An Investigation into Stratosphere-Troposphere Exchange using Air-Particle Trajectories

Aaron Billingham

Doctor of Philosophy
Institute for Meteorology
The University of Edinburgh
2003

Acknowledgements

Thanks to Bob, my supervisor. For some unknown reason I tried to do this PhD alone. Inevitably, of course, I could not.

Thanks also to all those who were completing, or finished, a tour in the terminal room whilst I was there. It is worth it in the end.

Final thanks to all the members of GEAS and to a certain Time Lord for providing that rather more abstract inspiration necessary to finish. Oh, and Mum, thanks for the scarf. Who could have foreseen how important it would become?

And for anybody reading this thesis with a PhD to write I offer some words of wisdom. When pursuing experiments and theories try to follow the example of the greatest investigator of all time:

"When you have eliminated the impossible, whatever remains, however improbable, must be the truth."

Sherlock Holmes
Sir Arthur Conan Doyle's The Sign of Four

And when feeling down, as will happen now and again, do not worry about it. Just acknowledge the reality, let it out and then move on:

"OK, I give up! What's goin' on?!?"

Johnny Cage
Mortal Kombat

This Doctor of Philosophy was funded by the Natural Environment Research Council.

Abstract

Tropical stratosphere-troposphere exchange is examined by the use of water vapour data and trajectory calculations. Water vapour data from the Microwave Limb Sounder (MLS) instrument and two-dimensional trajectories calculated from the assimilated data of the United Kingdom Meteorological Office (UKMO) are used to examine the evolution of water vapour upon isentropes near the 68 hPa surface. Three-dimensional trajectories calculated from the assimilated data of the European Centre for Medium-Range Forecasts (ECMWF) are used to examine the flow of air across the tropopause.

Combination of the MLS and UKMO data allows the construction of purely-isentropic evolutions of water vapour. On timescales less than those characteristic of diffusion and of methane oxidation, comparisons of these evolutions to the observed cases can be used to show where vertical motions must cross isentropic surfaces. As such, a comparison of monthly-averaged, water-vapour maps on isentropic surfaces near 68 hPa to monthly-averaged maps of the same data after ten-day isentropic-advections is presented for most of the operation time of the 183 GHz antenna of the MLS instrument — November 1992 to March 1993. The comparison shows that the two evolutions rarely match each other and thus that vertical airflows must be present over most of the tropical region, throughout the year, near 68 hPa.

The use of three-dimensional trajectories allows for a more-direct and more-detailed analysis of tropical, cross-tropopause motion. Though the lesser reliability of vertical wind-data does mean that only those three-dimensional-trajectory results that were in basic agreement with the results of the two-dimensional case described above could be considered useful, such an agreement was generally found during this study.

Three-dimensional trajectories are presented to show that though cross-tropopause motion does occur throughout the tropical region a persistent longitudinal-preference in the motion existed for all times investigated — the winters of 1980, 1981 and 1993 and all seasons of 1992. Crossing frequencies are shown to be much higher over the mid-Pacific throughout the year and much lower over the Indonesian and Asian monsoons, both extrema being visible at the ECMWF model-levels at 110 and 90 hPa. The peak crossing was stronger during the 1993 winter than in any other winter and stronger in autumn than in any other season of 1992. Furthermore, whenever the peak crossing showed an increase in magnitude it was accompanied by an increase in the concentration of particle crossings into the mid-Pacific.

Taken together, the results of the two- and three- dimensional experiments also suggest that longitudinal variations in the 68 hPa, MLS water-vapour-concentrations occur not through differential uplift but by variations in the height of the tropopause.

Contents

List of Figures

List of Tables

Chapter 1

Trajectories and Stratosphere-Troposphere Exchange

Stratosphere-troposphere exchange describes the material coupling, both dynamical and chemical, of the lowest two layers of the atmosphere and can, in turn, affect their radiative coupling as well. The exchange occurs across the tropopause, a surface defined to separate the two very different environments of the troposphere and stratosphere. Below the tropopause lies the unstable troposphere, the atmospheric layer that contains the majority of human activity and the rapid vertical motions of convection. Above the tropopause lies the calmer stratosphere, a layer free from chaotic weather conditions and where horizontal flows dominate over a much smaller vertical motion. Stratosphere-troposphere exchange therefore entails not just an airflow between two atmospheric layers but also a transition from one airflow regime to another.

Stratosphere-troposphere exchange (hereafter STE) comprises a net downwards motion in the extratropics and a net upward motion in the tropics. The majority of the extratropical, downward flow occurs through tropopause-folding events, a well-documented phenomenon (for example: World Meteorological Organisation (1986); Holton *et al.* (1995); VanHaver *et al.* (1996)). The tropical, upwards airflow is less well-described and it is not yet known by what method this cross-tropopause motion

primarily occurs.

Tropopause-folding events are fuelled by a downward motion in the stratosphere and controlled by weather in the troposphere. The integral cross-tropopause airflow takes the form of long, tangled filaments of stratospheric air reaching down into the troposphere. At the start of their lifetime the filaments are contained by strong gradients of potential vorticity but these gradients weaken with time, causing the stratospheric air to irreversibly join the troposphere.

It is not clear whether the existence of a spatially-confined phenomenon is necessary to explain the tropical exchange and its temporal variability. Indeed, no mesoscale, cross-tropopause motions have been confirmed to frequently occur there. Moreover, it is not even yet known whether the forcing of the tropical, cross-tropopause airflow is dominated by tropospheric or stratospheric phenomena.

An estimate of the overall mass-flux from the troposphere to stratosphere can be made however, by considering the stratospheric air-motion. The first description of this airflow was made by Brewer (1949) in an effort to explain the very low water-vapour concentrations found in the stratosphere. He hypothesised the now-accepted theory that air rises into the stratosphere in the tropics, thus crossing the coldest part of the tropopause, where the temperature minimum is capable of freeze-drying air down to the low water-vapour concentrations observed. Brewer's hypothesis goes on to describe the airflow continuing up into the higher tropical-stratosphere before being drawn out toward the poles, whereupon it travels back down into the extratropical troposphere.

By considering this motion Rosenlof and Holton (1993) were able to estimate the tropical, cross-tropopause mass-flux, as a function of season, that must occur to replace the air drawn up into the higher tropical-stratosphere. However, though their estimate indicates how much air must cross the tropical tropopause, the details of the how and where of the crossing remain unclear; it is not yet known what relative contribution convection, wave motion and the slow uplift of the stratosphere make to the forcing of the tropical exchange. Hence, the details of the spatial and temporal distribution of the tropical crossing are still undescribed.

Previous investigations into the details of the tropical exchange have made use of both global-scale, atmosphere models and regional observations of tropical air -flows and -characteristics. Many of the modelling studies have suggested that tropics-wide stratospheric-forcing causes tropics-wide exchange (Appenzeller *et al.*, 1996; Gettelman *et al.*, 2000; Gettelman and Sobel, 2000). Many of the purely-observational studies advocate the importance of local convection in fuelling the tropical exchange (Danielsen, 1993; Kelly *et al.*, 1993; Sherwood, 2000), particularly the strongest convective activity that occurs over the Indonesian island chain in the northern winter and over the Bay of Bengal in the northern summer. The results of all these investigations are extremely informative but inconclusive nonetheless.

A combination of global-scale modelling and regional observations can be put to greater use in the investigation of STE when in the form of assimilated-data sets. This combination provides globally-covering wind-data in a single dataset, allowing the motion of particles of air that would occur under the observed winds to be tracked and so the particles' trajectories to be plotted. Air-particle trajectories have been well used to investigate tropospheric motions but only one study has so far used trajectory calculations to examine the tropical, cross-tropopause motions (Jackson *et al.*, 2001) and this study only looked for exchange forced by convection from below.

Since assimilated-data sets cover the entire tropics at many levels of both troposphere and stratosphere however, it is possible to directly show the path that air takes across the tropopause throughout the tropics. Thus trajectory calculations can be used to investigate the tropics-wide exchange, to directly search for all the mechanisms of cross-tropopause motion that might be occurring. This thesis describes an effort to do just that, to use trajectories to examine the exchange at all longitudes and latitudes and to determine the temporal variability in the crossing locations found.

No previous study of tropical STE has made such an extensive use of trajectories. The greatest reason for this is the low reliability of vertical wind-data in comparison to other quantities. This fact makes it necessary either to treat three-dimensional trajectory results with great care or to compare them to the results of a second,

separate investigation. In the latter case a greater degree of confidence can be taken in the details of the trajectory results if the two investigations are in basic agreement.

This thesis uses the latter technique, comparing the trajectory data to the differences between isentropic and observed evolutions of water-vapour data. Estimates of isentropic evolutions are created by advecting water-vapour data with the winds of assimilated-data sets after interpolation onto isentropes. On timescales less than those characteristic of diffusion and of methane oxidation, comparisons of these evolutions to the observed cases are used to show where vertical motions must cross isentropic surfaces. The results of this water-vapour investigation not only provide a reasonable gauge of the reliability of the three-dimensional trajectory results but also provide independent information about uplift in the stratosphere.

1.1 Regions of Interest

In the chapters that follow, references are made to land and ocean areas in order to describe the extent of water vapour features and the positions of trajectory clusters. This is done to aid comparison between plots. The latitudinal and longitudinal extents of features and clusters may vary slightly between plots but still be found within similar areas of the tropics. As such, named positions become more useful than numerically defined areas when comparing plots, especially when considering many plots at one time.

On the following three pages therefore, three maps are presented as a guide to the tropical locations that will be used in the discussions of later chapters (figures 1.1–1.3).

Map 1

Figure 1.1 shows all tropical longitudes at up to thirty degrees from the equator. Islands and major land masses mentioned in later chapters are named. In the case of the former their co-ordinates are also supplied to the nearest half degree.

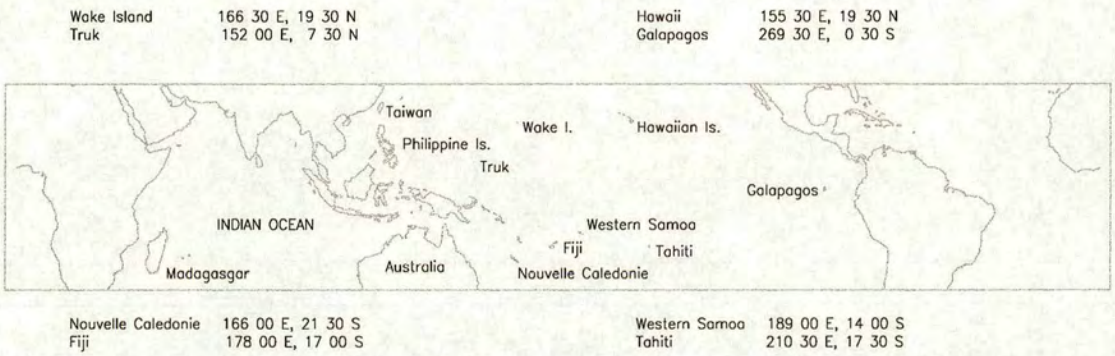

Figure 1.1: **Map of the Tropics.** Shows tropical countries and ocean areas at all longitudes up to thirty degrees from the equator. Island locations are given in degrees and minutes to the nearest half degree.

Map 2

Figure 1.2 shows five regions of the tropics that are more regularly discussed:

1. southeast Asia, see top panel of figure 1.3
2. Indonesia and neighbouring countries, see middle panel of figure 1.3
3. Central and South America, see bottom panel of figure 1.3
4. Micronesia
5. Polynesia

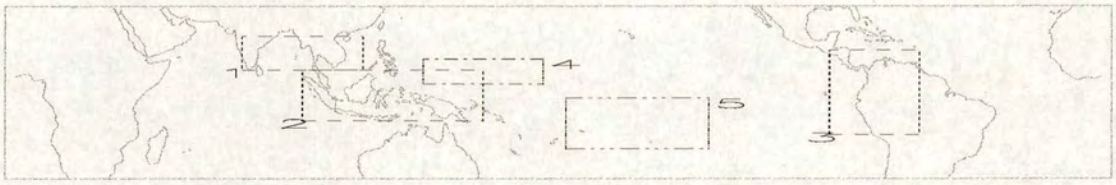

Figure 1.2: **Regions of Interest.** Shows five regions that are referred to by name within the following chapters. Those three regions indicated by dashed boxes are expanded upon in figure 1.3. The region denoted by dot-dash outline contains within it, but does not mark the political border of, the islands of Micronesia. The region denoted by triple dot-dash outline contains within it, but does not mark the political border of, the islands of Polynesia.

Map 3

Figure 1.3 shows three of the regions highlighted in figure 1.2 in greater detail.

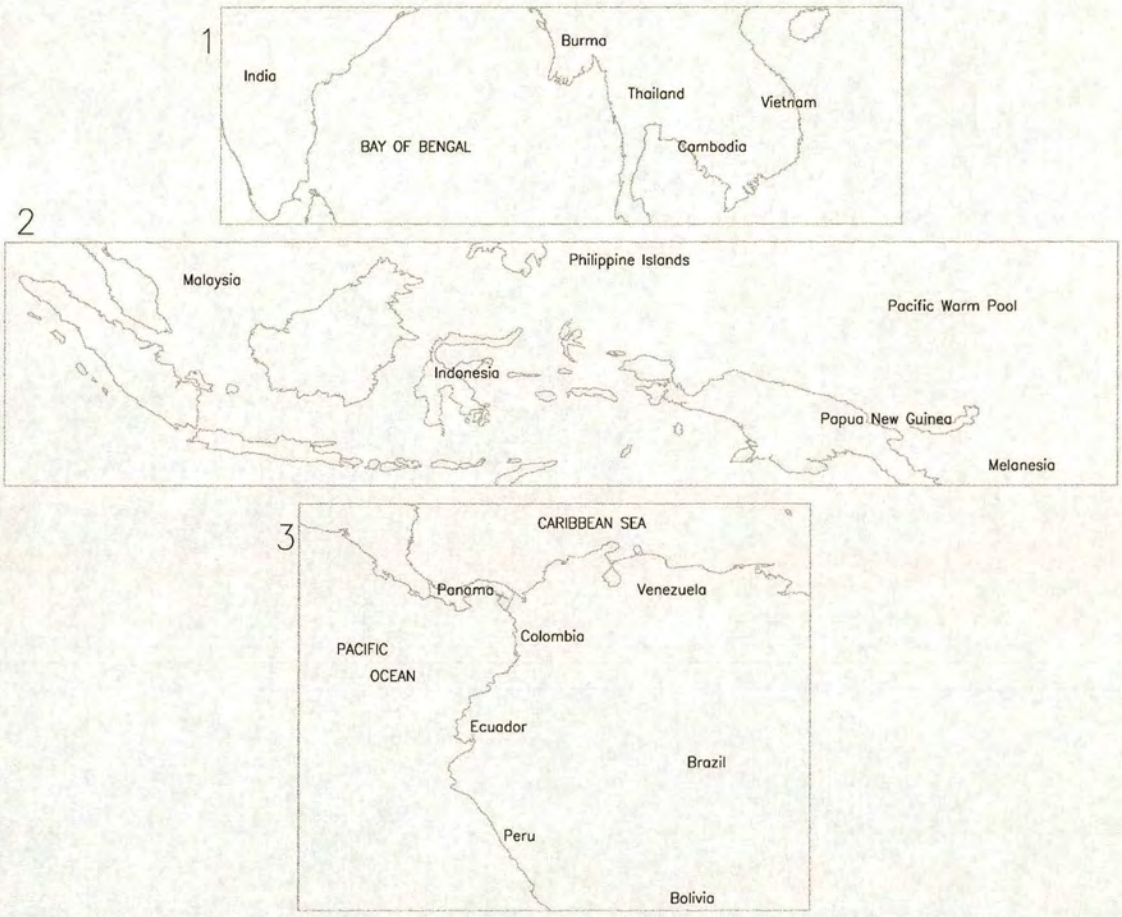

Figure 1.3: **Regional Maps.** Shows in greater detail the three numbered regions of figure 1.2: 1, southeast Asia; 2, the Indonesian island chain and neighbouring countries; 3, parts of Central and South America.

1.2 Aims of this Thesis

This thesis examines tropical stratosphere-troposphere exchange using both two- and three- dimensional trajectory-calculations.

The two-dimensional air-particle trajectories are used to advect water-vapour data from the Microwave Limb Sounder instrument, allowing the estimation of purely-isentropic evolutions of water vapour. These artificial evolutions are compared to the observed evolutions of the same data interpolated onto the same isentropes. In regions where the comparison reveals differences between the two evolutions, vertical motions can be said to have occurred across the isentrope.

The three-dimensional air-particle trajectories are used by themselves to analyse the tropics-wide, cross-tropopause motion. This examination highlights areas of preferential entry into the stratosphere (assuming basic agreement of the locations with those identified in the two-dimensional study). Temporal variations in the cross-tropopause motion are also examined.

Together these investigations will be used to show that:

- There exists a region of heightened tropical-exchange in the mid-Pacific.
- Cross-tropopause motion occurs throughout most of the tropical region, the exceptions being those areas above the most intense, wide-spread convection.
- The distribution of tropical, cross-tropopause motion does not change significantly between the early 1980s and the early 1990s.

1.2.1 Outline of the Thesis

Chapter 2 discusses in greater detail what was known about the exchange of air before the conclusions of this thesis were drawn. The background atmospheric motions within the troposphere and stratosphere are described, revealing the dynamics of the region surrounding the tropopause. The discussion then focuses on the tropopause

and suggests that the tropical exchange might be better examined as the motion across a layer rather than a surface. This distinction allows for the fact that, realistically, air will change from having tropospheric to stratospheric properties gradually through time rather than abruptly at the tropopause. The airflows either side of this layer that may affect either its size or position are then detailed.

Chapter 2 also discusses the first working theory of tropical STE, as put forth by Newell and Gould-Stewart (1981), the validity of which is still under consideration. This discussion is accompanied by reviews of more recent theories, both those adapted from the original idea and those suggesting alternative flows. From the sum of all these ideas, three hypotheses are proposed, which are disproved in turn throughout later chapters.

Chapter 3 discusses the technical details of trajectory and advection calculations and the errors associated with them. This chapter also discusses the datasets used in, and their selection for, the two means of investigation.

Two wind datasets are introduced — the assimilated data of the European Centre for Medium-Range Weather Forecasts (ECMWF) and of the United Kingdom Meteorological Office (UKMO). Both are discussed, along with a comparison of both to winds measured by the Changi Airport radiosonde in Singapore. The results of this comparison are then used to explain the separate use of the UKMO data in the creation of isentropic, water-vapour evolutions and the ECMWF data in the creation of three-dimensional trajectories.

A single water-vapour dataset is introduced — that of the Microwave Limb Sounder (MLS) instrument aboard the Upper Atmosphere Research Satellite. Data from the MLS instrument provide a tropics-wide, daily-updated view of the water vapour upon levels surrounding the tropopause. This continual coverage of the entire tropics proved to be ideal for the estimation of isentropically-advected evolutions of lower stratospheric water-vapour.

Within chapter 4, monthly-averaged and five-day-averaged isentropic and observed evolutions of water vapour are presented and compared for most of the lifetime of the 183 GHz antenna of the MLS instrument — November 1992 to March 1993. This

investigation focuses upon isentropes near the 68 hPa, the lowest level above the tropical tropopause layer for which the MLS retrievals provide useful data. Vertical motions are then inferred from this comparison.

These results are compared to the proposal of Newell and Gould-Stewart (1981), which suggests that tropical exchange occurs only over those areas of the most intense, wide-spread convection. It is shown, however, that uplift can only be inferred to occur in most places *other* than over this convective activity.

Chapter 5 shows the results of a three-dimensional trajectory analysis of cross-tropopause motion during the years 1980, 1981, 1992 and 1993. The trajectories are used to show that, at 90 and 110 hPa, a preferred region for the cross-tropopause motion exists in the mid-Pacific. The same results also confirm that tropical exchange is minimal over regions of the most intense convection. This crossing distribution is shown to persist throughout all seasons and years analysed.

The nature of the mid-Pacific crossing is also discussed, with evidence to indicate that it occurs an order of magnitude faster than the global-mean upwelling velocity seen in the stratosphere and with limited horizontal motion. Though this peak crossing does not significantly alter in position during the times analysed, it is shown to be stronger during the 1993 winter than in any other winter and stronger in autumn than in any other season of 1992. Furthermore, the analysis shows that whenever an increase in number of trajectory crossing-events occurred over the mid-Pacific the crossings were always concentrated into a smaller horizontal area. These inter-year and inter-season variations in the crossing-distributions do not appear to be linked to those of the Quasi-Biennial Oscillation or the El Niño Southern Oscillation.

Finally, chapter 6 discusses the results of this thesis as a whole and their implications for stratosphere-troposphere exchange, eliminating descriptions of the tropical exchange that the trajectory analyses have shown to be inviable. The remaining possible descriptions of the cross-tropopause flow are then examined along with proposals for further experiments that might help to eliminate more of this remainder.

Chapter 2

Stratosphere and Troposphere

The relative contributions from stratospheric and tropospheric motions to the forcing of tropical stratosphere-troposphere exchange (hereafter STE) are unknown. Any theory that hopes to properly describe the detailed exchange must therefore consider all the motions, in both layers, that can affect the environment near the tropical tropopause.

Newell and Gould-Stewart (1981) proposed the first theory to describe the detailed tropical exchange. Believing that not all parts of the temperature minimum near the tropopause were capable of drying air down to the low stratospheric water-vapour concentrations, they suggested that air only crossed the tropopause in restricted places. They further noted that the only regions with a cold enough temperature-minimum were those above the strongest convective activity. Thus Newell and Gould-Stewart (1981) proposed convection as the dominant force for tropical exchange. Their theory suggests that air would spread to the remaining tropical stratosphere by isentropic advection, implying that the influence of the cross-isentrope stratospheric-uplift would be confined above the tropopause.

The validity of this theory is still under question, since it is not clear that a significant amount of convective activity penetrates the tropopause (Gettelman *et al.*, 2002). Recent work has also suggested that the entire tropopause region may be cold enough to provide sufficient drying after all (Dessler, 1998). If correct, both of these facts would suggest that convection does not play a considerable role in the

forcing of the tropical exchange.

Newer theories discussing the detailed tropical-exchange thus rely less on the direct action of convection, some even splitting the drying and final-crossing into separate processes. Potter and Holton (1995) suggested that exchange might occur upon the crests on Kelvin waves generated by tropospheric disturbances. Sherwood and Dessler (2000) proposed that the drying occurs through convective overshoot that then detrains, for the most part, into the upper troposphere. Holton and Gettelman (2001) proposed that the drying occurs above areas of convection but a kilometre or more below the tropopause. In the latter two cases the final uplift would occur downstream of the drying event, dependent only on the stratospheric uplift.

Further observational or experimental evidence is required to differentiate between the suggested possibilities for the detailed tropical-exchange. Possibly the most useful observations to date are of tropical cirrus cloud. Such observations have already shown a strong link between the variations in the frequency of high cirrus and in the stratospheric-uplift (Zhang, 1993). Further analyses of high cirrus could go so far as to aid the differentiation between the rapid uplift of convection and the slow uplift of the stratosphere. This latter analysis would, however, require a large campaign of *in situ* measurements, in order to examine the relative fraction of the different isotopic compositions of water that occur during the different types of uplift (Moyer *et al.*, 1996).

Lack of observations therefore, makes a long-running, tropics-wide cirrus-cloud-study impossible, as yet, and a long-running, tropics-wide dataset is crucial to an investigation into the relative contribution of stratospheric and tropospheric motions to the forcing of tropical STE. As such, a trajectory study may succeed where other studies cannot.

Within this chapter the current understanding of the tropical exchange is reviewed as a foundation for the research presented in later chapters. Section 2.1 discusses what is currently known about the dynamics of the tropical tropopause region in which the exchange occurs. Section 2.2 reviews the "stratospheric fountain" of Newell and Gould-Stewart (1981). Section 2.3 then reviews the theories of tropical

exchange that have been proposed since. Section 2.4 discusses the information that studies of tropical, high-cirrus cloud have provided. Finally, in section 2.5, the possibilities for the exchange are gathered together such that a proposal for their investigation can be given. The proposal takes the form of three hypotheses, which are each disproved in later chapters using the results of trajectory studies.

2.1 Dynamics of the Middle Atmosphere

The tropopause separates the more radiatively-dominated stratosphere from the more convection-dominated troposphere. In the extratropics the separation is well defined by strong gradients in potential vorticity. In the tropics the situation is not so simple, as the tropopause does not so clearly separate tropospheric and stratospheric phenomena and the current World Meteorological Organisation definition of the tropopause serves a more conceptual rather than practical purpose. For these reasons, other definitions of the tropopause have found contemporary use in the study of tropical cross-tropopause motions.

Each new definition of the tropical tropopause suffers from the same problem however — they only separate the stratosphere and troposphere in terms of one atmospheric characteristic, for example, temperature or potential vorticity. This is because there is no definite division between *all* tropospheric and *all* stratospheric phenomena. Rather each phenomenon may overlap any and all other phenomenon, to a degree that is a function of height over some finite layer. Unravelling the relative contributions of each phenomenon throughout this layer, thus properly describing the region of cross over, is the key to understanding tropical STE. As such, all tropospheric and stratospheric motions that take effect near their mutual tropical-border must be considered when investigating STE.

2.1.1 The Troposphere

The primary force of disturbance in the tropical troposphere is the convection that results from surface heating and convergence of air. The strongest tropical convec-

tion is usually found along the Intertropical Convergence Zone (ITCZ), which marks the boundary and meeting point of the northeasterly and southeasterly Trade Winds. Furthermore, the strongest tropical convection usually occurs during the monsoon seasons of tropical countries: The northern-hemisphere summertime sees monsoons over India and Mexico, the southern-hemisphere summertime sees them over Australia and South America.

This strongest convective-activity can reach up to, and sometimes even beyond, the tropopause near 16 km. However, the main tropical outflow is thought to be near 200 hPa, at around 12 km, with nearly all outflow topped by a level near 140 hPa, at around 14 km, (Highwood and Hoskins, 1998). These figures are not universally accepted however; it was proposed by Sherwood and Dessler (2001) that the main outflow occurs higher up, at ~150 hPa, and that significant penetration of the tropopause occurs. If this latter estimate were correct then convection would be very important contributor to local STE.

Convection along the ITCZ makes up the rising-motion half of the Hadley Cell, which describes the basic flow pattern of the tropics and subtropics. The true distribution of convection is, of course, somewhat more complex but can be depicted using increasing levels of detail, up to that of daily weather, superimposed over the Hadley Cell; the contribution to STE from convection may then occur at any, or even all, of these levels.

The next level of detail up from the basic flow is a zonal asymmetry described by the Walker Circulation, a representation of which can be seen in figure 2.1, which is a copy of figure 11.10 of Holton (1992). The top panel of the diagram shows the undisturbed Walker Circulation, with convective activity caused by the warm surfaces of Africa, South America and the Pacific Warm Pool. Their high surface temperatures cause convection within each region and a corresponding downflow within relatively cooler neighbouring areas. The Pacific Ocean cell of the Walker Circulation is created by the Trade Winds, which drag ocean currents westward, causing the colder, deep waters off the coast of Peru to rise to the surface. Thus a cell forms with a rising motion over the relatively warm west Pacific and a sinking motion over the cooler east Pacific.

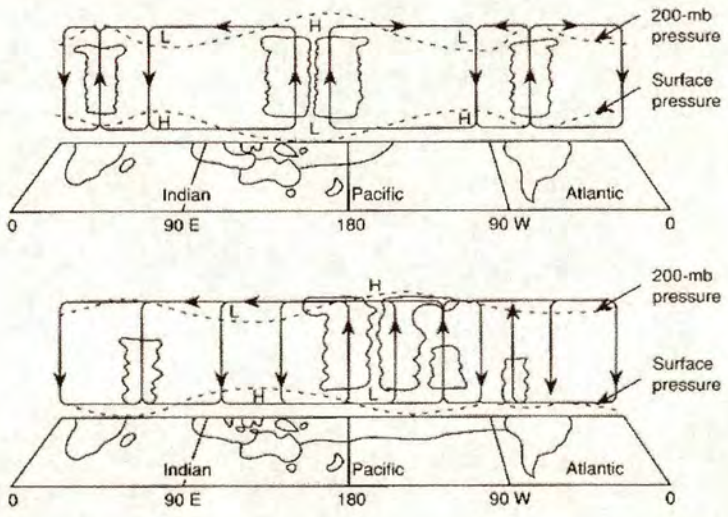

Figure 2.1: **The Walker Circulation.** As figure 11.10 of Holton (1992), page 381. The upper panel shows the convective cells of the Walker Circulation, the lower panel shows this circulation altered by the El Niño phase of the El Niño Southern Oscillation.

Further detail in the distribution of convection comes from the El Niño Southern Oscillation or ENSO. This tropical phenomenon disturbs the Walker Circulation to an extent that can be appreciated in the bottom panel of figure 2.1. The ENSO has a period somewhere between 3 and 5 years, marked by warm events, called El Niño, and cold events, called La Niña. Though the ENSO can alter atmospheric conditions worldwide, its strongest effects are felt in Indonesia and Peru.

El Niño conditions occur when the Trade Winds relax, no longer dragging ocean currents to the western Pacific. As such, the convection that would normally be seen over the Pacific Warm Pool and Indonesia instead rises over the central Pacific. The accompanying downflow of air over Indonesia during these times can bring severe drought to the islands. This period is labelled as a "warm phase", since the coastal waters of Peru are no longer cooled by upwelling from below. During El Niño conditions the surface waters rise in temperature by between 1 and 4 degrees, causing the death of much of the surface-water marine-life.

La Niña conditions cause the opposite effects — increased convection over Indonesia, and so flooding, and a decrease in surface water temperatures (by 2–5 degrees)

off the coast of Peru. In this case the convection patterns remain similar to the undisturbed Walker Circulation, it is only the intensity of the activity that changes.

2.1.2 The Stratosphere

Increasing absorption of solar energy with height in the stratosphere creates stable layers that suppress convection. Dynamical effects in the stratosphere are instead the result of wave-forced motions. Vertical motions there can be determined by comparison of the radiatively-forced- to the observed- temperature-distribution. Where there are differences between the two, there must be dynamical effects present to disturb the atmosphere away from its radiative-equilibrium state towards the observed condition. Figure 9.6 of James (1994) illustrates the two temperature distributions and are reproduced here in figure 2.2.

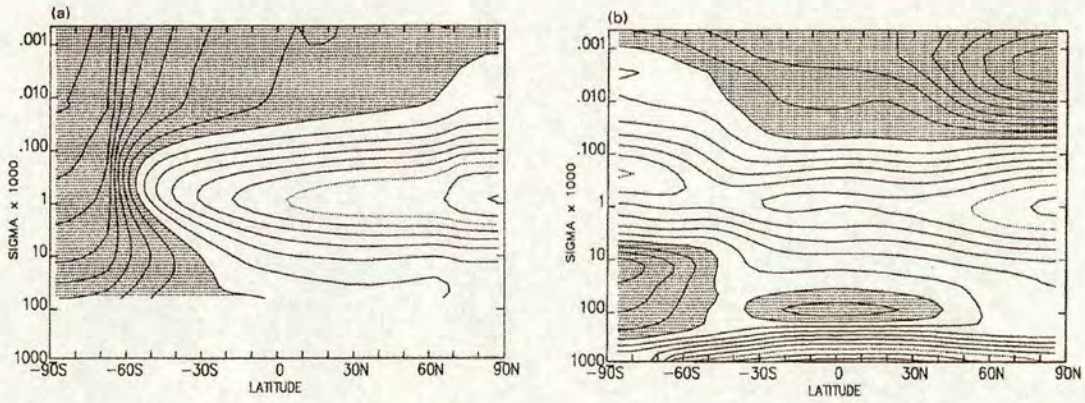

Figure 2.2: **A Comparison of Radiative and Observed Temperature.** As figure 9.6 of James (1994), page 311. Panel (a) shows the radiatively determined temperature of the stratosphere and mesosphere and panel (b) the observed temperature distribution. Both panels are a climatology for July. The vertical scale is approximately pressure in hPa. The contour interval is 10 K with shaded regions indicating temperatures less than -60°C.

A comparison reveals that there must be dynamical effects occurring at the tropical tropopause, in the summer mesosphere and in the winter stratosphere and mesosphere. In the former two locations there must be adiabatic ascent, whereupon expansion will cause rising air to cool below radiative equilibrium. Conversely, the winter stratosphere and mesosphere must both experience adiabatic descent, caus-

ing air to warm to temperatures above that of radiative equilibrium. These airflows are illustrated in figure 2.3 (obtained from the British Atmospheric Data Centre; produced by the NASA Goddard Institute for Space Studies, July 1999).

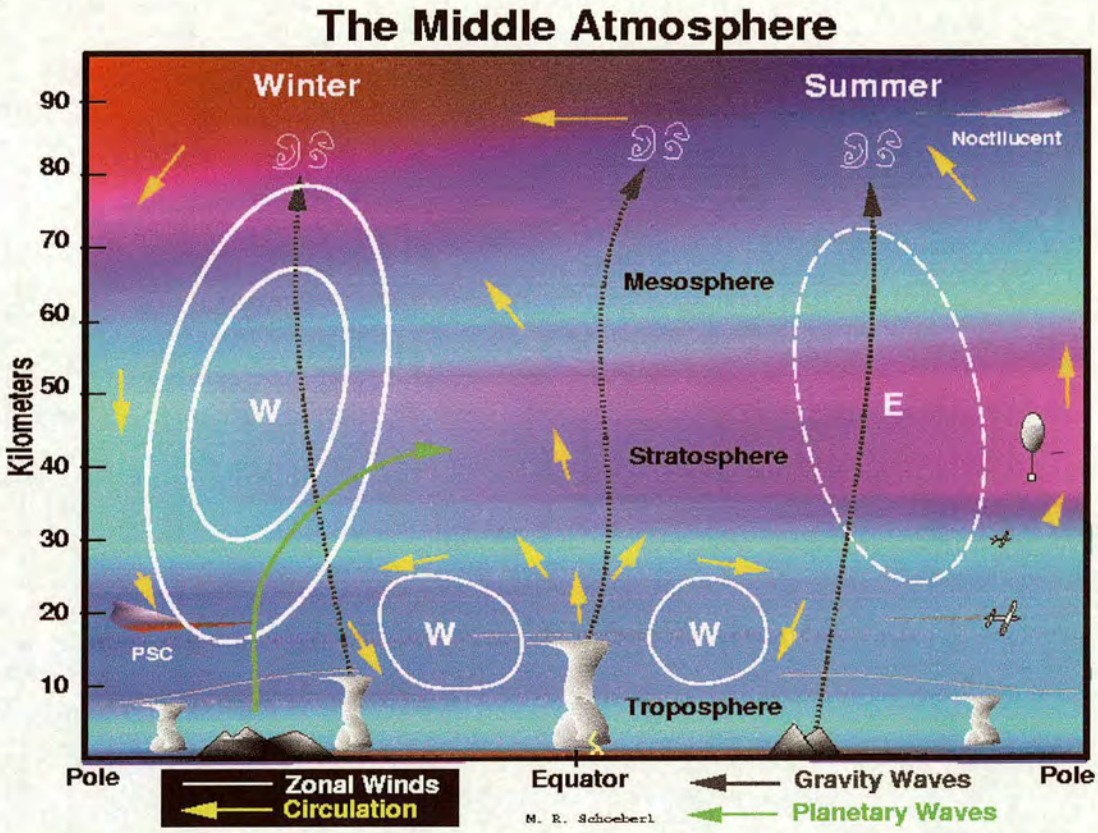

Figure 2.3: **The Middle Atmosphere.** Obtained from the British Atmospheric Data Centre; produced by the NASA Goddard Institute for Space Studies, July 1999. The diagram shows the circulation in yellow arrows and the propagation of waves up from the troposphere in green and black. Regions of wave breaking are marked in white at the tip of the arrows. Also drawn are noctilucent and polar stratospheric clouds (the latter marked as PSC).

The Brewer-Dobson Circulation comprises the upward motion across the tropical tropopause and the downward flow in the winter stratosphere. This wave-driven circulation connects the two flows via an equator-to-pole motion in the high stratosphere and is completed by a return flow to the troposphere at mid-latitudes. The Brewer-Dobson Circulation is important to STE because of the air it draws up across the tropical tropopause and hence is discussed in detail later in this chapter.

Also visible in the figure are:

- The wave-driven, Murgatroyd-Singleton Circulation — that connects the rising motion in the summer mesosphere to the falling motion in the winter mesosphere via a pole-to-pole flow near the mesopause (Murgatroyd and Singleton, 1961).
- The subtropical jets — that are important for extratropical STE as tropopause folds often occur in their vicinity (van Velthoven and Kelder, 1996; Gouget *et al.*, 2000).
- The stratospheric summertime-easterlies and wintertime-westerlies — that form under the thermal wind relation due to stratospheric heating.

The high latitudes of the stratospheric summer-hemisphere are well heated by the sun, the long days more than making up for the low angle of incidence, causing a temperature gradient to form between the summer pole and the cooler equator. In the winter hemisphere a stronger temperature gradient occurs as temperatures fall off much more sharply towards the limit of incident sunlight, at around 66 degrees latitude, where the heating rate is zero. These gradients cause an airflow from the summer pole to the equator and on to the winter pole. Under the Earth's rotation the resulting airflows are turned easterly in the summer hemisphere and westerly in the winter hemisphere, as indicated in figure 2.3.

At the equator thermal wind balance does not hold and so the winds there are not so simply forced. However, as shall be discussed later in this chapter, any indigenous flow that would result here is swamped by a motion forced from the troposphere — the Quasi-Biennial Oscillation.

To enable the reader to better picture the three-dimensional flow of the upper troposphere and lower stratosphere reproductions of figures 9.1 and 9.2 of James (1994) are supplied here in figure 2.4. It shows the streamfunctions for a northern hemisphere January and July at four levels of the atmosphere. By mentally combining figures 2.3 and 2.4 it is possible to envisage the transition from the depression-

dominated, transient conditions of the troposphere to the more stable, persistent and spatially-uniform conditions of the stratosphere.

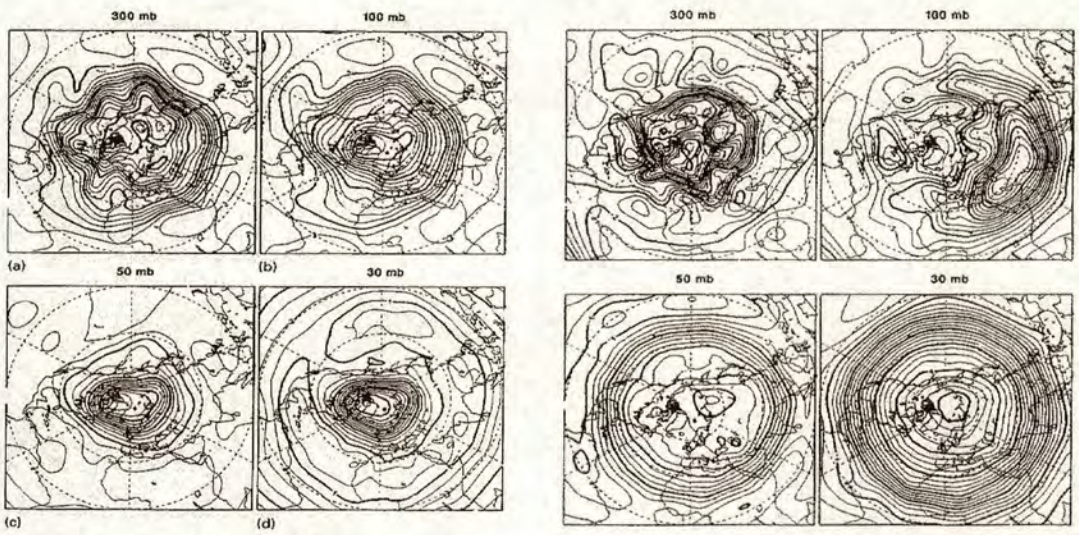

Figure 2.4: **Upper Troposphere and Lower Stratosphere Streamfunctions.** As figures 9.1 and 9.2 of James (1994), pages 303–304. Shows the streamfunction for four levels of the atmosphere as indicated by the left panel: (a) 300 hPa, (b) 100 hPa, (c) 50 hPa and (d) 30 hPa. The levels are the same in the right panel. On the left the streamfunctions are for 22^{nd} January 1987, with contour interval 10^7 m^2s^{-1}, and on the right for 22^{nd} July 1986, with contour interval 5×10^6 m^2s^{-1}. All maps are centred upon the north pole.

Figure 2.4 shows that stratospheric flows are, though more uniform than tropospheric motions, not completely uniform around a latitude circle. This is apparent in the 30 mb January picture of the figure, in which the polar night jet is not axisymmetric. The Rossby waves that drive the Brewer-Dobson Circulation also disturb the stratospheric airflow as they travel up from the troposphere to the high stratosphere. However, they are only able to propagate up through the wintertime westerlies and hence the 30 mb July map is free of disturbance. A map of the south pole in July would still show lesser disturbance than the north pole, January map however, since the greater amount of orography of the northern hemisphere generates more waves.

Rossby wave disturbances to the stratospheric westerly conditions can also cause more dramatic effects than asymmetric streamlines. The easterly momentum imparted by breaking Rossby waves can slow and sometimes even reverse the westerly

flow. This produces regions of easterly shear with height and, by thermal wind balance, a gradient of increasing horizontal temperature towards the winter pole. Such warmings events are referred to as "stratospheric sudden warmings" and usually occur over the space of one or two weeks, though on occasion can do so much faster. These sudden warmings are generally seen during the mid- to late winter but may occur at any point throughout the time of westerly conditions.

The final warming of the polar region occurs during the spring with the return of sunlight. Increasing solar heating disrupts the cyclonic circulation of the polar vortex and its westerly winds break down, sometimes on timescales of only a few days. Anticyclonic circulations displace the polar vortex from the pole before it breaks up entirely, after which the summer-like easterly winds take over and the temperature of the polar region rises substantially. The duration of the change between conditions depends upon the degree of interaction with Rossby waves.

The autumn transition tends to be far gentler than the spring, typically occurring over radiative timescales (between 5–20 days). Around the autumn equinox the summer pole cools and a small cyclonic vortex forms over the pole, replacing the summer anticyclone. The easterlies of the summer regime persist in mid-latitudes, only slowly being hedged out as the polar vortex strengthens and expands equatorward. Eventually a strong polar night jet will form as the easterlies retreat into the tropics. This slow progress of easterly winds is not affected by Rossby waves.

The Brewer-Dobson Circulation

It was Brewer (1949) who first proposed a stratospheric circulation, entailing a tropical, rising motion, connected by a high altitude poleward drift to an extratropical, downward flow that returned air to the troposphere. Brewer (1949) proposed this theory to explain the observed dryness of the stratosphere, that the tropical tropopause could conceivably freeze-dry crossing air to stratospheric values. Some time later Dobson (1956) provided the first observational evidence to support the suggested flow, also showing that a poleward, then downward flow was qualitatively consistent with the observation of high concentrations of ozone in the lower polar

stratosphere, far from its production region.

This circulation, the Brewer-Dobson circulation, has been shown to be driven by the breaking of Rossby waves in upper stratosphere (Andrews and McIntyre, 1976, 1978; Dunkerton, 1978; McIntyre and Palmer, 1984; Haynes *et al.*, 1991). Excited by the orography of, and diabatic heating in, the troposphere, Rossby waves travel predominantly equatorward and upward. They can only propagate in westerly flow however, and so, upon reaching the stratosphere, only penetrate into the winter hemisphere. Furthermore, for each wavelength there exists a critical velocity of the background flow, whose strength is inversely proportional to that wavelength. Only when the background flow is less than this velocity can the Rossby waves propagate within it. Thus, the winter stratosphere also filters waves down to the longer wavelengths. Hence the use of "planetary waves" as opposed to Rossby waves in figure 2.3.

As the waves propagate in height their amplitudes increase in inverse proportion to the air density. The propagation continues until the waves break, which generally occurs at a height where the wave amplitude becomes comparable to the wavelength. As the waves break, their westward momentum is imparted to air within the stratosphere, slowing the environment's westerly flow. This breaking occurs at all longitudes of the stratospheric mid-latitudes[†], creating a well-mixed "surf zone" (McIntyre and Palmer, 1984).

Under the turning of the Earth, slowed air parcels move polewards, leaving behind an area of low pressure. Neighbouring air then moves towards this low pressure, causing another region of low pressure to form in *its* wake. This action repeats, describing a chain of motion connecting the mid-latitude upper-stratosphere to the tropical lower-stratosphere and possibly down into the tropical troposphere. Overall, the motion is said to work under the "downward control principle" (Haynes *et al.*, 1991), since the response to the driving force occurs below the point of action.

The Brewer-Dobson circulation is present all year round, following the strato-

[†]However, it is not known if the wave breaking occurs evenly around the planet and hence whether or nor the forcing of the stratospheric uplift is horizontally uniform.

spheric winter-westerlies, but with noticeable asymmetry between the northern and southern hemispheres. Rosenlof and Holton (1993) calculated the mass flux across the 100 hPa surface, as a function of season, as an estimate of the global-scale STE resulting from the pumping mechanism described. Their results show that the larger number of planetary waves of the northern hemisphere lead to greater extratropical downwelling and tropical upwelling during the northern winter. The information from their tables 1 and 2 are gathered together here as table 2.1.

	DJF	MAM	JJA	SON	Annual Mean
NH extratropics	-81	-46	-26	-43	-49
Tropics	114	76	56	70	79
SH extratropics	-33	-30	-30	-28	-30

Table 2.1: **Mass Flux Across the 100 hPa Surface.** After tables 1 and 2 of Rosenlof and Holton (1993), page 10473. Units are 10^8 kg s^{-1}. Negative signs indicate downward flux. Abbreviations are: DJF, December, January and February; MAM, March, April and May; JJA, June, July and August; SON, September, October and November; NH, northern hemisphere; and SH, southern hemisphere.

These 100 hPa mass-fluxes are not necessarily evenly distributed throughout the tropics and extratropics. However, a full description of the spatial variation of the mass flux would require better knowledge of the distribution of planetary-wave propagation in the stratosphere than is currently available. To date, only the sources of the waves in the troposphere and the latitudinal extent of the forcing have been determined.

Becker and Schmitz (1999) showed that only the combined action of orographic and mid-latitude-thermal wave-forcing can induce a realistic circulation, *i.e.* one that continuously bridges the tropics and polar latitudes in the stratosphere. They also showed that solar heating of the tropics does not influence the magnitude of the forcing. Such heating may affect the latitudinal extent of the uplift however, since it has some influence over the radiative equilibrium of the lower stratosphere, which in turn controls the filtering of propagating waves (Becker and Schmitz, 1999; Plumb and Eluszkiewicz, 1999).

Plumb and Eluszkiewicz (1999) suggested that the equatorward extent of the wave

breaking is critical in determining the tropical coverage of the lower-stratospheric uplift. Using a non-linear, two-dimensional model of Rossby wave forcing in the stratosphere they determined that a steady and linear circulation, with a qualitatively-reasonable upwelling, can be obtained if the wave drag occurs to within 20 degrees of the equator. None of their experiments were able to reproduce the observed maximum upwelling in the summer hemisphere however, even with the wave drag extending to within 12 degrees of the equator.

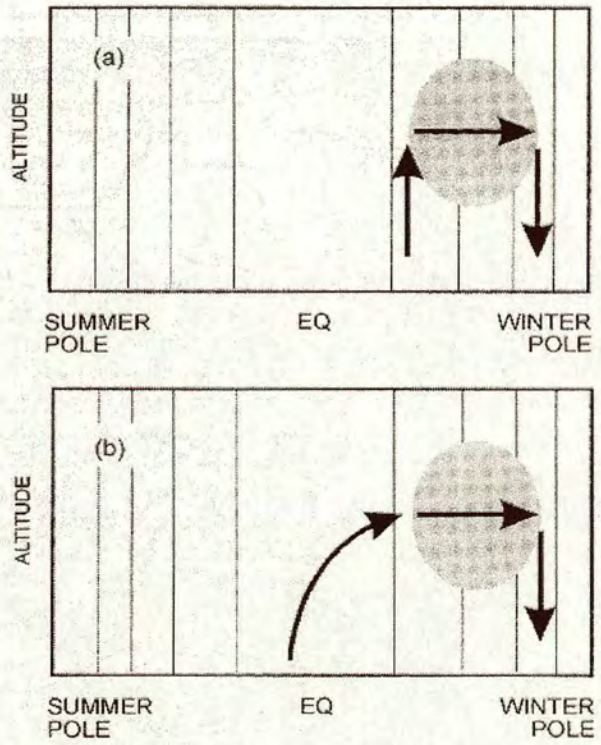

Figure 2.5: **Wave-Driven Uplift.** As figure 1 of Plumb and Eluszkiewicz (1999), page 869. The vertical lines mark contours of angular momentum and the shaded area shows the region of wave breaking that drives the Brewer-Dobson circulation. The arrows of panel (a) mark the steady state circulation that might be expected from theory (see text) and those of panel (b) mark the circulation observed.

Figure 2.5 is a copy of figure 1 of Plumb and Eluszkiewicz (1999), showing a theoretically expected upwelling (a) and the observed case (b). Observations show that the contribution from Rossby-wave drag is concentrated within the surf zone (McIntyre and Palmer, 1983; Murphy *et al.*, 1993; Randel *et al.*, 1993; Grant *et al.*, 1996). By analysis of the angular momentum budget, Haynes *et al.* (1991) showed that,

given this wave-breaking limit, there can only be motion across angular momentum contours within this surf zone, as shown in panel (a). Mass continuity demands some air flows into the shaded area but this will occur along angular momentum contours, i.e. in the vertical[†]. Outside of the shaded region there can be no flow across the angular-momentum contours as there is no local force to drive it. As such, a stratospheric flow forced by Rossby-wave breaking alone would look like figure 2.5a.

However, such a flow is not seen, as can be shown through observations of tropical vertical-velocities. Figure 2.6 is a reproduction of figure 2 of Plumb and Eluszkiewicz (1999). It shows the residual vertical velocity at 68 hPa as determined from temperature and constituent data, acquired by the Microwave Limb Sounder and Cryogenic Limb Array Etalon Spectrometer instruments aboard the Upper Atmosphere Research Satellite, and radiative transfer code.

The vertical velocities show a definite shift toward the summer hemisphere, with the exception of only one northern winter period in both data sets. Furthermore, annual mean upwelling is depicted out to at least to 20 degrees from the equator. Hence observations would tend to suggest that the response to wave drag is more like that of figure 2.5b, which requires some local force acting within deep tropical latitudes, equatorward of the Rossby-wave forcing.

The necessity of this force has been discussed by previous authors (Dickinson, 1971; Held and Hou, 1980; Haynes *et al.*, 1991) but no explanation of its nature or source has yet been found. From their model results Plumb and Eluszkiewicz (1999) deduce that the "numerically necessary but otherwise arbitrary viscosity" that they had to apply to their model to obtain a realistic flow must be much weaker than thermal dissipation, with a relaxation timescale some fifty times smaller than for the thermal case. They therefore suggest that molecular viscosity would be too weak, implying that must be an eddy viscosity, the best candidates for which are the vertically propagating equatorial waves of the Quasi-Biennial Oscillation.

[†]See Haynes *et al.* (1991) for discussion of the downward connection at high latitudes.

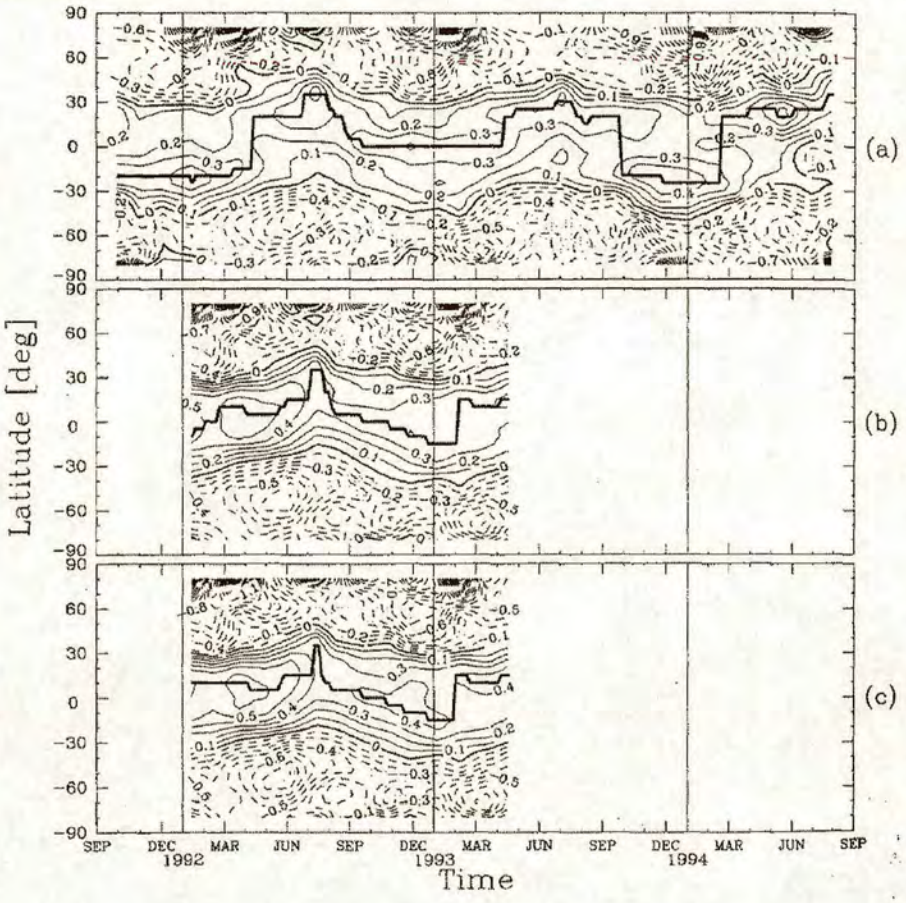

Figure 2.6: **Vertical Velocities at 68 hPa.** As figure 2 of Plumb and Eluszkiewicz (1999), page 870. Panel (a) shows Microwave Limb Sounder data, panels (b) and (c) Cryogenic Limb Array Etalon Spectrometer data. The effects of aerosols are included in panel (c). Contour interval is $0{\cdot}1\times10^{-3}$ ms^{-1}; negative values are shaded. The bold, solid line indicates the point of maximum upwelling.

The Quasi-Biennial Oscillation

The Quasi-Biennial Oscillation (hereafter QBO) is a wave-driven motion, exhibiting easterly and westerly winds that alternately descend through the stratosphere, dominating the tropical airflow and its variability. Though it is called an oscillation the QBO is better described as an alternation, for it has no fixed cycle or amplitude but rather a period varying from 22 to 34 months and wind strengths that vary with height. Both easterly and westerly winds propagate down from a height of about 50 km in the upper stratosphere to the tropopause, near 16 km, with the phase

reversal tending to occur during the northern spring. An excellent review covering further details of the QBO can be found, along with the history of its discovery, in Baldwin *et al.* (2001), the most important points of which are reproduced here in the following text.

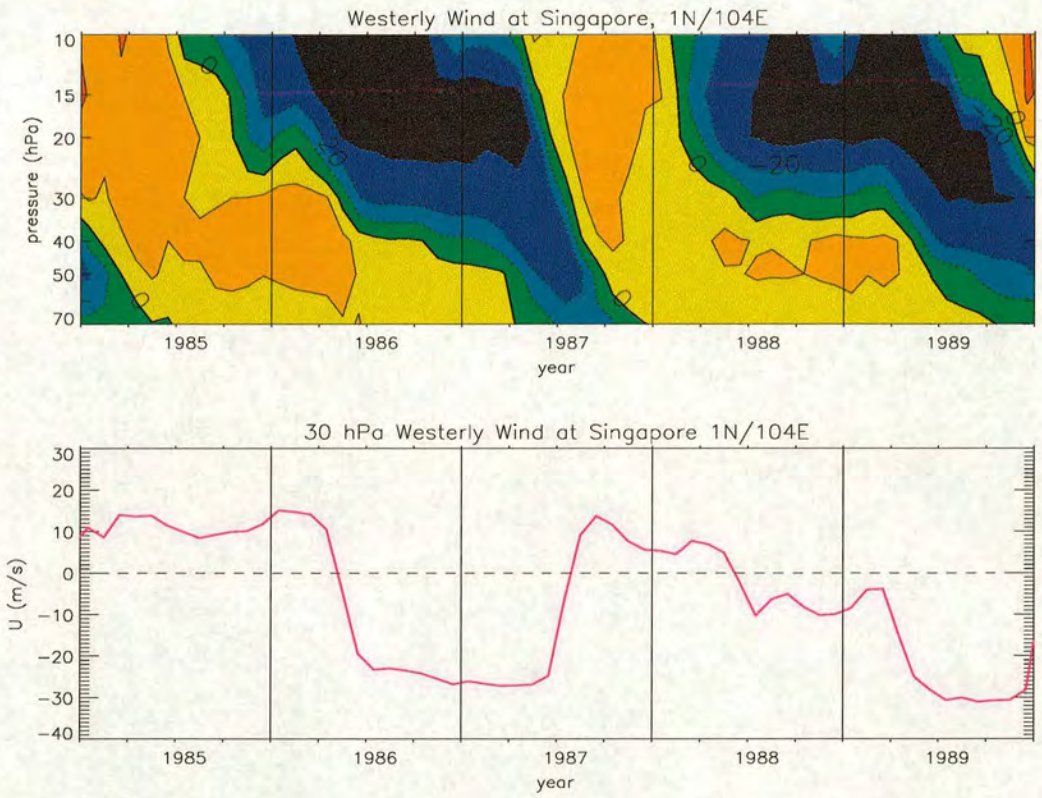

Figure 2.7: **The Quasi-Biennial Oscillation as Observed by the Singapore Radiosonde.** Supplied by Vicky West at The University of Edinburgh (personal communication). The contours of the top panel are 10 ms^{-1} with westerlies in yellow and orange and easterlies in green and blue. The bottom panel shows the wind reversals at 30 hPa.

Figure 2.7 shows the QBO in a timeseries of zonal wind measured by the Singapore radiosonde station at 1·36 °N, 103·98 °E. Some of the general properties of the QBO can be appreciated in the figure: The change from easterly to westerly winds propagate downward much faster than the change from westerly to easterly; the westerly phase tends to be more regular in duration; the easterlies are usually stronger than the westerlies.

QBO winds tend to be relatively small near the stratopause, with speeds up to 5 ms^{-1}. Between 5 and 20 hPa the wind speeds are larger, the easterlies reaching up 30 ms^{-1} and the westerlies up to 20 ms^{-1}. Both easterlies and westerlies remain approximately constant over this height range. Below 20 hPa, QBO winds decrease, falling off rapidly after 50 hPa. The amplitude of all winds are approximately Gaussian about the equator and approximately longitudinally symmetric (Baldwin *et al.*, 2001).

That the QBO cannot simply be the result of a single downwardly-propagating wave can be appreciated from the fact that the amplitude of such a wave would exponentially decrease in proportion to increasing air density. Such an amplitude change is not evident in figure 2.7. Also, the forcing for the alternation must propagate downward with the change in wind direction to overcome losses by dissipation.

The now generally-accepted theory that best describes the QBO was put forth by Holton and Lindzen (1972), was furthered by Plumb (1977) and realised in experiment by Plumb and McEwan (1978). From the work of these authors it was determined that the driving force for the QBO originates in the troposphere. Motions there, particularly convection, can force a spectrum of waves that propagate up through the tropical stratosphere. The QBO results from an interaction between equatorially-trapped, vertically-propagating waves and the mean flow. The interaction occurs in such a way however, such that the period of the overall phenomenon is not related to that of the driving waves.

As occurs with Rossby waves in the extratropical stratosphere, the mean flow in the tropics acts as a filter on waves propagating up from the troposphere below. Only those waves moving against the mean flow are able to penetrate the tropopause and propagate into the stratosphere. In the extratropics, only the easterly, or westward, propagating Rossby waves can penetrate into the extratropical, wintertime westerlies. In the tropics however, the alternating mean flow means that different waves can propagate at different times — when the flow is westerly, Rossby-gravity waves will pass up into the tropical stratosphere, when it is easterly, Kelvin and gravity waves can propagate.

All these wave types will, under their respectively-required mean flow conditions, propagate up into the higher stratosphere and then break. The Rossby-gravity waves will deposit easterly momentum and the Kelvin and gravity waves westerly momentum. In all cases the waves slow down the mean flow, eventually stopping, then reversing it. This flow reversal becomes a cap on the upward propagation of following waves, which are therefore forced to break at a lower height. The reversed flow then propagates down through the stratosphere, ultimately reaching the tropopause, whereupon the alternative waves can then penetrate the stratosphere. This process repeats and the flow continues to change back and forth between the two directions.

The effects of the QBO are felt throughout the entire stratosphere, not only modifying the wave propagation through both the tropics and extratropics but also altering tropopause characteristics, stratospheric dynamics and stratospheric chemistry.

Planetary wave breaking: These waves predominantly propagate equatorwards and have been observed to break across the equator in the stratospheric summer-hemisphere (Holton and Tan, 1980, 1982; Hitchman *et al.*, 1987). However, both the zonal mean wind direction at 30 degrees latitude in the winter hemisphere and the phase of the QBO are crucial in determining the degree to which such penetration occurs (Chen, 1996). If either the QBO or the 30-degree wind are easterly then planetary waves cannot cross into the tropics and will be forced out into the mid- and high latitude stratosphere. At the highest latitudes the waves can converge and slow down the zonal mean flow of the stratospheric polar vortex, causing the vortex to break up more rapidly[†] (Polvani *et al.*, 1995; Chen, 1996). Conversely, if both the QBO and the 30-degree wind are westerly the polar vortex can be stronger (Dunkerton and Baldwin, 1991).

Stratosphere: Niwano and Shiotani (2001) observed vertical velocity anomalies, with QBO-related variations, of magnitude $0{\cdot}10$–$0{\cdot}15\times10^{-3}\mathrm{ms}^{-1}$ between 20 and 40 hPa and $0{\cdot}1\times10^{-3}\mathrm{ms}^{-1}$ at 50 hPa. (Both of these values were obtained for equatorial winds, the anomalies diminishing in magnitude away from the equator.)

[†]See the discussion on the wintertime stratospheric vortex in the first part of this section.

The changing vertical zonal-wind shear of the QBO require changes in the latitudinal temperature gradient to balance them, allowing the atmosphere to remain in thermal wind balance. These temperature gradients come about through adiabatic vertical motion. Increasing westerly shear with height requires a increasing temperature towards the equator, giving rise to descent. Conversely, increasing easterly shear with height gives rise to ascent. These vertical motions in turn also cause changes in some stratospheric species. The slowed stratospheric uplift during westerly anomalies leads to air parcels spending greater time below ~28 km in the region of greater ozone production and so increased ozone concentrations. Conversely, the increased uplift during easterly anomalies leads to decreased ozone concentrations.

Tropopause: Randel *et al.* (2000) found a QBO signal in the variation of lapse-rate tropopause characteristics that can be well correlated to changes in the 50 hPa zonal, equatorial wind. The temperature of the tropopause was found to be higher when the stratospheric uplift was slowed by the QBO westerly anomalies and lower when the stratospheric uplift was enhanced by easterly anomalies. Using data for the years 1979 to 1997 from the reanalyses of the National Centres for Environmental Prediction they found temperature and pressure variations of $\pm 0{\cdot}3$ K and ± 1 hPa respectively.

A Tropical Pipe

The tropical rising motion of the Brewer-Dobson Circulation is not the only consequence of Rossby-wave breaking in the extratropical stratosphere, since air is drawn poleward at all heights not just in the upper stratosphere. This is apparent from the seasonal cycle in CO_2 and H_2O signals observable in the extratropical stratosphere, whose periods match those of the cycles in the tropospheric sources of both species (Boering *et al.*, 1996; Strahan *et al.*, 1998). The extent to which air is drawn out of the tropics is a function of height.

In the low to mid- stratosphere there are barriers inhibiting air motion between the tropics and extratropics. The first observation of such a barrier was made by

Trepte and Hitchman (1992), who discovered that the isentropic motion of volcanic species into the winter extratropics considerably decreased above 21 km. Similar barriers were later found in the summer subtropics and at the equator (Chen *et al.*, 1994), the latter only being present during the northern winter however.

These barriers create a vertical channel, some 40 degrees of latitude wide, constraining the mid-stratospheric flow. They do not completely isolate the tropics from the extratropics however, leading to an analogy describing the region as a "leaky pipe" (Neu and Plumb, 1999). The walls of the pipe are defined much as is the extratropical tropopause — by strong gradients of potential vorticity. Permeation of the walls occurs in a similar fashion to the tropopause folds seen in the troposphere, though in the stratosphere it is Rossby waves that contort contours of potential vorticity by drawing out tongues of air (Randel *et al.*, 1993; Polvani *et al.*, 1995; Chen, 1996).

Above and below the tropical pipe the subtropical gradients of potential vorticity are overcome by other forces. In the higher stratosphere the barriers are overcome by breaking Rossby waves (Mote *et al.*, 1998). In the lower stratosphere Mote *et al.* (1998) suggest that tropospheric motions cause sufficient disturbance for two way exchange between tropics and extratropics to be possible. Within the pipe most air parcels follow the Brewer-Dobson circulation. Some however, may be drawn out of the pipe half way up it and then be subject to the extratropical downwelling. This brings with it the possibility that some air may complete several smaller circuits of the lower stratosphere before returning to the troposphere via the Brewer-Dobson circulation.

The tropical pipe covers the height range ~20–24 km, which bridges approximately 60 and 35 hPa and the 450 and 600 K isentropes (Mote *et al.*, 1998; Rosenlof, 1995; Haynes and Schuckburgh, 2000a). The strength of its barriers vary with the QBO, being stronger during its easterly phase (Trepte and Hitchman, 1992; Chen *et al.*, 1994). As a whole, the pipe is thought to shift into the summer hemisphere (Randel *et al.*, 1998; Haynes and Schuckburgh, 2000a). However, contemporary estimates disagree as to the magnitude of the shift. Randel *et al.* (1998) found little shift below 600 K, suggesting only the top of the pipe is found 10 to 15 degrees toward

the summer hemisphere. Haynes and Schuckburgh (2000a) however, suggest that the entire pipe shifts with season, by approximately 10 degrees at 450 K and 20 degrees at 550 K.

2.1.3 The Tropical Tropopause

The tropopause as defined by the World Meteorological Organisation is: "The lowest level at which the lapse rate decreases to 2 degrees Celsius per km or less, provided also the average lapse rate between this level and all higher levels within 2 km does not exceed 2 degrees Celsius per km" (WMO, 1957). This surface, the lapse-rate tropopause, is easy to measure but since it has little physical meaning its use in the investigation of STE is questionable.

The greatest difficulty in defining a useful tropical tropopause lies in overcoming the fact that it takes a finite time for air parcels to take on stratospheric characteristics and thus become part of the stratosphere. In practice, measurement of the exchange of air between the troposphere and stratosphere can only be performed by observing some transition or motion across some critical surface, either side of which the air-parcel characteristics have a clear difference in a respective property. But which transition or surface is the most appropriate?

Potential vorticity gradients are large between the two atmospheric layers, implying that a surface of constant potential vorticity might be used as the critical surface. However, within the deep tropics the contours of such surfaces become almost vertical.

Hoskins (1991) defined the regions overworld, middleworld and lowerworld such that parts of the troposphere and stratosphere could be separated by the types of motions necessary to enter them rather than by a material characteristic. Figure 2.8, which is a copy of figure 1 of Holton *et al.* (1995), illustrates the three separate "worlds" and their partitions.

The middleworld is defined to be those parts of the stratosphere and troposphere that can interact by isentropic means. The remaining stratosphere forms the over-

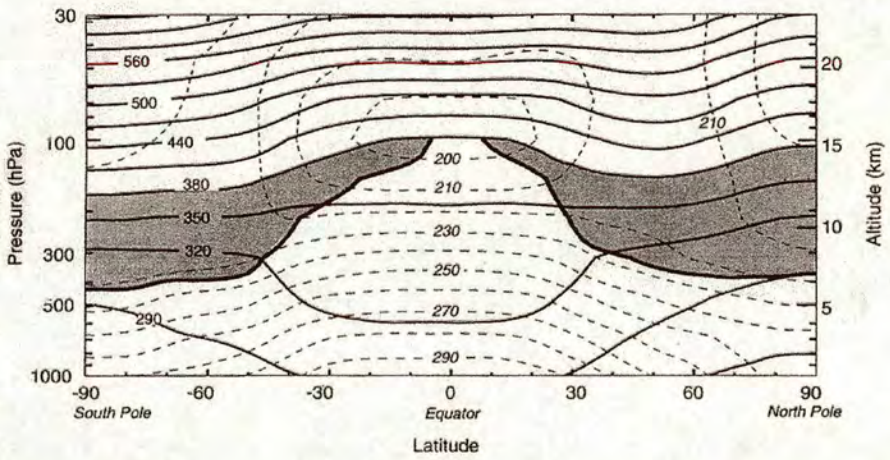

Figure 2.8: **Cross Tropopause Motions.** As figure 1 of Holton *et al.* (1995), page 405. The dashed contours show temperature (K) and the solid contours potential temperature (K). The heavy, solid line indicates the 2 PVU potential vorticity contour, marking the extratropical tropopause. This line cuts off at the 380 K isentrope, here used to approximate the tropical tropopause. The shaded area indicates the region of the stratosphere that may be entered from the troposphere by isentropic motion.

world and the remaining troposphere the lowerworld. In the diagram the stratospheric part of the middleworld is shaded. This region is also known as the lowermost stratosphere (Holton and Austin, 1991).

Two types of STE are now differentiated by this division — adiabatic and diabatic. Adiabatic exchange occurs purely in the middleworld, across the 2 PVU potential-vorticity contour, which serves as a good extratropical tropopause (Holton *et al.*, 1995). Diabatic exchange is the only method by which the overworld stratosphere can be reached from the troposphere. In this case Holton *et al.* (1995) use the 380 K isentrope to separate the overworld from the tropical middleworld.

Though this definition separates the tropical STE from the extratropical and provides a surface to measure the exchange across it is still inadequate for study of tropical STE for one reason. Plumb and Eluszkiewicz (1999) show that positive vertical velocities can be found at up to, and sometimes beyond, 20 degrees from the equator at 68 hPa. Though this does not prove that the uplift covers such a wide range at the height of the 380 K isentrope, the possibility cannot be ignored.

Therefore, since the limit of the diabatic partition lies at around ten degrees from the equator (see figure 2.8) the three-worlds partitioning is not suitable for study of tropical STE.

The most useful distinction between the stratosphere and troposphere for the study presented in this thesis is the sharp difference in water vapour concentrations. The critical surface for water vapour being that of the temperature minimum. This surface, the cold-point tropopause, can be used to split the troposphere and stratosphere across the whole tropics.

The Cold-Point Tropopause

Seidel *et al.* (2001) use radiosonde data from 83 tropical stations between the years 1961 and 1990 to determine the climatological characteristics of the cold-point tropopause (hereafter CPT) in comparison to the lapse-rate tropopause (hereafter LRT). They discovered that, at up to 25 degrees from the equator, the mean CPT height lies near to 96 hPa (16·9 km), always above the mean LRT height, the mean separation between the two surfaces varying from 4 hPa (∼0·4 km) in the deep tropics to 14 hPa (∼0·9 km) 25 degrees north and south. They also found that the two tropopauses exhibit similar height variations in time and longitude. Throughout the year the CPT height varies between 92 hPa (17·1 km) in the northern winter and 102 hPa (16·4 km) in the northern summer.

These intrayear variations, along with those of other tropopause characteristics are well summarised by figure 5 of Seidel *et al.* (2001), which is shown here as figure 2.9. This figure shows the variation of quantity equally as important to the study presented in later chapters as the tropopause temperature — q_s, the mean saturation mixing ratio of air entering the stratosphere. Figure 2.9 shows that the climatological average q_s varies between around 4 ppmv in the northern winter and around 7 ppmv in the northern summer.

The figure also compares the tropopause variations to those of the 100 hPa surface, suggesting that this pressure level cannot be used as a proxy for either the LRT or CPT.

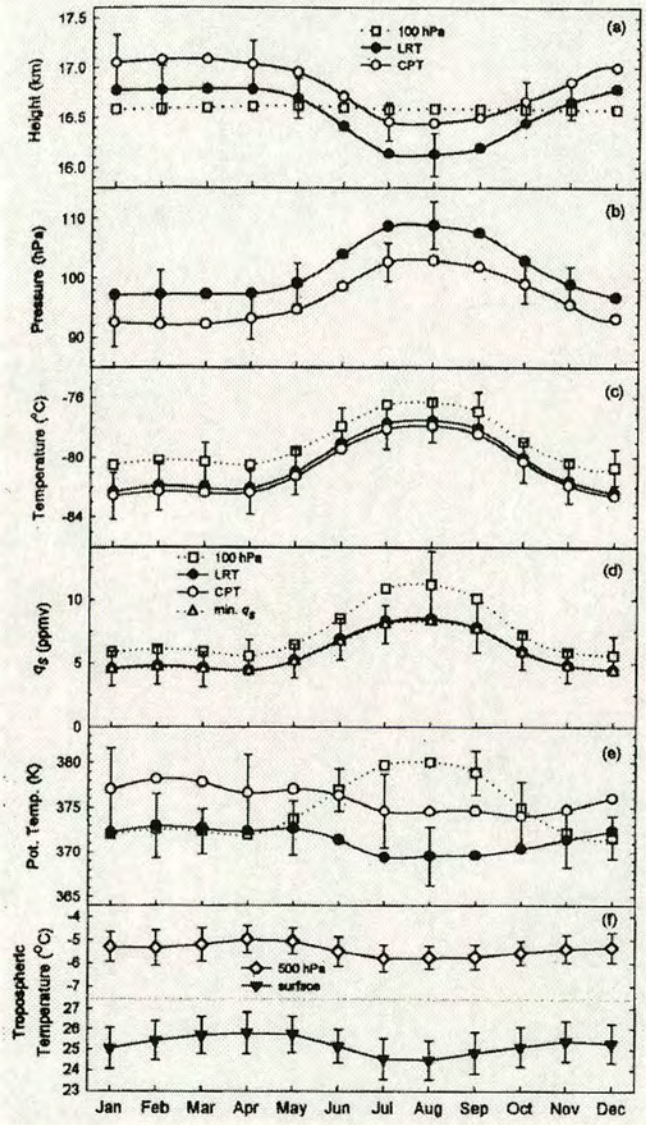

Figure 2.9: **Climatological Seasonal Cycles of Tropopause Characteristics.** As figure 5 of Seidel *et al.* (2001), page 7863. Seasonal cycles are of (a) height, (b) pressure, (c) temperature, (d)water vapour saturation volume mixing ratio, and (e) potential temperature in the equatorial zone (10°N–10°S) at the LRT, CPT and 100 hPa levels. Tropospheric temperatures at the surface and 500 hPa level in the same region are shown in panel f. Error bars indicate ±1 interannual standard deviations about the 1961–1990 monthly means. Except in panels d and f, error bars are shown every third month, alternating among the three levels, to avoid clutter. In panel d, error bars for the 100 hPa level fall within the square symbols.

The longitudinal variations of the tropopause can be appreciated by considering figure 2.10, which is a copy of figure 6 of Seidel *et al.* (2001), showing the climatological mean height of the LRT. Seidel *et al.* (2001) do not show the corresponding map for the CPT since the longitude variations for both tropopauses are similar.

From this figure it can be seen that the northern hemisphere tropopause is generally higher than its southern counterpart, particularly so during the northern winter. Between the months of December and March the climatological CPT has a maximum height over Central America at 17·6 km (Seidel *et al.*, 2001). During the remaining months of the year the maximum lies over Africa (Seidel *et al.*, 2001).

These height variations are not necessarily correlated with the variations in CPT temperatures. Seidel *et al.* (2001) found that in 91 percent of the months comprising their dataset the position of the minimum temperature of the CPT (the Pacific Warm Pool) was different to that of the maximum height (the western Atlantic). By obtaining correlations of tropopause characteristics with those of the troposphere and stratosphere, Seidel *et al.* (2001) show that the height and temperature of the CPT (and equally the LRT) are forced by different atmospheric motions. They showed that the tropopause height has a correlation of 0·5 or better with surface temperature, the height and temperature of the 500 hPa layer and the virtual temperature of the 850 to 100 hPa layer. The tropopause temperature, on the other hand, has higher correlations with the temperature and pressure at 18km than with tropospheric characteristics. From this Seidel *et al.* (2001) deduced that the height of the tropopause reflects the temperature of the underlying troposphere and will be a strong function of convection. The tropopause temperature however, shows a greater connection to the stratospheric forcing.

Evidence to support this latter connection can be found in the work of Yulaeva *et al.* (1994), which shows that the lower-stratospheric temperatures follow an annual cycle. Yulaeva *et al.* (1994) analysed data from the Microwave Sounding Unit instrument MSU-4 aboard the National Oceanic and Atmospheric Administration's operational weather satellites. Their figure 2 is replicated here in figure 2.11, showing the annual march of climatological-mean, lower-stratospheric temperatures for the tropics, extratropics and the globe.

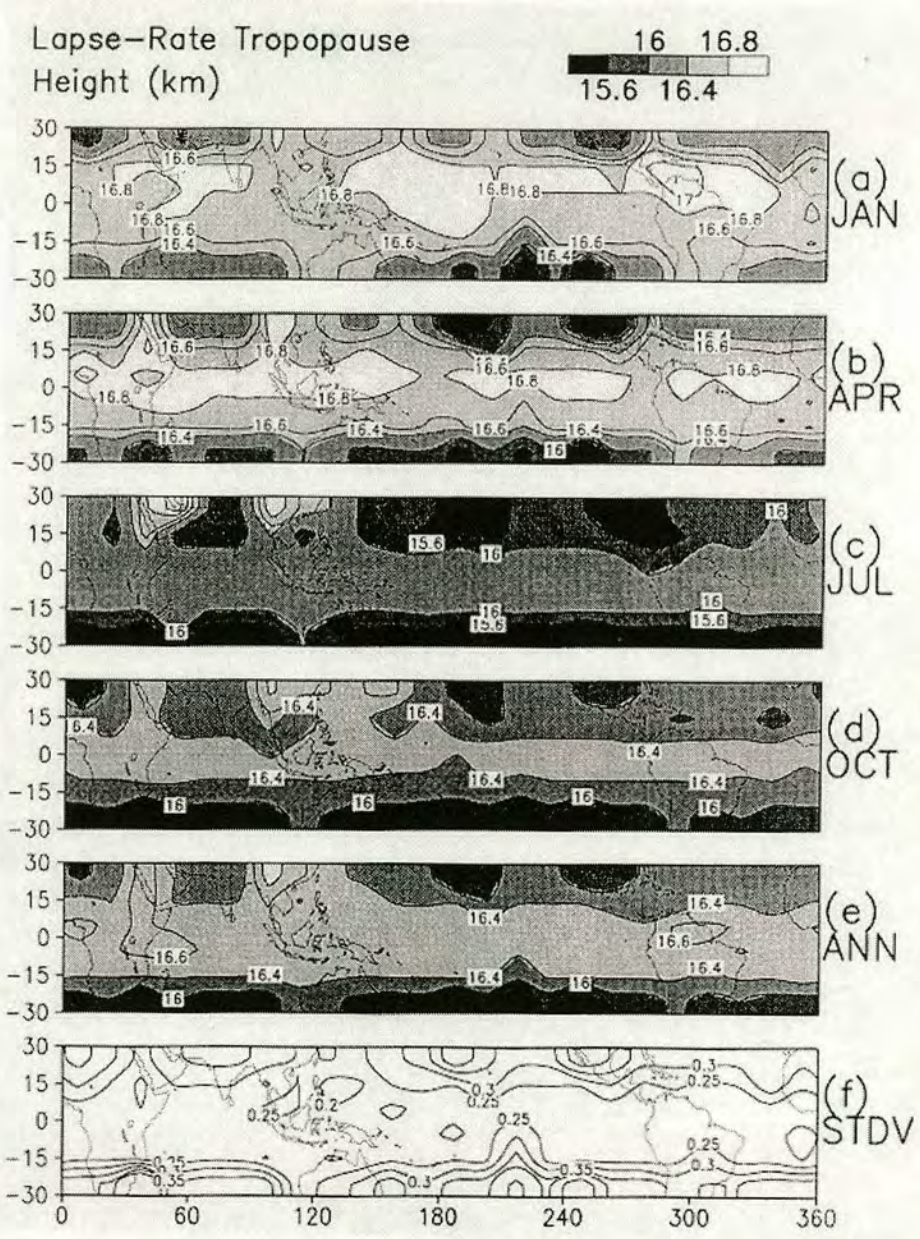

Figure 2.10: **Climatological Mean Height of the Lapse-Rate Tropopause.** As figure 6 of Seidel *et al.* (2001), page 7864. Shows the climatological mean height of the lapse-rate tropopause in kilometres based on 0000 and 1200 UTC radiosonde data for 1961–1990. Panels (a)–(d) are averages for four months of the year, panel (e) is an annual mean. Contours on panels (a)–(e) are every 0·4 km; additional contours are shown at 16·6 and 17·0 km. Panel (f) shows the inter-annual standard deviation of the individual annual means about the long-term annual means.

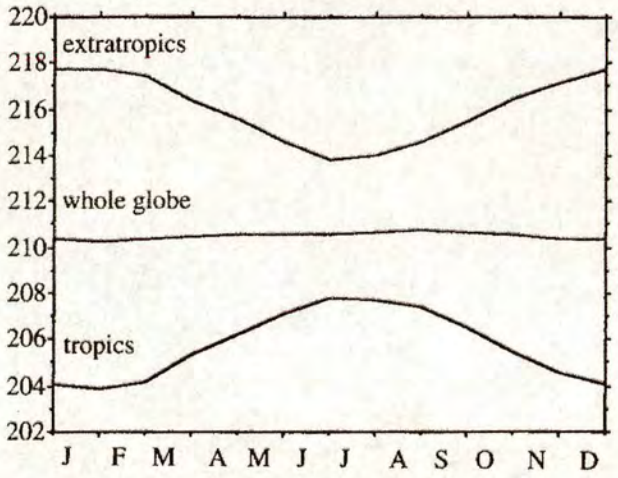

Figure 2.11: **Annual March of the Climatological-Mean, Temperature in the Lower Stratosphere.** As figure 2 of Yulaeva *et al.* (1994), page 171. Data is from 1979–1991 measurements of the Microwave Sounding Unit MSU-4, averaged over the tropics (30°N to 30°S), the extratropics (poleward of 30° north and south) and the entire world.

The increased uplift of a stronger Brewer-Dobson Circulation is evident from the lower temperatures of the tropical, lower stratosphere during the northern-hemisphere winter. Moreover, the seasonal variation in the temperatures follows that of the strength of the wave-driven, Lagrangian-mean, meridional circulation as indicated by table 2.1. Greater uplift in the tropics gives rise to lower temperatures there. Weaker uplift in the tropics gives rise to higher temperatures. Figure 2.11 also shows the corresponding inverse temperature cycle of the extratropical stratosphere, balancing the tropical change and leaving the global-average almost constant. (A very slight variation is visible in the global-average but this is consistent with the annual cycle in diabatic heating of ozone (Yulaeva *et al.*, 1994).)

Across the Tropical, Cold-Point Tropopause

A consequence of the transport of air across the tropical cold-point tropopause is that tropical, stratospheric air will exhibit a seasonal variation in water-vapour mixing-ratios. In the lower stratosphere this variation will be in phase with the variation in the height of the cold-point tropopause. Higher in the stratosphere the variation in

mixing ratio will be a function of the magnitude of the Brewer-Dobson circulation and of methane oxidation as well.

The flow of air crossing the tropical, cold-point tropopause has been likened unto magnetic tape passing a recording head, for just as a signal is recorded onto the tape so is a water vapour signal appreciable in air rising through the stratosphere (Mote *et al.*, 1995, 1996). Though there will be some degradation of this signal above and below the tropical pipe by exchange of air between the tropics and mid-latitudes, within the pipe the change in water-vapour mixing-ratio will be mostly due to methane oxidation alone. This source of water vapour has no strong seasonal variation in the tropics, increasing water-vapour concentrations throughout the year. As such, it does not obscure the water vapour signal. Mote *et al.* (1996) suggest that the water vapour signal has an e-folding time of 7–9 months in the lower stratosphere. Hence, air entering the stratosphere with water vapour mixing ratios of around 4 ppmv could be expected to see a change in this concentration of up to 1·5 ppmv within around 8 months, or approximately 0·06 ppmv in 10 days[†].

The water vapour signal is visible at up 10 hPa (Mote *et al.*, 1995, 1996), above which height it is destroyed by the motion excited by planetary-wave breaking. At any given time there will be two maxima and two minima in the water vapour signal between 100 and 10 hPa (Mote *et al.*, 1996), since the signals take approximately 6–8 months to reach 46 hPa, 15 months to reach 22 hPa and 18 months to 10 hPa. Variation occurs in the time taken to reach the lower height due to the difference in strength of the Brewer-Dobson between northern winter and northern summer. The speed of the uplift is approximately 0·4mms^{-1} during the former and 0·2mms^{-1} at other times of the year (Mote *et al.*, 1996). This difference also causes the signal minimum to spread out more in the vertical compared to the height range covered by the signal maximum. The time taken to reach heights up to 22 hPa can be further modified by up to two months under the action of the QBO (Mote *et al.*, 1996).

The vertical progress of the water-vapour signal up from the tropopause helps to make better sense of previous measurements taken by ER-2 aircraft in the lower

[†]This unit of time is relevant to chapter 4.

stratosphere as described by Kelly *et al.* (1993). These authors, during flights over Darwin, Australia, discovered a water vapour minimum of 3·5 ppmv near 19 km, far too low a value to be explained by the height of the cold-point tropopause at that time of year. Similar measurements around northern Australia and Central America confirmed the existence of this hygropause. Only with the proposal of the rising water vapour minimum from an earlier time of year was this tropics-wide hygropause explained.

A Tropical Tropopause Layer

Use of a critical surface allows determination of when air takes on a certain stratospheric characteristic. It provides an approximate time and an approximate place for the start of the exchange. However, the crossing process will most likely be more complex, given the number of different forces acting in upper troposphere and lower stratosphere.

This can be appreciated by considering the evolution of an air parcel in a convective overshoot. The parcel may rise up beyond the cold-point tropopause and so dehydrate. After this point the parcel may detrain into the stratosphere and then be taken up by the Brewer-Dobson Circulation. Equally, it might fall back down into the troposphere only to cross the tropopause a second time under the action of the stratospheric wave-driven motion elsewhere. In this latter case[†] the dehydration process and final crossing into the stratosphere would be two separate processes with different timescales. Furthermore, the relative contribution to parcel motion from both of these forces may change throughout the tropics.

Hence, in order to investigate the complete exchange, it is necessary to consider two processes — when and where air obtains stratospheric qualities and when and where it irreversibly passes into the stratosphere. These events may occur together but, if they do not, then the intervening air-motion becomes an important consideration. This motion will occur within some finite region that can be called a tropical tropopause layer. This layer will cover a tropical height-range that comprises the

[†]This possibility, proposed by Sherwood and Dessler (2000) is fully detailed later in section 2.3.

troposphere down to the lowest point the stratospheric forcing has influence and the stratosphere up to the highest level tropospheric motions have influence.

Table 2.2 is a list of possible limits suggested by previous authors. Based on the results of this table, a tropical tropopause layer that considers the overlap of all motions would lie between 215 and 50 hPa.

Author(s)	**Boundary height**
- *Upper Boundary*	
Dunkerton (1995)	50–30 hPa — exhibit significant meridional velocities associated with monsoon circulations
Rosenlof (1995)	60 hPa — where the average transformed-Eulerian-mean, tropical, vertical-velocity is a minimum; the mass flux across the tropical, 60 hPa surface being 6 times less than that crossing 100 hPa
Mote *et al.* (1998)	60 hPa — the bottom of the tropical pipe
Sherwood and Dessler (2000)	70 hPa — highest level convection can reach
Gettelman *et al.* (2001a)	80 hPa — the highest ENSO signal
- *Lower Boundary*	
Sherwood and Dessler (2000)	150 hPa — the level of zero net radiative heating
Reid and Gage (1996) Folkins *et al.* (1999) Thuburn and Craig (2000)	215 hPa — the level reached by the stratospheric wave-driven action

Table 2.2: **The Extent of the Tropical Tropopause Layer.** A list of possible height limits for the tropical tropopause layer based on extent of the influence of tropospheric and stratospheric motions as determined by previous authors.

Long-Term Trends

Mastenbrook and Oltmans (1983) and Oltmans and Hofmann (1995) show a net increase in lower-stratospheric water-vapour between the mid-1960s and the mid-1990s (net since there was a decrease in the 1970s). Michelsen *et al.* (2000) evaluate the increase at 0·041±0·007 ppmv per year (1·2±0·2 %) using Atmospheric Trace Molecule Spectroscopy experiment data from 1985–1994. This change however, cannot be attributed to long-term trends in the cold-point tropopause, which was observed to

rise and cool during the same time period (Randel *et al.*, 2000; Zhou *et al.*, 2001; Seidel *et al.*, 2001). Were the lower-stratospheric water-vapour only a function of the tropopause temperature then its concentrations would be expected to be decreasing. The degree of the change in tropopause characteristics is indicated in table 2.3.

Seidel *et al.* (2001) — *lapse-rate tropopause*	
Height	+20 m per decade
Pressure	-0·5 hPa per decade
Temperature	-0·5 K per decade
Potential Temperature	no significant change
Saturation Mixing Ratio	-0·3 ppmv per decade
Randel *et al.* (2000) — *lapse-rate tropopause*	
Temperature	-0·57 ±0·18 K per decade
- without the effects the El Chichón eruption	-0·28 ±0·17 K per decade
Zhou *et al.* (2001) — *cold-point tropopause*	
Temperature	-0·57 ±0·06 K per decade

Table 2.3: **Trends in the Tropopause Characteristics.** Seidel *et al.* (2001) use radiosonde data from 83 tropical stations between the years 1961 and 1990. Randel *et al.* (2000) use radiosonde data from 12 tropical stations between the years 1979 and 1997. Their trend without the influence of the El Chichón eruption were calculated by omitting data from the years 1982 and 1983. Zhou *et al.* (2001) use rawinsonde data from 70 tropical stations between the years 1973 and 1998.

The decadal temperature trend is quite significant when compared to other variations in tropopause temperature: inter-annual — 1–2 K; caused by the QBO — ±0·3 K; caused by the ENSO — -0·4 – +0·6 K per unit of the Southern Oscillation Index (Randel *et al.*, 2000). (The Southern Oscillation Index is calculated as the pressure anomaly at Tahiti minus the pressure anomaly at Darwin, Australia. Randel *et al.* (2000) show that the index falls approximately between ±4 for their data period — 1979 to 1997.)

A large part of the negative trend in the cold-point-tropopause temperature results from the eruption of El Chichón (Randel *et al.*, 2000). Care is therefore required when determining the long-term change in tropopause characteristics. Nevertheless, the observed change in lower-stratospheric water-vapour concentrations is in contrast to that which would occur by a change in tropopause temperature, even discounting

the effects of El Chichón. This therefore implies that the water-vapour trends result, instead, from an alteration in the dynamical connection between the stratosphere and troposphere.

Zhou *et al.* (2001) suggest that, of the three factors that can influence stratospheric water-vapour, only one could be responsible for its observed long-term trend. Increases in methane emission cannot explain the increase in water vapour (Nedoluha *et al.*, 1998) and, as mentioned above, neither can changes in the tropical tropopause. This leaves only a change in the wave-driven motion of the stratosphere. Using a two-dimensional model Zhou *et al.* (2001) found that a decrease in the residual circulation of the stratosphere would increase stratospheric water vapour. They also found that an increase in the latitudinal extent of the stratospheric uplift would do the same, since cold-point tropopause temperatures are larger in the subtropics than the tropics.

In searching for a change in tropical dynamics that might give rise to a decrease in the residual circulation of the stratosphere or an increase in the latitudinal extent of the stratospheric uplift, Zhou *et al.* (2001) observed rising sea-surface temperatures and decreasing outgoing longwave radiation over most the tropics. These observations imply a general increase in the mean strength of tropical convection over the period analysed — 1973 and 1998. Though Becker and Schmitz (1999) showed that the strength of the wave-driven forcing of the stratosphere is not a function of tropical convective activity, they did propose that the latitudinal extent of the stratospheric motion could be. Hence, the long-term trends in lower-stratospheric water-vapour may be indirectly affected by changes in convective activity.

2.2 The Stratospheric Fountain

Observations of lower-stratospheric, water-vapour mixing-ratios in various regions of the tropics in the 1970s revealed concentrations too low to be explained by air rising through the local tropopause (Mastenbrook, 1974; Kley *et al.*, 1979). At the measurement sites the cold-point tropopause was too warm to freeze-dry passing air

down to stratospheric concentrations. This led Kley *et al.* (1979) to the conclusion that stratospheric air must enter from the troposphere only over specific geographic regions with the coldest local-tropopause temperatures.

That the uplift across the tropopause is not a uniform motion throughout the tropics was supported by Robinson (1980). He, among other authors, commented that such uplift would lead to widespread, thick cirrus in the tropics, which is not observed. Robinson (1980) further suggested that cross-tropopause flow would therefore most likely result from deep tropical convection and that this had not been verified because experimentation had not been carried out in suitable places at the correct times.

As such, Newell and Gould-Stewart (1981) examined the temperatures of the entire tropical tropopause. They used radiosonde measurements of temperature to determine, for all seasons of the year, over which areas the tropopause was sufficiently cold to produce the observed low-concentrations of stratospheric water-vapour. They confirmed that suitable regions existed over the areas of strongest convection, changing with time of year, and named the areas "stratospheric fountains".

Figure 2.12 shows the January and July maps of figure 2 of Newell and Gould-Stewart (1981), indicating the percentage of radiosonde stations reporting monthly-mean temperatures of less than -82·4 °C at the 100 hPa level. Newell and Gould-Stewart (1981) were clear that this surface would not always best represent the minimum temperature level but did not have access to a more appropriate data set at that time.

The figure shows a January fountain over the western tropical-Pacific, Indonesia, Malaysia and northern Australia. Newell and Gould-Stewart (1981) also showed that similar areas of low temperature existed between November and March in their ten-year average data (maps not reproduced here). During the northern summer they found a "fountain" over the Bay of Bengal and India, covering the region of, and persisting for the time of, the Asian monsoon (Newell and Gould-Stewart, 1981). (See the July map in figure 2.12 as an example.) All the regions highlighted by their study are those that experience intense convection during the respective times of

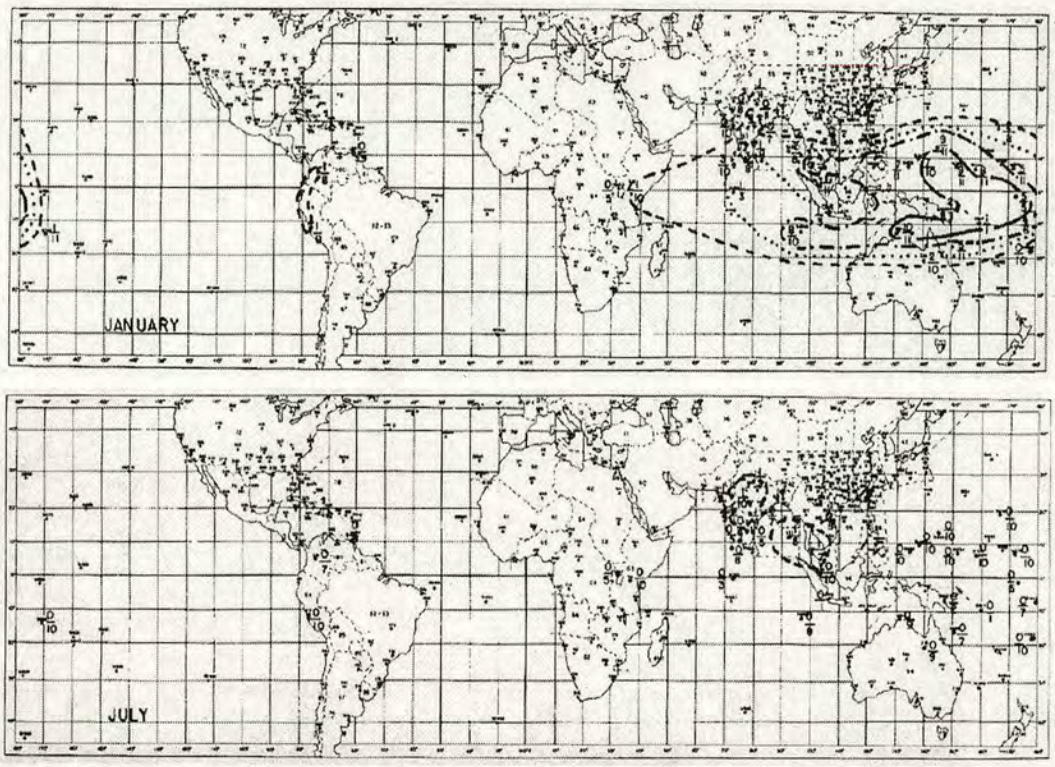

Figure 2.12: **Stratospheric Fountains.** Shows the January and July maps of figure 2 of Newell and Gould-Stewart (1981), pages 2791 and 2792 respectively. The maps indicate whereabouts radiosonde stations report monthly-mean temperatures of less than -82·4 °C at the 100 hPa level. Numbers near stations denote the fraction of months during 1970–1980 which had mean temperatures below -82·4 °C. Contours indicate 90% (solid), 50% (dot-dash), 30% (dotted) and 10% (dashed) occurrence.

year. Newell and Gould-Stewart (1981) suggested therefore, that strong convection, followed by isentropic motion, could ventilate the lower tropical stratosphere.

A mechanism for the dehydration of air through the fountain regions was suggested by Danielsen (1982), whereby the dehydration occurs by fallout of ice crystals that form in anvil cloud. He proposed that the anvil outflow of convective turrets penetrating the tropopause could settle in the stratosphere. This would occur if the mean potential temperature of the turret rises above that of the tropospheric environment by absorption of stratospheric air. Assuming little overlying and underlying cloud the anvil would radiatively cool at its top and heat by absorption of longwave radiation from below. Within this framework the anvil would not subside

but rather overturn, with a turbulent flux of heat and water vapour up within the cloud. Danielsen (1982) suggested that there would be sufficient time for crystal growth and fall-out before the anvil air completely entrained into the stratosphere.

Together these two ideas formed the first theory for the mechanism of tropical STE, a theory that has only relatively recently been challenged. Some modelling studies have suggest that uplift into the stratosphere occurs outside the fountain regions (for example Appenzeller *et al.* (1996); Gettelman *et al.* (2000); Gettelman and Sobel (2000)). Furthermore, observations of stratospheric water-vapour and carbon-dioxide suggest that air enters the stratosphere in amounts that make limited spatial regions of entry seem unlikely (Boering *et al.*, 1995; Mote *et al.*, 1996).

Dessler (1998) goes further still, suggesting that the time-averaged tropopause-temperature *is* cold enough to dry air to stratospheric concentrations throughout the tropics. By examining the temperature of the cold-point tropopause, as measured by tropical radiosondes for the years 1994 to 1997, he found that the saturation volume-mixing-ratio of the tropopause region was $4{\cdot}0 \pm 0{\cdot}8$ ppmv and that the volume mixing-ratio of air entering the stratosphere was $3{\cdot}8 \pm 0{\cdot}3$ ppmv. These values are not however, universally accepted (Vomel and Oltmans, 1999; Dessler, 1999).

Though Zhou *et al.* (2001) believe that the suggestion of Dessler (1998) is correct, they found that the saturation mixing-ratio and the entry mixing-ratios only agree for the 1990s. From this stand-point Zhou *et al.* (2001) discuss a compromise between the two possibilities. They suggest that the fountain theory may have been necessary during the timeframe of the data used by Newell and Gould-Stewart (1981) but not during the timeframe of those data used by Dessler (1998), since the long-term trends in the lower stratospheric water vapour show it to be rising[†].

2.3 Current Theories of Exchange

Holton and Gettelman (2001) sum up the current appreciation of tropical STE with the following paradox:

[†]See section 2.1.3 — Long-Term Trends.

" Freeze drying to the saturation mixing ratio characteristic of the exceptionally cold tropopause of the tropical Western Pacific is apparently required to account for the the observed very low stratospheric water vapour mixing ratios. Such freeze drying would appear to require slow upwelling in that region to produce cooling and condensation and to allow time for the ice crystals formed in the freezing process to sediment out. Observations, however, suggest that the mean vertical motion is downward at the tropopause over the Western Pacific, not upward. Thus the term "fountain" is not appropriate. Rather this region will be referred to as the "cold trap". "

Several theories have been presented to explain tropical STE since the "stratospheric fountain" of Newell and Gould-Stewart (1981) that attempt to get around this problem. Though distinct, all can be broadly categorised into two groups — those that maintain that the drying occurs coincident with the exchange and those that suggest the drying and exchange can be split into two entirely separate processes.

The former category encompasses two possibilities for STE:

- The original "stratospheric fountain" theory.
- That the exchange occurs through diffusion or turbulent motion at the crests of equatorially-trapped, Kelvin waves (Potter and Holton, 1995; Alexander *et al.*, 1995).

The latter category encompasses two theories of STE that advocate equally the importance of the strong horizontal winds near the tropopause and the coldest tropopause regions:

- That the drying occurs by overshooting convection, which passes air through the "cold trap" region. Air may detrain into the stratosphere but most will fall back down to lower levels. The subsequent uplift into the stratosphere then occurs under the stratospheric, wave-driven motion downstream of convection. (Sherwood, 2000; Sherwood and Dessler, 2000)

- That the dehydration occurs as strong horizontal winds advect most of the upper tropospheric air through the "cold trap" region. The drying occurs in the upper troposphere, in the relatively cold air produced by radiative effects of cirrus overlying convection. Air may then exchange into the stratosphere at any subsequent point in the flow. (Holton and Gettelman, 2001; Hartmann *et al.*, 2001)

The latter three proposals are discussed in the following text.

2.3.1 Kelvin-Wave Exchange

Cooling occurs in the crests of buoyancy waves near the tropopause (Alexander *et al.*, 1995). It is possible that the dehydrated air at these crests might be drawn into the stratosphere (Potter and Holton, 1995). However, it is not yet clear if wave crests pass slowly enough or if ice removal proceeds rapidly enough to know whether this method would remove enough moisture to be a significant part of STE.

2.3.2 Convective-Drying and Subsequent Exchange

In the separated drying and exchange mechanism proposed by Sherwood and Dessler (2000) the former process occurs on a much shorter timescale than the latter. They propose that the dehydration of air occurs by the method discussed by Danielsen (1982), through the action of convection in regions below the coldest tropopause areas. In this way convection could move air up to and possibly beyond the minimum temperature level, dehydrating the air. The final, irreversible cross-tropopause motion could then occur at any point in the tropics under the influence of the stratospheric, wave-driven motion. Figure 2.13 is a reproduction of figure 1 of Sherwood and Dessler (2000), showing their rapid drying and downstream-uplift mechanism compared to STE under the stratospheric, wave-driven motion alone.

Within panel A the dehydration is shown to occur only in one small area of the tropical tropopause layer. The most energetic convection will penetrate this area and detrain air directly into the stratosphere. Less energetic convection may still

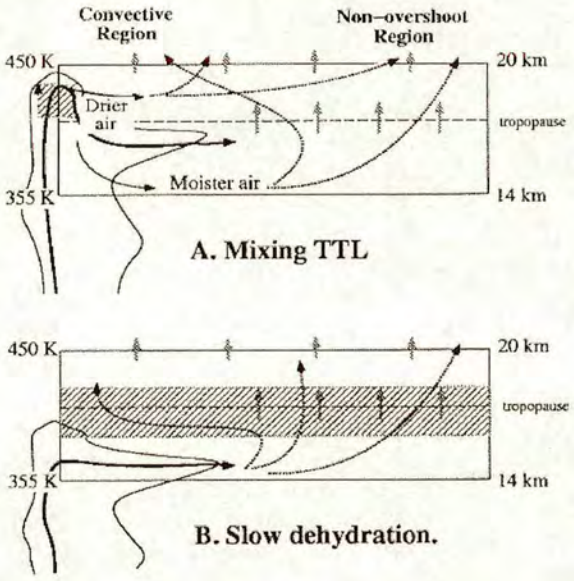

Figure 2.13: **The Mixing Tropical Tropopause Layer** As figure 1 of Sherwood and Dessler (2000), page 2514. Panel (A) illustrates the separation of drying and exchange and panel (B) the processes coincident. The hatched areas mark regions of final dehydration. The small, grey arrows show the ubiquitous ascent due to the wave-driven forcing. The dotted, black arrows show air parcel movements, which are significantly affected by horizontal motions. Convective turrets enclosed by thin black lines. Within the mechanism of panel (A) the large horizontal mixing occurs between dehydration and final crossing is visible.

pass through the dehydration region but may detrain lower. As such, the detraining air will have a range of water vapour concentrations — the higher the detrainment the lower the concentration. This distribution would be visible in the horizontal plane, as the air detraining higher would be pulled up into the stratosphere earlier, closer to the convective centre. Thus the relative amount of air with higher water vapour concentrations would increase away from the convective centre. Sherwood and Dessler (2000) expect the majority of detrainment to occur in the uppermost troposphere. As such, the majority of the cross-tropopause motion associated with this mechanism could occur after considerable horizontal movement away from the region of convection.

Increasing water vapour concentrations away from the centres of convection has been observed in the upper troposphere (Vomel *et al.*, 1995). Furthermore, the idea

that the uplift occurs away from convective regions is consistent with observations of strong downfluxes of air over the cold-trap region (Sherwood, 2000; Gettelman *et al.*, 2002). As with all theories reliant on convection however, it is not yet clear if this mechanism will significantly contribute to STE because of the lack of observed overshooting convection.

There is evidence that some convection does penetrate the stratosphere from the Stratosphere-Troposphere Exchange Project (STEP), which flew an ER-2 aircraft within and downstream of eleven tropical storms. One of the flights revealed cirrus anvils in the stratosphere (Danielsen, 1993). Four of the flights showed evidence of dehydration down to 2·5 ppmv (consistent with stratospheric values) in the convective turrets, the radon content of the turrets suggesting recent contact with the troposphere (Kritz *et al.*, 1993). Other flights indicated vertical mixing occurred to levels beyond 400 K, some hundreds of metres into the stratosphere (Kelly *et al.*, 1993). Nevertheless, Gettelman *et al.* (2002) found that convection penetrates the tropopause less than 2 % of the time, suggesting that it would be insufficient to explain the mass fluxes across the 100 hPa surface presented in table 2.1.

2.3.3 Advective-Drying and Subsequent Exchange

The companion works of Hartmann *et al.* (2001) and Holton and Gettelman (2001) also suggest that air enters the stratosphere in all areas of the tropics and that convection only plays a part in the dehydration of air. However, they propose a drying mechanism that does not require overshooting convection, suggesting that horizontal advection in the upper troposphere above convective activity is sufficient.

Rosenfield *et al.* (1998) found that free cirrus would heat its environment by absorption of upwelling longwave radiation. Thus free cirrus at the tropopause would serve only to raise the stratospheric water-vapour entry-value. However, Hartmann *et al.* (2001) show that if cirrus at the tropopause lies above convective outflow (see figure 2.14), thus shielding the cirrus from longwave radiation, then the cirrus cloud will instead radiatively cool. Should that cirrus cloud lie at the level of the tropopause then it will lower the tropopause temperature below the longitudinal

mean, as observed in the cold-trap region (Highwood and Hoskins, 1998).

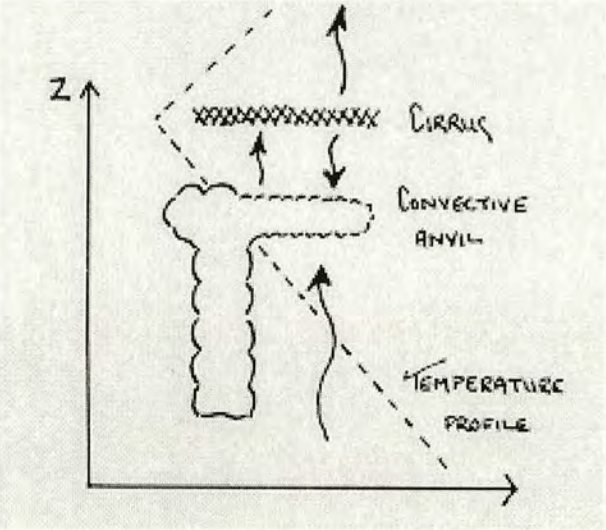

Figure 2.14: **Dehydration by Horizontal Motion.** Shows a convective event with a anvil outflow. The wavy lines lines indicate the emission of radiation. A temperature profile as a function of height (z) is also shown.

Although most convection detrains below 140 hPa (Highwood and Hoskins, 1998), a large amount of optically thin cloud does occur above this level. Kent *et al.* (1995) show that thin cirrus can be observed at the tropopause about 50 % of the time in the west Pacific, generally in regions where lower altitudes are more frequently cloudy. Also, Winker and Trepte (1998) show that 20 % of the tropics are covered by thin cirrus at any one time.

The origin of this upper tropospheric cloud is likely to be the remnants of previous uplift (Prabhakara *et al.*, 1993; Folkins *et al.*, 1999; Winker and Trepte, 1998), which have been advected away from their production region. Upon reaching areas of persistent convection, where potential temperature contours slope upward towards the convective centre, further isentropic advection will displace the moist air upwards, over and above the level of mean convective outflow. This vertical motion will then cause cirrus to form as the air rises and cools. Ice sedimentation downstream of the cooling then removes the moisture.

Hartmann *et al.* (2001) show that in order for the cirrus to obtain radiative equilibrium at a temperature less than that of mean tropopause (195 K), the temperature of

the underlying anvil must be less than about 232 K, which usually occurs at around 10·5 km. In the western Pacific the mean tropopause temperature are generally lower at around 188 K, which requires that anvils be present at 13 km to sufficiently cool the tropopause cirrus, a level just above that of the mean convective outflow. The anvils would not have to be quite so high if the cirrus cloud occurred with an optical depth slightly thicker than is currently predicted. This is not impossible however, as there are currently insufficient observations of the optical depth of cirrus cloud over the western Pacific to be sure of the true value.

To dehydrate sufficient amounts of air, this mechanism requires a large horizontal advection of moist air to maintain the cirrus cloud despite the loss of water vapour from sedimentation. However, the strong horizontal winds near the tropopause would be capable of this and, given the magnitude of the mean horizontal-winds to the mean vertical ($\sim$5 ms^{-1} compared to $\sim$0·5$\times$10^{-3} ms^{-1}), all upper tropospheric air could be cycled through the cold-trap area in a matter of a few days (Hartmann *et al.*, 2001). Thus all upper tropospheric air could be dehydrated to stratospheric values before uplift could draw air into the stratosphere.

This mechanism provides a method by which tropical STE could occur and that explains tropospheric observations. The cooling would be sufficient to offset the heating caused by the large-scale descent observed above the widespread convection of the cold-trap region (Holton and Gettelman, 2001). It also explains the frequently observed thin cirrus above the main convective outflow and the lack of thick cirrus everywhere despite an observed tropics-wide uplift (Gettelman *et al.*, 2000).

2.4 Cirrus Cloud

Observations of cirrus cloud may become the key to determining the mechanism of tropical STE. If the distribution and composition of cirrus cloud throughout the tropics could be determined, then differentiation between the proposed mechanisms of exchange might be achieved. Convective and gradual uplift cause different relative

concentrations of H_2O^{18} and HDO[†] to occur by the different amounts of condensation that result from their slightly different vapour pressures. Hence, distributions of uplift could be determined from distributions of cirrus cloud. To date, tropics-wide cirrus data are unavailable but existing cirrus data are still useful.

There are several recent works that suggest humidities in the upper troposphere are higher than was previously expected; higher to the extent that laminar optically-thin cirrus is very common near the tropical tropopause (Wang *et al.*, 1996). Jensen *et al.* (1999) show that humidities in the extreme upper troposphere are often near saturation with respect to ice, rather than being at the more generally accepted figure of 10–50 %. Wang *et al.* (1996) estimate that, up to 10 degrees from the equator, even at the 147 hPa level, the mean average humidity is around 66 %. Wang *et al.* (1996) also found cirrus in the descending branch of the Walker Cell, over the east Pacific and west Africa. This high frequency lends credence to the two theories presented in the last section that separate dehydration and uplift mechanisms, since both would tend to spread air close to saturation throughout the tropics.

Furthermore, both of these theories advocate the stratospheric, wave-driven uplift as important to the cross-tropopause motion throughout the tropics, which is also apparent from cirrus observations. Massie *et al.* (2000) report that the EL Niño of 1996 increased the upper tropospheric cirrus over the mid-Pacific and decreased it over Indonesia, as might be expected. However, even though the ENSO event moved the cirrus by around 25 degrees in longitude, Massie *et al.* (2000) observed no change in the number of cirrus events in the tropics between 50 and 240 degrees east between the years 1993–1998, implying another influence on its frequency.

Whereas lower, warmer cloud has a cycle that is dominated by the onset and waning of summertime monsoons and other convective events, the frequency of the highest and coldest clouds (those with temperatures less than 200 K) also show a pronounced annual cycle, one similar to that of the Brewer-Dobson Circulation (Zhang, 1993). High cirrus also exhibits no longitudinal preference, as occurs with lower cloud (Zhang, 1993). Thus, though the total cloud amount is controlled by

[†]HDO: where water is composed of one atom each of hydrogen, deuterium and oxygen.

solar heat input, the amount of cirrus that forms is linked more strongly to the stratospheric cycle, maximising with the coldest, highest tropopause (Zhang, 1993).

Confirmation of the gradual uplift throughout the tropics would be possible given further measurements of upper-tropospheric and lower-stratospheric cirrus. Nevertheless, observations to date suggest that stratospheric HDO is too abundant for all water vapour to have entered by convection (Moyer *et al.*, 1996).

2.5 Summary and Discussion

The motions of the upper troposphere and lower stratosphere are well summarised by figure 1 of Haynes and Schuckburgh (2000a), which is reproduced here as figure 2.15.

Convection in the tropics raises air up into the upper troposphere, whereupon cross-tropopause motion subsequently occurs by a mechanism or mechanisms yet to be fully determined. From there, air continues up in the Brewer-Dobson circulation, passing through the tropical pipe. If it is not drawn out to the extratropics by the breaking of Rossby waves before reaching the upper stratosphere it will then be drawn out at this height, moving into the winter-hemisphere westerlies. From the top of the pipe air is drawn polewards and eventually downwards through the polar vortex into the lowermost stratosphere. Air will then be released back into the troposphere through tropopause folds, the greatest frequency of which occurs in the northern winter and spring. Assuming air does not get trapped into additional circuits in the lower stratosphere[†], this process will take between 2 and 3 years (Rosenlof, 1995).

The motion across the tropical tropopause is possibly the least understood leg of the whole journey. Air might be dehydrated down to the low stratospheric values in passing some part of the cold-point tropopause before moving on into the stratosphere. However, it is not yet clear if this dehydration occurs across the whole tropics or just in some specific location, through which therefore, all rising tropical

[†]See section 2.1.2 — A Tropical Pipe.

Figures

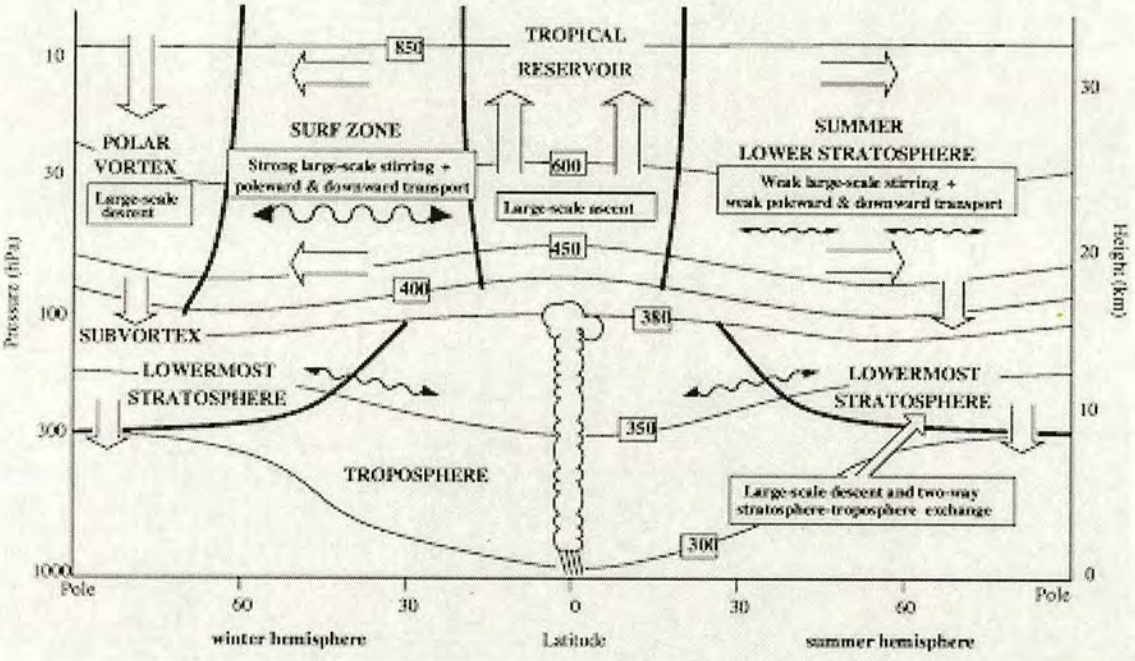

Figure 2.15: **Motions in the Upper Troposphere and Lower Stratosphere.** As figure 1 of Haynes and Schuckburgh (2000a), page 22778. Thin, labelled lines are isentropes; thick, black lines denote barriers to isentropic motion. The large arrows show transport due to the zonally-averaged, diabatic circulation, the vertical of which can be ascribed to the Brewer-Dobson circulation. Wavy lines indicate eddy transport along isentropic surfaces. Convection is shown in the tropical troposphere.

air would have to pass.

The first theory of tropical STE, the "stratospheric fountain" theory of Newell and Gould-Stewart (1981), suggested that the dehydration and cross-tropopause motion were both controlled by the strongest of tropical convective-activity. The strongest activity is found over Indonesia in the northern winter and over India in the northern summer, This mechanism however, requires that convection frequently penetrates the tropopause, to a degree that could explain the mass flux observed to cross the 100 hPa surface.

Recent work suggests that although convection is required to bring about the lower-than-mean tropopause temperatures of the "cold-trap" region, it need not necessarily

be important in controlling the cross-tropopause motion. Moreover, observations of tropics wide uplift at and below the tropopause (see Gettelman *et al.* (2000) and Plumb and Eluszkiewicz (1999) respectively) suggest that the stratospheric, wave-driven motion is dominant in moving air into the stratosphere. This is supported by observations of upper tropospheric cirrus cloud, the frequency of which shows an annual cycle as well as a dependence upon convection. Hence, it seems likely that the dehydration and cross-tropopause mechanisms are two separate processes.

It is also possible however, that the mechanism of the cross-tropopause motion has changed over time. Rising lower-stratospheric water-vapour concentrations may mean that the "cold-trap" region is no longer as necessary a part of the dehydration process as it might have been two decades ago (Zhou *et al.*, 2001).

2.5.1 Experimental Aims

From consideration of the issues raised in this chapter, three hypotheses concerning the detailed tropical-STE are proposed below. These hypotheses were investigated by examining the evolution of water vapour in the tropical tropopause layer and by direct examination of airflows. The results of this investigation are presented in the following chapters.

1. **Fountain Hypothesis.** Cross-tropopause motion only occurs over the area of strongest convection, the remaining tropical stratosphere being ventilated by adiabatic redistribution of the air from the convective source-region.

2. **Uniform-Entry Hypothesis.** No preferential region of cross-tropopause motions exists; air enters the stratosphere in an even distribution in both space and time throughout the tropics.

3. **Flow-Change Hypothesis.** A significant change occurs in the mechanism of cross-tropopause motion between the early 1980s and the early 1990s.

The first hypothesis is tested using water vapour data to see if the evolution of this species in the lower stratosphere is consistent with a "stratospheric fountain".

The second hypothesis concerns the tropics-wide, cross-tropopause motion. This hypothesis will be disproved if there exists a longitudinal or latitudinal preference in the cross tropopause motion, as might occur if the dominant forcing of this crossing were convection or if there were a horizontal variation in the stratospheric uplift.

The third hypothesis is investigated to determine whether or not a change in the cross-tropopause mass-flux occurred between the times when it was thought that passage through the cold-trap was and was not required to dehydrate air down to stratospheric values.

Chapter 3

Data and Methods — Trajectories and Advections

The investigation discussed in chapter 1, which will test the hypotheses put forth in chapter 2, requires the use of wind and water-vapour datasets that cover the entire tropics and a method of moving air-particles under the wind data. This allows a trajectory and advection study to search for tropical, stratosphere-troposphere exchange (hereafter STE) across the entire region in which it might occur. Tropics-wide coverage, throughout the upper troposphere and the lower stratosphere, is achieved for wind data by assimilated-data sets and for water-vapour data by some satellite-borne instruments.

Assimilated-data sets provide four-dimensional wind data on regular grids. In producing assimilated-data sets, atmospheric models combine radiosonde and satellite data under theoretical constraints that keep model parameters within realistic ranges. This allows a single dataset to provide atmospheric information on a global scale. Some models are also used to provide data at a greater time resolution than observations are taken, evolving data on from measured states.

Trajectories can be created from this data by moving a point particle[†] of air at the speed of, and in the direction of, wind data interpolated to its location. The

[†]The use of the term particle here, rather than parcel, is intentional, as all trajectories presented in this thesis are used to study the motions of point sources of air and not the development of malleable packets.

trajectory is created by moving the air particle for many small timesteps (much shorter than the temporal resolution of the wind dataset) at the end of each, winds are interpolated to the new particle co-ordinates. In this way the particle's trajectory can, technically, be mapped out for as long as desired.

The greatest practical limit on the length of the trajectory comes from the errors in its calculation. These calculations are prone to errors that grow with the length of the trajectory, since once a particle is moved under an incorrect wind it can only continue to stray into different wind regimes. Further complicating matters is the inherently random nature of these errors. Ideally it would be possible to ascribe a probability distribution for the end-point of each trajectory. It is however, too computationally expensive to perform this calculation for the large number of trajectories proposed in this study. Nevertheless, useful, empirical constraints on the accuracy of trajectories have been established by previous authors (see Stohl (1998), table 2). As such, if these constraints are applied, along with a reliability test from the advection of water-vapour data, trajectory calculations can still provide much useful information about tropical STE.

The water vapour data used for the reliability-testing in this thesis comes from the Microwave Limb Sounder (hereafter MLS) instrument flown aboard the Upper Atmosphere Research Satellite (hereafter UARS). The MLS instrument is an excellent choice for the advection study since it provided a continuous observation of the tropical region between 34 °N and 34 °S, from which daily maps of water-vapour concentration can be created. This high-frequency of updates allows the investigation to be performed on a daily basis or to be performed with good temporal-averaging such that daily fluctuations can be ignored in the study of long-term motions.

In the following chapter the technical details of trajectory calculations and advections are discussed. Section 3.1 discusses trajectories and their associated errors. Section 3.2 compares observed-wind data to the winds of assimilated-data sets. This comparison determines the degree to which the model physics for such datasets causes departure from observed values in the data-sparse, and so heavily model-dependent, tropics. This section then explains the use of data from the United Kingdom Meteorological Office (UKMO) in creating isentropic advections

and from the European Centre for Medium-Range Forecasts (ECMWF) in creating three-dimensional trajectories. Section 3.3 details the creation of isentropic advections using water vapour data from the MLS instrument. Section 3.4 details the creation of three-dimensional trajectories. Finally, a summary of the use of both types of calculation in the investigation of the hypotheses presented in chapter 2 is given in section 3.5.

3.1 Trajectories and Errors

Trajectory calculations suffer from three sources of error: truncation errors in the advection routine, spatial- and temporal- interpolation errors from data points to air-particle positions and data errors. The first are virtually eliminated in modern computing, since the processing power required to deal with the higher-order terms of advection equations is readily accessible. The latter two sources can, however, still be cause for concern.

3.1.1 Interpolation Errors

Interpolation errors will always occur with assimilated data since air-particle positions will never lie at exactly the positions and times of the gridded wind-data. However, these errors can be minimised by using the highest possible resolutions of data in both space and time and by using the most suitable interpolation methods.

Waugh and Plumb (1994) investigated the effect on the accuracy of trajectory calculations that results from degrading the spatial and temporal resolutions of the wind data used. Figure 3.1 is figure 3 of Waugh and Plumb (1994) and shows four contours distorted by their contour advection with surgery technique. This technique advects species contours under the motion of isentropic trajectories.

The four contours were initially-concentric circles, centred at the cross-hairs origin of each plot, whose scope covers one hemisphere of the globe. By initialising trajectories around each contour, they were advected forwards in time for twelve

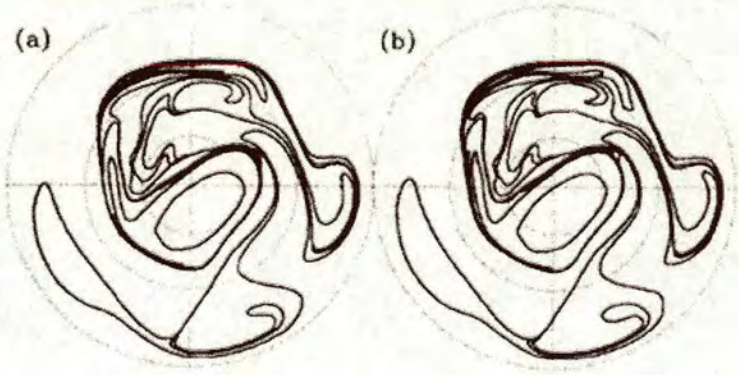

Figure 3.1: **Trajectory Accuracy and Wind Data Resolution: Spatial.** As figure 3 of Waugh and Plumb (1994), page 533. Shows four contours, initially concentric circles, after a 12-day isentropic advection using a contour advection with surgery technique and a constant temporal resolution. The spatial resolution of the wind dataset used was — 5° latitude by 10° longitude (a), 1° latitude by 3° longitude (b).

days, giving the shapes visible in figure 3.1. In figure 3.1a the wind data used had a spatial resolution of 5° latitude by 10° longitude and in figure 3.1b 1° latitude by 3° longitude. Both advections were performed with wind data at a temporal resolution of 12 hours. The comparison reveals that degrading the spatial resolution of the data has little effect at this temporal resolution. This concurs with the findings of Rolph and Draxler (1990), who suggest that for temporal resolutions of 6 hours or greater, differences caused by degradation of the spatial resolution of the wind dataset are minimal.

Figure 3.2 is figure 4 of Waugh and Plumb (1994), investigating the effects of degrading the temporal resolution of the wind dataset at a constant spatial resolution of 2° latitude by 5° longitude. Again, four initially-concentric circles have been advected for twelve days, once with wind data at each of the temporal resolutions 6, 18 and 24 hours. In this case, there is a noticeable difference in the contours after advection — more spurious, small-scale features appear as the temporal resolution decreases. Nevertheless, the larger-scale information is the same throughout figures 3.2 a–c.

The findings of Waugh and Plumb (1994) agree with the suggestion of both Knud-

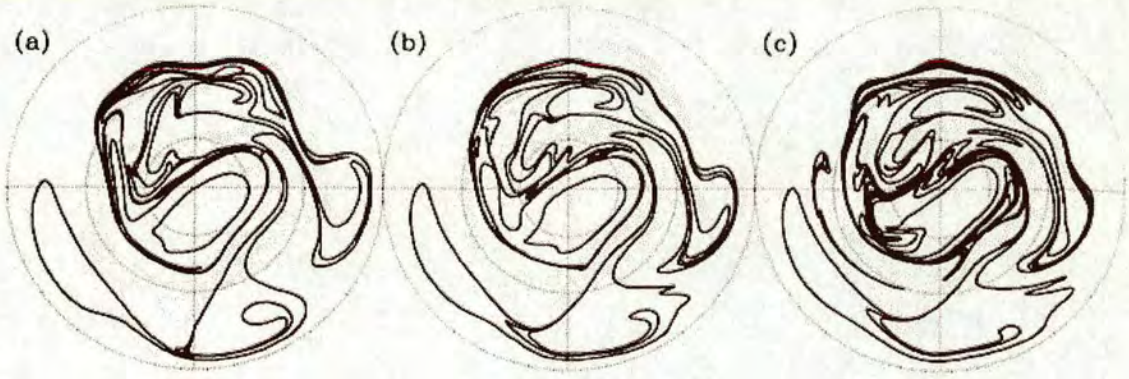

Figure 3.2: **Trajectory Accuracy and Wind Data Resolution: Temporal.** As figure 4 of Waugh and Plumb (1994), page 534. Shows four contours, initially concentric circles, after a 12-day isentropic advection using a contour advection with surgery technique and a constant spatial resolution. The temporal resolution of the wind dataset used was — 6 hours (a), 18 hours (b) and 24 hours (c).

sen and Carver (1994) and Stohl (1998) that improvements in the temporal resolution of the data have greater effect than improvements in the horizontal spatial-resolution. Knudsen and Carver (1994) and Stohl (1998) also note that the vertical-spatial resolution is more important than the horizontal-spatial and temporal resolutions when calculating three-dimensional trajectories.

Minimising the error by interpolation between the data spaces and times can be done by using a linear method in time (Stohl *et al.*, 1995) and in the horizontal (Walmsley and Mailhot, 1983). In the vertical, higher order terms are required to capture the higher frequency variability of the wind fields. Methven (1997) found that a cubic Lagrange method gives the most accurate results.

3.1.2 Data Errors

Data errors are caused by assimilation of inaccurate data or misjudgement of air-particle starting positions, for example when trying to initialise a particle within a smoke plume. The latter is a lesser problem for the study of STE, since contours of species data enclosing much larger areas can generally be used. The former source of data error often comes about due to sparse data coverage, a problem that can only be

dealt with by interpolation or empirical estimation. In the troposphere this can be a distinct problem in areas where the horizontal scale of the flow is much less than that of the radiosonde network, occurring, for example, within mountain ranges. In the stratosphere such tropospheric effects are greatly diminished but paucity of data is still a problem over remote land areas and the oceans. In these situations assimilated data sets rely on satellite measurements. However, such instruments then introduce a problem of poor vertical resolution in comparison to radiosonde measurements.

3.1.3 Overall Errors

Stohl (1998) suggests that three-dimensional trajectories are now the most accurate calculations. Isentropic trajectories are more readily calculated but cannot provide information concerning diabatic motions. These motions are included in three-dimensional calculations but their accuracy is dependent on that of vertical-wind data. Though contemporary vertical-wind data is far from perfect, it is sufficiently accurate to make three-dimensional calculations more valuable, in general, than isentropic ones. Isentropic calculations find use only in hypothetical situations and in regions where effects of diabatic heating and of synoptic and geographic disturbances are small or unexpected.

In the case of the *fountain hypothesis* all regions away from the "fountains" are assumed to be free of convection and so diabatic motions minimal. The hypothesis therefore implies that all these regions must be connected to the "fountains" by isentropic motions on timescales less than those typical of tropical diabatic motions, *i.e.* less than approximately twenty days (Holton *et al.*, 1995). As such, the comparison between artificially-created, purely-isentropically-advected evolutions to observed evolutions is valid and useful in the tropics if performed over periods somewhat shorter than twenty days.

Position errors of 20 % the total travel length[†] are "typical for trajectories com-

[†]Total travel length refers to that of the curved path of the trajectory not just the straight line distance between start and end points.

puted from analysed wind fields" (Stohl, 1998). This number was determined by considering all previous studies comparing trajectories calculated from analyses wind data to, for example, balloon flights, smoke plumes and other analyses data. One of these studies, Knudsen *et al.* (1996), compared calculated trajectories from ECMWF data to balloon flight paths in the stratosphere, also finding position errors to be typically around 20 %.

3.2 Wind Data

Assimilated-data sets that could be used to create air-particle trajectories are produced by several organisations:

- the European Centre for Medium-Range Weather Forecasts (ECMWF)
- the Goddard Space Flight Center (GSFC)
- the National Centers for Environmental Prediction (NCEP)
- the National Meteorological Center (NMC) of the United States
- the United Kingdom Meteorological Office (UKMO)

In selecting a data set to use for trajectory calculations a crucial consideration is the effectiveness of the model and so the extent to which output data may be disturbed away from the "real" radiosonde observations. Many previous authors have found the analysed winds of the ECMWF to be more accurate than several of the other assimilated-data sets. Trenberth and Olson (1988a,b) found that ECMWF data are more consistent with other instruments than are NMC data. Pickering *et al.* (1996) suggest that ECMWF trajectories might be slightly more accurate in the data-sparse south Atlantic than NMC trajectories. Pawson and Fiorino (1998) found that ECMWF temperatures at 100 hPa were considerably closer to observations than NCEP data.

The UKMO model has also been shown to have good qualities. Swinbank and O'Neill (1994b) show that the UKMO analysed winds agree well with available

radiosonde data in the tropical lower-stratosphere. Coy and Swinbank (1997) show that reasonable agreement extends to the winds of the GSFC model as well. At levels near 100 and 68 hPa the two models produce zonal winds that are generally within 2 ms^{-1} of each other, although a comparison of both horizontal wind-components at 68 hPa did show the GSFC winds to be greater than those of the UKMO by 3–5 ms^{-1}. Furthermore, the UKMO analyses would seem to be inherently suitable for use in conjunction with the MLS water-vapour data, since they were produced using a method of data assimilation to complement the Upper Atmosphere Research Satellite project (Swinbank and O'Neill, 1994a).

In order to determine which set of analysed winds might be most suitable for the isentropic advection of water vapour both the ECMWF and UKMO winds were compared to radiosonde data from the Changi Airport station in Singapore. In this way the analyses that best recreated the winds in the data sparse tropics could be appreciated. Figure 3.3 shows three time series of zonal and meridional winds — those of the ECMWF ERA-15 and the UKMO analyses and those of the Changi Airport radiosonde, the analyses data having been interpolated onto the radiosonde's location. The time series runs from 2^{nd} February and 29^{th} April 1997. A comparison for an earlier time would have been more appropriate but data for before December 1996 was not readily available from the British Atmospheric Data Centre when this comparison was undertaken. However, it is not thought that the error statistics will change significantly between the data used for the comparison and that used for the trajectory studies (see chapters 4 and 5).

Both analyses reproduce the variability of the radiosonde data well. However, the UKMO data better capture the height and timescale of the radiosonde features whilst the ERA-15 data follow the smaller-scale variation to a greater extent, specifically the meridional detail. Below the tropopause both analyses perform well. Above this surface the remnant of the QBO easterlies at 50 hPa are better represented in the UKMO dataset, whereas the magnitude of the QBO westerlies above 30 hPa are better represented in the ECMWF dataset. Overall, the UKMO data are closer to the radiosonde data in the case of zonal winds and the ECMWF data are closer to the meridional observations.

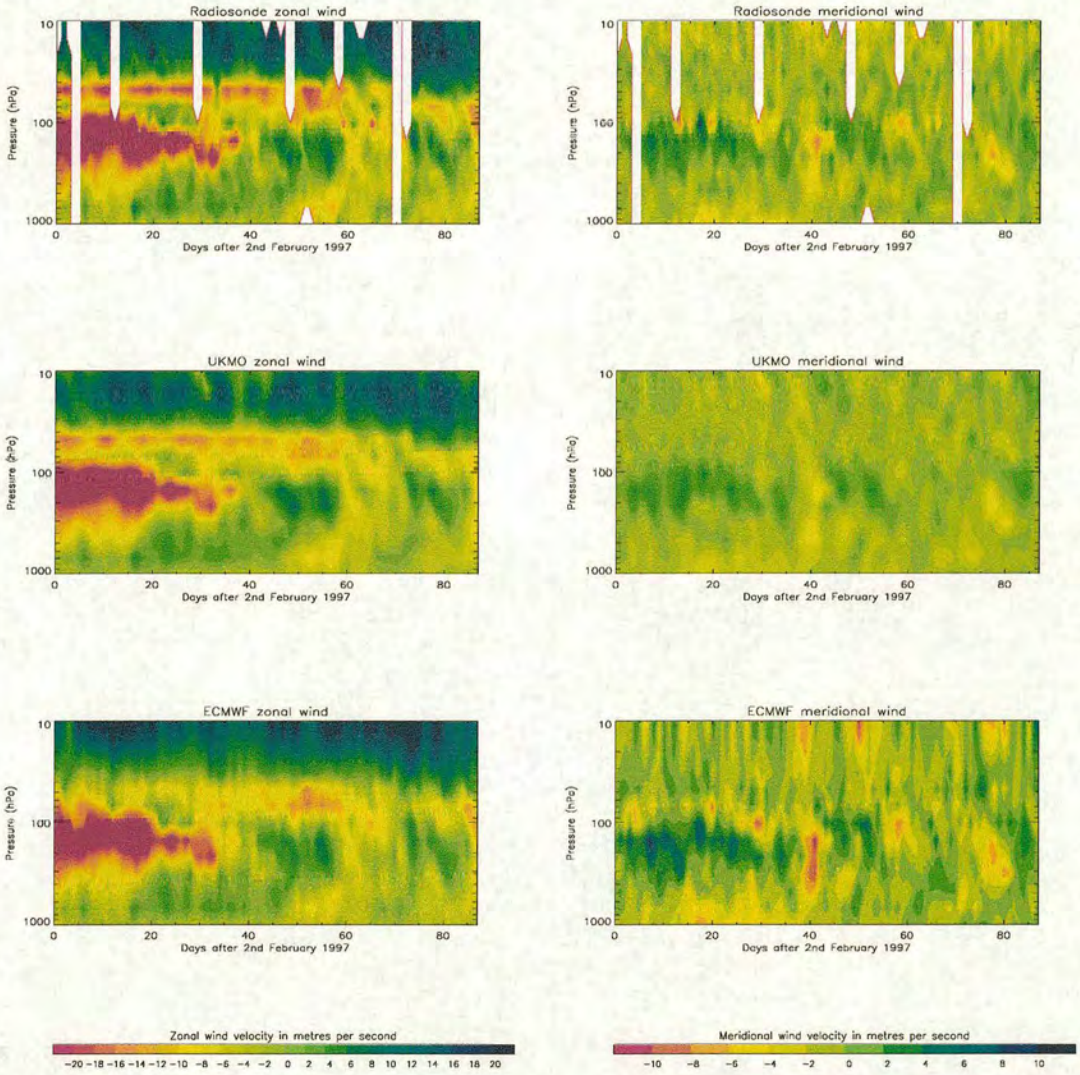

Figure 3.3: **Comparison of the Winds from Radiosonde and Analyses.** Shows timeseries of the zonal (westerly) and meridional (southerly) winds at 103·98 °E, 1·36 °N from the Changi Airport radiosonde in Singapore and the assimilated data of the United Kingdom Meteorological Office and the European Centre for Medium-Range Weather Forecasts. Assimilated data have been linearly interpolated to the radiosonde position. All panels cover the days between 2^{nd} February and 29^{th} April 1997. Whitespace on the radiosonde data plots indicate periods of no data.

This can be better appreciated through table 3.1, which presents average differences and correlations between the radiosonde and analyses winds for the 900 days between 1^{st} September 1997 and 30^{th} June 1999. The table shows data calculated for all heights and for 68 hPa alone, a surface near the top of the tropical tropopause layer. Both the radiosonde and the UKMO have data levels at this height. ECMWF data were linearly interpolated in $\log_n$[pressure] between 70 and 50 hPa analyses levels.

Zonal winds

	All heights			Single level: 68 hPa		
Analyses	mean dif.	r.m.s. dif.	correl.	mean dif.	r.m.s. dif.	correl.
UKMO	0·26	4·51	0·95	1·50	4·36	0·90
ECMWF	0·40	6·06	0·90	1·11	5·18	0·83

Meridional winds

	All heights			Single level: 68 hPa		
Analyses	mean dif.	r.m.s. dif.	correl.	mean dif.	r.m.s. dif.	correl.
UKMO	0·20	3·45	0·64	0·18	3·44	0·40
ECMWF	-0·06	2·97	0·75	0·13	2·98	0·60

Table 3.1: **Average Differences between Winds from Radiosonde and Analyses.** Shows the mean difference (mean dif.), root mean square difference (r.m.s. dif.) and the correlation (correl.) between winds from the Changi Airport radiosonde in Singapore and the assimilated data of the United Kingdom Meteorological Office (UKMO) and the European Centre for Medium-Range Weather Forecasts (ECMWF). Differences are in ms^{-1}. Assimilated data have been linearly interpolated onto the radiosonde position. Radiosonde and ECMWF data have been linearly interpolated onto the UKMO pressure levels between 1000 and 10 hPa. The differences and correlations are taken over the 900 days between 1^{st} September 1997 and 30^{th} June 1999.

Based on this result, the UKMO winds were selected for creating the isentropic advections of water vapour because they are closer to the radiosonde data in the zonal direction. Since trajectory errors are a function of their length, and in longitude air particles travel a distance that is generally three times that travelled in latitude, a lessening of the zonal error was considered more desirable. Though the UKMO model only updates its wind fields every 24 hours, compared to the 6-hourly updates of the ECMWF model, it was thought that this disadvantage was outweighed by the advantages of the UKMO data — the closeness of the UKMO and radiosonde winds

and the compatibility of the UKMO and MLS datasets. The loss of the small-scale information through lesser temporal resolution was considered acceptable[†].

In the case of the three-dimensional trajectories all considerations were outweighed by the importance of using the greatest temporal resolution possible, in order to cope with the vertical-wind variability. Thus the ECMWF data were required. This was not a problem however, since they are easily close enough to the radiosonde data not to cause concern over the model physics. The ECMWF dataset has a further advantage in terms of investigating the *flow-change hypothesis*: Whereas the UKMO data set begins with the activation of MLS on the 11^{th} September 1991, the ERA-15 data is available for December 1979 onwards, allowing study over a longer timeframe.

3.3 Isentropic Advection

The isentropic advections of water vapour data presented in chapter 4 were created using the UKMO wind data, MLS water-vapour data and an advection routine provided by Black (1997). The advection routine was originally developed for a contour advection process by Sutton *et al.* (1994) and Sutton (1994) that could be used to increase the resolution of existing species-concentration maps. The routine uses a fourth-order Runge-Kutta iteration to update air-particle positions based on assimilated wind data. This iteration was selected since the computational errors caused by it are negligible (Schoeberl and Sparling, 1995).

3.3.1 Water Vapour Data

The UARS flies at 585 km in a near circular orbit inclined at 57 degrees to the equator, completing almost 15 orbits of the Earth per day. All the solar panelling can be found one side of the satellite and the instrumentation on the other (Reber, 1993). In order to keep the solar panels illuminated and the instrumentation cool the satellite performs a "yaw manoeuvre" (an 180-degree turn within a plane parallel to the surface of the Earth) every 36 days. A consequence of this essential manoeuvre

[†]See section 3.3.4.

is a change in the coverage of some of the instruments' measurements.

The Microwave Limb Sounder scans at 90 degrees to the velocity vector of the satellite, scanning downwards at a tangent point of the atmosphere approximately 23 degrees great circle distance from the sub-orbital track of UARS. As such, it observes between 80 degrees of one hemisphere and 34 degrees of the other, each hemisphere receiving greater coverage during alternate 36-day yaw periods. Figure 3.4 shows the north-facing coverage of measurements taken on the 6^{th} March 1992.

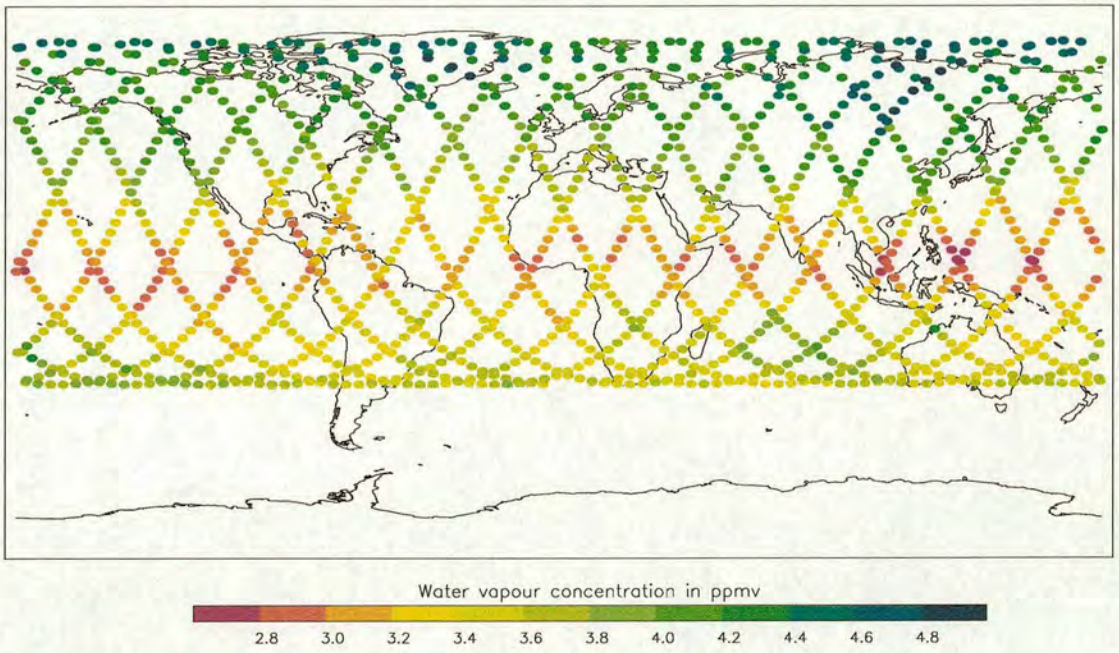

Figure 3.4: **Coverage of the MLS Instrument.** Shows the positions of the MLS measurements for one 24-hour period, when the UARS satellite was facing north. The data limits are 80 °N and 34 °S. When the satellite turns to south facing the coverage becomes 34 °N to 80 °S. Also shown are the retrieved water vapour concentrations at 68·1 hPa at the measurement points of 6^{th} March 1992. Within one day the satellite completes just under 15 orbits per day and hence the separation between the tracks of individual orbits is just over 24 degrees longitude.

Whilst being carried along the satellite track the MLS instrument scanned a vertical profile at each measurement point, each scan taking 65·5 seconds. The field of view of the instrument gives it a horizontal resolution of around 400 km along the line of sight, 5–10 km normal to the line of sight and approximately 2·5 km in the

vertical. Though early retrievals did not make full use of the vertical resolution of the instrument, providing data on a vertical grid chosen for computational speed and stability, later retrievals did. These later retrievals provide profiles that have the best agreement with the measured radiances on a grid with nodes spaced equally in $\log_n$[pressure] up to 0·046 Pa (approximately 90 km): 1000, 681, 464, 316, 215, 146, 100, 68·1, 46·4 ... 0·00046 hPa.

The MLS instrument carried three radiometers to detect radiation from the emission lines of various atmospheric species, water vapour being one of its primary targets. Other targets were oxygen, ozone and chlorine monoxide. The 63 GHz radiometer measured emission from the 63·0 and 63·5 lines of oxygen. Since the concentration of oxygen and its emission as a function of height are known this allowed the determination of temperature and pressure throughout the profile. The 183 GHz radiometer detected radiation from the emission lines of ozone at 184·4 GHz and water vapour at 183·3 GHz. The 205 GHz radiometer was sensitive to emissions from chlorine monoxide at 204·4 GHz and ozone at 206·1 GHz. The measurements of all radiometers were performed simultaneously and there was no degradation from ice clouds or by volcanic aerosol (Barath *et al.*, 1993). Further details on the MLS instrument can be found in Barath *et al.* (1993) and a comprehensive discussion on the techniques of microwave limb sounding can be found in Waters (1989) and Waters (1993).

The MLS, water-vapour dataset covers the time between 12^{th} September 1992 and 25^{th} April 1993, when the failure of 183 GHz radiometer ended data collection. The only notable interruption occurred between 2^{nd} June 1992 and 15^{th} July 1992, when the UARS developed a fault in its rotation mechanism such that instruments and solar panels alike could not be directed properly.

Retrieval Codes

Retrieval of MLS data was performed using the optimal estimation method described by Rodgers (1976). In this method an *a priori* estimate of the water vapour profile is combined with an estimate based on the measured radiances to provide a optimal

estimate. Each version of the retrieval code used a climatology for its *a priori* data made from a monthly average of the zonal-mean species data from earlier instrument records. Versions 3 (validated by Lahoz *et al.* (1996)) and 4 used data from the Limb Infra-Red Monitor of the Stratosphere (LIMS), whereas version 5 used Stratosphere Aerosol and Gas Experiment II (SAGE II) data for the lower stratosphere and version 17 data from the Halogen Occultation Experiment (HALOE) for the upper stratosphere and mesosphere.

The official version 5 retrieval was developed from a prototype, version 0104[†], created by H. C. Pumphrey at the Institute for Meteorology of the University of Edinburgh. This prototype adapted the official version 4 retrieval away from the previously-used, linear retrieval-technique to use of an iterative method. The linear retrieval assumed that the radiances received were proportional to the concentration of the emitting species. However, this assumption does not hold in the troposphere and lower stratosphere, where the atmosphere at the tangent height may no longer be the most opaque point along the scan. As such, the 46 hPa level was the lowest, stratospheric pressure-level to which water vapour was retrieved for the version 4 and earlier datasets. The iterative retrieval however, allowed much useful information at 68·1 hPa (Pumphrey, 1999) and a small amount of useful information at 100 hPa (Pumphrey *et al.*, 2000) to be retrieved.

The prototype retrieval (validated by Pumphrey (1999)) improved upon the previous versions in several other ways:

1. An improved forward model reduced systematic errors.
2. The use of SAGE II and HALOE data for the *a priori* proved to be a better choice than the LIMS data, which caused problems that increased with height and the retrieval to be useless at 100 hPa.
3. The vertical resolution of the retrieval grid was improved to the greatest resolution of the MLS instrument.

[†]This different naming system simply indicates the first (01) creation of a new retrieval scheme based upon the official version 4 (04) data.

4. The difference between concentrations observed on ascending and descending legs of the satellite motion were reduced.

These changes severely reduced the problems seen in the version 4 data, providing a retrieval with no major flaws. This is shown by Pumphrey (1999), who compared the prototype retrieval data with other instrumentation. He found the prototype showed better agreement with the other instruments than did previous retrievals. The 0104 data show good agreement with balloon-mounted, frost-point hygrometers between 100 and 3 hPa and agree generally with the Water Vapour Millimetre-Wave Spectrometer (WVMS), a ground-based instrument. The prototype also shows better agreement with HALOE (version 18) and Atmospheric trace Molecule Spectroscopy (ATMOS) data than its precursors, though is nevertheless uniformly drier than both instruments between 100 and 0·1 hPa, by between 0·1 and 0·4 ppmv. Pumphrey (1999) does note that the version 4 data are closer to that of ATMOS but point out that the prototype better captures ATMOS's variation with height.

Versions 0104 and 5

The official version 5 retrieval made use of the iterative technique tested by the prototype and of the improved forward model. Several further changes were also made to the retrieval for version five, in particular improved temperature and pointing code. This code lessened the dependence on the *a priori* in the mesosphere by use of a treatment of pressure shifting of the 183 GHz lines, which was previously dealt with by arbitrary adjustments to filters rather than by correcting instrument parameters. These further changes caused the two iterative retrievals to have noticeable differences, as is shown in the following section, which presents the results of a comparison between the version 0104 and 5 datasets.

Figure 3.5 shows the water vapour mixing ratios determined by both retrievals for one day in March 1992 at 68·1 hPa. Both datasets have been interpolated onto a standard grid of 10 degrees longitude and 2 degrees latitude using a method of exponential weighting with distance. The figure is presented as an illustration of the differences between the retrievals that are common to all water vapour maps at

this pressure level. Two clear differences can be observed in the figure. Firstly, the version 0104 data show lower mixing ratios in all areas and secondly, the version 5 data show a greater small-scale noise. This greater small-scale noise can be consistently observed at node heights below 14·7 hPa. At and above this height however, the situation reverses and the prototype exhibits greater small-scale noise.

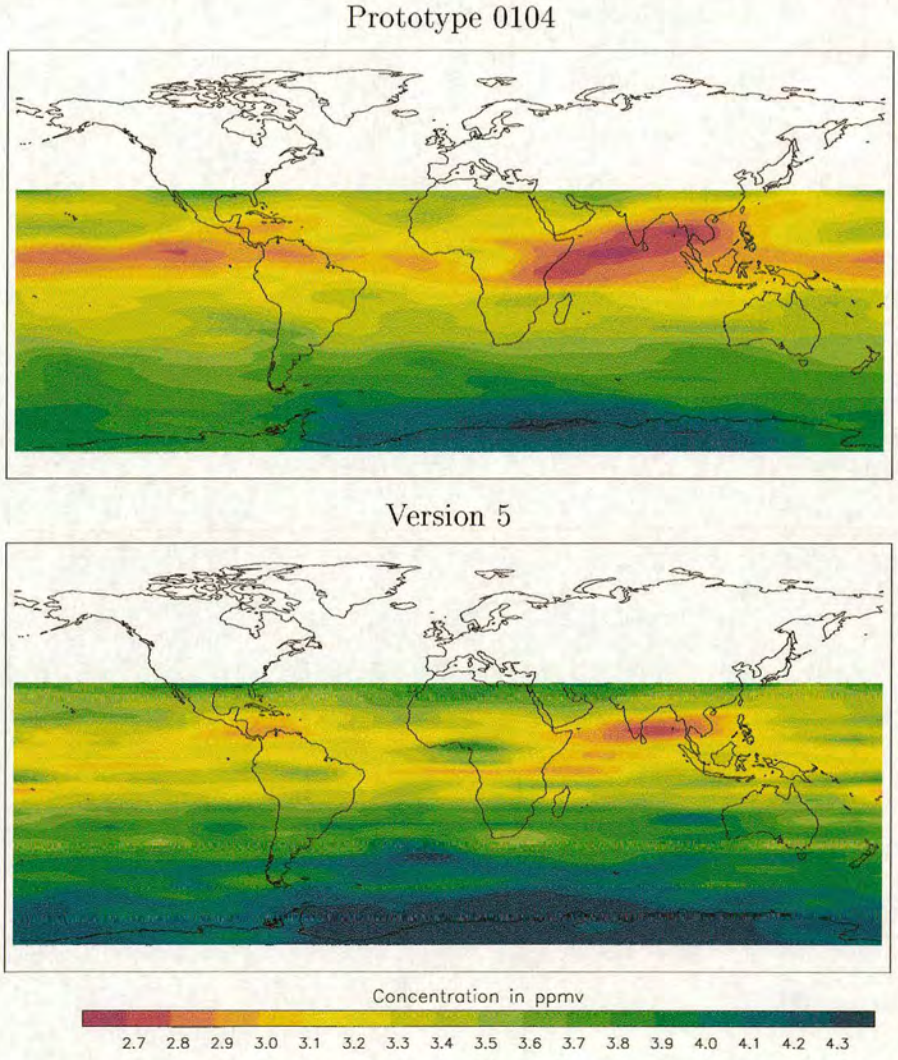

Figure 3.5: **Comparison of Version 0104 and 5 Retrievals.** MLS water vapour mixing ratio at 68·1 hPa for 27^{th} March 1992. Data have been interpolated onto a standard grid of 10 degrees longitude and 2 degrees latitude.

Figure 3.6 shows, as a function of height, the difference between the retrievals averaged over all grid points and days of the 183 GHz antenna lifetime. It indicates,

as can be appreciated in the maps of figure 3.5, that the version 0104 mixing ratios are generally around 0·3 ppmv lower at 68·1 hPa. Throughout the remaining lower stratosphere the prototype's mixing ratios are are lower by between 0·3 and 0·6 ppmv. In the low- to mid- mesosphere (0·68–0·10 hPa levels) the version 5 mixing ratios are higher, though the magnitude of the bias is smaller. Above these heights the version 0104 data are again generally lower. At all node heights the mean and root-mean-square differences are close, indicating small random errors and a mostly systematic separation.

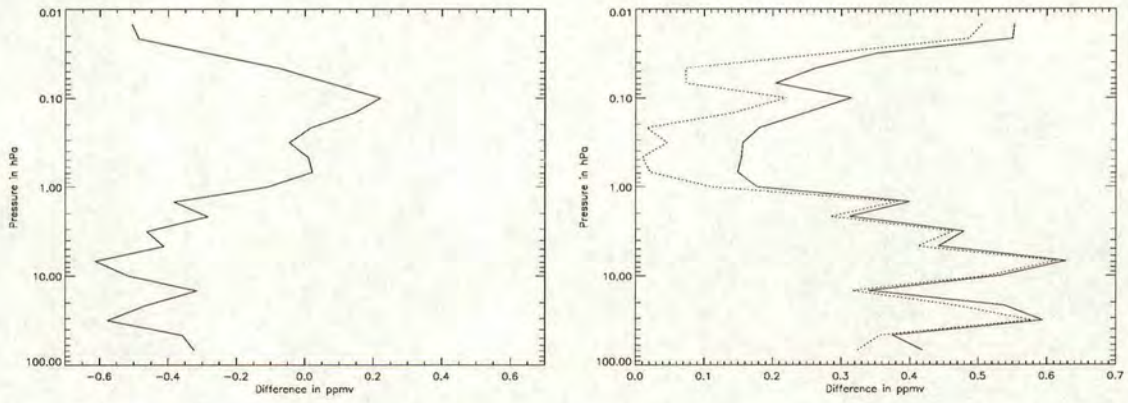

Figure 3.6: **Differences Between Version 0104 and 5 Retrievals.** The left panel shows the mean difference between the two retrievals as a function of height. The right panel shows the magnitude of this mean difference (dotted line) compared to the root-mean-square difference (solid line). Both the mean and RMS differences have been averaged over all grid points and all days of the 183 GHz antenna lifetime. The mean difference is calculated as the prototype data minus the version 5 data.

An advantage of the official version is a general lowering of the error as determined by the retrieval code. This can be appreciated through figure 3.7, which shows, averaged over all grid points and all days of the 183 GHz antenna lifetime, the retrieval error as a function of height for both versions.

Except for a small range between 0·46 and 0·1 hPa, where the errors are almost the same for both versions, the official retrieval has the lower error. However, since the advection study presented in chapter 4 makes use of difference plots between two maps of MLS data, a dataset with fewer random errors is more useful than one with smaller biases.

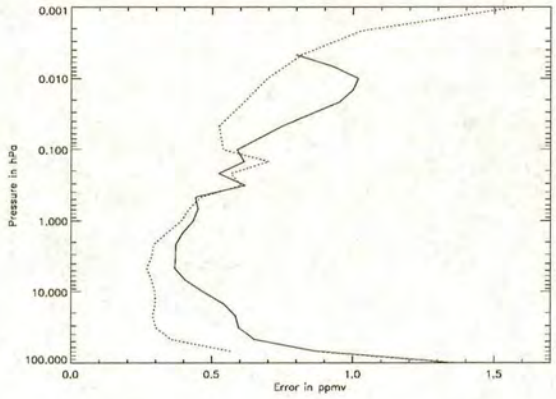

Figure 3.7: **Mean Error of Version 0104 and 5 Retrievals.** Shows the mean error on the retrieved water vapour product, averaged over all grid points and all days of the 183 GHz antenna lifetime, as a function of height. The solid line indicates version 0104 data and the dotted line version 5.

Figure 3.8 shows the average differences between gridded, water-vapour maps created using data from ascending and descending legs of the UARS flight path separately. The mean and root-mean-square differences were averaged over all grid points and all days of the 183 GHz antenna lifetime. These differences were a significant problem in the linear retrievals and, though reduced by the use of an iterative

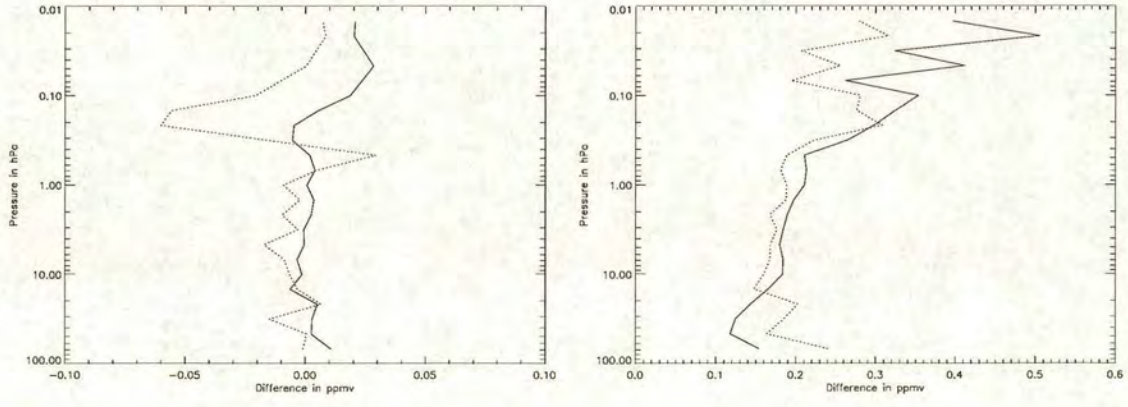

Figure 3.8: **Differences Between Ascending and Descending Orbits.** Shows the mean (left panel) and root-mean-square difference (right panel) between gridded, water-vapour maps created using data from ascending and descending legs of the UARS flight path. Data have been averaged over all grid points and all days of the 183 GHz antenna lifetime. The solid lines represent version 0104 data and the dotted lines version 5.

code, are still present at some heights of the versions 0104 and 5 data.

The mean difference is less than one percent of the average concentration at almost all heights for both versions. For the version 5 data the mean difference is negligible at all but one height. By comparing figures 3.8 and 3.7 it can be seen that the r.m.s. differences are about half the size of the total error in the version 5 data and about twenty percent of the total error in the version 0104 data. Nevertheless, the r.m.s. differences are similar between versions and for both increase with height as do water-vapour concentrations. Though the prototype data show larger r.m.s. differences than the version 5 data in the mid-stratosphere and above, it has smaller random differences in the lower stratosphere, the level of interest for the advection study of chapter 4.

That the version 0104 data are more suitable for study of the lower stratosphere is a fact supported by Pumphrey *et al.* (2000). They suggest that, for this height range, the version 5 data have too strong a dependence upon its *a priori* and that they contain a strong, monthly-varying signal that is more likely an artefact of the yaw manoeuvre than an atmospheric phenomenon. The signal is most likely due to a change in the small offset in antenna-measured radiances by absorption of solar radiation, which is larger at the beginning and end of the yaw period. Though the version 0104 minimised errors caused by the yaw manoeuvre, these errors returned in the version 5 retrieval.

In summary:

- In the case of both the iterative retrievals, the 100 hPa, MLS data is not good enough for the advection study and hence the 68·1 hPa data was used to investigate vertical motions in the lower stratosphere.
- Though the official version 5 retrieval may have improved information about upper stratosphere and about the mesosphere, information about the lower stratosphere is still better in the version 0104 retrieval and so the prototype retrieval was used in the advection study.

Managing Errors in the Water-Vapour Data

Though correct, it would be impractical to calculate and manage an error for each measurement made by the MLS instrument, therefore a broader error is used in the advection study. Clark *et al.* (2001) estimate the precision of a single profile, at 68·1 hPa, to be 0·3 ppmv and the accuracy to be 0·75 ppmv[†]. The value of this precision will be shown to be large in comparison to some of the concentration differences presented in chapter 4. For the purposes of that advection study it was therefore necessary to find some way of improving the precision of the data used, particularly as the combination of the water vapour with wind data would only serve to increase errors.

Adding spatial smoothing to the data was considered undesirable since there was no accurate way of deciding how much of the spatial fluctuation in the water vapour maps could be considered noise and how much was natural, horizontal variation. Temporal smoothing provided the answer, with five days providing a suitable time-frame for the averaging. Though this prevents consideration of daily variations in STE, short timescale events will still be visible. The loss of daily variations in the study of year-round STE was considered acceptable.

Figure 3.9 is presented here as an example of the water vapour fields used later. It shows version 0104 water-vapour data as retrieved for 68·1 hPa on 6^{th} March 1992. The top panel was created by taking the data from figure 3.4 and interpolating them onto the regular grid as introduced through figure 3.5. The bottom panel of figure 3.9 uses the same gridding of data but shows an average of the water vapour maps of the five days, or pentad, centred upon 6^{th} March 1992. Use of this averaging gave each grid-point on the mixing ratio maps a standard error of 0·13 ppmv.

The Retrieval at 68·1 hPa

The five-day-averaged distribution of figure 3.9 suggests that longitudinal variations in water vapour concentration persist into the lower stratosphere. If air rises slowly

[†]This accuracy can be appreciated from figure 3.7.

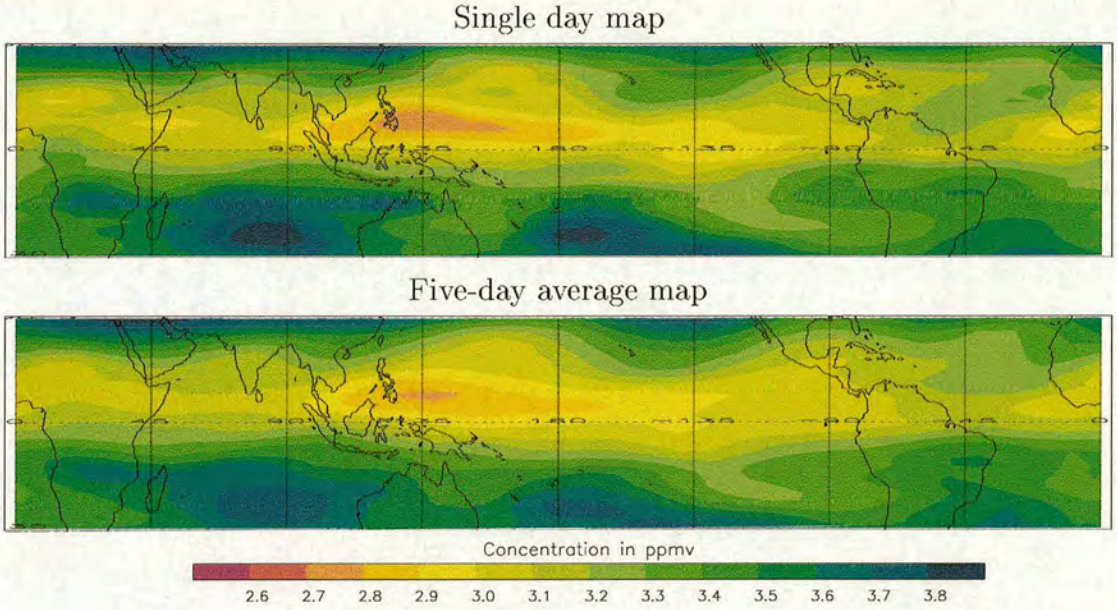

Figure 3.9: **Gridded Water Vapour at 68·1 hPa.** Shows version 0104 data for the 6^{th} March 1992. The top panel shows the individual day's data, shown in figure 3.4, interpolated onto a regular grid. The bottom panel shows a five-day average, or pentad, of the gridded water vapour, centred on 6^{th} March 1992.

from the tropopause to 68·1 hPa evenly and throughout most of the tropics, as implied by study of the "tape recorder effect" (Mote *et al.*, 1998), then a zonally symmetric pattern in the water vapour would be expected, the stratospheric winds smearing out any variations during the approximately thirty day travel time. These variations are therefore key to investigating the *fountain hypothesis*, since they could be explained by new air of lower mixing ratios arriving first at 68·1 hPa under the influence of convection. However, they could also be the result of the limited vertical resolution of MLS and the thickness of the retrieval's weighting function. If this were the case then features at 68·1 hPa could be the product of a contamination from signals at other pressure levels.

Figure 3.10 is figure 5 of Clark *et al.* (2001), showing the averaging kernels of the version 0104 retrieval and hence the weight with which variations in the true profile are felt at the retrieval-grid nodes. Ideally the kernel for each node would have a value of one at the node height and zero elsewhere. Where this is not the case

reflections of perturbations elsewhere will be observed at the node height.

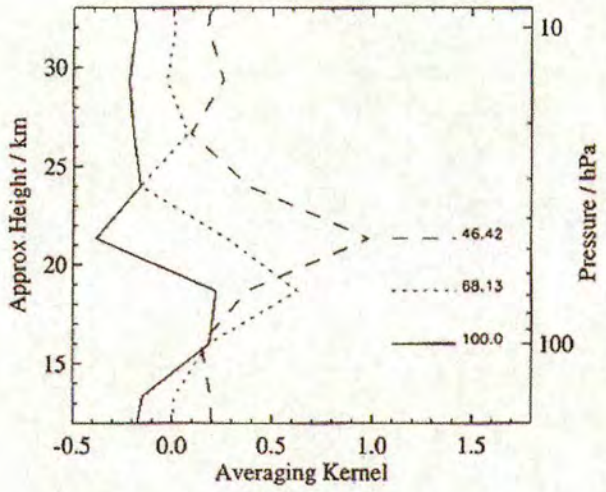

Figure 3.10: **Version 0104 Averaging Kernels.** As figure 5 of Clark *et al.* (2001), page 22701. Shows the kernels for three consecutive nodes of the version 0104 retrieval. The 100 and 46·4 hPa kernels have been offset by -0·2 and 0·2 respectively to aid clarity.

The 68·1 hPa kernel has a value 0·63 at 68·1 hPa and 0·18 at 100 hPa. Thus a perturbation of about 2 ppmv in the true profile at 100 hPa produces about a 0·6 ppmv perturbation in the retrieved profile at 68·1 hPa and so a pattern at 68·1 hPa could be the result of the same pattern at 100 hPa with a larger amplitude. However, Clark *et al.* (2001) show that, though 100 hPa data do show some correlation with those at 68·1 hPa, the variations at 100 hPa in these cases are smaller than those at 68·1 hPa. Hence they conclude that contributions at 68·1 hPa from effects below 90 hPa are small.

3.3.2 Selection of Isentropic Level

Though the MLS data were retrieved to pressure levels, the two-dimensional trajectory study was necessarily performed upon isentropes, given the assumption of adiabatic motion. As such, it was further necessary to determine upon which isentrope the investigation would be best performed and so to which isentrope the MLS data had to be interpolated.

It was desirable that the investigation be performed with data in close proximity to 68·1 hPa. In this way, a minimal amount of information from the 100 and 46·4 hPa retrieval nodes would be used, the 100 hPa data being unreliable and the 46·4 hPa data being information about the stratosphere outside the tropical tropopause layer. As a consequence, different isentropes were required for different times of the year, since the height of isentropes vary with season. Though this forbids comparison of inferred vertical-motions between months, such a loss was considered acceptable.

Suitable isentropes were determined by considering the MLS-retrieved potential temperatures upon the 68·1 hPa surface for all days of the 183-GHz-antenna lifetime. Potential temperature data were therefore gridded to the same resolution as was used to map water-vapour mixing-ratios. In this case however, it was only necessary to consider latitudes at up to fifteen degrees from the equator, since isentropes bow upwards toward zero latitude (see figure 2.8) and a focus towards the deep tropics was desired. Histograms of these data were then created for each month of the 183-GHz-antenna lifetime, beginning with November 1991[†]. All histograms used had bins of 1 K.

The histograms for all seventeen months exhibited a Gaussian distribution of potential temperature. The histograms for the months between and including November 1991 and May 1992 showed a Gaussian full width at half maximum (FWHM) of 9 K. The histograms for the months between and including June 1992 and March 1993 showed a Gaussian FWHM of 6 K. The mean values of each Gaussian, rounded to the nearest 5 K, are shown in table 3.2. These potential temperatures were used as the surfaces for the isentropic advections presented in chapter 4.

There does exist some variation in the mean potential temperature found at the 68·1 hPa level during each month — somewhere between 2–3 K. However, in working to an accuracy of 5 K the mean potential temperatures could be considered to be constant during each month.

There also exists a small inter-year variation for December and January but since no

[†]The retrievals of MLS water-vapour are unreliable for many days of September 1991, October 1991 and April 1993 and so data for these months were not used in the advection study presented in chapter 4. As such, these months are ignored here as well.

Month and Year	Isentropic level (K)	Month and Year	Isentropic level (K)
— 1991 —		— 1992 —	
November	445	November	445
December	445	December	440
— 1992 —		— 1993 —	
January	445	January	440
February	440	February	440
March	435	March	435
April	435		
May	435		
June	no data		
July	no data		
August	450		
September	450		
October	445		

Table 3.2: **Best-Representative Isentropic Surfaces.** Shows the isentropic level whose water vapour distribution best represents that retrieved for 68·1 hPa by the Microwave Limb Sounder (MLS) instrument. An isentrope is given for each whole month of the instrument's 183 GHz antenna lifetime.

inter-month comparison of the isentropic advections is to be performed this causes no problem. As an aside, chapter 4 will show that this inter-year variation in potential temperature does accompany an inter-year variation in water-vapour concentration: During 1993, when the 68·1 hPa surface has increased water vapour mixing ratios, the surface exhibits lower potential temperatures.

3.3.3 Advection Routine

The UKMO model updates its wind fields daily at 12 noon, GMT, on a grid whose horizontal resolution is 3·75 degrees longitude by 2·5 degrees latitude and vertical resolution matches that of the MLS instrument retrievals[†]. Its horizontal winds were interpolated in $\log_{10}$(pressure) co-ordinates onto potential temperature surfaces and then linearly in space and time to obtain the intermediate winds required by the advection routine.

[†]See section 3.3.1.

The trajectory calculation of Black (1997) makes use of a spherical co-ordinate system over most of the globe but switches to polar stereographic when particles are moved beyond 60 degrees latitude to avoid problems associated with co-ordinate singularity at the poles. Sutton *et al.* (1994) considered the loss of accuracy that occurred when using ever equatorward limits of the polar stereographic co-ordinate system. They suggest that there is no significant difference in particle distribution between having limits at 60 and 80 degrees. This thesis follows the work of Black (1997) in considering that sufficiently accurate results are achieved by changing co-ordinate systems at 60 degrees.

Though the advections of water presented following do use trajectories calculated after Black (1997), his "trajectory-mapping technique" is not applied to the MLS data prior to estimating isentropic evolutions of water vapour. Black (1997) applied the ideas of Pierce *et al.* (1994) and Morris *et al.* (1995) to MLS, water-vapour data, allowing synoptic maps to be produced from originally-asynoptic data. By advecting particles labelled with water-vapour mixing-ratios Black (1997) was able to produce water-vapour maps for any time within one 24-hour measurement period. This avoids the approximation that the MLS measurements in one 24-hour period are coincident in time and representative of the concentration distribution throughout the whole day.

For the purposes of this thesis, this synoptic approximation was used however. If synoptic maps of MLS data had been used as starting points for the estimation of isentropic evolutions then trajectory calculations would have been needed twice for each result — once to advect the data to the same time and once again to create the estimated evolutions. Since trajectory calculations are the largest source of error in the proposed study, extra calculations were not desirable. In the case of MLS, water-vapour data the synoptic approximation is not thought to cause large errors however. Water vapour does not exhibit large changes within a single day, as does ozone, for example, which has a diurnal cycle. Furthermore, chapter 4 will show that, in the deep tropics, individual particles of air are rarely transported more than a few degrees longitude or latitude during one day. Thus if a synoptic map of MLS, water-vapour data were to be created for midday few air particles would transport

water concentrations very far.

Estimated Isentropic-Evolutions

The maps of advected data which will be presented in chapter 4 were produced as follows. Air particles were initialised on a regular, equal-area grid that covered all longitudes up to thirty degrees from the equator. The grid resolution was 10 degrees in longitude and 2 degrees in latitude, matching that used to create the water vapour maps introduced in chapter 3. The particles were then advected backwards in time under the UKMO winds. At the end-points of these backward trajectories, at this chronologically earlier time, MLS water vapour data were interpolated from the measurement points onto the particle positions. The interpolation used was a method of exponential weighting with distance, again matching that used to create the gridded, water-vapour maps. The particles were then brought back along their paths of advection, onto the equal-area grid once more, thus allowing their water-vapour mixing-ratios to be mapped. Considered chronologically, the particles, with their water vapour, were advected forwards in time from seemingly random positions to arrive on the regular grid.

Figure 3.11 shows an example advection, under which version 0104, MLS, water-vapour data have been transported by trajectories upon the 435 K isentrope. The top panel is a pentad[†] of observed water vapour centred upon 5^{th} March 1992. In the bottom panel, the data from each of the five days have been advected forwards in time for ten days, so as to form a new pentad centred upon 15^{th} March 1992. The westward QBO-winds of this time cause the water vapour features of the top panel to shift westwards and to distort somewhat.

White space in the bottom panel indicates missing data, which comes about due to the viewing angle of the (UARS)[‡]. When the satellite is north-facing there is often advection of air into the southern portion of the map from outside the area of water vapour measurement (*i.e.* beyond 34 °S), and vice versa. This loss of data

[†]A five-day average; see section 3.3.1 — Using the Version 0104 Water-Vapour Data.

[‡]Section 3.3.1 — The Microwave Limb Sounder Instrument, discusses the satellite's viewing angles.

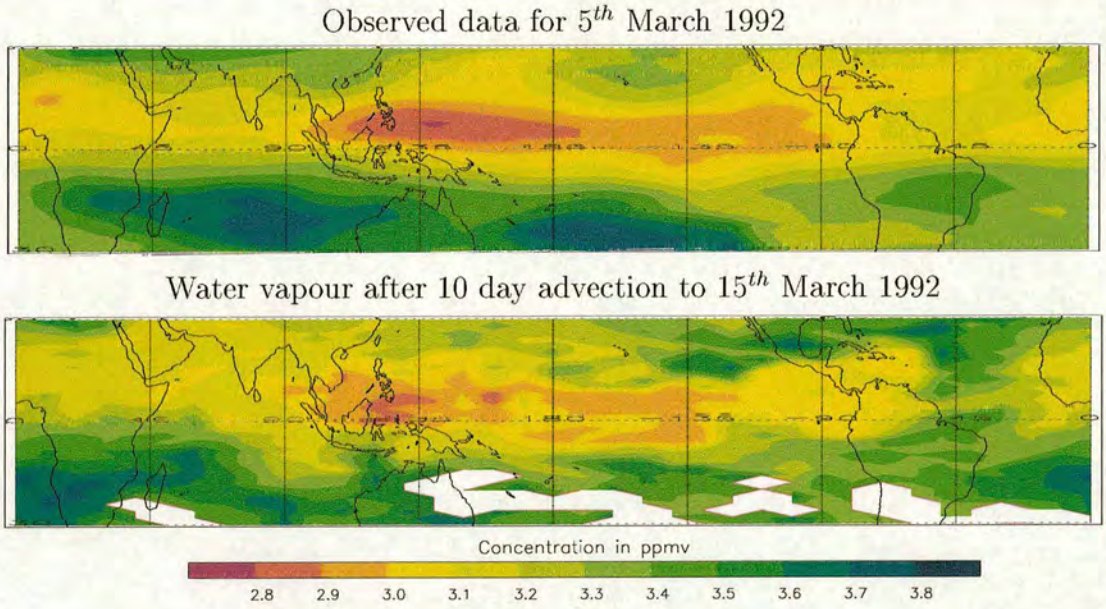

Figure 3.11: **An Example of Advected Water Vapour.** Version 0104 water vapour data on 435 K isentrope. Top panel: a pentad of observed data centred upon 5^{th} March 1992. Bottom panel: data from each day of this observed pentad advected forwards for ten days under UKMO winds allowing the creation of a new pentad centred upon 15^{th} March 1992. Whitespace in the bottom panel indicates regions where air was advected into the tropics from outside the field of view of the MLS instrument for three or more days of the pentad.

can still provide useful information about the flow on the surface however, since it is an indication of the amount of extratropical air that is advected into the tropics.

The after-advection plot shows seemingly greater detail than its data source. This an unavoidable, but not necessarily flawed, artefact of trajectory calculations. Indeed Sutton *et al.* (1994) and Sutton (1994) attempted to capitalise on the increased resolution added by the wind data, since such detail cannot be expected from maps of satellite data. Only wind data can provide the higher resolution as satellite measurements are limited by the instrument resolution and smoothing inherent in retrieval methods and since the advection can show how the species distribution would have occurred before other atmospheric motions smooth it out.

It might also be thought that the water vapour is not conserved between the two plots of figure 3.11, as the area inside each contour is not conserved and the

range of mixing ratios is less on the after-advection map. This is to be expected however, for three reasons: The advection does not take into account horizontal or vertical divergence; there will have been some advection of water vapour across the 30 degree latitude bounds of the plots; the data from each day of the pentad will undergo different trajectory motion, hence causing extreme values to be averaged away.

Altering Routine Parameters

The isentropic-advection routine has three parameters that may be altered: The method of interpolating water vapour data onto air particles; the length of the advection and the timestep of the Runge-Kutta iteration. As previously mentioned, the interpolation was chosen to be the same as that used to create maps of the unaltered MLS data. The other two parameters were set after considering Black (1997) and references therein.

Morris *et al.* (1995) examined atmospheric motions such that they might determine the timescale under which they could be expected to remain adiabatic. To this end they correlated the trajectory paths of adiabatic and diabatic advections initialised upon the same isentropic surface. They show that the isentropic approximations (that radiative heating and large vertical gradients of concentration have little effect on particle motion and species concentration) may hold for individual trajectories for one or two weeks and that large scale features may be preserved for periods of the order of a month.

It was desirable that the trajectories be run for a reasonably long time such that water vapour features would visibly move. Bearing in mind the considerations of Morris *et al.* (1995), the typical timescale of tropical diabatic-motions being around 20 days (Holton *et al.*, 1995) and timescales of diffusion and methane oxidation (see section 2.1.3) it was decided that the advection length should not be longer than ten days.

The timestep of the Runge-Kutta routine controls the accuracy and computational expense of the trajectory calculation, where one is traded off against the other. Fig-

ure 3.12 is figure 4.5 of Black (1997) and shows how the accuracy of the calculations changes with the length of the timestep, all other parameters of the advection and particle initialisation being constant. Test iterations with timesteps between two minutes and six hours are compared to a control, which had timesteps of one minute (set as the most accurate and so the most computationally expensive). In each case the root mean square difference between the test and control particle positions is shown.

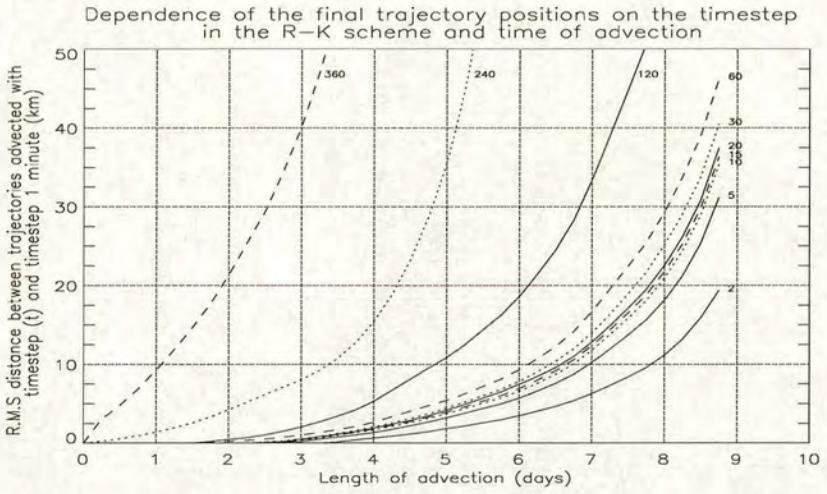

Figure 3.12: **Trajectory Accuracy as a Function of Timestep.** As figure 4.5 of Black (1997), page 86. Shows the sensitivity of the final particle positions with respect to the timestep of the iteration as compared to a control using a timestep of 1 minute. The advections were performed on the 800 K isentrope, initialised at 12 Z on 9^{th} January 1992. Numbers at the tails of each curve indicate the timestep of the advection used.

The map of advected water vapour in figure 3.11 was created using a timestep of thirty minutes. An extrapolation of the curve for the thirty-minute timestep of figure 3.12 would indicate a particle position error of around 100 km for a ten-day advection, which would be approximately one degree of longitude at the equator. To see what difference this would create to the advection plots the data shown in

the top panel of figure 3.11 was advected for ten days again, but this time using a timestep of one minute. At each grid point the difference between the two pentads of advected data was found to be less than 0·002 ppmv[†]. As such, a thirty minute timestep was used in the creation of all following advections of water vapour.

3.3.4 Errors

More than 5500 trajectories are required to create each pentad of advected data as introduced in section 3.3.3. The computational expense incurred in managing an error estimate for each of these trajectories, even when using the simplified recommendation of Stohl (1998), is an impractical consideration. The expense becomes even more unmanageable when studying isentropic evolutions for all the days spanning November 1991 and May 1992 and August 1992 to March 1993[‡], thus making use of over more than 500 000 trajectories. As such, it was decided that twenty percent of some average trajectory length would be a more appropriate error estimate.

Trajectory lengths were calculated as the total travel distance of the air particles by summing the great circle distance moved in each timestep, evaluated for the direct motion and separately in longitude and latitude. The great circle distance in longitude was calculated at an average latitude for each timestep. This approximation is not thought to cause a large error since the mean change in latitude per timestep was only 0·41 degrees, an average considerably increased by a small number of air-particles escaping to mid-latitudes.

Separation of the trajectories into two components was performed since their errors are expected to be proportional to wind strength, which generally has a much greater east-west than north-south component. This therefore reflects the probability distribution of final particle positions that would be the best trajectory error estimate, which would similarly be expected to have a greater spread in the zonal direction providing an oval-shaped distribution. The average trajectory length of

[†]The two maps are very similar and hence the pentad created with a timestep of one minute is not shown for comparison.

[‡]The months for which the retrievals of MLS water-vapour were missing data for less than three days. These months are those used in the experimental results presented in chapter 4.

the ten-day, isentropic trajectories was found to be 6170 km in longitude, 1850 km in latitude and 6800 km overall, each to the nearest 10 km. These distances lead to estimated errors of 1240 km in longitude (approximately 11 degrees of longitude at the equator), 370 km in latitude (approximately 3 degrees) and 1360 km overall, again to the nearest 10 km.

These mean trajectory lengths show some change with season and, given the increase in wind speed away from the equator, with latitude. Table 3.3 shows the estimated error calculated for four groups of months. The groups are approximately the seasons shifted back by one month; June and July are discounted because of the lack of MLS data during these months. This configuration takes into account the fact that air crossing the tropopause during each season takes approximately one month to reach the top of the tropical tropopause layer, where the *fountain hypothesis* is tested.

Months averaged over	JFM	AM	AS	OND
Longitude error (km)	1200	1200	1760	1060
Latitude error (km)	390	410	300	360

Table 3.3: **Trajectory Error Estimate by Season.** Shows, to the nearest 10 km, twenty percent of the average trajectory length in kilometres for tropically-initialised, ten-day, isentropic trajectories. Trajectory lengths have been evaluated in great circle distances separately in longitude and latitude directions. The abbreviations represent: JFM - January, February and March, AM - April and May, AS - August and September, OND - October, November and December. See text for details on days of release.

The average east-west distance travelled shows a significant increase in August-September accompanied by a decrease in the average north-south motion. Neither the QBO or ENSO exhibit two changes of phase within a single year period, leaving the seasonal variation in the Brewer-Dobson circulation, or rather in the waves that force it, as the most likely explanation of the flow change. The time of the decrease in north-south motion corresponds to that of the strengthening in the barriers of the subtropical pipe[†]. The increase in zonal flow might therefore come about if, during this time, wind vectors are not pulled so far north or south, though this does assume

[†]As discussed in section 2.1.2 — A Tropical Pipe.

airflows retain a similar speed throughout the year.

The inter-year differences in the trajectory lengths for the JFM (January, February and March) and OND (October, November and December) seasons are small in latitude but in longitude are comparable to the inter-season difference between the JFM and OND averages of table 3.3.

Table 3.4 shows the variation in trajectory length averaged over all seasons. Trajectories were assigned to the latitude band they spent the most time in. The data show that trajectories near 10 °S cover the shortest distance on average and that the average length increases symmetrically away from this latitude.

Latitude (degrees)	-30:<-20	-20:<-10	-10:<0	0:<10	10:<20	20:<30
Longitude error (km)	1090	970	950	1080	1240	1680
Latitude error (km)	420	290	250	270	340	480

Table 3.4: **Trajectory Error Estimate by Latitude.** Shows, to the nearest 10 km, twenty percent of the average trajectory length in kilometres for tropically-initialised, ten-day, isentropic trajectories. See text for days of release. Trajectories lengths have been evaluated in great circle distances separately in longitude and latitude directions.

Making Use of the Error Estimate

The error estimates discussed above will, in chapter 4, be used as horizontal length scales, below which the size and detail of water vapour features on post-advection plots cannot be considered believable. Figure 3.13 highlights three features of a ten-day advection of data ending on a pentad centred upon 18^{th} April 1992. The features were chosen to provide an indication of the level of detail that can and cannot be considered believable on the maps of the next chapter. Each feature is highlighted separately in its own panel: The top panel shows a large-scale, believable feature; the middle panel a feature large enough to be believable but with unreliable detail; the bottom panel a feature too small for its existence to be reliable.

The top panel feature is much larger than the error estimates in both table 3.3 and table 3.4. The highlighted range covers 50 degrees of longitude and 12 of

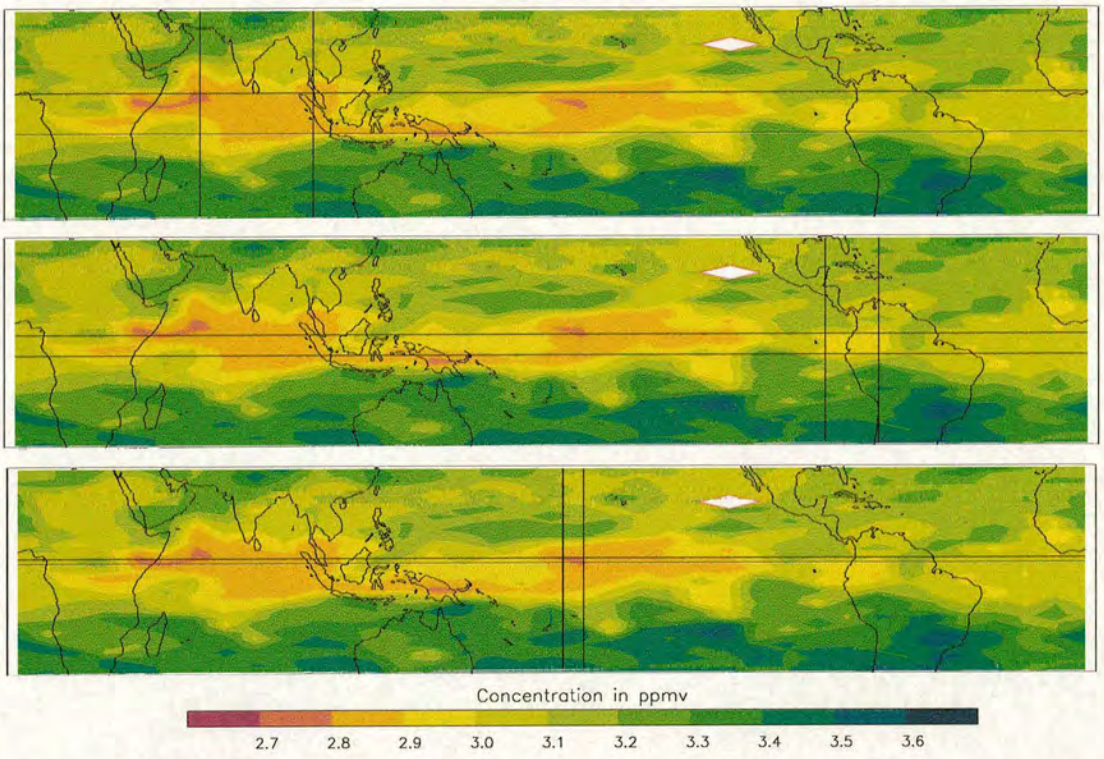

Figure 3.13: **Believability of Post-Advection Water-Vapour Features.** Each panel shows the same pentad of advected water-vapour data. The data were advected from 8^{th} to 18^{th} April 1992. In order to judge the believability of any water-vapour feature it must be larger than the appropriate length scale of both table 3.3 and table 3.4. As a guide three different features are analysed here, each highlighted in a separate panel: The top panel shows a large-scale, believable feature; the middle panel a feature large enough to be believable but with unreliable detail; the bottom panel a feature too small for its existence to be reliable.

latitude, covering more than 5500 km east-west and more than 1300 km north-south. Features of around this size and larger are the main focus of the following work. Some tendrils of the feature's 2·8 ppmv contour do fall below the April and equatorial error estimates and so details to this level are never considered.

At the equator in April, a water-vapour feature must be larger than 1200 km east-west and 410 km north-south in order to be believable (since the April length scales of table 3.3 are larger than the near-equator length scales of table 3.4). The highlighted feature in the middle panel of figure 3.13 therefore represents the smallest

feature that can be reliably considered at this time of year. No useful statement can be made about the feature's shape however, this level of detail is not believable.

The feature in the bottom panel of figure 3.13 has an east-west and north-south extent that are smaller than the respective length scales of tables 3.3 and 3.4. Features of this size are never considered in chapter 5.

3.4 Three-Dimensional Trajectories

The results of the three-dimensional calculations presented in chapter 6 were created using ECMWF wind data and a routine described by Methven (1997), which was originally designed and used for tropospheric experiments (see, for example, Methven *et al.* (1999); Evans *et al.* (2000)). Methven (1997) shows that the routine has negligible errors by the strong reversibility of trajectory calculations.

3.4.1 Trajectory Routine

The routine takes in pressure and horizontal wind strength from the ECMWF model output. From these data the vertical winds are then calculated from the vorticity and divergence at each model grid-point and from the pressure in the column below. In this way a vertical velocity is calculated that conserves angular momentum, energy and mass (after the method of Simmons and Burridge (1981)). This is used in preference to the existing, ECMWF, vertical-wind data, which have a dubious accuracy due to the large ratio of signal to noise that occurs during their measurement. Four-dimensional wind data are then interpolated linearly in time and the horizontal onto air-particle positions and by cubic Lagrange in the vertical. These positions are then advanced using a 4th order Runge-Kutta iteration.

ECMWF winds from the ERA-15 data set were used to investigate the *uniform-entry* and *flow-change* hypotheses. This ECMWF model updates its wind fields every six hours from midnight, four times daily, on a grid whose horizontal resolution is 2·5 degrees in both longitude and latitude. The vertical grid resolution of the

ERA-15 model has changed over the years but for those years before 1995 there are thirty one pressure levels spanning 1000 and 10 hPa. Near the tropopause the resolution is: 238, 209, 181, 156, 132, 110, 90, 70, 50 hPa.

3.4.2 Errors

The total error in an air-particle position can only increase with time during a trajectory calculation. However, the total error will have a far larger random component than a bias. Assuming that the majority of particles remain in the correct wind regime then cancellation of random errors allows the larger-scale position-structure of calculations to remain reasonably accurate (Morris *et al.*, 1995). The degree of accuracy and timescale the assumption holds for will, of course, be dependent on the scale of individual wind regimes. The calculations presented in chapter 6 use thirty days as an upper limit, based on the discussion presented in section 3.3.3: Altering Routine Parameters.

Use of many thousands of trajectories may serve to improve large-scale accuracy but it makes the calculation of trajectory errors impractical in terms of computational expense. As such, errors of the calculations shown in chapter 5 are instead considered in terms of the significance of the air-particle distributions. Both the *uniform-entry* and *flow-change* hypotheses suggest that no variation exists in the cross-tropopause flux, the former in space, the latter in time. The likelihood of calculated, air-particle crossing-patterns randomly occurring are therefore considered with respect to a uniform crossing-distribution.

3.5 Summary and Discussion

Though trajectory calculations can suffer quite large errors it has been shown that they can be reasonably estimated and dealt with. The two-dimensional experiments discussed by this thesis make use of the empirical estimate of Stohl (1998) — that trajectories will generally have errors of up to 20 % of their total travel distance. This estimate allows an error length-scale to be deduced, after-advection, water-

vapour features smaller than which must be considered unbelievable. In the case of the three-dimensional experiments discussed by this thesis there are no species features to apply the length scale to. Instead, a significance analysis is applied to air-particle distributions along the trajectories with respect to uniform distributions throughout the tropical tropopause layer.

Errors in calculating trajectories can be reduced by selecting the most suitable wind dataset. In the case of three-dimensional trajectories used to investigate tropics-wide STE, a tropics-wide dataset with the greatest temporal resolution possible was required — assimilated data from the ECMWF. A tropics-wide dataset was also required in the case of the two-dimensional trajectories used to investigate the *fountain hypothesis*. However, in this case a high temporal resolution was not as important. The UKMO assimilated-data were therefore selected, since their zonal winds were closest to those observed by a radiosonde in a data-sparse, tropical region.

Both two- and three- dimensional trajectories then, have the potential to be well used in the investigation of stratosphere-troposphere exchange. The former can provide simulated evolutions that enable a search for areas of uplift, thereby allowing a test of the *fountain hypothesis*. The latter enable a more direct analysis of air flows, allowing investigation of the *uniform-entry* and *flow-change* hypotheses by consideration of the nature of and yearly-change of the cross-tropopause flows.

The Microwave Limb Sounder instrument provides daily-updated, tropics-wide, water-vapour data throughout the lower stratosphere and is an ideal dataset for use in the estimation of the isentropic evolution of water vapour there. Though the dataset does not provide useful information at the tropical tropopause it can provide useful information at 68·1 hPa, towards the top of the tropical tropopause layer.

The version 5 retrieval of MLS data is superior to the prototype version 0104 except in the lower stratosphere. At these heights it has been shown that the former has increased differences between data obtained on ascending and descending legs of the satellite motion. Also, Pumphrey *et al.* (2000) show that in its lower stratosphere data the version 5 retrieval has too strong a dependence upon its *a priori* and

contains a strong, monthly-varying signal that is an artefact of the yaw manoeuvre rather than an atmospheric phenomena. As such, the version-0104, water-vapour retrieval is more suitable for examination of tropical STE.

In chapter 4 the *fountain hypothesis* is tested using estimates of the isentropic advection of MLS, water-vapour data under UKMO winds by the advection routine of Black (1997). This combination is used to search for the coincident drying and exchange suggested by Newell and Gould-Stewart (1981) and detailed by Danielsen (1982, 1993) that relies on the rapid action of convection. If uplift could be found in regions other than Indonesia in the northern winter and India in the northern summer then the *fountain hypothesis* would be disproved.

In chapter 5 the *uniform-entry* and *flow-change* hypotheses are tested using three-dimensional trajectories calculated from ECMWF winds and the routine developed by Methven (1997). Though experiments using these trajectories cannot yet differentiate between the two proposed mechanisms of STE (coincident and non-coincident drying and exchange) they can show whether the exchange occurs in preferred regions or equally throughout the tropics. Therefore, such calculations suggest whether localised mechanisms, such as those proposed by Newell and Gould-Stewart (1981), Danielsen (1982, 1993), Sherwood (2000) and Sherwood and Dessler (2001)[†], or mechanisms with tropical coverage, such as those of Potter and Holton (1995), Alexander *et al.* (1995), Holton and Gettelman (2001) and Hartmann *et al.* (2001), take precedence. Thus the *uniform-change hypothesis* is tested. By continuing this analysis back from the time of the MLS instrument, in the early 1990s, to the early 1980s, it is possible to determine if a significant change in the cross-tropopause flow occurred between these times. Thus the *flow-change hypothesis* is tested.

[†]The latter must be included here since they promote the importance of areas of high convective activity.

Chapter 4

Two-Dimensional Advections

With adequate water-vapour and wind data established and a suitable advection routine in place it was possible to test the *fountain hypothesis* proposed in chapter 2. The Microwave Limb Sounder (hereafter MLS) and United Kingdom Meteorological Office (hereafter UKMO) data were combined under the advection routine developed by Black (1997) to create estimates of isentropic evolutions of water vapour. These evolutions, on timescales less than those characteristic of methane oxidation and diffusion, were compared to observed evolutions upon the same isentropes. In regions where the comparison revealed differences, vertical motions were said to have occurred across the isentrope. The vertical motions discovered not only indicate whether or not the proposed "fountains" exist but also provide constraints for the reliability of vertical motions highlighted by the three-dimensional trajectories presented in the next chapter.

If the *fountain hypothesis* were correct then air-motion in the tropical tropopause layer would comprise two distinct aspects. The first would be a rapid uplift, penetrating the tropopause, in regions of strong convection. The second would be a slower, quasi-horizontal redistribution of this air new to the stratosphere, transporting it from the regions of strong uplift to the remaining tropics.

There is some indication in the MLS data that such a redistribution of water vapour may have occurred during the late winter and mid-summer of 1992. In winter 1992, lower-stratospheric MLS-data shows relatively dry air appearing first

over Indonesia and then later throughout the remaining tropics. In summer 1992, relatively moist air appears first over the Asian monsoon region before seemingly spreading east. These evolutions could be respectively explained by cross-tropopause motion through the higher, winter tropopause over Indonesia and the lower, summer tropopause over India, followed by quasi-horizontal, stratospheric motions from these regions.

Section 4.1 shows monthly-averaged data from the MLS instrument, detailing the longitudinal variations in water-vapour concentration that are visible at the 68·1 hPa level; the times when a "stratospheric fountain" might be acting are highlighted. Section 4.2 discusses the UKMO wind data, specifically those data used to create the results presented in this chapter. Section 4.3 presents the isentropic advections that test the *fountain hypothesis*. Section 4.4 expands on this investigation by determining where vertical motions can be inferred to have crossed the isentropes near 68·1 hPa for the whole lifetime of the 183 GHz antenna of MLS. A summary and discussion is then given in section 4.5.

4.1 Evolution of Water Vapour at 68·1 hPa

Throughout the lifetime of the MLS instrument's 183 GHz antenna the water vapour mixing ratios retrieved for 68·1 hPa range from 2·5 ppmv, found in March and April 1992 data, to 4·8 ppmv, occurring over the Asian monsoon regions in August 1992 data. The distribution of water vapour at this level varies from taking a band-like structure, most clearly observed during the northern summertime, to exhibiting a more patchy nature, particularly visible in the 1993 data. In the following section, monthly and five-day averages are examined and possible "stratospheric fountain" signatures are highlighted.

4.1.1 Monthly-Averaged, MLS Water-Vapour

Figure 4.1 shows monthly-averaged, version-0104 water-vapour distributions at 68·1 hPa for all months of the lifetime of the MLS instrument's 183 GHz antenna possible.

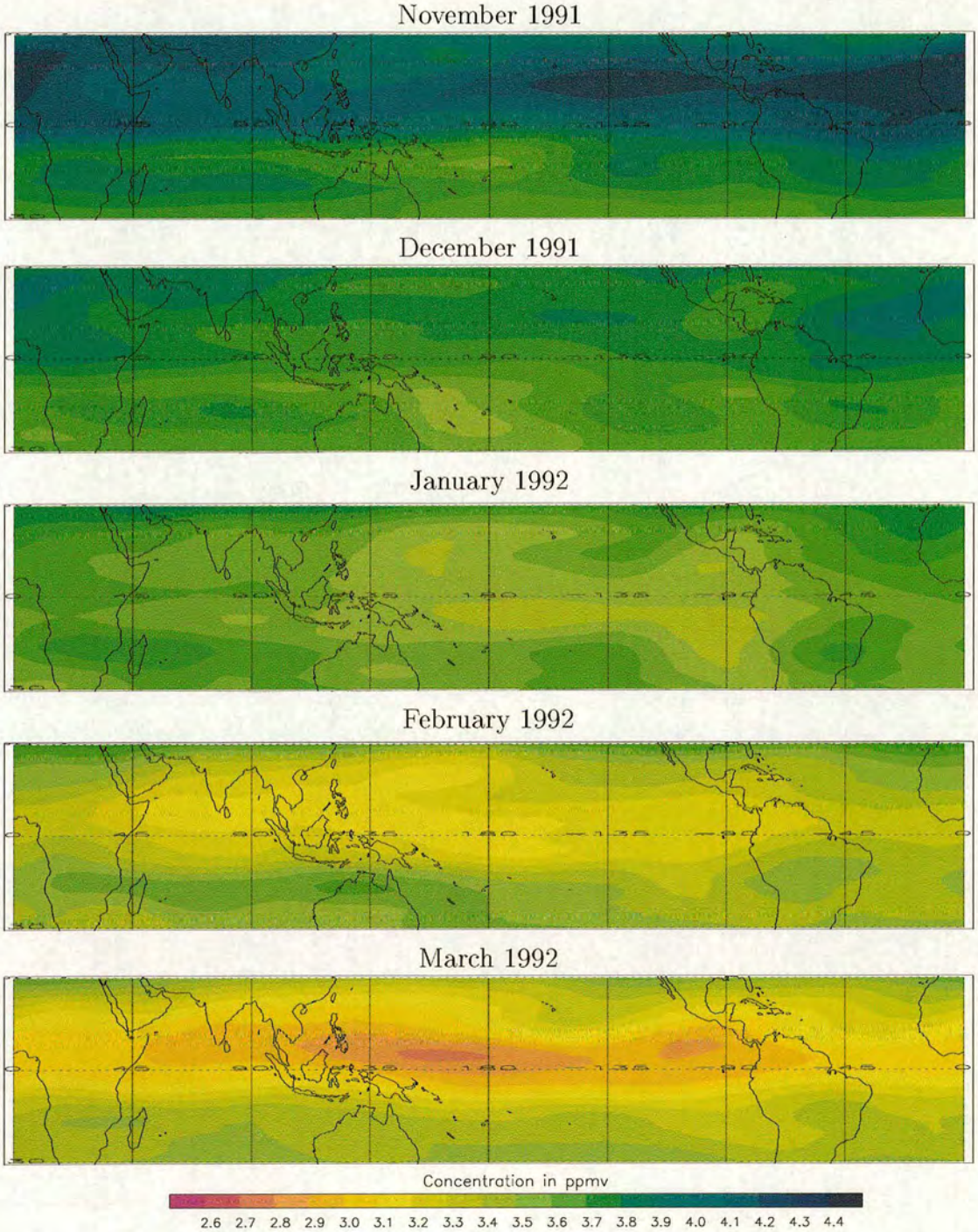

Figure 4.1: **Monthly-Averaged, MLS, Water-Vapour at 68·1 hPa.** Shows monthly-averaged mixing-ratios calculated from the MLS, version-0104 retrieval. Though the MLS instrument went online in September 1991, the retrievals were incapable of providing useful data for all days of September and October 1992. As such, there are no maps for these months.

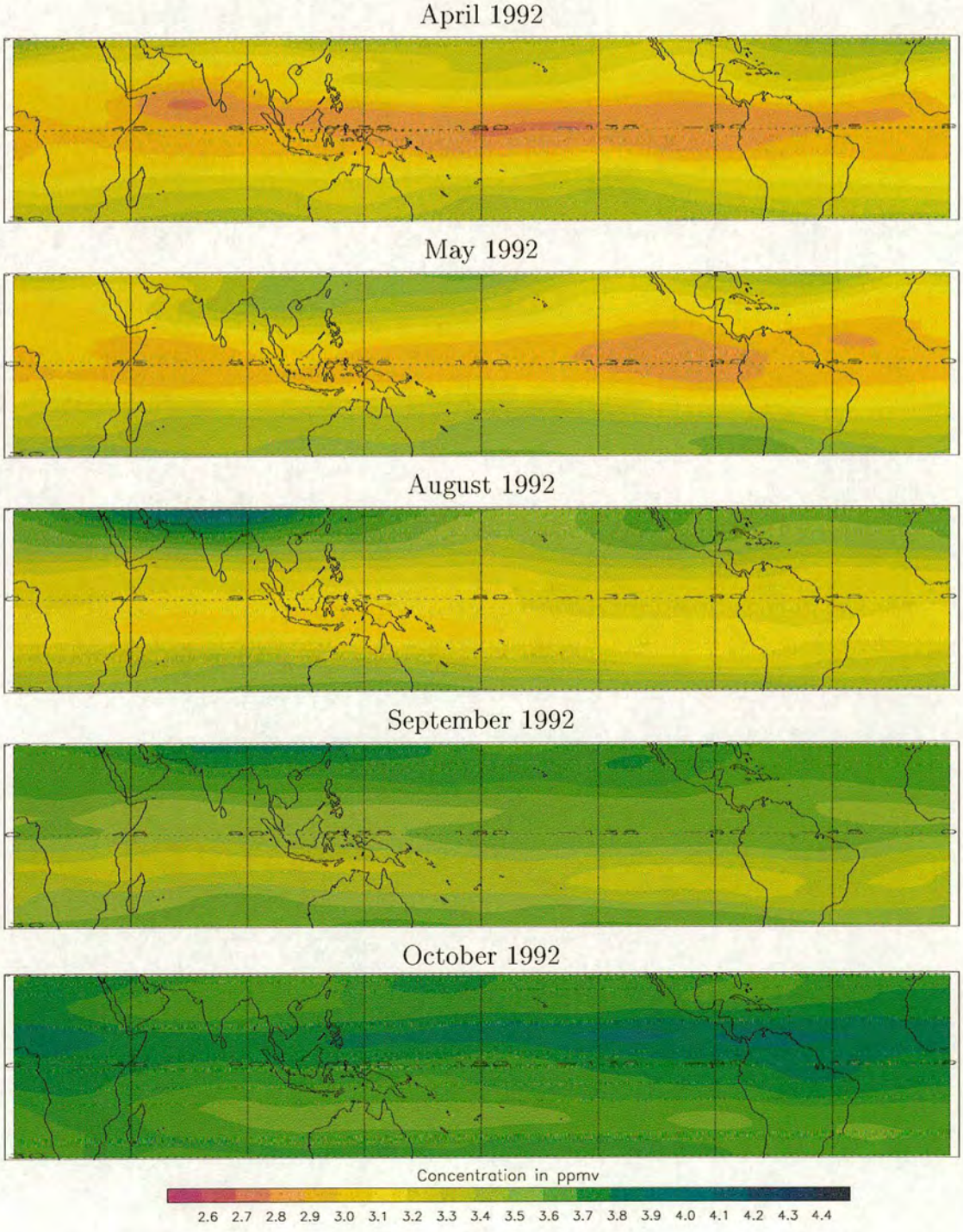

Figure 4.1: **Monthly-Averaged, MLS, Water-Vapour at 68·1 hPa.** Continued from previous page. There are no maps for June and July 1992 as the MLS instrument was not operational for all days of these months.

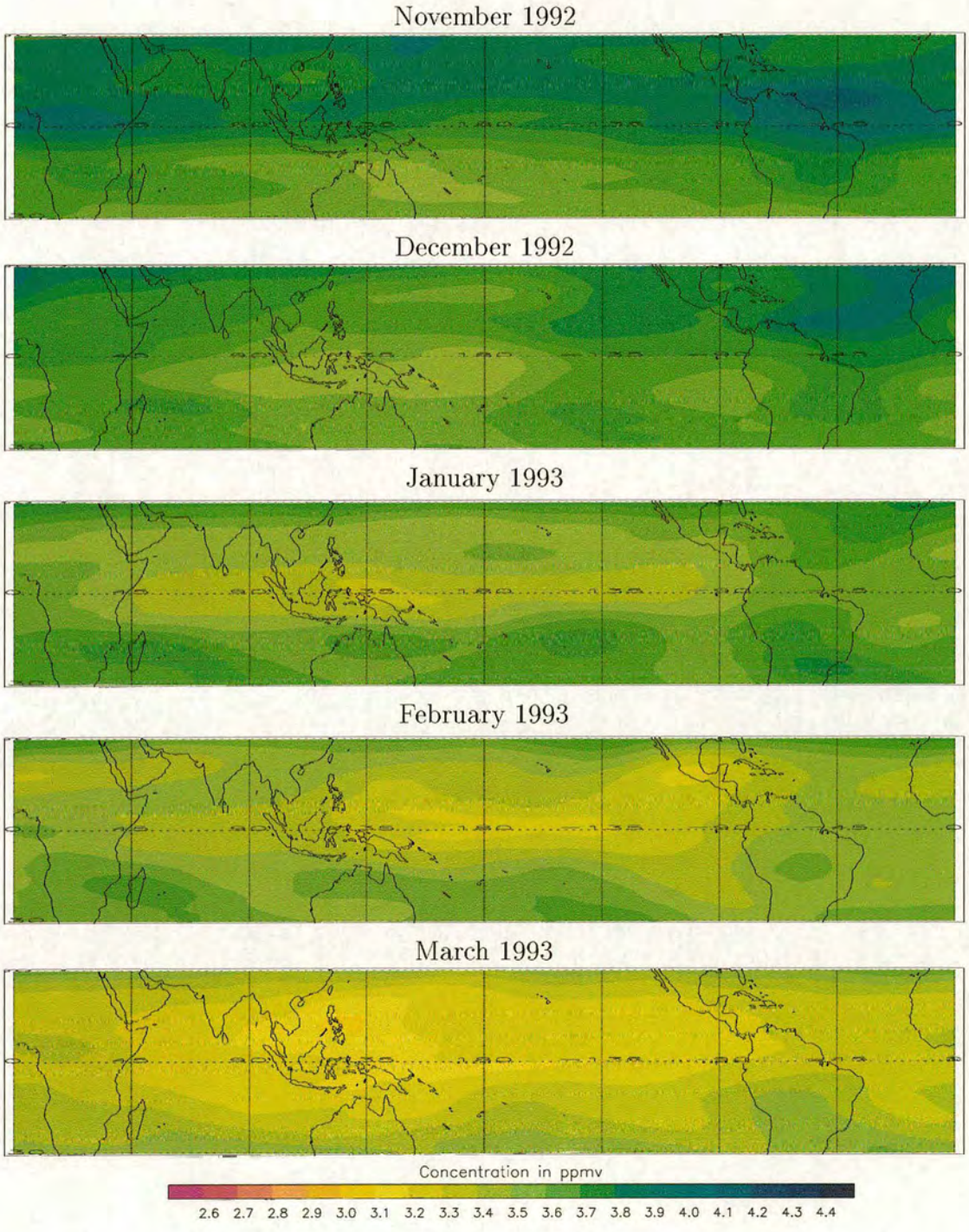

Figure 4.1: **Monthly-Averaged, MLS, Water-Vapour at 68·1 hPa.** Continued from previous page. Though the 183 GHz antenna functioned into April 1993 it failed before the end of the month and so an April map is not possible.

Although the highest water-vapour concentration on an individual day's map is found in August 1992 data, the monthly-mean data show the highest values in the November months. After November 1991, mixing ratios on the 68·1 hPa surface tend to fall, most rapidly over the Pacific Ocean but throughout the whole tropics nonetheless. This drying persists until March 1992, whereupon the smallest mixing ratios of the retrieval period can be observed to the east of Indonesia.

Though mixing ratios drop no lower in April the area of lowest values spreads further along the equator during this month. May 1992 then sees the last of the lowest concentrations as the effects of the tropopause temperature rising again[†] are felt at 68·1 hPa, particularly over Indonesia and the Indian Ocean, where mixing ratios rise the quickest. The change is not felt in all areas however; the eastern Pacific Ocean shows no increase in mixing ratio from the April case.

It is within the March and April data that the clearest "possible stratospheric-fountain" can be seen at the 68·1 hPa level. Though no regional development from Indonesia to the remaining equatorial longitudes can be appreciated in the monthly-average, it is clear on five-day-average maps, which are shown in the next section. These maps show a pattern developing throughout March (that repeats in April), which could be explained by relatively dry air spreading from Indonesia.

That these water-vapour distributions could be caused by atmospheric phenomena moving up from the tropopause is supported by lower-stratospheric data from the Halogen Occultation Experiment (hereafter HALOE). Figure 4.2 shows HALOE water vapour at 100 hPa, averaged over the winters (December, January and February) and springs (March, April and May) of 1993 to 1996, and at 83 hPa, averaged over the springs of 1993 to 1996.

The HALOE data is averaged over different years to the MLS data presented in figure 4.1. However, given the temporal proximity of the data in figure 4.1 to those in figure 4.2, it is reasonable to assume there will be some similarity in the long-term-averaged water-vapour between the two time periods in question. Hence, it is further reasonable to assume that a similar low water-vapour concentrations would

[†]See figure 2.9, which shows the seasonal variation in the tropopause temperature.

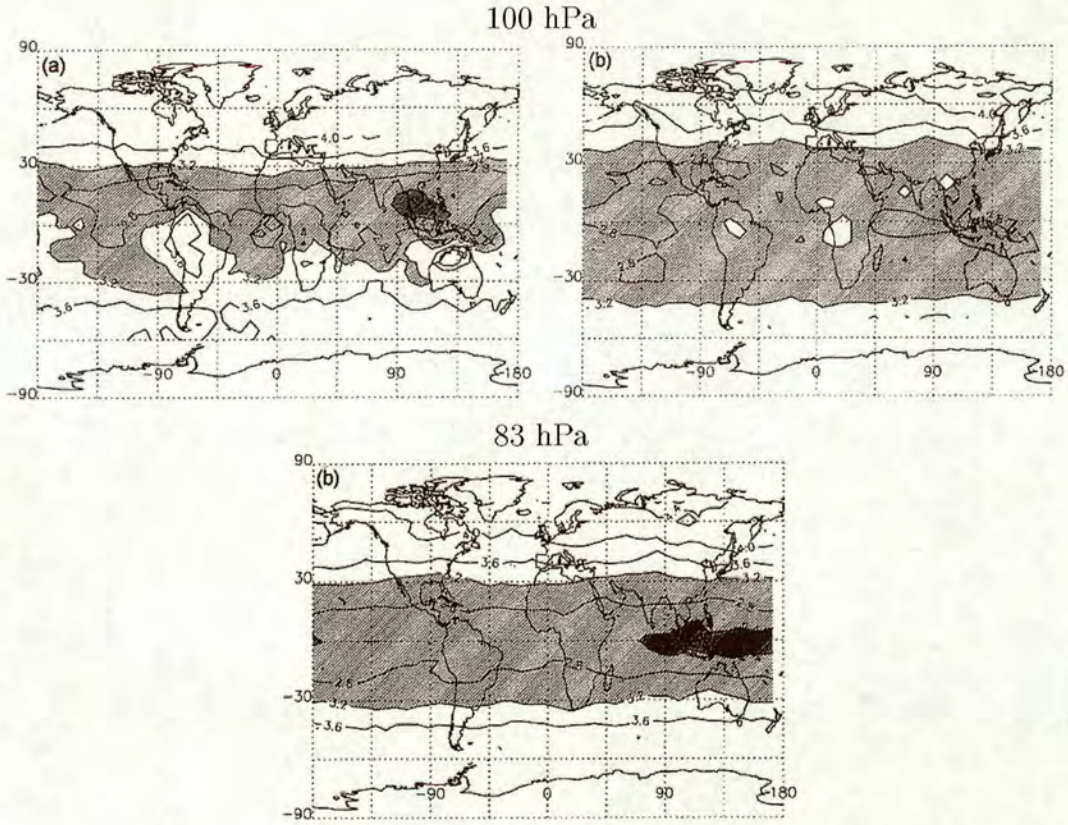

Figure 4.2: **Seasonally-Averaged, HALOE, Water-Vapour Maps.** As the first and second panels of figure 2 and the second panel of figure 3 of Jackson *et al.* (1998), pages 177 and 178 respectively. Top panels: Show the mean HALOE, water-vapour mixing-ratio at 100 hPa for December, January and February (a) and for March, April and May (b) of the years 1993–1996. Bottom panel: Shows the mean HALOE, water-vapour mixing-ratio at 83 hPa for March, April and May of the years 1993–1996. Contour interval is 0·4 ppmv. Broken contours indicate regions not covered by HALOE. Lined shading indicates values less than 3·2 ppmv, heavy shading indicates values less than 2·4 ppmv.

be found over Indonesia and neighbouring countries, at 100 and 83 hPa, during the spring of 1992. Thus it is possible that the observed distribution of low values at 68·1 hPa originates at the tropopause, near 100 hPa, in the winter- or spring- time and is then drawn up to the 83 and 68 hPa levels during the spring.

Lack of data from MLS prevents analysis of the water vapour field of the early summer of 1992 — June and July. However, given the August 1992 data, it is reasonable to assume that the water vapour at 68·1 hPa continued to increase during

June and July, albeit somewhat slowly (the difference across most of the tropics between May and August being not more than 0·2 ppmv). Only over the Asian continent is the increase large, most likely because of the monsoon below. In September a sharper, tropics-wide increase in water vapour concentration is seen and with it the loss of most of the longitudinal variation, leaving a band-like distribution with mixing ratios increasing away from a minimum at around 10 degrees south.

That the largest northern-summertime change occurs at the equator is clear when the difference between the September 1992 and August 1992 maps is taken, as can be seen in the bottom panel of figure 4.3. With the exception of the monsoon signature over the Asian continent the change in water-vapour becomes greater towards the equator. This is markedly different from the changes occurring during the spring months of the same year, which are far less band-like. The March 1992 to April 1992 case is a good example and is shown in the top panel of figure 4.3.

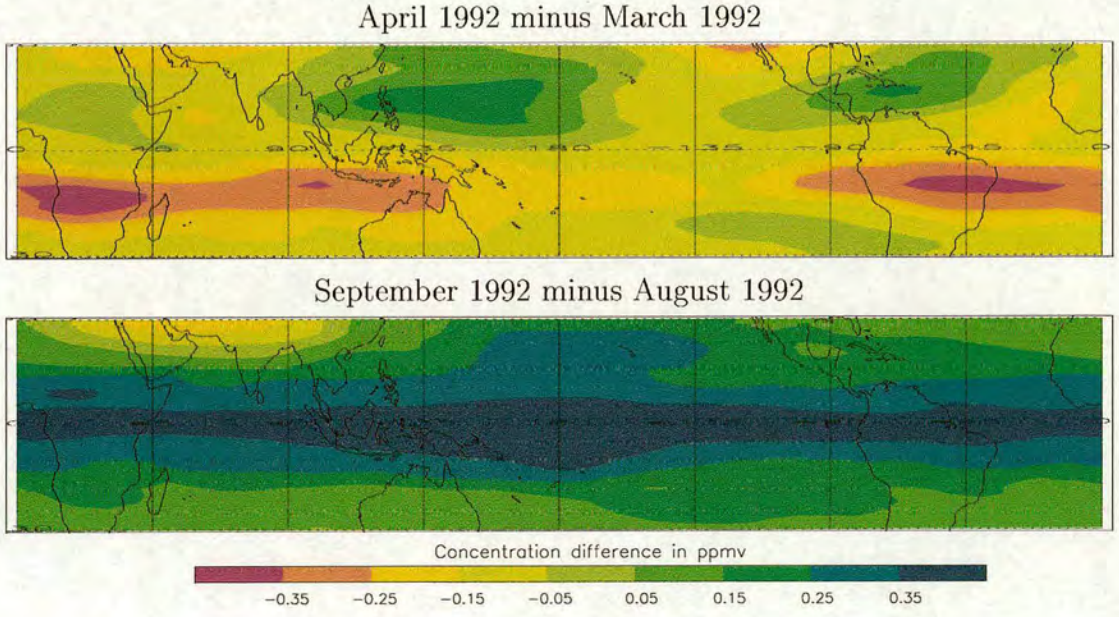

Figure 4.3: **Change in Monthly-Averaged Water-Vapour at 68·1 hPa.** Shows the difference in the monthly-averaged maps of figure 4.1. The top panel shows the April 1992 data minus the March 1992 data and the bottom panel September 1992 minus August 1992.

Though the equatorial water-vapour distribution loses longitudinal variation in

August 1992, the appearance of relatively moist air over India at that time still marks a "possible stratospheric-fountain". The five-day-average maps of the next section will show a developing area of relatively moist air that appears to spread away from the region of the Asian monsoon. Though this is a weaker case for a stratospheric fountain than that of the northern springtime since the greatest areas of change in mixing ratio between August and September 1992 occurred near the equator, it is considered for completeness.

By November 1992 the highest monthly mean values of the year occur, just as they did in the November of the previous year. These highest values occur in the northern hemisphere, where the greatest change from the October mixing ratios can also be observed. At 68·1 hPa the northern hemisphere shows a tendency to lead the changes in water vapour, changing from drying to moistening earlier in the year than the southern hemisphere. Furthermore, the November mixing ratios are the highest in the north and the March to May mixing ratios are the lowest in the north. Thus the northern hemisphere also exhibits a greater range of mixing ratios than its southern counterpart.

Four interyear differences can be appreciated by comparing the panels for December 1992 to March 1993 with the respective panels corresponding to one year previous. Firstly, the position of the minimum in the water vapour mixing ratio features is closer to Indonesia in 1993 than in 1992. Secondly, mixing ratios are generally lower in November and December 1992 than those months in the previous year. Thirdly, mixing ratios are generally higher between January and March 1993 than those months in the previous year. Finally, in 1993 the water vapour distribution is less band-like than in corresponding months of 1992.

Changes in the QBO or the ENSO can explain the first three of these four differences. Table 4.1 shows the state of the QBO and the ENSO for the lifetime of the MLS, 183 GHz antenna. In the table winter is taken to be January, February and March; spring to be April, May and June; summer to be July, August and September; autumn to be October, November and December. Under the wave-driven motion of the stratosphere air passes from 100 hPa (approximately the tropopause) to 68 hPa in around one month (Mote *et al.*, 1996, 1998). Therefore, it is appropriate

to examine 68 hPa data for January, February and March when investigating the cross-tropopause motion of the northern winter months; April, May and June for northern spring and so on.

Northern Hemisphere Season		QBO	ENSO
1991	Autumn	Westerly	Moderate warm
1992	Winter	Easterly	Strong warm
	Spring	Easterly	Strong warm
	Summer	Easterly	Weak warm
	Autumn	Easterly	Weak warm
1993	Winter	Westerly	Weak warm
	Spring	Westerly	Moderate warm

Table 4.1: **Phases of the QBO and ENSO — Inter-Season Comparison.** Shows whether the QBO exhibited westerly or easterly winds at 68·1 hPa and the relative strength of the El Niño as a function of season for the MLS, 183 GHz antenna lifetime. (There were no La Niña events during this time.) The QBO direction is that which occurred for the majority of each season. The QBO data is determined using data from the Singapore radiosonde station and the ENSO event is as reported by for Environmental Prediction (2002). Winter indicates the months January, February and March; spring — April, May and June; summer — July, August and September; autumn — October, November and December (see text for details).

Assuming a rapid, convection-dominated vertical-motion connects the cold-point tropopause and the 68·1 hPa level then variation in the horizontal position of the "fountain" should be consistent with changes in the ENSO. Figure 4.1 shows that this is the case for January and March. In 1992 the lowest mixing ratios seen in both months occur further from Indonesia than in 1993, consistent with a weakening ENSO in the latter year and convection returning westward.

Other inter-year differences do not appear connected to changes in the ENSO. The distribution of convection in the ENSO cycle always has longitudinal variations. Therefore the change from a band-like, water-vapour distribution to a more-patchy distribution seems unrelated to the ENSO phase.

Unless the QBO changed from being longitudinally invariant to longitudinally variant from one year to the next, it is also not likely to be responsible for this inter-year

difference. However, QBO-induced changes in the tropopause height† can explain the yearly difference in zonal mean mixing ratio. Westerly shear gives rise to decreased stratospheric uplift and increased tropopause temperatures. Easterly shear gives rise to increased stratospheric uplift and decreased tropopause temperatures. Thus under the influence of the QBO it is expected that autumn 1992 easterly conditions would give rise to lower mixing ratios than the autumn 1991 westerlies. Furthermore, it would similarly be expected that the winter 1992 easterly conditions would give rise to lower mixing ratios than the winter 1993 westerlies. Both of these conditions can be observed in figure 4.1.

That this inter-year difference is truly a function of the QBO can be further appreciated from figure 4.4, which comprises figures 3a and 2a of Gray and Russell III (1999), showing potential temperature versus time water-vapour cross-sections for the winters of 1992 and 1993. The top panel shows the easterlies of January and February 1992 and a water vapour minimum of less than 3·0 ppmv. The bottom panel shows the westerlies of January and February 1993 and a water vapour minimum of greater than 3·2 ppmv.

4.1.2 Five-Day-Averaged, MLS Water-Vapour

The low mixing-ratios seen on the March and April 1992 plots of the previous section are the result of the highest, cold-point tropopause. In the case of both months the lowest mixing-ratios are seen to spread across most of the equatorial region. Five-day-average maps of water-vapour mixing-ratios show that these equatorial patterns develop through both months, possibly as the result of an Indonesian fountain. Such maps, spanning March and April of 1992, are shown in figure 4.5.

The 2·9–3·0 ppmv contour can be seen only over the Pacific Warm Pool at the beginning of March. After this time it develops first eastward across the Pacific then, towards the end of March, westward across the Indian Ocean. During April the 2·9–3·0 ppmv contour connects across the Atlantic to cover the entire equatorial circle.

†See section 2.1.2 — Quasi-Biennial Oscillation.

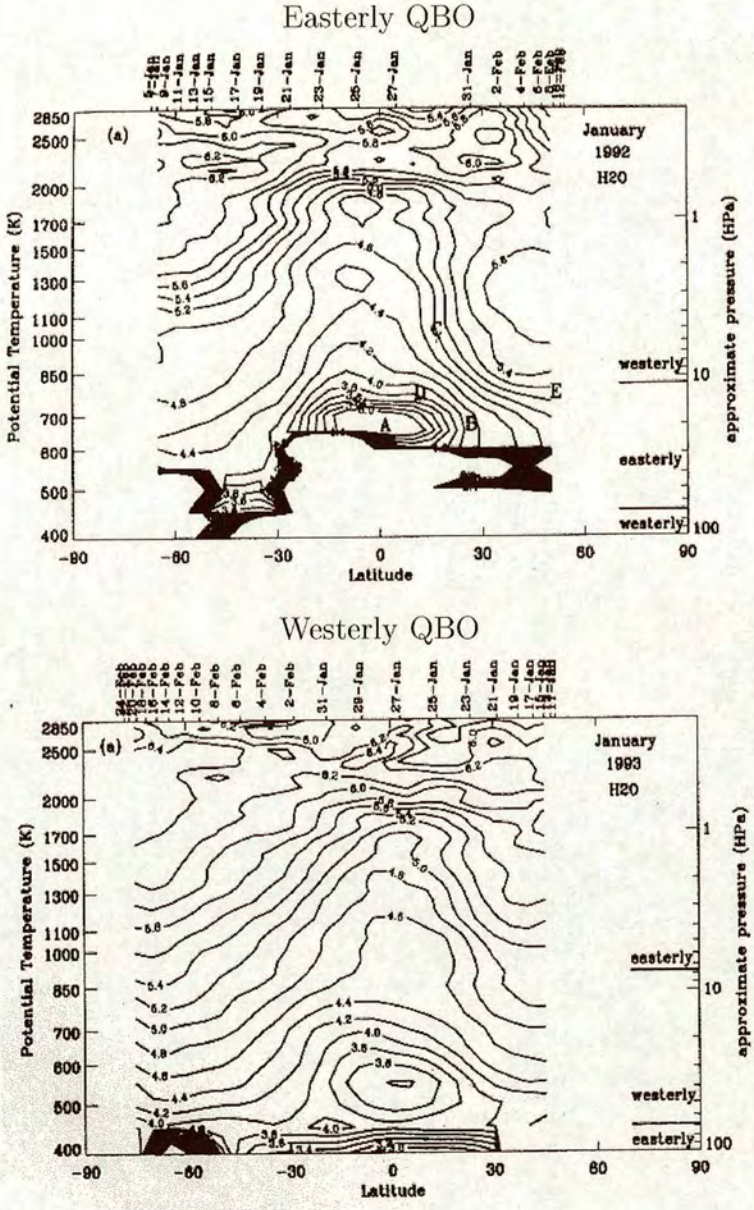

Figure 4.4: **QBO Effects on Lower Stratospheric Water Vapour.** As figures 3a and 2a of Gray and Russell III (1999), pages 981 and 980. Shows latitude versus potential temperature cross sections of zonally-averaged HALOE water vapour (ppmv). Top panel: sunset observations from 5^{th} January 1992 to 13^{th} February 1992. Bottom panel: sunrise observations from 10^{th} January 1992 to 25^{th} February 1992. Contour interval is 0·2 ppmv. Negative latitudes are south. The direction of the Singapore equatorial winds is also marked.

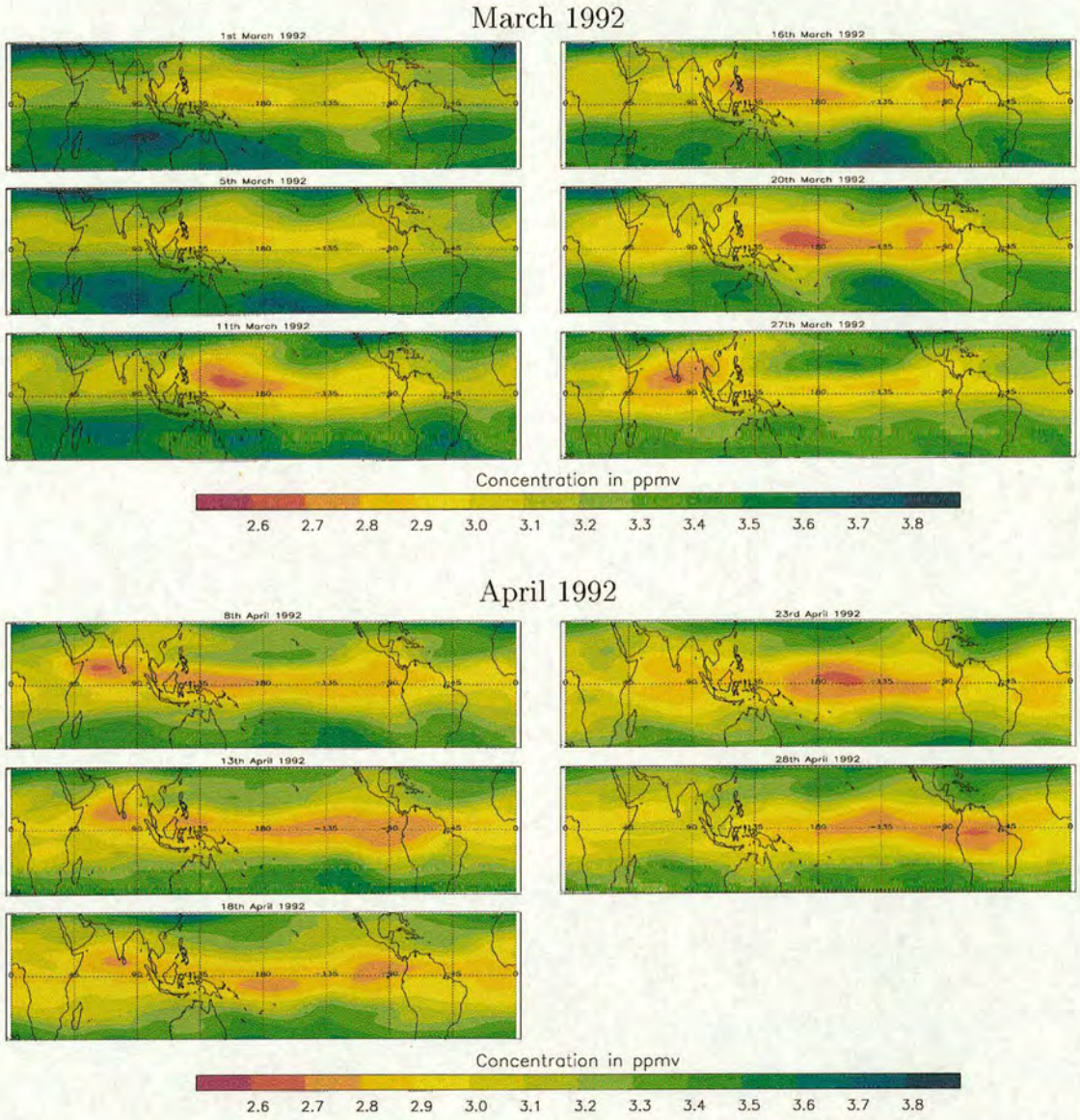

Figure 4.5: **MLS-Observed Water-Vapour for March and April 1992.** Shows the observed evolution of the five-day-averaged, MLS, version 0104 water-vapour at 68·1 hPa.

The developments of the lowest mixing-ratio contours (those of 2·8 ppmv and less) also begin over, and spread from, Indonesia. Though these contours never span the entire equatorial circle, their progress could still be explained by an Indonesian fountain that spreads relatively dry air out across the Pacific to Panama. This development occurs in March then repeats in April, the lowest mixing ratios having

almost vanished at the end of March.

The only interruption to this development is the appearance of a relatively high mixing-ratio feature near Hawaii on 27^{th} March. This feature occurs simultaneously with the disappearance of most of the very low (2·8 ppmv and less) mixing-ratios and may indicate that vertical motions other than a "fountain" were present at this time.

The northern-summertime fountains were suggested to occur over the Asian monsoon (Newell and Gould-Stewart, 1981). Figure 4.6 shows five-day-average maps of MLS water-vapour for August 1992.

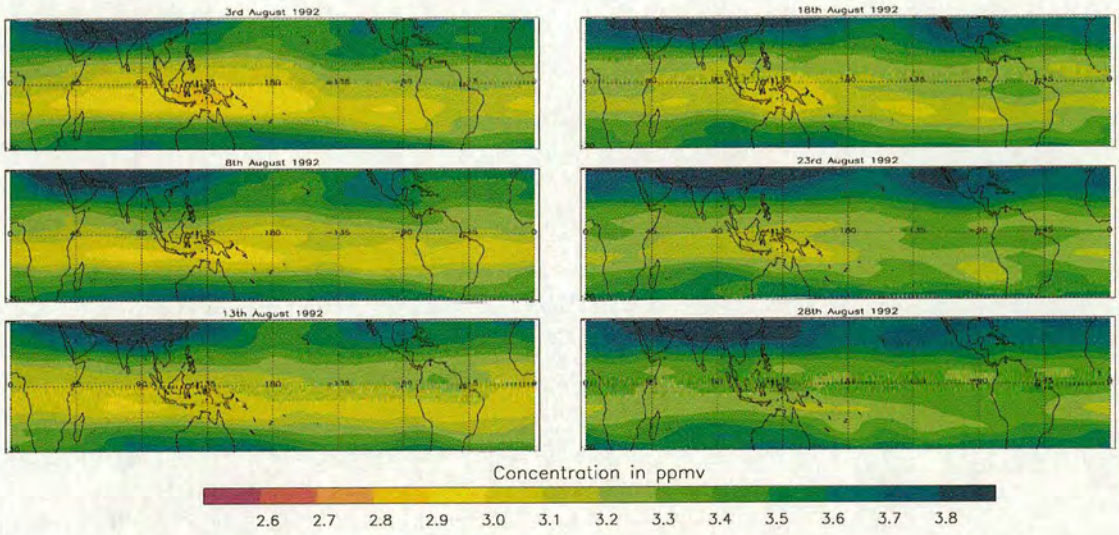

Figure 4.6: **MLS-Observed Water-Vapour for August 1992.** Shows the observed evolution of the five-day-averaged, MLS, version 0104 water-vapour at 68·1 hPa.

In figure 4.6 the Asian monsoon is marked by relatively moist air, consistent with the suggestion of Dethof *et al.* (1999) that the Asian monsoon hydrates the stratosphere. Nevertheless, this does not mean that the August development is inconsistent with the *fountain hypothesis*, since the lower stratosphere is expected to increase in water vapour whilst the tropopause is falling and warming. The injection of water vapour filling the equatorial dry area that formed during the previous springtime may have spread from the monsoon region during August.

4.2 UKMO Winds

Figure 4.7 shows three seasons' worth of UKMO zonal and meridional winds as an example of those data that were used to create the advection plots that are presented in the following sections. The panels are created in the same manner as was used for the UKMO winds of figure 3.3, with the UKMO analyses interpolated to the location of the Changi Airport radiosonde in Singapore. Note that the height range used differs between the figures however; figure 4.7 concentrates on the stratosphere and tropical tropopause layer.

The phase of the QBO, as indicated in table 4.1, can be appreciated from this figure. The westerlies of the previous year are still just visible above 100 hPa at the start of 1992 (top, zonal-wind panel). These winds are gradually replaced by descending easterlies throughout the year (middle zonal-wind panel), easterlies which are, in turn, replaced by westerlies in 1993 (bottom zonal-wind panel).

Consideration of this figure suggests that a possible increase in vertical interpolation errors might occur at times when the winds are changing from easterly to westerly at the 68 hPa level. Hence extra care is needed when interpreting trajectory results for these time periods. In the case of the monthly-averaged data however, the averaging period should reduce this problem. In the case of five-day-average data, the months examined fall well within the easterly regime at 68 hPa, thus avoiding the problem entirely.

4.3 Fountains

In the following section the water vapour and wind data discussed above are combined; each of the three "possible stratospheric-fountains" identified in the five-day-averaged, MLS water-vapour are examined using isentropic advections. In each case (March, April and August) water vapour on an appropriate isentrope is compared to an "after-advection" plot. From these two evolutions, difference plots are then created to highlight existing differences.

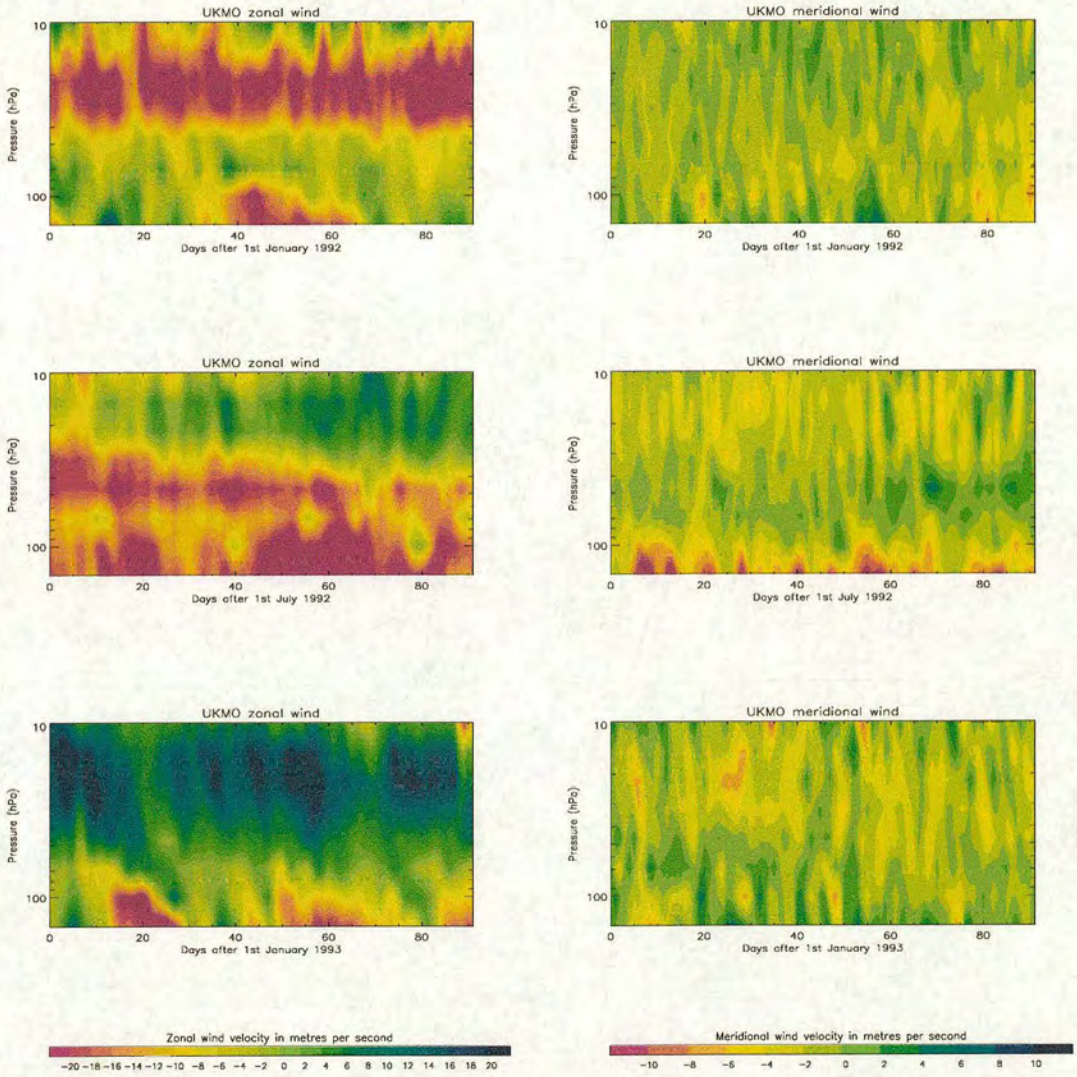

Figure 4.7: **Examples of UKMO Analyses Winds for 1992 and 1993.** Shows timeseries of the zonal (westerly) and meridional (southerly) winds of the assimilated data from the United Kingdom Meteorological Office. The data have been linearly interpolated to the location of the Changi Airport radiosonde in Singapore — 103·98 °E, 1·36 °N. All panel s cover the height range of the TTL and lower stratosphere — 150 to 10 hPa. The top panels cover the days from 1^{st} January 1992 to 31^{st} March 1992. The middle panels cover the days from 1^{st} July 1992 to 30^{th} September 1992. The bottom panels cover the days from the 1^{st} January 1993 to 31^{st} March 1993.

4.3.1 March Fountain — Indonesia

Figure 4.8 shows pentads of MLS-observed and isentropically-advected water-vapour mixing-ratios spanning March 1992. All maps show water vapour upon the 435 K isentrope. The after-advection maps show the date upon which the ten-day advections ended, thus the observed and advected panels can be directly compared.

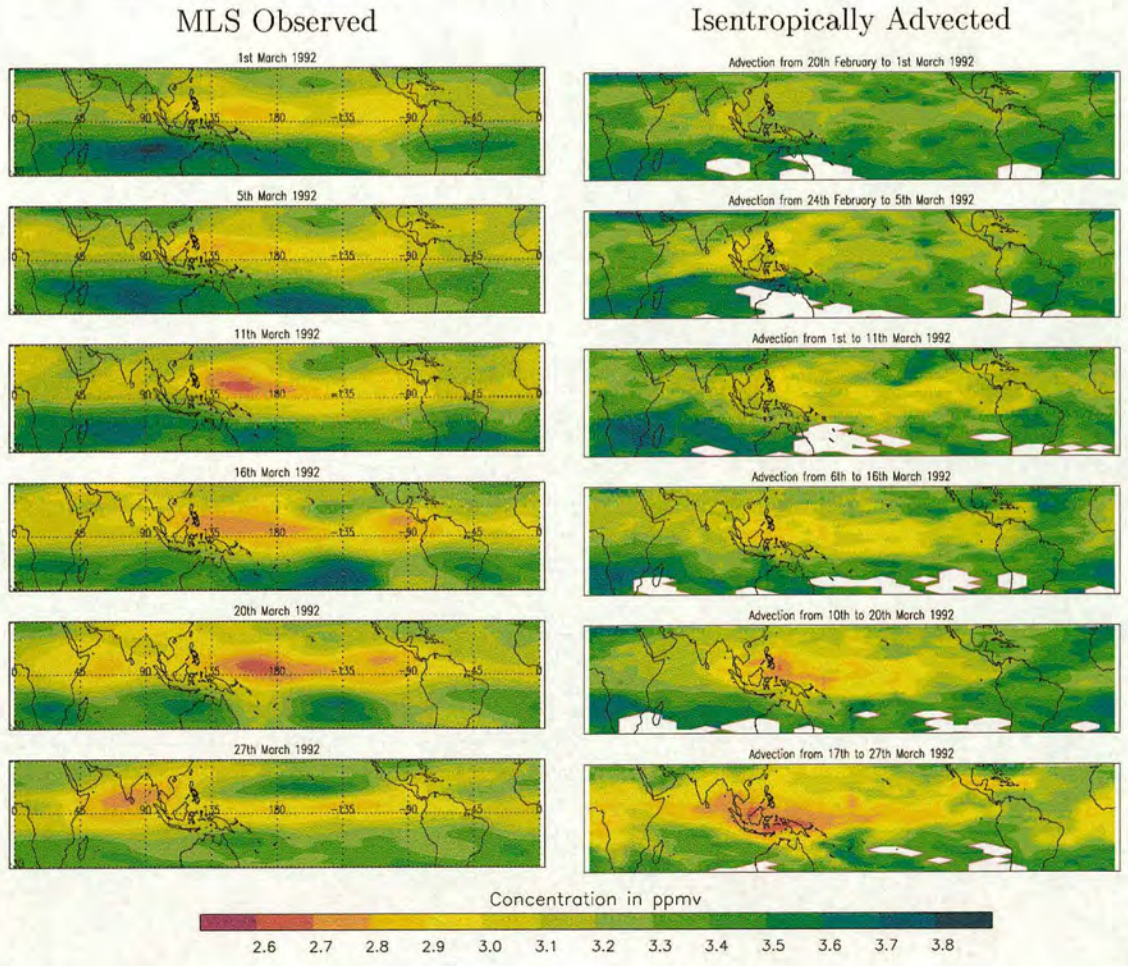

Figure 4.8: **MLS-Observed and Isentropically-Advected H_2O for March 1992.** Shows the observed (left) and ten-day-advected (right) evolutions of the five-day-averaged, MLS, v0104 water-vapour field upon the 435 K isentrope. The advections end on the marked days and so can be directly compared to the corresponding observed maps. White-space on the advection plot indicates that, for at least three of the days in the average, parcels were brought in from outside the field of view of the MLS instrument.

The two evolutions are dissimilar. The easterly QBO-winds (see table 4.1) present throughout 1992 advect the equatorial features westward. Hence, no significant feature bounded by the 2·8 ppmv contour is ever isentropically advected to the eastern Pacific or Panama from Indonesia or the Pacific Warm Pool.

Though the water vapour fields ten days prior to the isentropic advections (the fields from which the advections are created) are not shown, their make up can be appreciated from nearby days shown on the left-hand side of figure 4.8[†]. A pentad for the 17^{th} March would not be dissimilar to that shown for the 16^{th} March. Thus it can be appreciated that the advection has caused only minor changes to the water vapour distribution, changes that do not appear to account for most of the deep-tropical distribution of the 27^{th} March.

Two clear examples of this failure can be seen when comparing the data for the 27^{th} March in figure 4.8 — the feature centred upon the southern tip of India and the feature near Hawaii. Both are larger than the error length-scales given in tables 3.3 and 3.4 and could be believably represented by the isentropic advection. Neither, however, are seen in the final after-advection plot. Furthermore, the MLS-observed data for 27^{th} March suggest that, upon the 435 K surface, the majority of tropical regions exhibit water-vapour mixing-ratios of greater than 2·8 ppmv.

If the *fountain hypothesis* were correct in that there was a single location at which air reaches the 68·1 hPa level, then the evolution of the observed flow and of the estimated isentropic-flow should be similar except in that region. The maps for March 1992 thus imply that isentropic advection cannot alone explain the evolution of water vapour at 68·1 hPa during this time. Furthermore, the widespread dissimilarity implies that vertical motions are common throughout the whole tropical region. This is supported by figure 4.9, which shows the difference between the MLS-observed and isentropically-advected water vapour fields presented in figure 4.8.

Where the difference plot shows a positive value the isentropic advection did not

[†]The dates used to create the pentads are defined by the availability of data for pentads at the beginning and end of the advection.

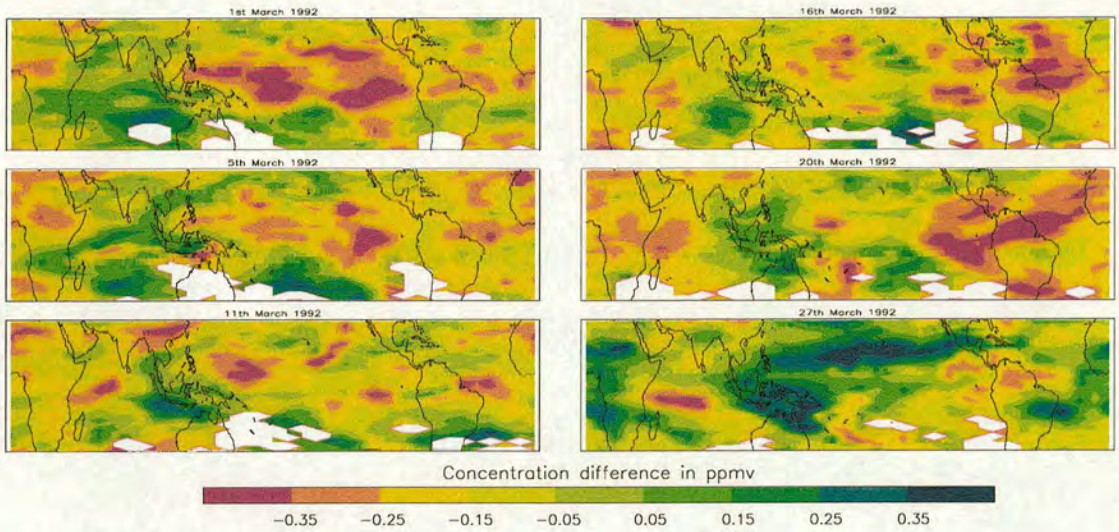

Figure 4.9: **Observed − Isentropically-Advected H_2O Fields for March 1992.** Shows the change due to all non-isentropic-advection processes that occurred during the ten days up to the dates marked in March 1992 on the 435 K isentrope. White-space indicates that during creation of the advection plot parcels were brought in from outside the field of view of the MLS instrument for at least three of the days in the average. A negative difference indicates dry air was brought to the surface, which at this time of year must have come from below. Positive differences indicate wetter air arrived from above.

bring as much water vapour to the area as was observed to arrive. Where the plot shows a negative value the isentropic advection brought more water vapour to the area than was observed to arrive. Where the difference approaches zero, isentropic advection is capable of explaining the evolution alone. In this latter case however, it is not certain that there was no vertical motion across the isentrope, since diabatic and isentropic winds may have each brought air to the region with the same water-vapour mixing-ratios. It should also be noted, for all cases, that nothing can be inferred about the strength of the vertical flow, only its duration, as water vapour concentrations will have been defined by processes occurring below 435 K; the concentrations are not a function of flow strength.

Nevertheless, figure 4.9 does suggest where vertical flows have crossed the 435 K surface during March 1992 and, by consideration of the vertical water-vapour profile, the figure can also be used to indicate the direction of the flow. During the northern

winter and spring falling tropopause temperatures will cause water vapour mixing ratios to increase with height in the lower stratosphere. Hence, at these times, positive evolution differences will imply air falling from above and negative differences air rising from below. During the northern summer and autumn the opposite will occur giving decreasing mixing ratios with height. In this case positive evolution differences will imply rising air and negative differences falling air. The exact times of the change between two cases will vary between years and the effect of the QBO on tropopause temperatures.

March lies well within the winter-spring period. Hence, except on the 27^{th}, uplift can be inferred to have occurred throughout most of the tropical region. Only above Indonesia, Australia, the Indian Ocean and the southwestern tropical-Pacific can believable downflow be inferred. On the 27^{th} March the believable downfall spreads further, covering the region of anomalous moistening over Hawaii seen in figure 4.8. Though the presence of whitespace in figures 4.8 and 4.9 does indicate clear isentropic advection into the tropics, vertical motions must also have been prevalent there during March 1992.

Significance

Since the differences between the observed and isentropically-advected evolutions are relatively small (for example, considering differences of 0·2 ppmv in figure 4.9 compared to the 2·8 ppmv concentrations of figure 4.8) the significance of the difference contours was examined. By considering a random distribution of observed and advected mixing ratios, with the same standard deviations as occurred in the maps created, the probability of a gridpoint exhibiting difference values of each chosen contour, relative to the mean difference, was determined. The results as a function of month are presented in table 4.2.

Difference values at or above 0·15 ppmv are always more than 99 % significant and, for the most part, values at or below -0·15 ppmv are equally as reliable. The significance of values between -0·15 ppmv and 0·15 ppmv are not usually so high however. Nevertheless, it was always possible to work to a confidence level of at

Month		Contour value, ppmv			Month		Contour value, ppmv		
		-0·15	-0·05	0·05			-0·15	-0·05	0·05
1991	Dec	98	73	>99	1992	Sep	>99	>99	58
1992	Jan	95	90	>99		Oct	>99	96	73
	Feb	99	66	>99		Nov	>99	88	93
	Mar	92	88	>99		Dec	>99	58	>99
	Apr	>99	50	>99	1993	Jan	>99	62	>99
	May	>99	79	93		Feb	>99	54	>99
	Aug	>99	>99	73		Mar	>99	58	>99

Table 4.2: **Significance of Difference Contours.** Shows the one-tailed significance of four contour values used in creating maps of the difference between observed and isentropically-advected evolutions of water vapour. Percentages are given for each whole month of the MLS instrument's 183 GHz antenna lifetime. Other contours all have significances higher than 99·9 %.

least 92 % if only considering difference values lying outside the -0·15 ppmv and 0·15 ppmv limits.

This consideration does not, therefore, change the conclusions drawn for March 1992. Significant uplift can be seen throughout most areas of the tropics and significant downfall can be seen over Indonesia and the Indian Ocean during most of March. The downfall over Indonesia and Hawaii shown by the difference pentad for the 27^{th} March also remains significant.

4.3.2 April Fountain — Indonesia

Figure 4.10 shows the difference between MLS-observed and isentropically-advected water-vapour fields for five pentads spanning April 1992. The evolution differences of April 1992 indicate vertical motions of the same directions as can be inferred from the March 1992 differences. Vertical-motions inferred from figure 4.10 can be compared to the April, MLS-observed, water-vapour features of figure 4.5.

The April differences are similar to the March differences. Significant uplift across the 435 K surface can be inferred to have occurred throughout much of the tropical region, frequently so over the Pacific, South America and parts of Africa. Significant downfall across the isentrope also occurs near Nouvelle Calédonie, Fiji, Tahiti and

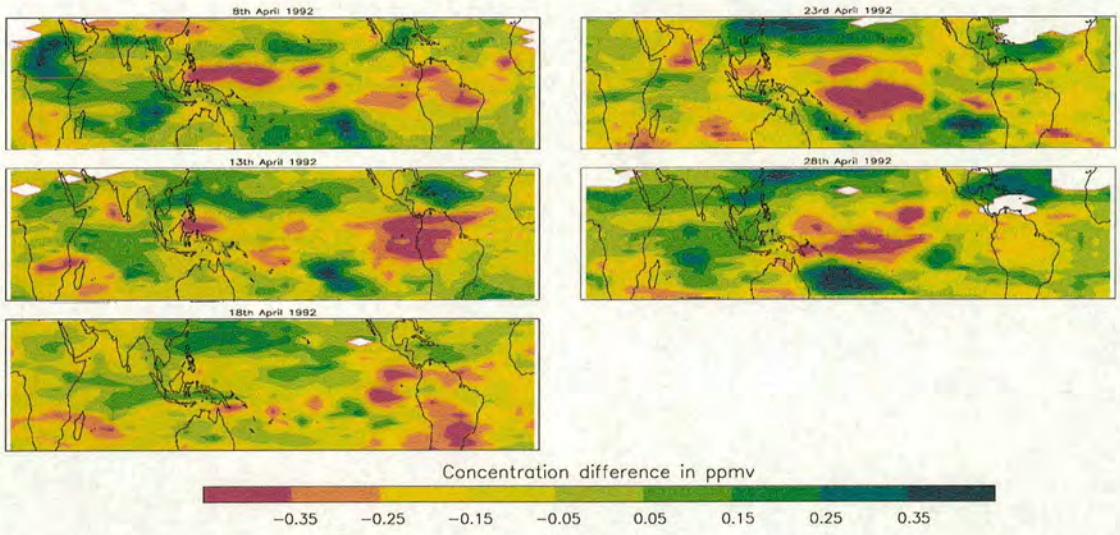

Figure 4.10: **Observed − Isentropically-Advected H_2O Fields for April 1992.** Shows the change due to all non-isentropic-advection processes that occurred during the ten days up to the dates marked in April 1992 on the 435 K isentrope. White-space indicates that during creation of the advection plot parcels were brought in from outside the field of view of the MLS instrument for at least three of the days in the average. A negative difference indicates dry air was brought to the surface, which at this time of year must have come from below. Positive differences indicate wetter air arrived from above.

the Indian Ocean, as occurred during March 1992.

Some dissimilarities between the March and April 1992 cases can be seen. Towards the end of April the Caribbean region sees significant downfall, as opposed to the uplift present there throughout March. A reversal in the flow direction between the two months also occurred over Indonesia, which, in April, frequently sees uplift. This latter change could be attributed to lessening convection there as the northern-winter conditions subside. Seeing as convection is thought to be responsible for causing the widespread descent over Indonesia during the northern winter (Sherwood, 2000; Gettelman *et al.*, 2002) then a reversion to the standard stratospheric conditions after the period of strong convection would be expected.

Direction aside, it is still clear that significant vertical motions existed outside the Indonesia region during April as well as March 1992, the "possible fountain" region of both months. Therefore the *fountain hypothesis* does not appear to hold for either

month, since isentropic advection cannot alone explain the evolution of water vapour on isentropes near 68·1 hPa.

Vertical Motions Throughout the Tropics

It can be inferred that some of the vertical flows identified as crossing the 435 K isentrope must be part of a connection between the tropopause and 68·1hPa comprising a motion faster than the "tape recorder" signal. If such a rapid connection did not exist, then the clear longitudinal variation in the water-vapour distribution at 68·1 hPa could not be present. However, the exact nature and distribution of the connection cannot be determined from the advection analysis presented above. Even assuming that the majority of the observed descent occurs above the strongest convection (Sherwood, 2000; Gettelman *et al.*, 2002) there are still two possibilities for stratospheric uplift — one comprising a uniform stratospheric-uplift, the other comprising an uplift with longitudinal variations.

If the stratospheric uplift were uniform across the tropics then the 68·1hPa, water-vapour distributions would have to have been imposed at a lower level, most probably by variations in the tropopause height. If the vertical motions were uneven in time or space however, then the water-vapour distribution could equally be the result of an even tropopause as one with a varying height. In the case of uneven uplift, the March and April distributions could have resulted from sequential uplift above Indonesia, Central America and then the Pacific.

Figure 6 of Seidel *et al.* (2001), reproduced here in figure 4.11[†], shows the average height of the lapse-rate tropopause as determined by radiosonde data for the years 1961–1990. Comparison of this figure with the monthly-average, water-vapour distributions of figure 4.1 does reveals some similarity.

In both figures the January and April distributions exhibit longitudinal variations and in both figures the October distributions approach a more zonally-symmetric pattern. This lends some credence to the suggestion that the 68·1 hPa water vapour features are the function of a tropopause-defined distribution preserved by rapid

[†]Also shown in figure 2.10.

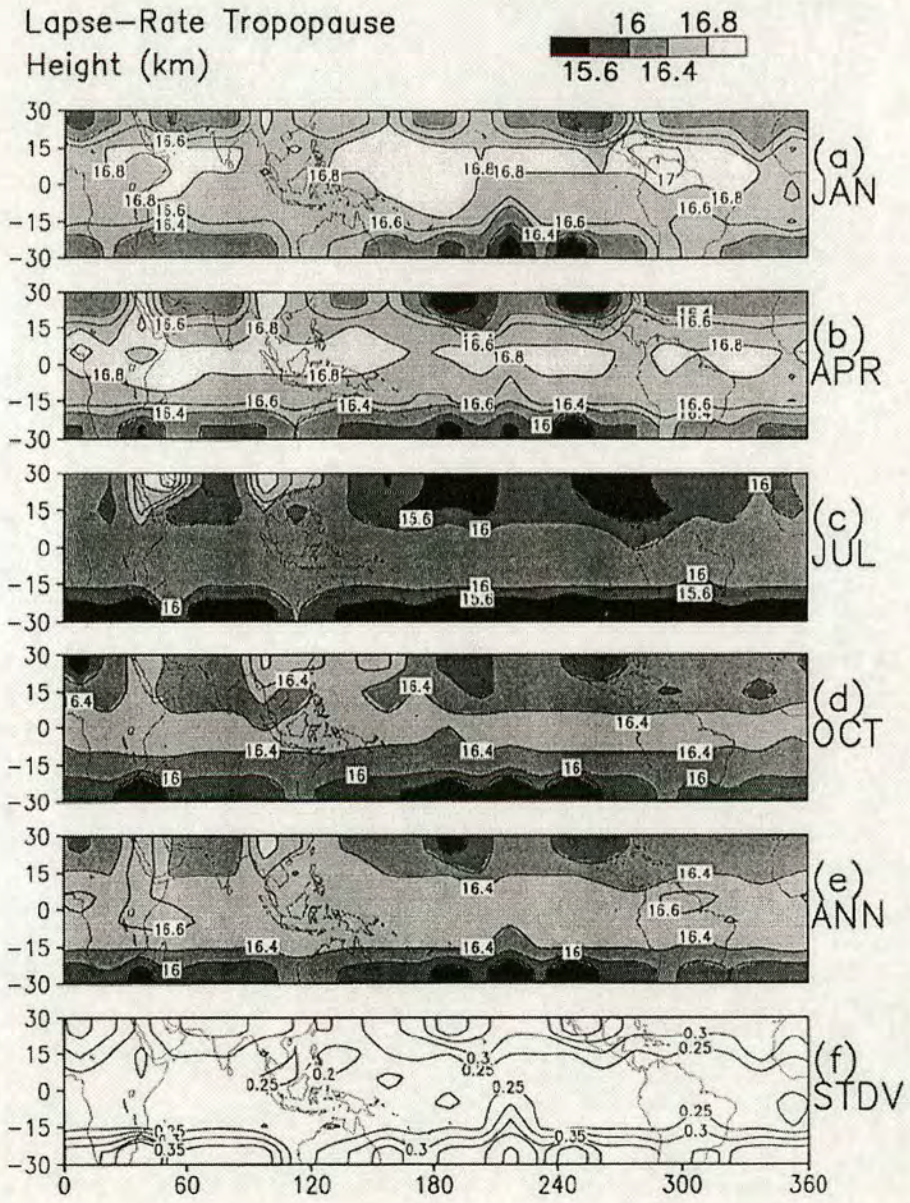

Figure 4.11: **Climatological Mean Height of the Lapse-Rate Tropopause.** As figure 6 of Seidel *et al.* (2001), page 7864. Shows the climatological mean height of the lapse-rate tropopause in kilometres based on 0000 and 1200 UTC radiosonde data for 1961–1990. Panels (a)–(d) are averages for four months of the year, panel (e) is an annual mean. Contours on panels (a)–(e) are every 0·4 km; additional contours are shown at 16·6 and 17·0 km. Panel (f) shows the inter-annual standard deviation of the individual annual means about the long-term annual means.

uplift through the lower stratosphere before being destroyed by horizontal motions. Though the observed patterns could be the result of a differential stratospheric

uplift, given the basic similarity of the distributions of figures 4.1 and 4.11, the simplest explanation would comprise a rapid, even uplift that preserved a water-vapour distribution established at the tropopause.

It would be possible to correlate the positions of the minimum water vapour with the height of the cold-point tropopause. However, the three-dimensional trajectory study presented in the next chapter seemed a much more worthy examination of lower stratospheric airflows, especially as they determine the vertical speed of air particles in the lower stratosphere.

4.3.3 August Fountain — Asian Monsoon

Figure 4.12 shows the difference between MLS-observed and isentropically-advected water-vapour fields for five pentads spanning August 1992. The vertical motions inferable from this plot can be compared to the August, MLS-observed, water-

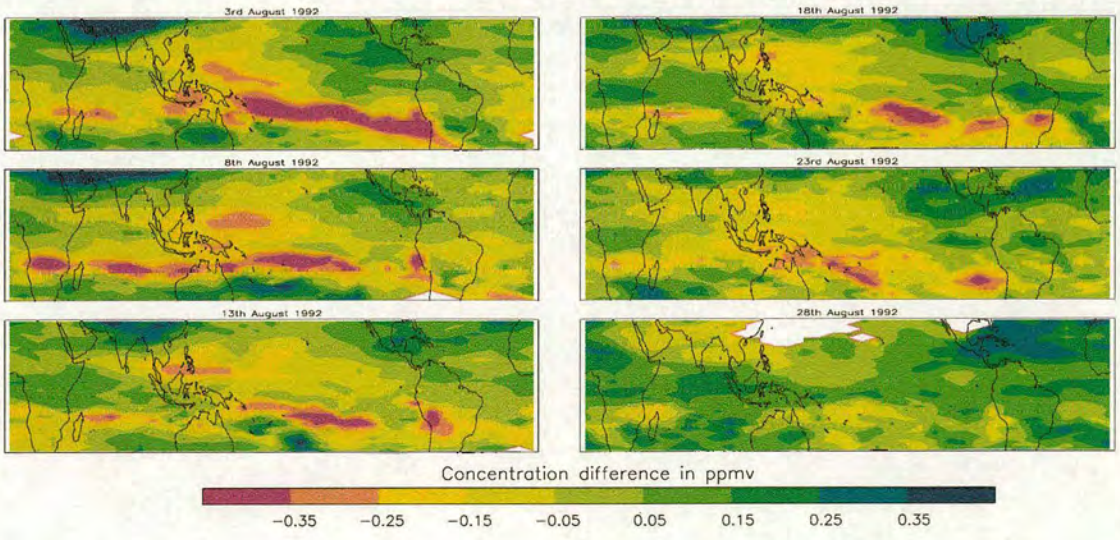

Figure 4.12: **Observed − Isentropically-Advected H_2O Fields for August 1992.** Shows the change due to all non-isentropic-advection processes that occurred during the ten days up to the dates marked in August 1992 on the 450 K isentrope. White-space indicates that during creation of the advection plot parcels were brought in from outside the field of view of the MLS instrument for at least three of the days in the average.

vapour features of figure 4.6. The fountain theory of Newell and Gould-Stewart (1981) suggests that entry into the stratosphere at this time of year occurs over the Asian monsoon.

The direction of the vertical motions implied by these August differences are difficult to interpret, since a change in the sign of the difference above the Asian monsoon can be observed mid-month. Since there is no reason to believe that the direction of the vertical motion above the monsoon changes throughout its lifetime between May and November it seems more likely that a change in the direction of the vertical motion implied by the sign of the differences occurs instead. This is substantiated by figure 2.9, which shows that the mean mixing ratio upon entry to the stratosphere reaches a peak in August. Thus rising air could be implied from positive differences at the start of August and from negative differences towards the end of August.

For the purposes of this section however, the direction of the flow is irrelevant. Irrespective of direction, significant vertical motion (indicated by differences less than -0·05 and greater than 0·15 ppmv in figure 4.12) can still be inferred to have frequently crossed the 450 K isentrope over the Pacific, the Indian Ocean and Asia during August 1992. Though isentropic advection *may* be able to explain the change in water-vapour over much of tropics in August 1992[†], vertical motions are not confined to the area of strongest, northern-summertime convection — above the Asian monsoon. Hence, the *fountain hypothesis* does not hold for August 1992.

4.3.4 Possible Stratospheric Fountains

The *fountain hypothesis* did not hold under the advection analysis of MLS, water-vapour data for the months of March, April and August 1992. Neither of the two regions proposed by Newell and Gould-Stewart (1981) — Indonesia in the northern winter and India in the northern summer, were the only source of vertical motions in the lower stratosphere from which quasi-isentropic motions might supply air to the remaining tropics. Furthermore, vertical motions were shown to be common in August and prevalent in March and April throughout the tropical region.

[†]This is not substantiable because zero difference in figure 4.12 cannot be considered significant.

4.4 Implied Vertical Motions

Both updraughts and downdraughts cross the isentropes near 68·1 hPa throughout the year and, though none of the motions persist uninterrupted for whole months at a time, regions with a clear net flow can be inferred from monthly-averaged, evolution-difference plots. Figure 4.13 shows the monthly-averaged, ten-day difference between the observed and isentropically-advected evolutions of water vapour on isentropes near 68·1 hPa. The isentropes used for each month are those discussed in section 3.3.2. The maps of figure 4.13 are constructed to allow inferences to be made concerning vertical motions near the top of the tropical tropopause layer, requiring the use of different isentropes throughout the year. As such, no inter-month comparison is drawn.

Throughout December 1991 to April 1992 negative differences indicate air rising to the surface from below and positive differences air falling from above. It can therefore be inferred, to a confidence level of 73 %[†], that during December 1991 there was a widespread uplift across most of the tropics. More-significant uplift occurred over the northwestern tropical-Pacific and over the Americas. A more-significant, net downflow during the same month can be inferred to have occurred over central Africa and Indonesia, though the feature over the latter is only just large enough to be believable given trajectory errors (see section 3.3.4).

The overall extent of the uplift decreases between December 1991 and April 1992 but is always present and significant over the west coasts of Central and South America and over parts of the Pacific and Asia. During January and March even the -0·05 ppmv difference contour is very significant (88 % or higher). This allows good confidence to be had in the fact that tropical uplift is so widespread throughout the northern winter, with significant downdraughts being confined to southern Africa, Madagascar, Tahiti and Indonesia and its neighbouring islands. The downflow is not prevalent before March 1992 but, during this month and April 1992, there is significant downflow over the northwestern tropical-Pacific, the Caribbean and most of the tropics poleward of 10°S.

[†]See table 4.2.

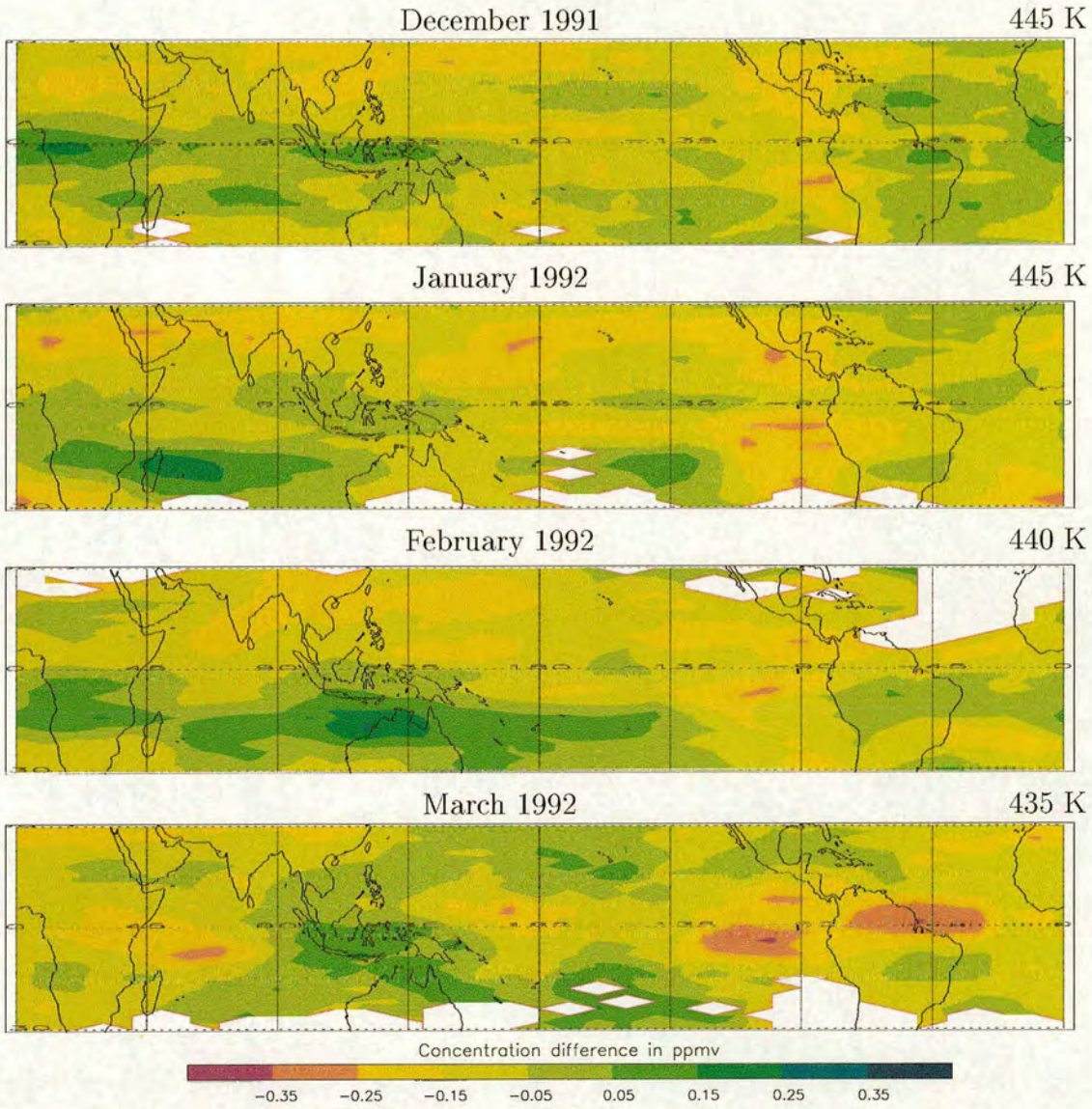

Figure 4.13: **Monthly-Averaged, Observed − Isentropically-Advected, H_2O Fields.** Shows the average change over ten days due to all non-isentropic-advection processes for the months indicated. Each map is constructed by subtracting the ten-day, isentropically-advected evolution from the observed data for evolutions ending on each day of the month and then performing an average. Water vapour data is from the MLS version 0104 retrieval. The same months are considered as were used in figure 4.1 except November 1991. This month required ten days of data from October 1991 to complete an advected evolution, these days were not available.

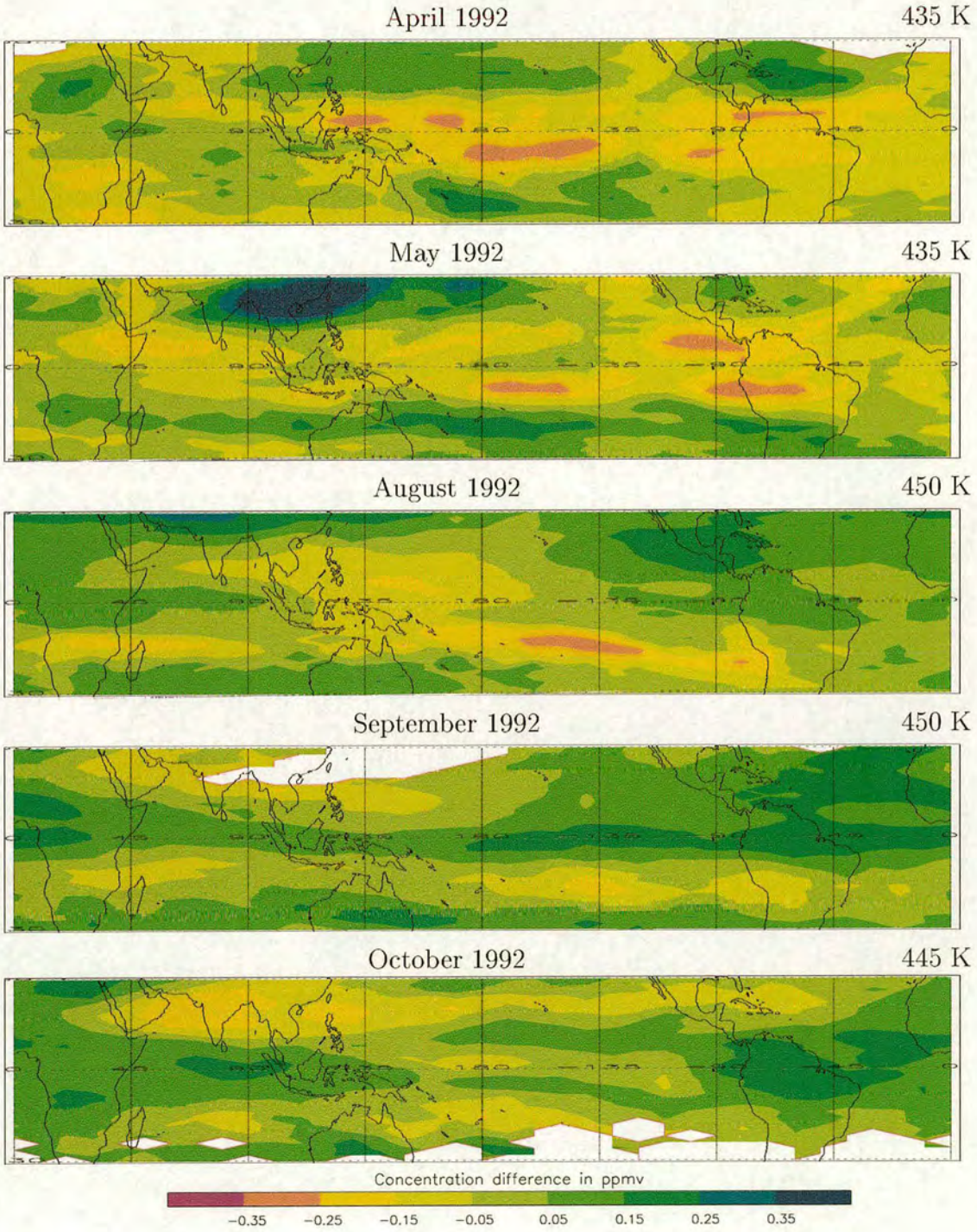

Figure 4.13: **Monthly-Averaged, Observed − Isentropically-Advected, H_2O Fields.** Continued from the previous page.

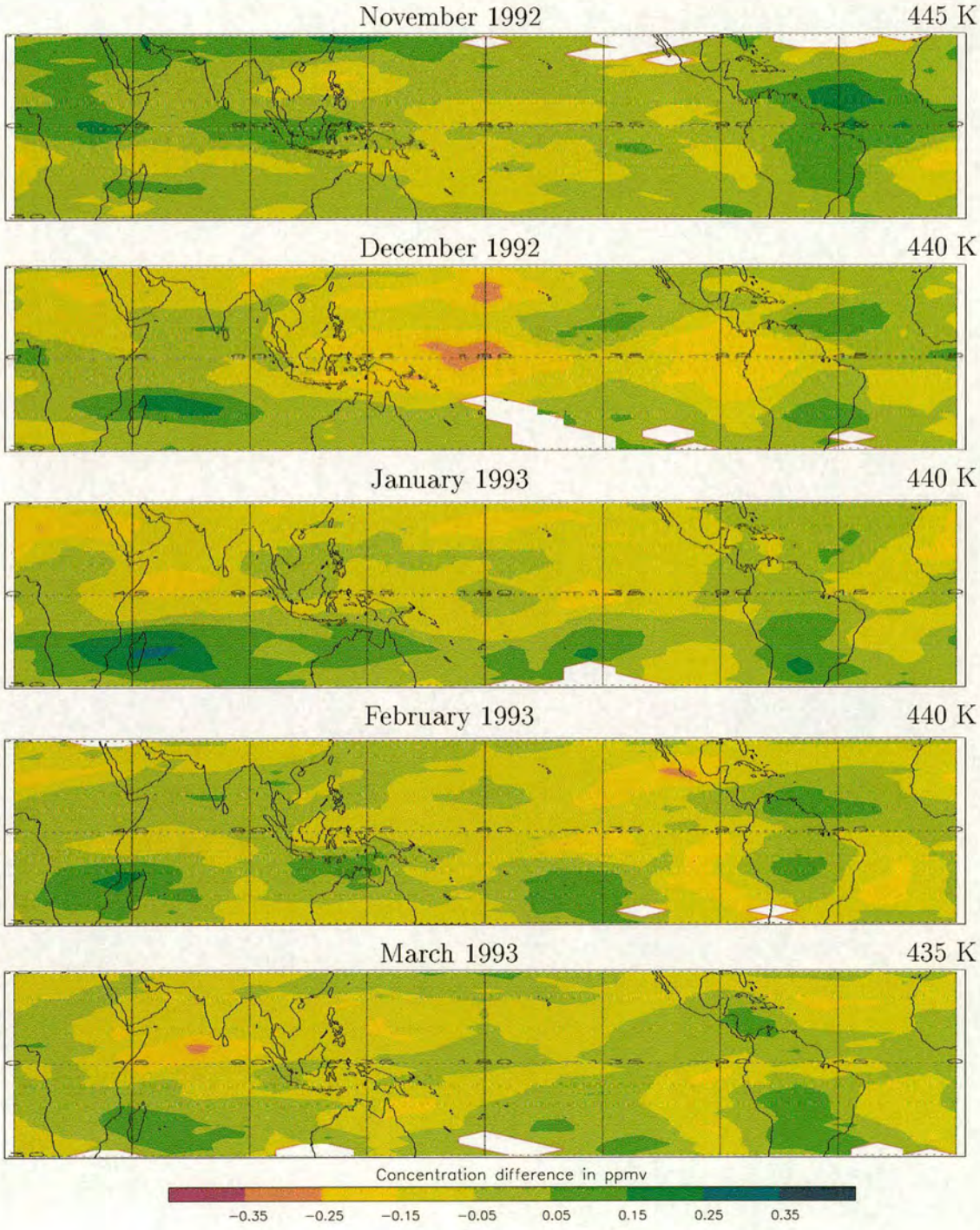

Figure 4.13: **Monthly-Averaged, Observed − Isentropically-Advected, H_2O Fields.** Continued from the previous page.

Figure 2.9 shows that the mixing ratios of water vapour entering the stratosphere begins to increase in May. At some point after this, therefore, the vertical, water-vapour profile in the lower stratosphere will change such that it decreases with height, thus changing the direction of the motion that can be inferred from the evolution difference plots. However, given that, in the mean, it takes air a month to travel from the tropopause to 68 hPa these changes may not be observable at 68 hPa by May.

The Asian monsoon offers another difficulty in interpreting the May difference values. Firstly, it will considerably alter the height of the local tropopause. Secondly, if strong convection does frequently penetrate the tropopause (as suggested by Sherwood and Dessler (2000) and Dessler (2002)) then new air entering the stratosphere could reach 68 hPa much earlier than elsewhere in the tropics. When combined with the moistening effect of the monsoon suggested by Dethof *et al.* (1999) this rapid connection could cause the water vapour profile over the monsoon to decrease with height around 68 hPa in May above the monsoon, even though it may be increasing with height elsewhere in the tropics at this time.

Given both these considerations, it is suggested that the negative differences shown across most of the equator in figure 4.13 for May 1992 still imply air rising from below and that the direction of the motion above the monsoon cannot be determined by this analysis for May 1992 (though the existence of a vertical flow can definitely be inferred).

Interpretation of September differences lead to the same difficulties as do May differences, as indicated by figures 2.9. At some point after August the vertical water-vapour profile in the lower stratosphere will reverse again to increase in height, but this will not necessarily have occurred at 68 hPa by September. Hence, it is suggested that the direction of the motions implied would be relatively dry air coming down from above and relatively moist air will have come up from below. This implies that a band of significant, believable uplift existed along the equator during September. Further significant, believable uplift during these months can also be inferred to have occurred over the Atlantic, Central America, Brazil, Venezuela and Ecuador. Further significant, believable downfall can be inferred to have occurred

over the southeastern tropical-Pacific during September 1992.

By November, given figure 2.9, the water vapour profile should have returned to the same gradient as would be observed between December through April. Unfortunately, figure 4.13 shows that much of the tropics is covered by differences between -0·05 and 0·05 ppmv at this time, values which provide no information on vertical motions since zero difference could be the result of both isentropic and diabatic motion.

Throughout December 1993 to March 1993 significant uplift becomes vanishingly small, only present over the west Pacific during the first month of the four. Not that the uplift is confined to smaller pockets during this time, but rather that there are larger areas of data with similar mixing ratios both before and after advection. This is most likely due to the higher tropopause temperatures observed during 1993[†], meaning the tropopause will most likely have reached its highest temperature earlier in the year. Thus throughout December 1993 to March 1993 the mixing ratios of air below 68 hPa will be similar to those at this level, obscuring the uplift in this analysis.

Significant downdraughts can, however, be inferred to have taken place over Madagascar, the southern-tropical Pacific and South America. The decreased significance of the 1993 data makes an inter-year comparison difficult but it does appear that there is some similarity in the distribution of the downdraughts between the two years.

4.5 Summary and Discussion

No evidence has been found to support the *fountain hypothesis* using isentropic-trajectory and water-vapour data for March, April and August 1992. By comparison of isentropically-advected and observed evolutions of water-vapour data near the top of the tropical tropopause layer it was shown that the observed evolutions near

[†]Recall the discussion on the QBO effects of the lower stratospheric mixing ratios in section 4.1.1.

68·1 hPa could not be explained by arrival to the surface over regions of strong convection followed by adiabatic redistribution. Furthermore, vertical motions were shown to be present across much of the tropical region throughout the year.

Downdraughts were shown to exist above Indonesia in the northern winter (in concurrence with the findings of Sherwood (2000); Gettelman *et al.* (2002)). Updraughts were shown to exist over much wider areas and, though not confined to specific regions, were more consistently inferable over the tropical Pacific and its coastlines. These updraughts were persistent throughout the year. Furthermore, it was inferred that the uplifts formed part of a rapid flow of air (in comparison to the speed of the "tape signal") that must connect the tropopause and 68·1 hPa in order to explain the existence of longitudinal variations in the water vapour distribution at the latter height.

Examination of the monthly-averaged, MLS version 0104 water vapour retrieved for 68·1 hPa revealed that mixing ratios showed a band-like structure in latitude throughout the year with the central band containing the lowest mixing ratios in the northern winter and the highest in northern summer. A longitudinal variation, which is strongest within the central band, is imposed upon this pattern in the northern winter.

Comparison of the longitudinal variation in the water-vapour distribution at 68·1 hPa to the longitudinal variation in the average lapse-rate tropopause height revealed similar structures. Since the lapse-rate and cold-point tropopause height variations in time and space are similar (Seidel *et al.*, 2001) and tropopause height is closely related to tropopause temperature, the comparison suggests that the water-vapour distribution at 68·1 hPa could conceivably be a pattern imposed by the cold-point tropopause that is rapidly carried up to 68·1 hPa.

Examination of the monthly-averaged, MLS version 0104 water vapour retrieved for 68·1 hPa also revealed four differences between the 1992 and 1993 water-vapour evolutions:

1. The position of the minimum water vapour feature was closer to Indonesia and

the Pacific Warm Pool in 1993 than in 1992. This would be consistent with the ENSO relaxing in 1993. If the position of this minimum concentration is a function of the ENSO variation then a rapid airflow between the troposphere and 68·1 hPa would have to exist, such that longitudinal variations in the water vapour field are not eliminated by stratospheric horizontal winds above the tropopause.

2. Mixing ratios were generally lower in November and December 1992 than in the previous year. This is consistent with the increased tropopause temperatures, and hence water vapour entry mixing ratios, that accompany the QBO easterlies during 1992.

3. Mixing ratios were generally higher between January and March 1993 than in the previous year. This is consistent with the increased tropopause temperatures, and hence water vapour entry mixing ratios, that accompany the QBO easterlies during 1992.

4. There is less of a band-like structure in the 1993 winter data than in the 1992 winter data. This is not consistent with changes in the QBO or ENSO.

The examination of the stratospheric fountain theory proposed by Newell and Gould-Stewart (1981), as presented in this chapter, was conducted for levels too high into the stratosphere to truly test the cross-tropopause motion. However, the investigation presented does show that the cold-point tropopause and the 68·1 hPa level must be connected by a rapid, vertical motion and that uplift reaching 68·1 hPa occurs throughout the tropics. Furthermore, the areas of uplift inferred during this investigation will be useful in the validation of the areas of uplift identified in the three-dimensional trajectory study presented in the next chapter, which does directly analyse cross-tropopause motion.

Chapter 5

Three-Dimensional Trajectories

The analysis of the previous chapter revealed no evidence to support the *fountain hypothesis* as stated in chapter 2. The evolution of water vapour near 68·1 hPa could not be characterised as arrival to the surface into a restricted source region by advection from below followed by adiabatic redistribution. This fact, however, does not disallow a fountain acting lower in the stratosphere (resulting from convection only just penetrating into it), since the 68 hPa surface lies between 1 and 2 km above the tropical tropopause. Neither does this fact disallow there being a region of preferential entry into the stratosphere.

The vertical resolution of the Microwave Limb Sounder (hereafter MLS) water-vapour data limited its potential use in the analysis of the last chapter to three levels of the tropical tropopause layer (hereafter TTL) — 146·4, 100·0 and 68·1 hPa. Furthermore, the confidence that can be had in the accuracy of the 100·0 hPa data is considerably less than can be had in the data at the other two retrieval nodes (Pumphrey *et al.*, 2000). As such, MLS water vapour data can only be used to infer the vertical motion of air near the top and bottom of the TTL.

Further detail about tropical, cross-tropopause motion can be achieved by the use of three-dimensional trajectories. Though the accuracy of an individual trajectory is questionable, the largest scale features of many-trajectory calculations are believable (Morris *et al.*, 1995). Furthermore, should the uplift suggested by trajectory calculations coincide with the inferred uplift suggested by the water-vapour analysis

of the previous chapter then a greater level of confidence can be had in both results.

Trajectory calculations were therefore used to investigate both the *uniform-entry* and *flow-change* hypotheses first presented in chapter 2:

- **Uniform-entry Hypothesis.** No preferential region of cross-tropopause motions exists; air enters the stratosphere in an even distribution in both space and time throughout the tropics.
- **Flow-Change Hypothesis.** A significant change occurs in the mechanism of cross-tropopause motion between the early 1980s and the early 1990s.

In both cases, maps showing the frequency of air-particles crossing specific surfaces within the TTL were created from the trajectory calculations. The *uniform-entry hypothesis* was tested by examining whether any particular region showed an increase in crossing frequency compared to the surface average. The *flow-change hypothesis* was tested by determining whether or not the crossing distributions significantly changed between the early 1980s and the early 1990s.

In the following chapter all results presented have been calculated from back-trajectories, *i.e.* trajectories run backwards in time. In this way, the chronological end-points of the air-particles' paths could be set to cover the whole tropics, thus showing the origins of all the air reaching the lower, tropical stratosphere. To avoid confusion however, air-particle trajectories will always be discussed in terms of the chronological path of the particles. Thus the direction air particles travel in the discussion is the same as would occur in the atmosphere.

Section 5.1 discusses the ECMWF winds data, specifically those data used to create the results presented in this chapter. Section 5.2 details the trajectory calculations and the general flow within the TTL observed from them. The investigation of the *uniform-entry hypothesis* is discussed in section 5.3 and the investigation of the *flow-change hypothesis* is discussed in section 5.4. Section 5.5 then discusses the nature of the air motion after the crossing of the tropopause up to the top of the TTL (between 90 and 68 hPa) in comparison to the cross-tropopause motion

itself (between 110 and 90 hPa). This comparison investigates changes in the air motion that occurs as particles move into the stratosphere and, more specifically, as they approach the pressure level used in the advection study presented in the previous chapter. Finally, section 5.6 discusses the results of this chapter and their implications with respect to the observations of previous authors.

5.1 ECMWF Winds

Figure 5.1 shows three seasons' worth of ECMWF zonal and meridional winds as an example of those data that were used to the trajectory plots that are presented in the following sections. The panels are created in the same manner as was used for the ECMWF winds of figure 3.3, with the ECMWF analyses interpolated to the location of the Changi Airport radiosonde in Singapore. Note that the height range used differs between the figures however; figure 5.1 concentrates on the stratosphere and TTL.

Figure 5.1 clearly shows the QBO easterlies of 1992 being replaced by the QBO westerlies of 1993, as did figure 4.7. Figure 5.1 also highlights the same potential problems with the change in wind direction passing 68 hPa. The results presented in this chapter should not be heavily influenced by increased interpolation errors however, as all results are presented as seasonal averages.

5.2 Trajectory Calculations

All trajectory calculations were run for thirty days[†] such that particles would end up on a regular two-dimensional grid upon the 68 hPa surface. The grid covered ten degrees of longitude, beginning at the Greenwich Meridian, and two degrees of latitude, extending out to thirty degrees either side of the equator. Trajectories were calculated which ended on the regular grid points at 1200 GMT each day of the period of investigation, the duration of which depended upon the investigation

[†]The limit on large-scale accuracy suggested by Morris *et al.* (1995). See section 3.3.3 — Altering Routine Parameters for discussion.

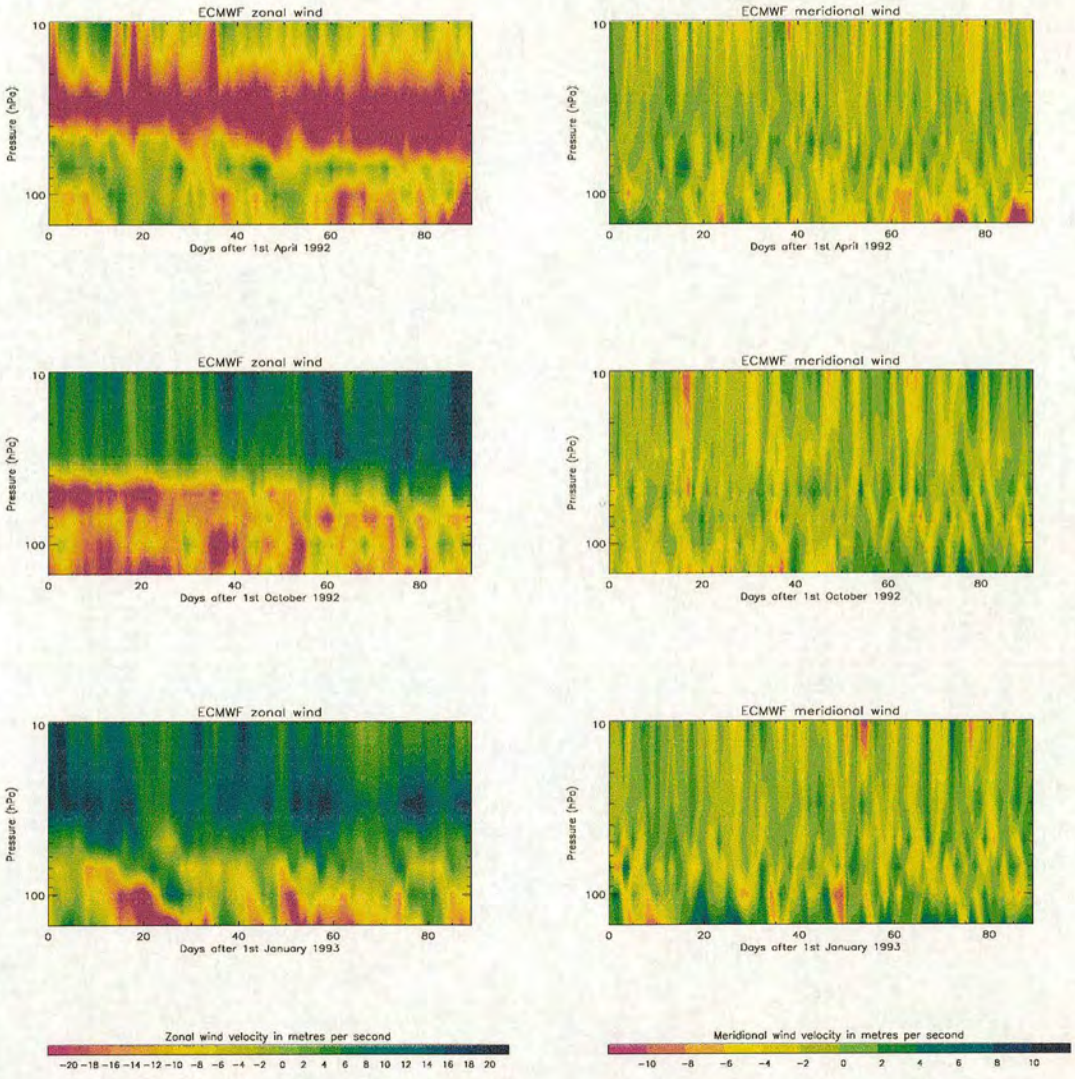

Figure 5.1: **Examples of ECMWF Analyses Winds for 1992 and 1993.** Shows timeseries of the zonal (westerly) and meridional (southerly) winds of the assimilated data from the European Centre for Medium Range Forecasts. The data have been linearly interpolated to the location of the Changi Airport radiosonde in Singapore — 103·98 °E, 1·36 °N. The top panels cover the days from 1^{st} April 1992 to 30^{th} March 1992. The middle panels cover the days from 1^{st} October 1992 to 31^{st} December 1992. The bottom panels cover the days from the 1^{st} January 1993 to 31^{st} March 1993.

(detailed later). The release from 68 hPa ensured that only air-particles that would not fall back down into the tropical troposphere were considered.

The investigations into both the *uniform-entry* and *flow-change* hypotheses were performed within the TTL, which could be considered to cover the height range between 215 and 50 hPa[†]. Particle motion between these surfaces would take much longer than 30 days however. Furthermore, in order to see the detailed flow occurring near the tropopause, the height range of study had to be quite narrow, as not all particles reaching the stratospheric, end-points will have come from the troposphere, some will have come from the stratospheric extra-tropics. Narrowing the height range of the study therefore minimises the number of particles arriving from the stratospheric extra-tropics.

As such, two height ranges of interest within the TTL were chosen for the investigations presented in this chapter — 110–90 hPa and 90–68 hPa. The first range covers the seasonal variation of the cold-point tropopause — 102 and 92 hPa (Seidel *et al.*, 2001). The second height range shows how particles reach 68 hPa and the distribution in the uplift reaching the pressure level that was the focus of the water-vapour study presented in the last chapter. A sufficiently large number of particles was found to travel from 110 to 68 hPa, within the tropical region, for a robust, detailed study of the cross-tropopause motion.

5.2.1 Motion in the Tropical Tropopause Layer

A cursory trajectory-analysis of the motion between 110 and 90 hPa reveals that the large-scale features of the tropical, vertical motion are captured by the combination of wind data from the European Centre for Medium-Range Weather Forecasts (hereafter ECMWF) and the trajectory routine of Methven (1997). Figure 5.2 shows that, though the assimilated data from the ECMWF is not capable of resolving convective events, the trajectory routine of Methven (1997) still captures the large-scale downflow deduced to occur over the strong, wide-spread convection of Indonesia (Sherwood, 2000).

[†]As discussed in section 2.1.3 — A Tropical Tropopause Layer.

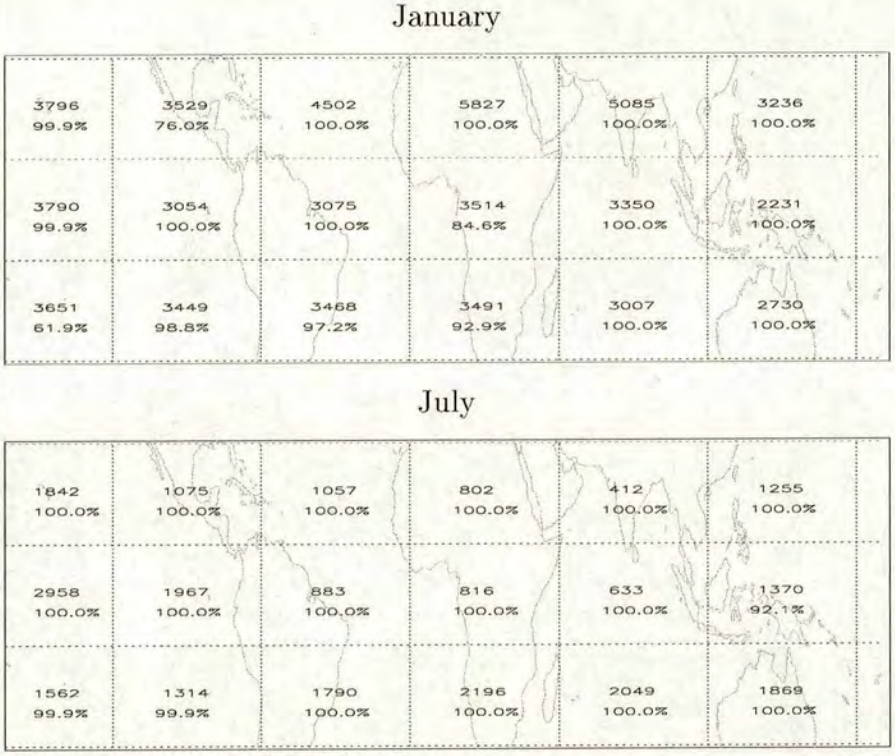

Figure 5.2: **Horizontal Motion of Trajectories Ascending from 110 to 90 hPa.** Shows all longitudes at up to thirty degrees latitude from the equator. The tropics have been split into eighteen regions, each of 60 degrees longitude by 20 degrees latitude. The upper number in each region denotes the number of times trajectory paths were found to cross the region in the horizontal whilst travelling up from 110 hPa to 90 hPa during January (upper panel) and July (lower panel) 1992. 6348 (18·3%) of the January and 2211 (6·4%) of the July trajectories crossed the total map area. The lower statistic of each region indicates the significance of the crossing number with respect to an even distribution of crossings spread throughout the layer. See text for details.

Figure 5.2 shows crossing statistics for trajectories, calculated for January and July of 1992, that passed from 110 to 90 hPa within thirty degrees of the equator, within the 30 day period. 39·9% of the January trajectories rose from 110 hPa to get to 68 hPa, 18·3% did so whilst always within thirty degrees of the equator. In July percentages were 16·8% and 6·4% respectively. Note that this does not indicate a difference in the crossing between months however, since the stratospheric circulation is weaker in the northern summer. As such, it is expected that fewer particles will have originated below 110 hPa in the case of trajectories calculated for the northern

summer.

In the figure the tropical tropopause is split into eighteen regions. The size of the regions was defined as approximately that of core area of regional dry-features observed by MLS and of the fountain areas designated by Newell and Gould-Stewart (1981). The regions are therefore of similar size to the area enclosed by the 2·8 ppmv contours of figure 4.5 and the 90 % contour of the January (top) panel of figure 2.12.

The upper value in each region indicates the number of times trajectory paths were found to cross the region in the horizontal whilst travelling up from 110 hPa to 90 hPa. In this way a trajectory that crossed the region twice (perhaps having gone completely round a latitude circle) counted twice towards the region's upper value. Figure 5.3 shows an example of the number of counts added to the tropical map by three, hypothetical trajectories. In these case the air particles moved from the starred positions at 110 hPa to the diamond positions at 90 hPa. The nature of the vertical path of the trajectories is not indicated since such detail is not included in figure 5.2.

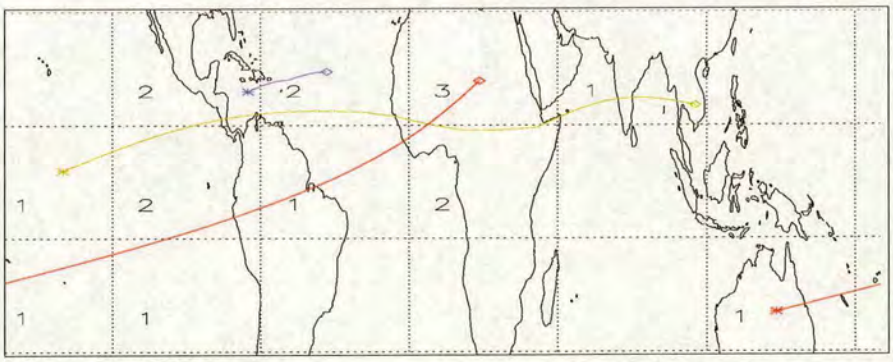

Figure 5.3: **Trajectory Example — Ascent from 110 to 90 hPa.** Shows three hypothetical trajectories that trace the motion of air-particles from the 110 hPa surface (starred positions) to the 90 hPa surface (diamond positions). The grid divides the tropics in the same manner as that of figure 5.2. The numbers in bottom left of all regions that have at least one trajectory passing through them indicate the total number of times a trajectory entered the region. This counting method is the same method as was used to create the statistics of figure 5.2. Note that the green trajectory adds to the count of the north-African region twice.

In the bottom left of all regions that have at least one trajectory passing through

them there is a number that indicates the total number of times a trajectory entered the region. Note that the green trajectory adds to the count of the north-African region twice. The value of such a count over simply registering the number of individual trajectories that cross the region is that it better approximates the total air flow through each region during the whole period of study.

The lower value in each region of figure 5.2 indicates the statistical significance of the number of crossings in relation to the null hypothesis of an even crossing-distribution throughout the tropics — the total number of region-crossing events divided evenly between the eighteen regions. In the January case of figure 5.2 this null hypothesis thus comprised a mean crossing distribution of 3599 crossing events (to the nearest whole event) and in the July case 1436 crossing events.

The amount of horizontal motion cannot be found from these crossing statistics of figure 5.2 and so in the case of low crossing numbers it is impossible to differentiate between two possible cases:

1. Few particles entered the region, as occurred over the Indian region of figure 5.3.

2. Trajectories crossing the layer exhibited little horizontal motion; it can be appreciated that the blue trajectory in figure 5.3 could have caused higher crossing statistics had its horizontal extent been greater.

However, regions of strong convection are still highlighted by low numbers of crossings. In these regions fewer crossings might indicate a lessening of the overall airflow through the region. Equally, the lower crossings could indicate a faster, more-direct, vertical-motion persists in the region. Whichever the case, low crossing values are found in all regions of heightened convection — over Indonesia and, to a lesser extent, the northerly ITCZ in January and over India and, to a lesser extent, the southerly ITCZ in July. The simplest interpretation of this similarity is that the downflow over strong convection proposed by Sherwood (2000) and Gettelman *et al.* (2000) to occur over Indonesia also occurs over the Asian monsoon and, to a lesser extent,

the ITCZ. If this were the case then STE over Indonesia could not be considered to be unique in any theory of exchange.

Such a distribution of descent between the 90 and 110 hPa surfaces would, however, be in contrast to previously-published, ECMWF, vertical-velocity data, which would suggest uplift occurs over the Asian monsoon (Simmons *et al.*, 1999). Figure 3 of Simmons *et al.* (1999), reproduced here as figure 5.4, shows tropical, and some mid-latitude, vertical velocities averaged over ECMWF data between 1979 and 1993. The figure implies that, during July, the Asian monsoon sends air up beyond 90 hPa and that some activity in the mid-Pacific causes a smaller area of concentrated upward motion at 110 hPa. In January the average upward motion is spread over a larger area, pockets being visible over the Pacific, Panama and Australia.

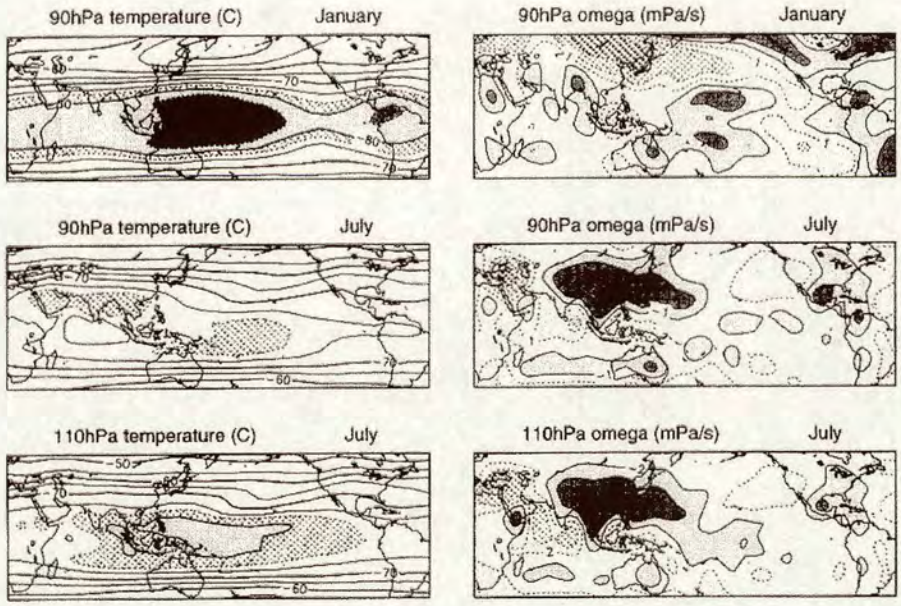

Figure 5.4: **Average Conditions near the Tropopause.** As figure 3 of Simmons *et al.* (1999), page 360. Temperature and vertical motion averaged from ECMWF reanalyses for the period 1979-1993. Temperature plots have contour interval 5°C in the unshaded regions (for temperatures below -77·5°C) and 2·5°C in the shaded regions. The darkest shading indicates temperatures below -85°C. Vertical motion is plotted with intervals at 1, 3 and 9 mPa s^{-1} at 90 hPa and 2, 6 and 18 mPa s^{-1} at 110 hPa. Solid contours and shading indicate ascent, dotted contours and stippled shading denote descent.

Taken together figures 5.2 and 5.4 thus suggest that the Indonesian region might

exhibit unique STE after all, concurring with current theories proposed to explain the exchange occurring there (Sherwood and Dessler, 2000; Hartmann *et al.*, 2001; Holton and Gettelman, 2001). Furthermore, given figure 5.4, the simplest interpretation of the low number of horizontal trajectory-crossings through regions over the Asian monsoon and the ITCZ becomes that they are instead the result of a more-direct vertical motion. If this were the case then extra credence would be given to the suggestion of Sherwood and Dessler (2001) and Dessler (2002) that convection does frequently penetrate the tropopause up to, and perhaps beyond, 90 hPa.

5.3 Uniform-Entry Hypothesis

Figure 5.5 shows boxed distributions of trajectory crossing points for the 68, 90 and 110 hPa surfaces, each created by considering a subset of all the trajectories calculated for January, February and March of 1992. As in chapter 4 these months are used to analyse the northern winter conditions. Since Mote *et al.* (1996, 1998) determined that air takes approximately one month to travel from the tropopause to 68 hPa it is appropriate to consider trajectories calculated for January, February and March when examining the cross-tropopause motion of the northern winter months.

In this figure the horizontal position of each trajectory is considered as it passes the surface in question. Hence the distributions indicate the number of trajectories that crossed the surface in each of the boxed regions. The size of the boxes was arbitrarily determined, but is small enough to provide a detailed distribution without spreading the crossing data too thinly.

The trajectory subset used to create figure 5.5 comprises only those trajectories that arrived at 68 hPa after having risen from 110 to 90 hPa within thirty degrees of the equator. Thus air-particles that reached 68 hPa in the tropical stratosphere after having crossed the extratropical tropopause or that originated anywhere in the stratosphere were discarded for the creation of the figure. Each map of figure 5.5 is created using the same 16553 trajectories. Note that the use of this subset is the reason why the 68 hPa crossing-distribution is not uniform.

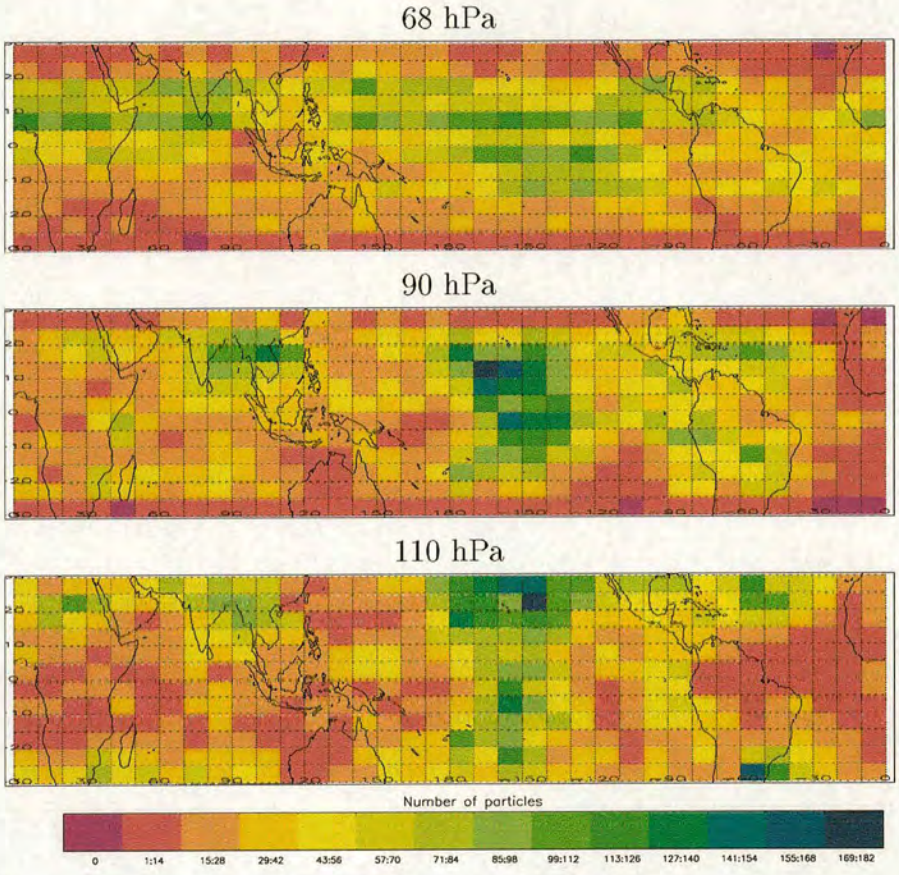

Figure 5.5: **Distribution of Trajectory Crossing Points: Winter 1992.** Shows the distributions of air particles crossing three pressure levels during a trajectory run for winter (January, February, March; see text) 1992. Each map is constructed from the same 16553 trajectories (16·3 % of the total calculated) that reached 68 hPa after having crossed from 110 to 90 hPa within thirty degrees of the equator.

Of the total 101556 trajectories calculated for the winter of 1992, 37·3 % rose from 110 hPa and 16·3 % did so within tropical bounds. Thus, around 56 % of air reaching 68 hPa from 110 hPa was of extratropical origin. This is consistent with the findings of, for example, Mote *et al.* (1998) and Haynes and Schuckburgh (2000a), who suggest considerable exchange occurs between the tropics and extratropics in the lower stratosphere. When all of the trajectory calculations for winter 1992 are considered, not just those that originated from 110 hPa, the percentage originating from the extratropics falls to 29·9 %. This figure is also consistent with the work of previous authors, for it lies within the error bounds of the estimate of Volk *et al.*

(1996), who suggest that 15 % (with an error range of −10 %, +15 %) of air at 68 hPa is of extratropical origin.

Figure 5.5 shows crossing-distributions that are far from even, especially at 110 and 90 hPa. At 110 hPa the distribution shows minima over the Indonesian island chain, the equatorial Atlantic and parts of Africa. The existence of a minimum crossing over Indonesia at this time is consistent with the observations of a predominant downflux of air there as observed by Sherwood (2000) and Gettelman *et al.* (2000). The same distribution also has maxima along a line between the Hawaiian islands and Polynesia. The significances of the minima and maxima, compared to an even distribution of 16553 trajectories crossing under purely-vertical motion (38 trajectories per box) are both high: The significance of 28 particles crossing is 90 % and the significance of 85 particles crossing is almost 100 %.

Similar extrema are visible in the 90 hPa crossing-distribution, though the minima are somewhat filled in compared to the 110 hPa case and the maximum is centred more towards the equator. Nevertheless, the number of air-particles crossing in this 90-hPa, mid-Pacific maximum remains over three times that crossing elsewhere. This pattern is still visible in the 68 hPa crossing-distribution, though somewhat more smeared out. A westward spread is to be expected at this level however, under the influence of the QBO, the phase of which in 1992 was indicated in table 4.1.

The only feature of figure 5.5 that is inconsistent with the findings of previous authors is that maximum in the uplift at 68 hPa occurs in the northern hemisphere at this time. Previous authors suggest that the maximum mass flux crossing the 68 hPa surface usually occurs in the summer hemisphere (for example Plumb and Eluszkiewicz (1999)). Nevertheless, the significance of both the maxima and minima of the crossing distribution at both 110 and 90 hPa suggests that the *uniform-entry hypothesis* does not hold, since this mechanism would result in a uniform distribution of crossing points and yet significant maxima and minima have been found to exist.

5.3.1 Cross-Tropopause Flow

Some of the details of the non-uniform, cross-tropopause motion can be determined by considering the nature of the air-particles' journey from 110 to 90 hPa. This nature can be appreciated from figure 5.6, whose three histograms indicate: The number of days taken to cross the layer; the number of horizontal boxes, as defined in figure 5.5, the particles moved through whilst crossing the layer; the number of up turning-points† that occurred along the trajectory paths during the crossing. These statistics were compiled for the winter 1992 crossing, using the same trajectory subset as was used to create figure 5.5.

Particle crossing times were binned in whole numbers of days, rounding up. The mode time taken for particles to cross the layer was thus two days. Particles crossing at this speed must have been travelling at greater than the global mean upwelling velocity, estimated to be around 0·5 mm s^{-1} (Mote *et al.*, 1998). The slowest-moving particles of the peak bin would have travelled between 90 and 110 hPa (of the order of 1 km) in two days, hence moving at just under 6 mm s^{-1} in the vertical. Thus they were travelling at more than eleven times the mean upwelling velocity.

The number of boxed regions crossed in the horizontal does correspond to the accepted, characteristic velocity of the lower stratosphere. Air particles travelling at 10 ms^{-1} in the zonal direction, a reasonable speed for the lower-stratospheric QBO-easterlies, would travel through two or three of the longitudinal box-lengths as defined in figure 5.5. This corresponds well with the peak number of boxes crossed indicated in the top-right histogram of figure 5.6.

The directness of the crossing is indicated by the number of up turning-points along the trajectory paths: The greater the number of up-turning points the greater the number of interruptions there were to the particles' uplift. The majority of particles therefore, move in a relatively uninterrupted direction with few turning points.

Whether the Brewer-Dobson circulation or convective updraught dominates the particle motion between 110 and 90 hPa, the figure shows a clear trend towards a

†Meaning the number of times an air particle changed from downward to upward motion.

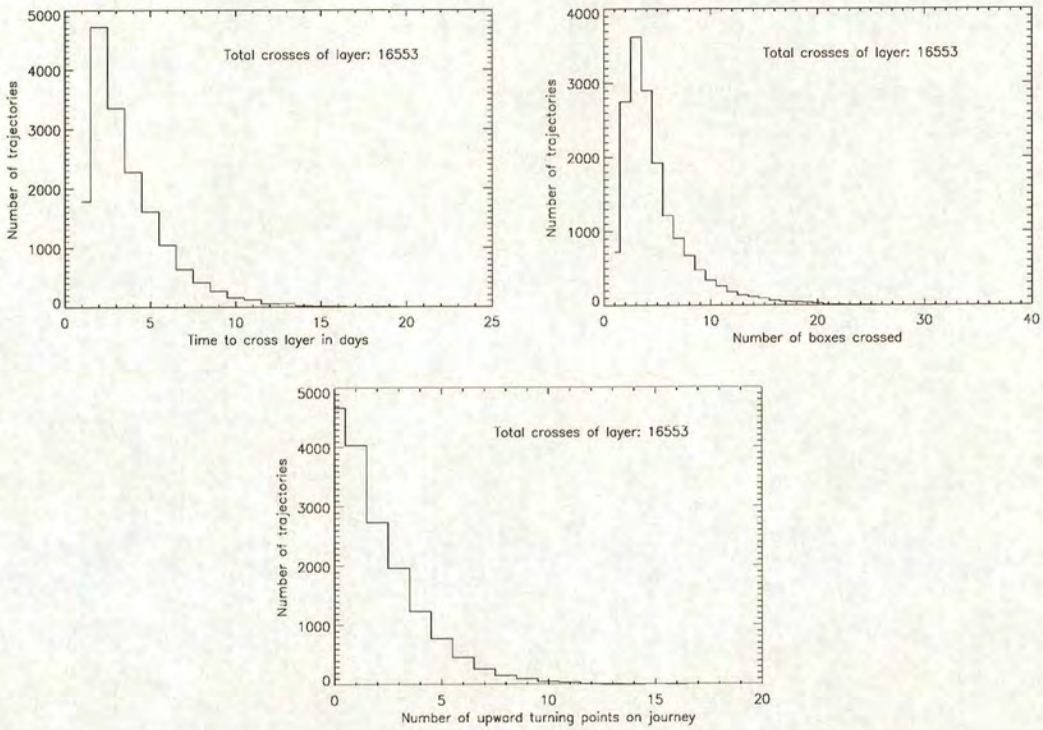

Figure 5.6: **Details of the Trajectory Paths: Winter 1992.** Indicates details of the crossing of the 110 to 90 hPa layer for winter of 1992. Only those trajectories that reached 68 hPa after having crossed between 110 and 90 hPa within thirty degrees of the equator are considered. The number of trajectories in this subset is also shown. The top-left panel shows time taken to cross the layer, with fractions of days rounded up. The top-right panel indicates the number of horizontal regions crossed by the trajectories when traversing the layer. The bottom panel shows the number of up turning-points along the trajectories.

rapid, direct crossing with limited horizontal motion.

Though the trajectories within the mode bin of each of the three histograms are not necessarily always the same (there being a different number forming each peak), the trajectories of those mode bins do all cross the 110 to 90 hPa layer in similar spatial distributions. Figure 5.7 shows the crossing distributions made from three trajectory subsets — those trajectories within the mode bins of the histograms in figure 5.6. All three maps show the distributions at 90 hPa. All three crossing-distributions show a similar pattern to that seen in figure 5.5, with a maximum in the crossing over the mid-Pacific and minima over Indonesia, the Indian Ocean and

Africa.

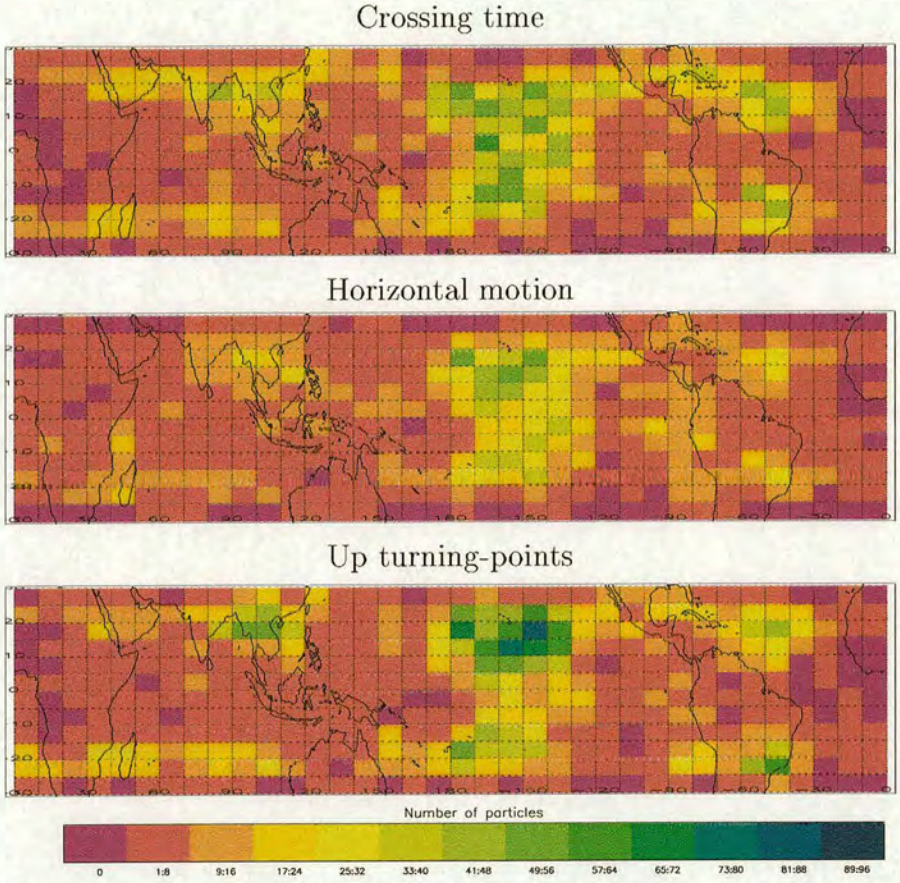

Figure 5.7: **Distribution of Trajectory Crossing Points: Mode Crossing, Winter 1992.** Shows the positions of air particles at 90 hPa during a trajectory run for winter 1992. Each map is constructed from a subset of those used to create figure 5.5. The top panel shows trajectories crossing in the peak time: 2 days. The middle panel shows trajectories crossing with the peak amount of horizontal motion: 3 boxes. The bottom panel shows trajectories crossing with the peak number of up turning-points: 0. The peak values are those determined in figure 5.6.

Figures 5.5 and 5.7 both show crossing-event maxima in the mid-Pacific. However, there is a difference in the distributions of the two figures. Though the ratio of crossing events in the mid-Pacific to the highest number elsewhere is approximately the same between the figures, the ratio of the strength of the maxima of each plot relative to their respective crossing-event minima increases in figure 5.7. For example, compare the mid-Pacific maxima to the local crossing-event maxima over Vietnam. In both figures the ratio is a little under 2 to 1. Then compare the

ratio of crossing events in the mid-Pacific to that of the distribution minima, for example over mid-Australia. This ratio increases from 6 or 7 to 1 in figure 5.5 to 10 to 1 in figure 5.7. Therefore, whereas there are particles moving rapidly and with little horizontal motion distributed throughout the tropics, there is a tendency for the air-particles moving with these characteristics to be concentrated towards the region of the mid-Pacific, crossing-maxima.

This concentration of faster vertically-moving particles into the mid-Pacific is made clearer when examining the crossing distributions created from the trajectories of successive groups of bins from any one of the histograms of figure 5.6. Three such groups have been used to create the crossing distributions at 90 hPa shown in figure 5.8. The three groups are: Those particles that traversed only one horizontal region in crossing the 110 to 90 hPa layer; those particles that traversed between 1 and 3 horizontal regions whilst crossing the layer; those particles that traversed eight or more horizontal regions whilst crossing the layer.

The top and middle panels of figure 5.8, comprising the more-rapidly-, more-directly- moving particles, both exhibit the same concentration into the mid-Pacific. The bottom panel, comprising only the slower vertically-moving particles, shows no such concentration. Though both the top and bottom panels of the figure comprise a differing number of particles to the middle panel, all three distributions have significant maxima and minima compared to an even distribution of trajectories crossing the 90 hPa layer. The mean number of trajectories crossing in the middle panel was 16, with the significances of 9 and 24 crossing events both being 96 %. The mean number of trajectories crossing in the upper panel was 2, with the significances of 0 and 8 crossing events being 95 and 100 % respectively. The mean number of trajectories crossing in the lower panel was 6, with the significances of 1 and 8 crossing events being 99 and 70 % respectively. Hence, the distribution in the bottom panel of figure 5.8 is significantly different to the distributions of the other panels, confirming the concentration of faster-crossing particles into the mid-Pacific.

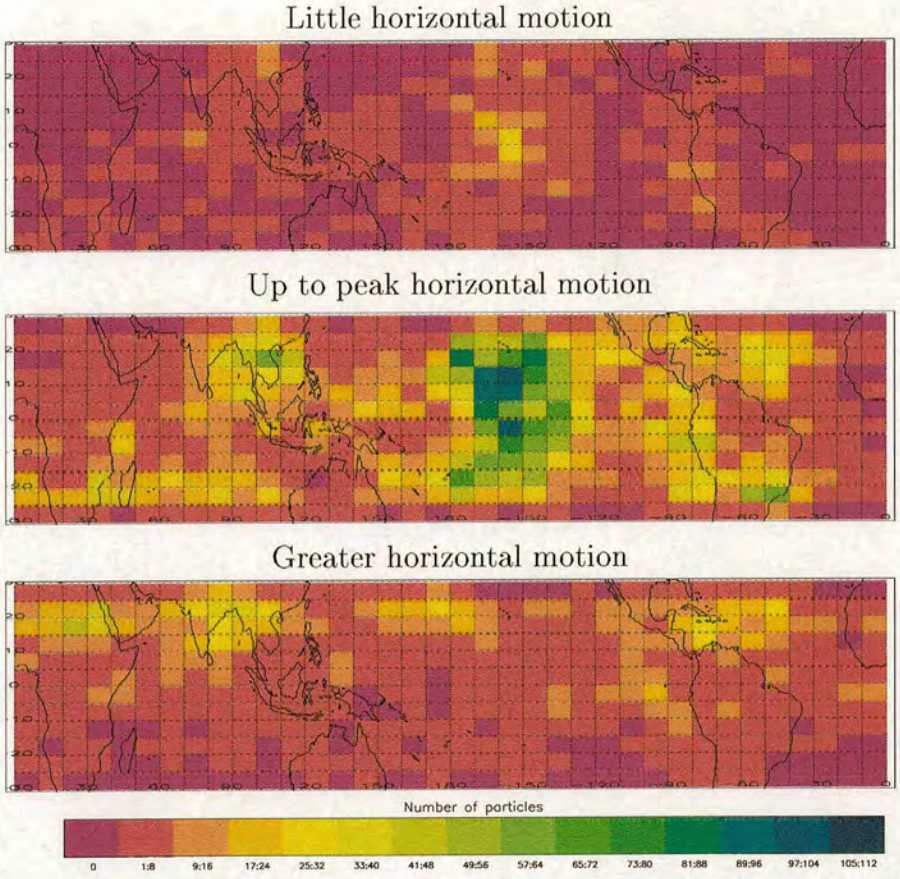

Figure 5.8: **Distribution of Trajectory Crossing Points: Horizontal Motion, Winter 1992.** Shows the positions of air particles at 90 hPa during a trajectory run for winter 1992. Each map is constructed from a different subset of those used to create figure 5.5. In the top map those trajectories crossing the 110 to 90 hPa through only one horizontal region are plotted. In the middle map trajectories crossing with the peak or lesser horizontal motion are shown, *i.e.* 3 or fewer boxes. In the bottom map the 90 hPa positions of trajectories crossing through eight or more horizontal regions are plotted. The number of trajectories used in each case is determined by adding up the number of trajectories in the respective bins of the top right histogram of figure 5.6.

5.3.2 Inter-Season Differences: 1992

In chapter 4 it was shown that the MLS, water-vapour distributions at 68·1 hPa exhibit longitudinal variations in the northern winter and spring but not in the northern summer and autumn. It was further suggested that these longitudinal variations would most easily be explained by variations in tropopause height rather

than by differential uplift. In the following section, seasonal variations in the surface crossing-distributions within the TTL are examined to determine whether or not a significant, seasonal difference is present that might explain the differing 68·1 hPa, MLS, water-vapour distributions.

None of the four seasons of 1992 were found to show an even crossing distribution throughout the tropics. This can be appreciated from figure 5.9, which shows air-particle positions at 90 hPa for trajectories calculated for winter, spring (April, May, June), summer (July, August, September) and autumn (October, November, December). Again, only those trajectories rising up to 68 hPa after having crossed the 110 to 90 hPa layer within thirty degrees of the equator have been considered. Note that the winter 1992 distribution in figure 5.9 is a repeat of the second panel of figure 5.5 but with a changed colour scale.

All seasons show a maximum in crossing events over the mid-Pacific, yet there are some inter-seasonal differences in the crossing distributions. The winter and spring distributions are similar. Both show a minimum in crossing events over Africa and the Indian Ocean but with some crossing in almost all areas of the tropics nevertheless. The autumn and summer distributions also exhibit crossing in almost all regions but show a concentration of crossing events into a smaller area than occurs in the winter and spring cases, the majority of summer and autumn events being confined to the Pacific and some of its neighbouring land masses. The autumn distribution also has the highest number of crossing events in a single region, approximately twice as high as the maximum of any other month.

The significances of the maximum and minimum crossing-events, compared to an even distribution, are high for all seasons of 1992. The significances of 23 and 66 crossing-events in the winter, spring and autumn cases are always greater than 98 %, except for 23 crossing-events, which has 88 % significance. The mean crossing-events during these seasons was 38, 40 and 31 respectively. The summer significances of 1 and 22 crossing events, compared to a mean of 14, are also high, both being greater than 98 %.

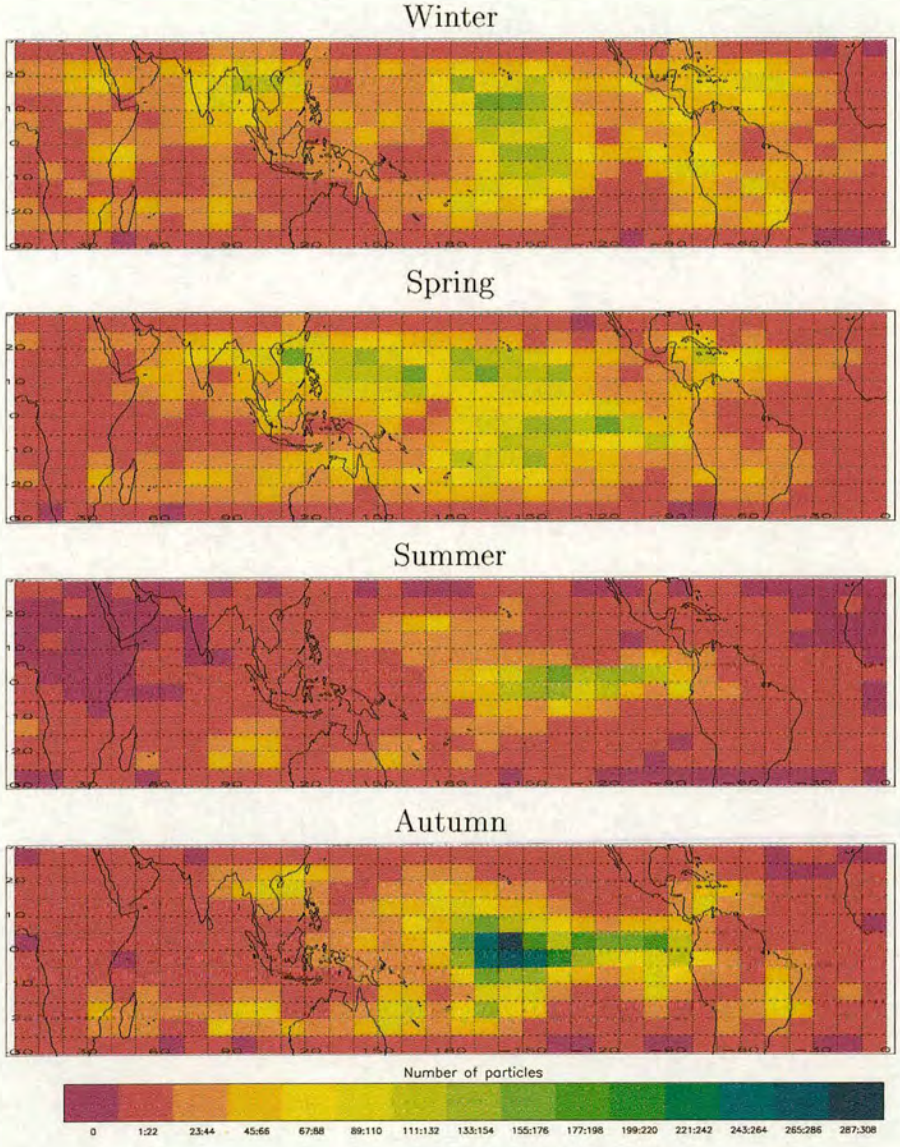

Figure 5.9: **Distribution of Trajectory Crossing Points: Seasons of 1992, 90 hPa.** Shows the positions of air particles at 90 hPa during four separate trajectory runs for the northern hemisphere seasons of 1992. The winter panel is a repeat of the middle panel of figure 5.5 but with a different colour scale. Each map is constructed from the trajectories that reached 68 hPa after having crossed the 110 to 90 hPa layer within thirty degrees of the equator during the respective season. The number of trajectories used in each case is: Winter (January, February, March), 16553; spring (April, May, June), 17151; summer (July, August, September), 6064; autumn (October, November, December), 13393.

Some of the temporal variation in the crossing clearly follows the seasonal cycle in the mass flux across the 100 hPa surface predicted to result from the residual stratospheric circulation[†]. Table 5.1 shows the total number of crossing events as a function of season. That the number of crossing events is highest in the northern winter and spring and lowest in the northern summer indicates the influence of the stratospheric, wave-driven motion on the magnitude of the cross-90-hPa flow.

Season	*Trajectories crossing the layer*	
	number of trajectories	% of total released
Winter	16553	16·3
Spring	17151	16·9
Summer	6064	6·0
Autumn	13393	13·0

Table 5.1: **Trajectories Crossing from 110 to 90 hPa Within Tropical Bounds.** Indicates the number of trajectories that reached 68 hPa after having crossed the 110 to 90 hPa layer within thirty degrees of the equator. These trajectories were those used to create figure 5.9. Statistics are given for each season (as detailed in previous figures) of 1992 as a raw number and as a percentage of the total released.

A slower mean-speed of air-particles in the northern autumn and summer can also be appreciated from histograms showing the time air particles took to cross between 100 and 90 hPa. Such histograms are shown in figure 5.10. The histograms of the figure are created from the same trajectory subsets as used to create the crossing distributions of figure 5.9. The winter histogram is the same as the time-of-crossing histogram of figure 5.6. Overall, the histograms of each season show distributions that favour their lower bin values. This further indicates a similar crossing mechanism acting between the seasons, even though the strength of that mechanism may be varying.

An interesting feature of figure 5.1 is the minimum in the crossing events over the Middle East in the northern summer. This Middle Eastern minimum lies to the west of a similar minimum that can be seen in the crossing distribution for 110 hPa for the same time. Such a map is presented in figure 5.11, which clearly shows a

[†]As determined, for example, by Rosenlof and Holton (1993), whose results were shown in table 2.1.

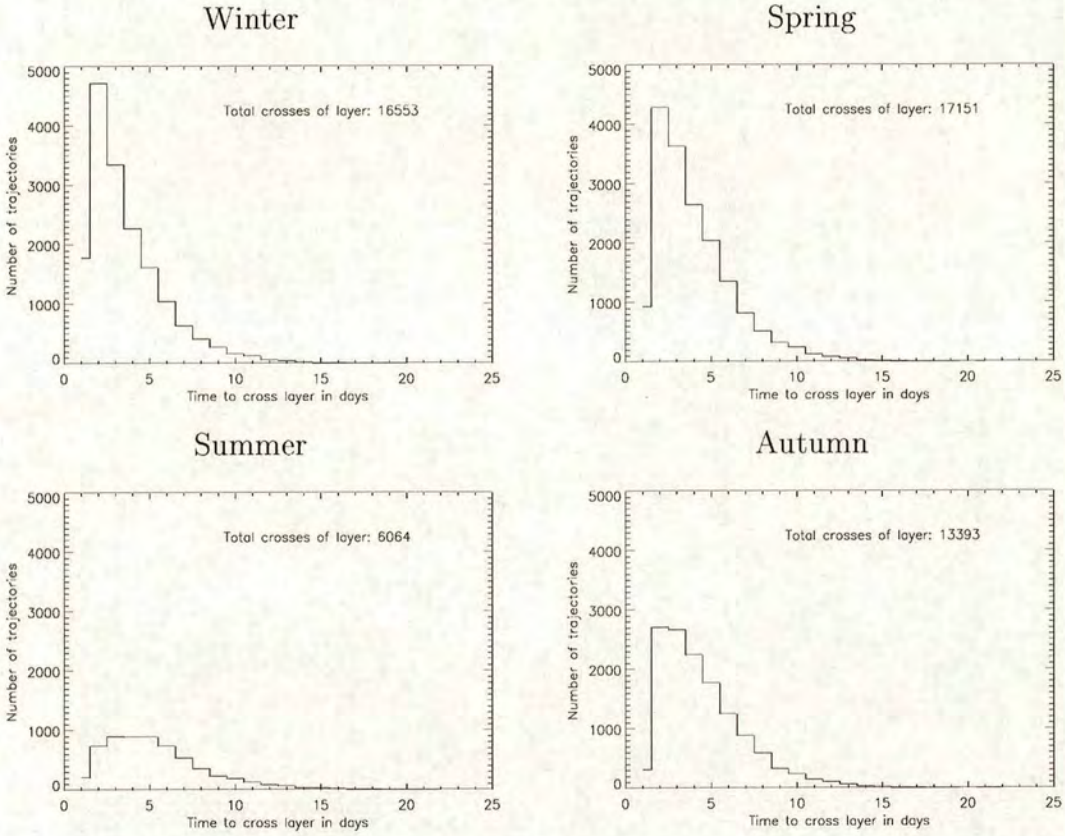

Figure 5.10: **Details of the Trajectory Paths: Seasons of 1992.** Indicates the time trajectories took to cross the 110 to 90 hPa layer during the seasons of 1992. Only trajectories that reached 68 hPa after having crossed between 110 and 90 hPa within thirty degrees of the equator are considered. The number of trajectories crossing in each season is also indicated.

wide-spread region of zero crossing-events centred just off the west coast of India. These distributions would be consistent with a feature rising from 110 hPa to 90 hPa being advected westward under the easterlies QBO winds of 1992. The statistical significance of zero crossing, compared to an even distribution of purely-vertical trajectories, approaches 100 %.

Such a minimum is not in contradiction to the uplift suggested to have occurred above the Asian monsoon by previous authors, since figure 5.4 shows a prior report of an area of descent to the southwest of the Asian monsoon. However, the mid-Pacific maximum in the crossing frequencies on the summer panel of figure 5.1 are still greater than crossing frequencies nearer the Asian monsoon. Combined with

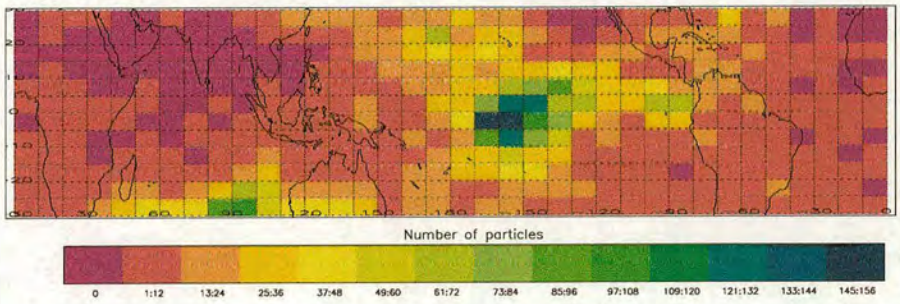

Figure 5.11: **Distribution of Trajectory Crossing Points: Summer 1992, 110 hPa.** Shows the positions of air particles at 110 hPa calculated for summer (July, August, September) of 1992. The trajectories are the same as used to create the summer plot of figure 5.9.

the minimum in the crossings observed over Indonesia in the northern winter, this implies that strong convection is not dominant in the control of tropical STE.

There are difficulties however, in ascribing the observed cross-tropopause motion to purely-stratospheric control. The primary difficulty is that a change in the overall airflow appears to occur somewhere between 90 and 68 hPa.

Figure 5.11 also shows that a mid-Pacific maximum in crossing events occurred in the northern summer at 110 hPa as well. This mid-Pacific maximum is common to all seasons at the heights 110 hPa (distributions for the northern autumn and spring 1992 not shown) and 90 hPa.

However, by 68 hPa the crossing distributions become spread out under the effects of the QBO winds such that crossing distributions become much more even around latitude circles. These can be seen from figure 5.12, which shows 68 hPa crossing-distributions for the same trajectory subsets as were used to create figure 5.9. The statistical significances of these maps is high, even in the summer case where the mean crossing frequency is 14. Though this causes the significance of the 1–14 bin to approach zero, all other bins of the summer case thus have significances approaching 100 %.

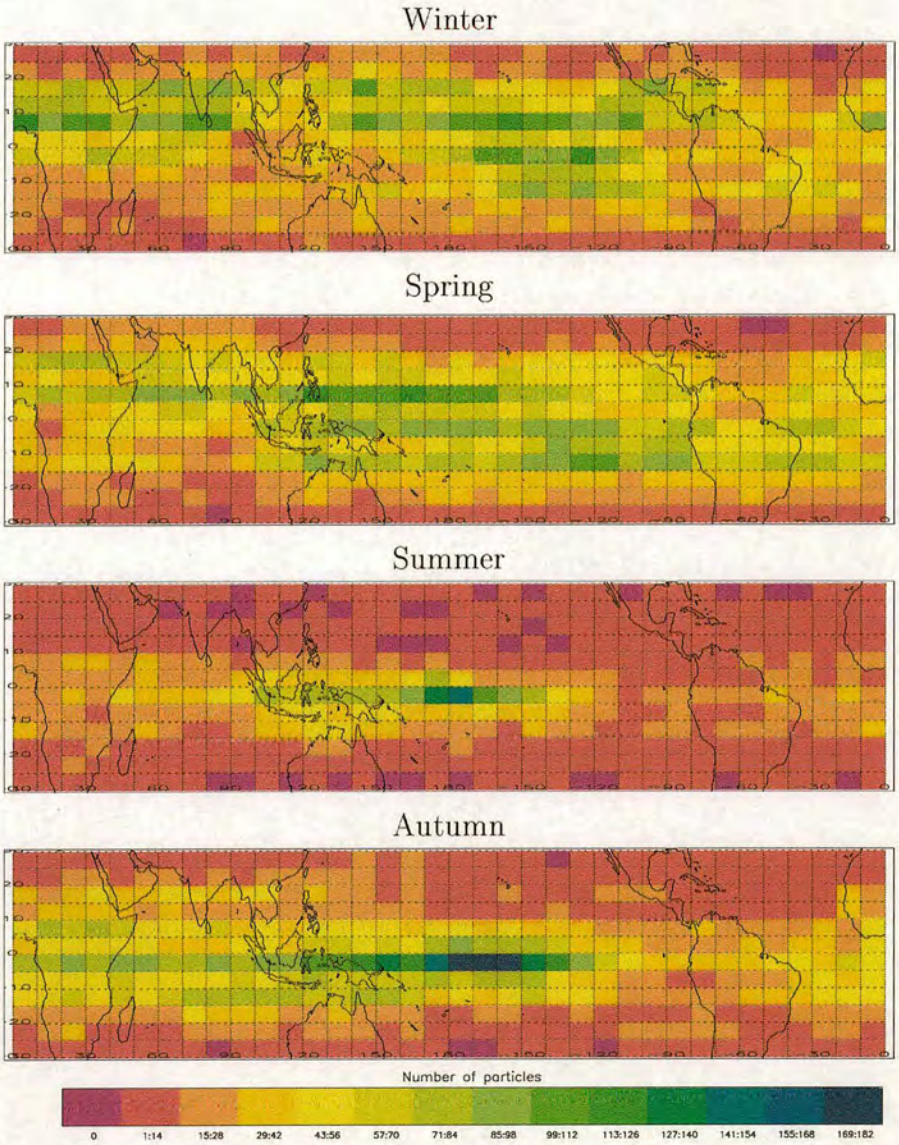

Figure 5.12: **Distribution of Trajectory Crossing Points: Seasons of 1992, 68 hPa.** Shows the positions of air particles at 68 hPa during four separate trajectory runs for the northern hemisphere seasons of 1992. The winter panel is a repeat of the top panel of figure 5.5 but uses a different colour scale. Each map is constructed from the trajectories that reached 68 hPa after having crossed the 110 to 90 hPa layer within thirty degrees of the equator during the respective season. (Note that this is the reason why the distributions are not uniform.) The trajectories used in each case are the same as those used to create figure 5.9, numbering: Winter (January, February, March), 16553; spring (April, May, June), 17151; summer (July, August, September), 6064; autumn (October, November, December), 13393.

If the cross-tropopause flow were controlled from below then a spread of the trajectories from a single region could easily be explained by the influence of the QBO winds. If the control comes from above however, then some force must limit the extent of the stratospheric, wave-driven motion or QBO in longitude. This would imply that either one or both of the wave-driven motions have an uneven distribution or their longitudinal extent reduces between 68 and 90 hPa. (This latter case might explain the increase in flow strength that comes with the decrease in area.) At this time is not possible to verify either suggestion as the current understanding of the longitudinal distribution of the stratospheric wave-breaking is insufficient[†].

Whatever the predominant force is that gives rise to the motions calculated, the statistical significances of the crossing-frequency distributions at all pressure levels are high. Furthermore, the uplift suggested by the maps of this section are in good basic agreement with the uplift inferred from the water-vapour analysis presented in the previous chapter for the 1992 data. The northern summertime uplift in both cases is seen to be confined along the equator, in a band some 20 degrees of latitude wide. The northern wintertime uplift in both cases is wide-spread across the tropics.

Note that it cannot be expected that the details of figure 4.13 will correspond to those of figure 5.12, since the former shows monthly averages and the latter seasonal. Nevertheless, the large-scale results of the separate investigations do corroborate each other. Hence, a good level of confidence can be had that the mid-Pacific, crossing-frequency maximum is a real, believable feature of tropical STE.

5.4 Flow-Change Hypothesis

The *flow-change hypothesis* was tested by examining the spatial, crossing-event distributions of trajectories created for the early 1980s and the early 1990s. In this way it was determined whether the crossing patterns discovered in the last section persisted through both decades or whether the distributions exhibited significant variation.

[†]For a discussion see section 2.1.2 — The Brewer-Dobson Circulation.

Figure 5.13 shows the crossing distributions at 90 hPa for trajectory subsets calculated for the winters (January, February and March) of the years 1980, 1981, 1992 and 1993. As in previous maps, the subsets comprise those trajectories reaching 68 hPa after having crossed between 110 and 90 hPa within thirty degrees of the equator. The panel for 1992 is a repeat of the middle panel of figure 5.5 but uses a different colour scale.

The crossing distributions in figure 5.13 all show the mid-Pacific maximum seen in previous distributions, with the statistical significances of 53 or more crossing events always being greater than 97 %. Furthermore, the inter-year variation in the 90 hPa crossing distributions is largely similar to the inter-seasonal variation. The crossing events always cover most of the tropics and an increase in crossing events in the mid-Pacific is again accompanied by tighter concentration of the overall crossing to the Pacific and its neighbouring land areas. This similarity extends to the connection between the magnitude of the total cross-tropopause flow and the concentration of crossing events to the mid-Pacific.

The total number of trajectories crossing the tropical layer each year, and hence the number in each subset, is shown in figure 5.14, which comprises histograms of the number of days taken to cross the tropical layer. When considered along with the distributions of figure 5.13 the crossing values show that the strongest concentration of crossing events to the mid-Pacific occurs when the overall cross-tropopause flow is weakest — in 1993. Though only four years of data have been analysed the pattern does hold for all four, with increasing overall flow strength and increasing spread of crossing events throughout the tropics occurring as — 1993, 1981, 1980, 1992.

Confirmation that the inter-year variations are small differences in the strengths of local crossing-frequencies and so not indicative of a change in the mechanism of the cross-tropopause flow can be taken from the histograms of figure 5.14. The figure shows that the distribution of times taken to cross the tropical layer are similar between the years. In all four cases the mode crossing times are small compared to the time that would be taken to cross between 110 and 90 hPa at the speed of the mean stratospheric upwelling as deduced by Mote *et al.* (1996, 1998) — 2 days compared to approximately 20 days.

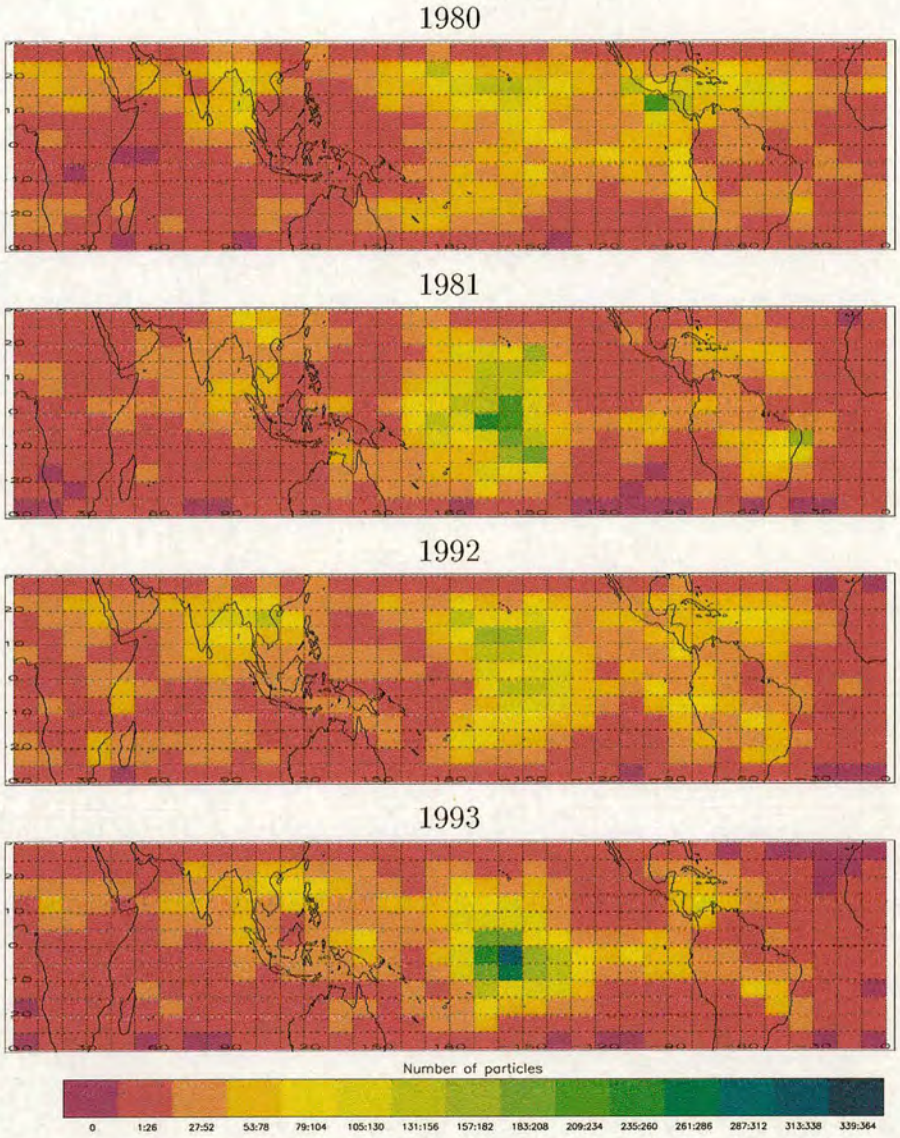

Figure 5.13: **Distribution of Trajectory Crossing Points: Four Winters, 90 hPa.** Shows the positions of air particles at 90 hPa during four separate trajectory runs for the northern winters of 1980, 1981, 1992 and 1993. The 1992 panel is a repeat of the middle panel of figure 5.5 but uses a different colour scale. Each map is constructed from the trajectories that reached 68 hPa after having crossed the 110 to 90 hPa layer within thirty degrees of the equator during the respective winter. The number of trajectories used in each case is: 1980, 15170; 1981, 14795; 1992, 16553; 1993, 13908.

Similar conclusions about the mechanism of the cross-tropopause motion can be drawn from histograms of the number of horizontal boxes crossed and of the number

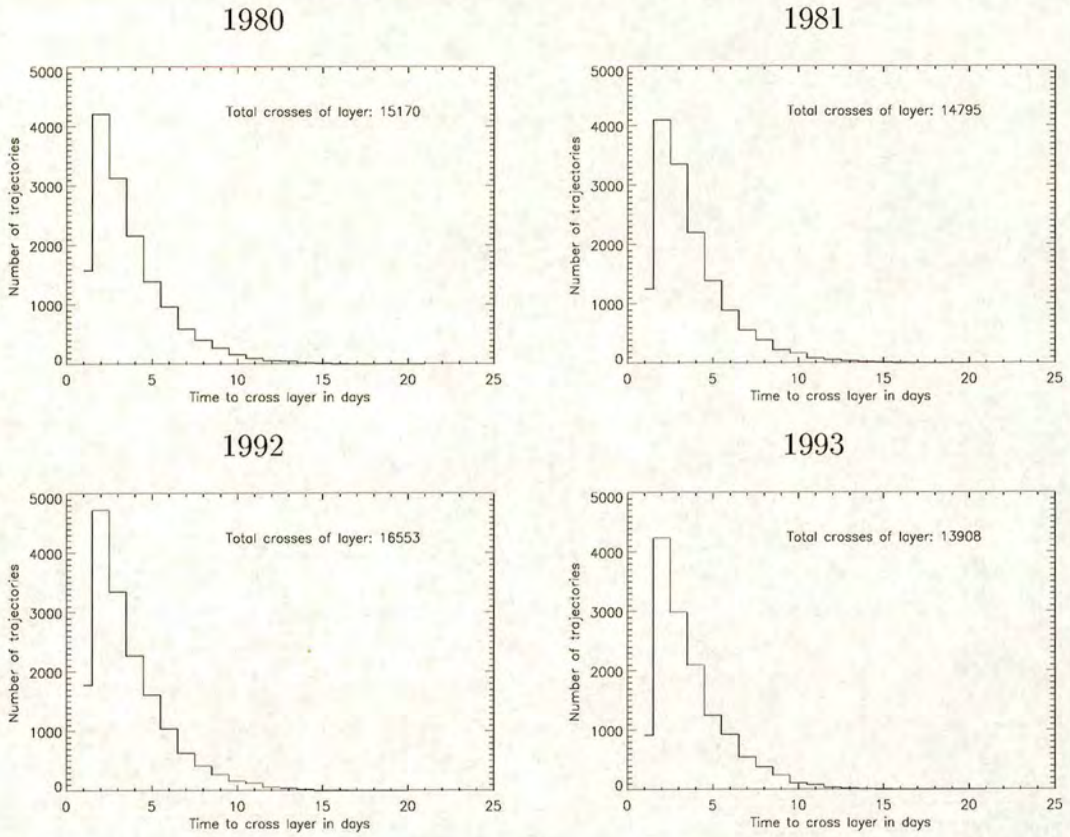

Figure 5.14: **Details of the Trajectory Paths: Four Winters.** Indicates the time trajectories took to cross the 110 to 90 hPa layer during four northern winters — 1980, 1981, 1992 and 1993. Only trajectories that reached 68 hPa after having crossed between 110 and 90 hPa within thirty degrees of the equator are considered. The number of trajectories crossing in this fashion, in each winter, is also indicated.

of upward turning-points. Since these histograms have similar relative patterns to figure 5.14 however, they not shown here. Taken together these results and distributions shown in figure 5.13 suggest that the *flow-change hypothesis* does not hold — there is no significant change in the mechanism of the cross-tropopause motion between the early 1980s and the early 1990s. There is not a change of cross-tropopause motion from occurring through a mesoscale region in the 1980s to a more tropics-wide uplift in the 1990s.

Nevertheless, inter-year variations can be observed, variations which might indicate whether tropospheric or stratospheric motions dominate the cross-tropopause flow. Once again, difficulties when trying to ascribe dominance to tropospheric and

stratospheric motions.

If tropospheric motions were dominant then variations in the trajectory crossing-point distributions of figure 5.13 would match ENSO variations, the phase of which, for the four years used in the figures above, is indicated in table 5.2. If the ENSO had strongly altered the magnitude of the cross-tropopause flow during the four years investigated then the strongest mid-Pacific crossing would be expected during the strongest warm phases of the ENSO[†]. Moreover, the positions of the highest crossing-frequencies would be expected to move in longitude with the position of the strong convection below. However, table 5.2 shows that there is no correlation between the strength of the crossing maxima and the phase of the ENSO. The strongest El Niño occurs with the weakest crossing-frequency maxima in 1992 and the ENSO exhibited a neutral phase when the mid-Pacific crossing frequency showed increase in 1981. Furthermore, the crossing-frequency maxima in figure 5.13 exhibit no significant longitudinal variation.

Northern Hemisphere Season		**QBO**	**ENSO**
1980	Winter	Easterly	Weak warm
1981	Winter	Westerly	Neutral
1992	Winter	Easterly	Strong warm
1993	Winter	Westerly	Weak warm

Table 5.2: **Phases of the QBO and ENSO — Inter-Year Comparison.** Shows whether the QBO exhibited westerly or easterly winds at 68 hPa and the relative strength of the El Niño as a function of season for the lifetime of the 183 GHz antenna. (There were no La Niña events during this time.) The QBO data is determined using data from the Singapore radiosonde station and the ENSO event is as measured by for Environmental Prediction (2002).

Nevertheless, if the stratospheric, wave-driven circulation dominates the cross-tropopause flow the decreasing area of the crossing-frequency maxima must still be explained. In the case of the winters of 1980, 1981 and 1993, the 68 hPa crossing-distributions are much less concentrated towards the Pacific than the 90 hPa distributions, just as in the 1992 case. This is apparent from figure 5.15, which shows the 68 hPa crossing distributions for the trajectories that crossed between 100 and

[†]Figure 2.1 shows the positions of convection under the neutral and warm phases of the ENSO.

90 hPa in the tropics for all four winters.

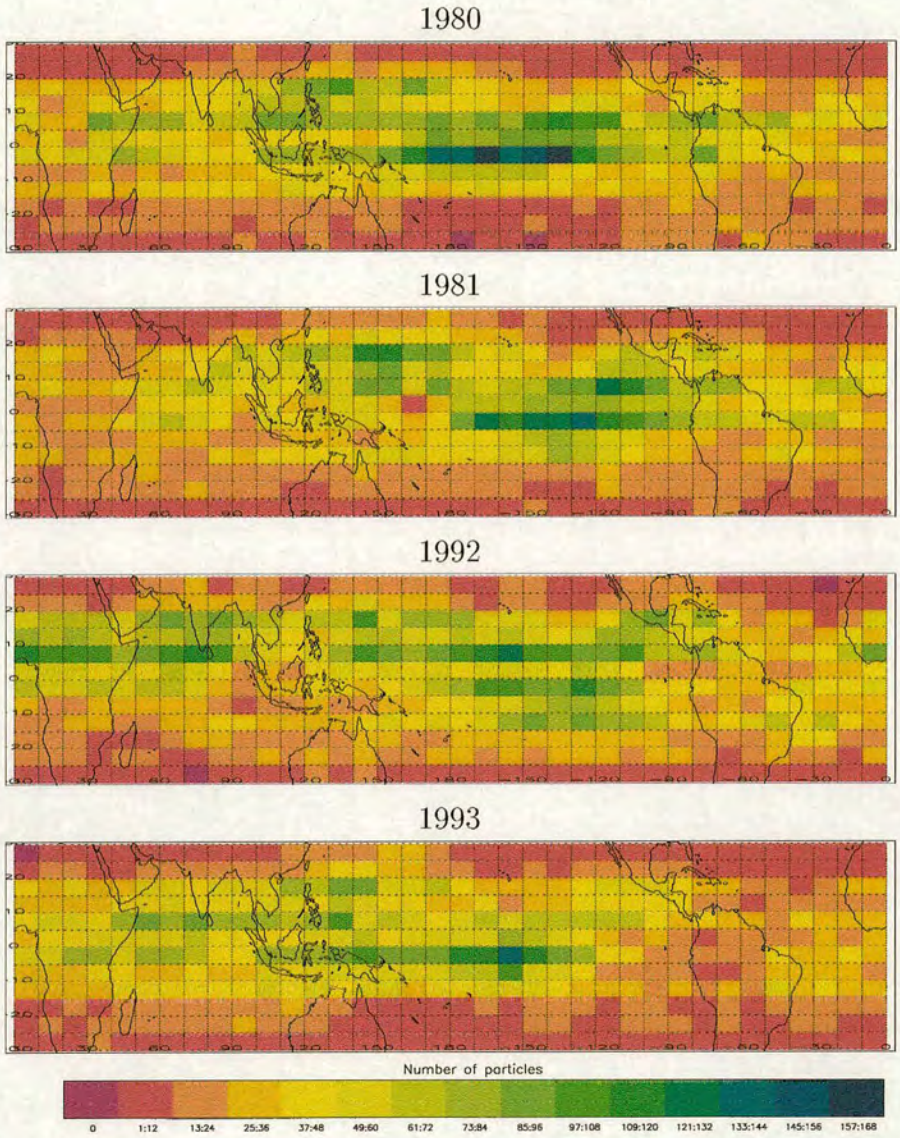

Figure 5.15: **Distribution of Trajectory Crossing Points: Four Winters, 68 hPa.** Shows the positions of air particles at 68 hPa during four separate trajectory runs for the northern winters of 1980, 1981, 1992 and 1993. The 1992 panel is a repeat of the top panel of figure 5.5 but uses a different colour scale. Each map is constructed from the trajectories that reached 68 hPa after having crossed the 110 to 90 hPa layer within thirty degrees of the equator during the respective winter. (Note that this is the reason why the distributions are not uniform.) The trajectories used in each case are the same as those used to create figure 5.13, numbering: 1980, 15170; 1981, 14795; 1992, 16553; 1993, 13908.

Again as in the 1992 cases, the simplest explanation for the increasing spread of the mid-Pacific, crossing-frequency maxima with height would be the influence of the QBO winds upon an exchange forced from below.

It is noted that the low significances of the 1993 difference maps presented in figure 4.13 mean that the uplift deduced by three-dimensional trajectory calculations cannot be verified for this year. Furthermore, a lack of MLS data for the years 1980 and 1981 means that no validation of the three-dimensional trajectory calculations can be performed for these years either. In the case of all three years, the results of this chapter must, therefore, be treated with caution. However, the significances of the distributions for these years are always high, giving some confidence that at least their large-scale detail is accurate. Nevertheless, their small-scale detail must be treated as unreliable.

5.5 Above 90 hPa

The results of this chapter so far have shown that there is some spatial preference in trajectory crossing-distributions at 110 and 90 hPa and a tendency for the tropical motion between these two levels to occur rapidly, with reduced horizontal motion. However, it was also suggested that a change in the uplift occurs somewhere between 90 and 68 hPa. In this section the nature of the uplift between 90 and 68 hPa is examined to determine how it differs from the cross-tropopause motion.

Figure 5.16 shows histograms of the time taken by air particles to travel between 90 and 68 hPa. The histograms are created from a subset of trajectories calculated for October 1992. The subset is again comprised of only those trajectories crossing between 110 to 90 hPa within thirty degrees of the equator. Histograms for other months of the years 1980, 1981, 1992 and 1993 show similar patterns, as do histograms of the horizontal motion travelled and of upward turning-points along the journey. As such, only the crossing-time data for October 1992 is displayed here.

The left-hand histogram shows two distributions. The solid-line histogram shows the number of days taken to move between 90 and 68 hPa by all trajectories in the

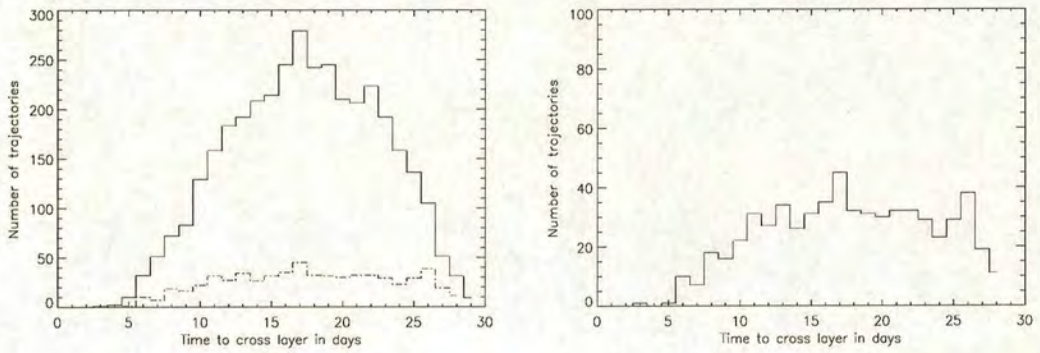

Figure 5.16: **Crossing Details — 90 to 68 hPa.** Shows histograms of the crossing times for trajectories moving between 90 and 68 hPa. Only trajectories that arose through the 110 to 90 hPa layer within thirty degrees of the equator from a release for October 1992 are considered. On the left all trajectories of this subset are binned in solid-line histogram. The dot-dash histogram on the same plot show a subset of these trajectories: Those particles that crossed the 110 to 90 hPa layer during the peak number of days. On the right the subset histogram is shown on a smaller scale.

subset described above. The right-hand histogram and the dot-dash histogram on the left show the time taken by a further subset of *these* trajectories — those that crossed between 110 and 90 hPa during the mode number of days for that crossing, *i.e.* 2 days.

Figures 5.12 and 5.15 suggest that the tropical flow between 90 and 68 hPa is more uniform in space than the cross-tropopause motion below. The histograms of figure 5.16 further suggest that this larger spatial spread is accompanied by a larger spread in the time of the crossing the upper layer.

Together the histograms show that the time taken for air to move between 90 and 68 hPa has a Gaussian-like distribution centred on around 18 days and that this time taken is independent of the method of crossing between 110 and 90 hPa. Furthermore, 18 days is close to the time of travel that would result from annual-mean upwelling velocity as deduced by Mote *et al.* (1998) at 0·5 mm s^{-1} — around 23 days (assuming a distance travelled of around 1 km). The Gaussian centre of similar histograms for the other months discussed in this chapter come even closer to this figure, varying between around 18 and 21 days.

Hence, somewhere between 90 and 68 hPa there is a change in the uplift. Below the change height there is a preferred region of uplift in the mid-Pacific and a tendency towards rapid-vertical, reduced-horizontal motion. Above the change height the uplift becomes spread throughout the tropics and its mean speed tends toward the annual-mean upwelling velocity of the stratosphere. Note that the exact height of the change cannot be determined from the results presented above since they are limited by the vertical resolution of the ECMWF wind-data.

5.6 Summary and Discussion

The *uniform-entry* and *flow-change* hypotheses were disproved by three-dimensional trajectory analysis. A preferential region of entry into the stratosphere has been shown to exist; despite the fact that air does enter the stratosphere throughout the tropics, a maximum in the crossing-distributions occurs in the mid-Pacific. Furthermore, this pattern in the cross-tropopause motion was found to have occurred throughout all seasons of 1992 and all winters of the years 1980, 1981, and 1993. Thus, though the distribution of crossing events in the tropics may have differed slightly within these time periods, the change was not significant and the same mechanism of cross-tropopause motion appears to have been working during them all.

Throughout all the time periods analysed a maximum in the crossing distributions was observed at both 110 and 90 hPa in the mid-Pacific between the Hawaiian islands and Polynesia. Crossing events were found to more concentrated towards this area during autumn and summer 1992 than during winter and spring 1992 and also more concentrated there during 1993 and 1981 than during 1980 and 1992. At all times when the crossing events were seen to be concentrated in this way the overall flow into the stratosphere was found to be weaker.

In chapter 4 evidence was presented to suggest, for the northern winter, first, that the Indonesian region is not the sole point of entry into the stratosphere and second, that Indonesia, Panama and the central Pacific are not *all* regions of preferred entry.

This led to the conclusion that the simplest explanation for the longitudinal variations in MLS, water-vapour data at 68·1 hPa is that they are caused by variations in tropopause height and a uniform uplift. The results of chapter 5 however, show that, though air does enter the stratosphere throughout the tropics, a preferential region of entry does exist in the central Pacific.

Nevertheless, the results of the separate chapters are not conflicting. Taken together, figures 5.7, 5.14 and 5.16 suggest that the first occurrence of the lowest mixing ratios outside the region of preferential entry (over Indonesia rather than the central Pacific in the northern winter, see figure 4.5) is a believable feature of the exchange. Taken together, these figures show that some particles reach 68 hPa much faster than would be expected under the global-mean, stratospheric upwelling-velocity and that particles travelling so are spread throughout the tropics. Hence, though the region of preferential entry does not occur over Indonesia, a tropics-wide uplift exists that is capable of preserving a water-vapour pattern, imposed at the tropopause, to 68 hPa. Moreover, the pattern is preserved despite a change in the mechanism that dominates the uplift, occurring somewhere between 90 and 68 hPa.

Since this distribution of uplift is present throughout all time periods analysed, the compromise offered by Zhou *et al.* (2001) cannot explain the increase in lower stratospheric water between the 1980s and 1990s. Zhou *et al.* (2001) suggested that the fountain theory may previously have been required to explain the low water-vapour values of the stratosphere but no longer, since the long-term trends in the lower-stratospheric water-vapour show it to be rising. A change in the mechanism of cross-tropopause flow could have caused such a water-vapour change. Though such a mechanism change was not observed between the 1980s and 1990s, it may still be the case that a mechanism change occurred before the 1980s. A future experiment might make use of the ERA–40 data, which was not available at the time this investigation was performed, to usefully extend examination of the *flow-change hypothesis* back to the 1960s.

The results of this chapter are an important addition to the trajectory study performed by Jackson *et al.* (2001). Their study also used ECMWF wind data in conjunction with the trajectory routine of Methven (1997) but they did not investi-

gate airflows throughout the entire tropical lower-stratosphere. Jackson *et al.* (2001) released three-dimensional trajectories over the four regions of strongest convective activity — Indonesia, the central Pacific, Africa and South America. They released forward trajectories from 150 hPa and from the lapse-rate tropopause height and backward trajectories from the cold-point tropopause height.

Jackson *et al.* (2001) found that trajectories released over the Indonesian and central Pacific regions described a rapid motion, associated with convective activity, up to the height of the lapse-rate tropopause and a slow ascent over these regions above around 100 hPa. The air particles they released over these regions showed a tendency to enter the stratosphere over the Pacific Warm Pool. The trajectories they calculated for regions above Africa and South America however, showed no such preferential entry, tending to cross the tropopause near to their areas of release.

Jackson *et al.* (2001) also note that the tropopause crossing-locations of the air-particles they released from 150 hPa did not correlate with the positions of the coldest tropopause temperatures. They further explain that the reason the African and South American trajectories did not reach a western-Pacific entry point was because the horizontal winds in the former locations were much smaller. Nevertheless, they suggest that a preferred region of entry into the stratosphere occurs over the western Pacific.

A simpler interpretation of their results however, is that there is no region of preferential entry. Their results could just as easily be explained by a uniform uplift and crossing locations determined by horizontal winds below the tropopause. This simpler explanation holds because of their use of spatially-confined release sites. The advantage of a release of trajectories across the entire tropics from 68 hPa, as used to create the results of this chapter, is that the origins of all air entering the stratosphere are determined. Release from individual locations could only determine part of the description of stratospheric entry.

The results of this chapter are also in contradiction to those of previous studies of stratosphere-troposphere exchange that do make use of assimilated-data sets but not of trajectory calculations. Such studies have not found a preferential region

of entry into the stratosphere. Gettelman and Sobel (2000) combined the Goddard Earth Observation System data with the analysis technique proposed by Wei (1987). Gettelman *et al.* (2000) combined the same data with the three-dimensional chemical transport model of the Goddard Space Flight Center. The former authors investigate the overall mass flux whilst the latter investigate developing distributions of water vapour. Both investigations found the cross-tropopause mass-flux to be horizontally uniform throughout all tropical latitudes and longitudes.

However, Gettelman and Sobel (2000) advise caution in interpreting their results, since the method proposed by Wei (1987) may not correctly diagnose the instantaneous, tropical, cross-tropopause mass-flux, specifically that associated with convection. Thus Gettelman and Sobel (2000) suggest that whereas their results should adequately represent the residual circulation of the stratosphere they will not include local phenomenon.

Furthermore, Gettelman *et al.* (2000) suggest that their model does not adequately represent observed, water-vapour distributions near 100 hPa. They also offer a lack of convection in their model as explanation, as well as unconsidered wave alteration of local tropopause height and temperature.

Clearly, the lack of a proper representation of convection cannot be the cause of a difference between the results of this chapter and those of Gettelman *et al.* (2000) and Gettelman and Sobel (2000), since the ECMWF model does not resolve individual convective events either. The clearest difference between the investigation reported in this thesis and the those reported in Gettelman and Sobel (2000) and Gettelman *et al.* (2000) is the use of different models and analysed-data. It is possible therefore that a different treatment of, for example, gravity waves is responsible for the difference in the vertical motions observed.

The final possible inconsistency between the results presented in this thesis with those of other authors occurs with the findings of Plumb and Eluszkiewicz (1999). These authors suggest that the maximum upwelling at 68 hPa is usually found in the summer hemisphere[†]. Having examined data for the years 1992 to 1994, they found

[†]Recall figure 2.6 and the discussion in section 2.1.2 — The Brewer-Dobson Circulation

the only exception to occur between September 1992 and March 1993. During these months they found the maximum upwelling to be at the equator. The results of this thesis did not concur for the winter 1992 case, finding instead that the maximum in the uplift occurred in the winter hemisphere for the January to March season. However, the winters of 1980 and 1981 showed a summer hemisphere maximum and the winter 1993 equatorial maximum is observed in both figures 2.6 and 5.15.

This final inconsistency could be explained by the assumption generally taken in this thesis that air takes a month to travel between the 100 and 68 hPa surfaces. The results of both chapters 4 and 5 have suggested, however, that a significant number of trajectories crossed between these surfaces an order of magnitude faster than the mean upwelling velocity of the stratosphere. Further work repeating the analysis with the standard seasons could therefore reveal different positions for the maxima in trajectory crossing-point distributions.

Nevertheless, the two-dimensional advection results of chapter 4 corroborate the large-scale uplift distribution deduced from the trajectory analysis presented in this chapter. Furthermore, the significances of three-dimensional trajectory results for all years examined were always high. This suggests that, though the position of the centre of the crossing-frequency maxima may sometimes be in doubt, the large-scale features of the crossing distributions are believable. Hence, good confidence can be had that there does exist a year-round maximum in the cross-tropopause over the mid-Pacific.

In the next and final chapter an explanation for the existence of this increased cross-tropopause flow is proposed. Moreover, an attempt is made to reconcile the fact that the rapid uplift calculated to have occurred between the 100 and 90 hPa surfaces, some eleven times the speed of the global-mean, stratospheric upwelling velocity, occurs away from the regions of strongest convective activity.

Chapter 6

Discussion

Using 68 hPa, water-vapour data from the Microwave Limb Sounder (MLS) instrument and trajectories calculated from the assimilated data of the United Kingdom Meteorological Office (UKMO) and the European Centre for Medium-Range Weather Forecasts (ECMWF), three hypotheses regarding stratosphere-troposphere exchange were investigated:

1. **Fountain Hypothesis.** Cross-tropopause motion only occurs over the area of strongest convection, the remaining tropical stratosphere being ventilated by adiabatic redistribution of the air from the convective source-region.

2. **Uniform-Entry Hypothesis.** No preferential region of cross-tropopause motions exists; air enters the stratosphere in an even distribution in both space and time throughout the tropics.

3. **Flow-Change Hypothesis.** A significant change occurs in the mechanism of cross-tropopause motion between the early 1980s and the early 1990s.

This investigation led to the following conclusions:

1. The evolution of water vapour between November 1991 and March 1993 at 68 hPa is inconsistent with the idea of a stratospheric fountain reaching this height. The 68 hPa evolution cannot be explained by isentropic redistribution from source regions over the strongest convective activity.

2. A region of preferential uplift exists at 110 and 90 hPa in the tropical mid-Pacific during all time periods examined — the winters of 1980, 1981 and 1993 and all the seasons of 1992.

3. There is no significant change in the mechanism of cross-tropopause flow between the early 1980s and the early 1990s, only in the strength of the preferential flow and its concentration into the mid-Pacific.

The first statement argues against the existence of a "stratospheric fountain" as suggested by Newell and Gould-Stewart (1981). If such a phenomenon existed and reached up to 68 hPa then the isentropic advections of water vapour presented in chapter 4 would have been far more similar to the observed evolutions. Though this does not disallow a "stratospheric fountain" reaching to a lower level of the stratosphere, the uplift deduced in chapter 5 does. In that chapter it was shown that some air particles travel rapidly between 110 and 68 hPa in most regions of the tropical Pacific. The combined results of both chapters make exchange through a small, confined area appear unlikely.

Statement two indicates that there is still a region of preferred entry into the stratosphere however, occurring over the tropical mid-Pacific between the Hawaiian islands and Polynesia. Though uplift was found to occur at 110 and 90 hPa throughout most of the tropics, the number of trajectories crossing both surfaces was found to be at least three times higher in the mid-Pacific than anywhere else.

The third statement argues that the mid-Pacific sees preferential entry throughout both decades examined, such that the cross-tropopause motion did not change from a "stratospheric fountain" mechanism in the early 1980s to a Pacific-dominated crossing-mechanism in the early 1990s. The limited time frame of the analysis of chapter 5 does mean however, that such a change could still have occurred at an earlier time.

6.1 On the Facts Discovered and the Data Used

During the investigation of the three hypotheses, other information about the nature of the motion in the tropical tropopause layer and about the characteristics of the three datasets used was discovered. The lists that comprise this section collect together all the conclusions from previous chapters, detailing them in three groups — motion across the tropopause, motion towards the top of the tropical tropopause layer and the three datasets used throughout the study.

The Cross-Tropopause Motion

- Uplift across the 110 and 90 hPa surfaces occurred over most of the tropical region.
- The uplift over areas of the strongest, most wide-spread convective activity (Indonesia in the northern winter and India in the northern summer) was much less frequent than the average for both the 110 and 90 hPa surfaces.
- The uplift across the 110 and 90 hPa surfaces was much more frequent over the tropical Pacific than anywhere else in the tropics for all times examined — the winters of 1980, 1981 and 1993 and all the seasons of 1992.
- The relative magnitude of the mid-Pacific maximum in crossing-frequency compared to the greatest frequency of crossing events elsewhere was:
  - Always less at 90 hPa than 110 hPa;
  - greater in the summer and autumn of 1992 than in the winter and spring of 1992;
  - greater in 1993 and 1981 than in 1992 and 1980.
- The mechanism of the uplift between the 110 and 90 hPa surfaces was not significantly different between all years examined — 1980, 1981, 1992 and 1993.
- The position of the crossing-frequency maximum did not exhibit variation that could be linked to the phase of the El Niño Southern Oscillation.

- The uplift between the 110 and 90 hPa surfaces showed a tendency towards being a rapid, uninterrupted motion partnered by little horizontal motion.
- A slightly higher percentage of particles crossing the 110 to 90 hPa layer in the mid-Pacific moved in this rapid manner than elsewhere in the tropics.
- The mode speed of the uplift between the 110 and 90 hPa surfaces was around eleven times the global-mean upwelling velocity of the stratosphere.

Motion Near the Top of the Tropical Tropopause Layer

- When the concentration of the cross-tropopause flow at 110 and 90 hPa in the mid-Pacific was greatest (autumn and summer 1992, winter 1981 and 1993) a mid-Pacific, crossing-frequency maximum was also visible at 68 hPa.
- The uplift between 90 and 68 hPa was different from the uplift between 110 and 90 hPa. Particles crossing the former layer exhibited Gaussian distributions of travel time, distance moved in the horizontal and interruptions to their journey, whereas the distributions of such characteristics for the crossing of the latter layer exhibited a strong bias towards low values.
- The total water vapour reaching 68 hPa and its distribution on this surface showed notable inter-year differences:
  - The position of the minimum in the water vapour mixing ratio features is closer to Indonesia in 1993 than in 1992, consistent with variations in ENSO strength and thus implying convective influence above 90 hPa;
  - mixing ratios were generally lower in November and December 1992 than in the previous year, consistent with the QBO easterlies of 1992 causing lower tropopause temperatures in 1992 relative to 1991;
  - mixing ratios were generally higher between January and March 1993 than in the previous year, consistent with the QBO easterlies of 1992 causing lower tropopause temperatures in 1992 relative to 1993;
  - there is less of a band-like structure in the 1993 winter data than in the 1992 winter data.

- Irrespective of the difference in concentrations of water vapour between 1992 and 1993 the lowest water-vapour concentrations arrive at 68 hPa in March of both years.

- The positions of extreme water-vapour concentrations at 68 hPa correspond better with the extreme values of the mean height of the tropopause indicated by Seidel *et al.* (2001) than with crossing-frequency maxima in the TTL. Given that rapidly moving air particles are found throughout the TTL, the 68 hPa water vapour distribution is more likely under the control of the local tropopause height than differential uplift.

The Three Datasets Used

- The version 0104 retrieval of MLS data was discovered to be more accurate than version 5 in representing the water vapour at the retrieval nodes 100·0, 68·1 and 46·4 hPa since:
  - the version 0104 retrieval showed a lesser dependence upon its *a priori*;
  - the version 0104 retrieval showed smaller differences between data obtained on the ascending and descending legs of the satellite path.

- Data from the UKMO better captured the zonal wind measured by the Changi Airport radiosonde in Singapore.

- Data from the ECMWF better captured the meridional wind measured by the Changi Airport radiosonde in Singapore.

- Errors in two-dimensional advections of water-vapour data were shown to be small enough not to obscure meaningful results.

6.2 On the Consequences for The Exchange

The mechanism or mechanisms that control the cross-tropopause motion give rise to a tropics-wide uplift and a further increased mass-flux crossing over the mid-Pacific.

The former uplift is well described by the stratospheric, wave-driven uplift but the second is not; it could be described equally well by:

1. A buoyancy force in the troposphere or at the tropopause, the magnitude of which decreases with height above the tropopause;

2. a concentration of part of the stratospheric, wave-driven motion or the QBO above the Pacific, whose effects decreases in horizontal area and correspondingly increases in mass-flux density as it reaches down to the tropopause.

There is no current evidence to suggest that the stratospheric motions will concentrate in longitude as they reach down to the tropopause. Moreover, a tropospheric buoyancy force would more easily explain the observed cross-tropopause flow, even though one of the strongest of such forces observed in the troposphere gives rise to a downflux of air in the tropical tropopause layer. Thus, though convection may play a part in the drying of air, it may not be important in the final exchange of air into the stratosphere. However, it is possible that the conditions above convection in differing regions are not the same across the tropics.

6.2.1 The Mechanism of the Tropical Drying and Exchange

In section 2.3, four current theories for the tropical drying and exchange of air into the stratosphere were discussed. They are each revisited here in relation to the results of this thesis.

The "Stratospheric Fountain" Theory.

The results of chapters 4 and 5 showing that uplift is common across the whole tropical region and throughout the year, in agreement with the findings of many previous authors (see, for example, Dessler (1998) and Gettelman *et al.* (2000)), show that this is most likely not the mechanism in operation.

Kelvin-Wave Exchange.

If the cold temperatures above the Pacific Warm Pool are required to freeze-dry air to stratospheric values then the fact that majority of cross-tropopause motion occurs in the mid-Pacific implies the drying and exchange processes are separate mechanisms. Hence Kelvin-wave exchange is most likely not the dominant mechanism for tropical STE.

Convective-Drying and Subsequent Exchange.

The results of chapter 5 showed minima in the trajectory crossing-point distributions at 110 hPa as well as at 90 hPa above Indonesia and the Pacific Warm Pool. Hence, whereas the results chapter 5 implied that convection does influence air motions above 90 hPa, they also implied that this is the case in most regions except those above Indonesia and the Pacific Warm Pool. This suggests that convective-drying and subsequent exchange is not the most likely of the four proposed mechanisms for the tropical stratosphere-troposphere exchange.

Advective-Drying and Subsequent Exchange.

This thesis focused upon motion in the tropical tropopause layer and in the stratosphere. Hence, no evidence can be drawn from this thesis to either support or contest the validity of the mechanism of advective-drying proposed by Hartmann *et al.* (2001). However, if this mechanism were in effect below 110 hPa then it could feasibly freeze-dry a sufficient amount of air to explain the average stratospheric, water vapour entry-value before the air is drawn up into the stratosphere via a mid-Pacific uplift.

6.2.2 A Possible Description of the Tropical Exchange

The proposal of Hartmann *et al.* (2001) and Holton and Gettelman (2001) would allow for differing air motions above the convection of Indonesia and the convec-

tion above India and the remaining ITCZ. The conditions placed on relative cloud heights and distributions required to support the subsidence and cooling above the Indonesian convection in their theory are very specific. Hence, they could conceivably be unique to this region and not necessarily occur in the mid-Pacific. This would allow convection to remain the dominant force for tropical exchange despite subsidence above one of the strongest of tropical convective regions.

The magnitude of a convective, buoyancy force would decrease with height above the temperature minimum and an airflow so forced would be increasingly disturbed by QBO winds upon moving into the stratosphere, characteristics that are necessary to explain the differing distributions of trajectory crossing-points at 110, 90 and 68 hPa presented in chapter 5. Buoyancy forces also occur across the entire tropics, which would explain the fact that particles moving rapidly in the vertical between 110 and 90 hPa were observed throughout the tropical region. The concentration of the buoyancy force to the mid-Pacific could be explained by the semi-permanent position of the ITCZ at the equator in that area. Moreover, this semi-permanent position would also account for the crossing-frequency maxima being found there all year round.

The only weakness to such a theory is the apparent lack of connection between the temporal variations of the ENSO and the crossing-frequencies. The semi-permanent position of the ITCZ allows the spatial variations of the ENSO and the crossing-frequencies to differ but an increase in magnitude of the cross tropopause flow in the mid-Pacific would still be expected during strong El Niño conditions. It is possible however, that this would not have been observed in back trajectories released from the stratosphere. Such a condition might require forward trajectories, released from the troposphere, to observe it. Furthermore, only four years' worth of data were used in this study; a repeated experiment with more data might well reveal a connection missed here.

6.3 Further Work

There are several experiments that would serve either to increase confidence in results already obtained or to gather further information on stratosphere-troposphere exchange:

1. **A re-analysis using longer running datasets.**

   (a) **Water vapour:** A limitation of the MLS data is that it covers only two winters, one spring, one autumn and half a summer. The launch of the EOS AURA satellite will hopefully provide the same high-frequency coverage of the entire tropical region that MLS did but for a longer time.

   (b) **Winds:** Use of the ERA-40 data would allow the investigation into the long term trends in the cross-tropopause flow to be extended back to the 1950s. The current investigation covered only ten years, which may be too short a time to reveal any trends.

2. **Trajectory runs released from 90 hPa and 110 hPa.** Trajectories initialised at 68 hPa were used to discover more about the origins of the extreme water-vapour concentrations seen at this level and to deduce air motion within the tropical tropopause layer. A more detailed study of the cross-tropopause motion could be obtained by releasing forward trajectories from 110 hPa and backward trajectories from 90 hPa. This is a change that could be applied to the experiments already performed. Using the same grid of initialisation more trajectories would cross the 110–90 hPa layer, making results more significant.

3. **Determining the height of the longitudinal preference in stratospheric motion.** Back trajectories could be released from higher in the stratosphere to determine the maximum height of the longitudinal preference for crossing frequency. This maximum height could then be compared to the height that could be reached by air with the energy obtained from buoyancy-forced uplift in the mid-Pacific.

4. **Determining the connection to convective activity.** The potential temperature and humidity changes that occur along trajectory paths could be traced to determine if the mid-Pacific, crossing-frequency maxima is connected to convection.

5. **Comparison of water vapour distributions to tropopause heights.** MLS water-vapour maps could be compared to monthly-mean and five-day-averaged tropopause heights. Correlation would reveal whether the water-vapour distributions could be explained by the rapid uplift of distributions imposed by local variations in the cold-point tropopause height.

6. **A clarification of directions implied from evolution differences.** The evolution differences could be put to greater use when partnered with vertical profiles of the water vapour mixing ratios for the specific times used in the experiments rather than deduced from climatological means. Furthermore, much greater accuracy would be obtained concerning change in the meaning of positive and negative evolution differences if the water vapour profiles were used on the timescales of the five-day average plots rather than the monthly-average data.

7. **A test of the three-dimensional trajectory routine used.** A test of the accuracy of the trajectory routine described by Methven (1997) could be performed by comparing the observed breakdown of a stratospheric polar-vortex to that indicated by a three-dimensional trajectory-calculation. Trajectory runs of greater than ten days would show if the calculations could reproduce a breakdown. During the first ten days of escape from the vortex, particle motions would be expected to remain approximately isentropic, after this time they would not. Note that this would not be a test of the reliability of vertical winds, only a validation of the use of large groups of trajectories.

References

Alexander, M. J., Holton, J. R., and Durran, D. R.: 1995. The Gravity-Wave Response Above Deep Convection in a Squall Line Simulation. *Journal of the Atmospheric Sciences* **52**(12), 2212–2226.

Andrews, D. G. and McIntyre, M. E.: 1976. Planetary Waves in Horizontal and Vertical Shear: The Generalised Eliassen-Palm Relation and the Mean Zonal Acceleration. *Journal of the Atmospheric Sciences* **33**(11), 2031–2048.

Andrews, D. G. and McIntyre, M. E.: 1978. An Exact Theory of Nonlinear Waves on a Lagrangian Mean Flow. *Journal of Fluid Mechanics* **89**(4), 609–646.

Appenzeller, C., Holton, J. R., and Rosenlof, K. H.: 1996. Seasonal Variation of Mass Transport across the Tropopause. *Journal of Geophysical Research-Atmospheres* **101**(D10), 15,071–15,078.

Baldwin, M. P., Gray, L. J., Dunkerton, T. J., Hamilton, K., Haynes, P. H., Randel, W. J., Holton, J. . R., Alexander, M. J., Hirota, I., Horinouchi, T., Jones, D. B. A., Kinnersley, J. S., Marquardt, C., Sato, K., and Takahashi, M.: 2001. The Quasi-Biennial Oscillation. *Reviews of Geophysics* **39**(2), 179–229.

Barath, F. T., Chavez, M. C., Cofield, R. E., Flower, D. A., Frerking, M. A., Gram, M. B., Harris, W. M., Holden, J. R., Jarnot, R. F., Kloezeman, W. G., Kloze, G. J., Lau, G. K., Loo, M. S., Maddison, B. J., Mattauch, R. J., McKinney, R. P., Peckham, G. E., Pickett, H. M., Siebes, G., Soltis, F. S., Suttie, R. A., Tarsala, J. A., Waters, J. W., and Wilson, W. J.: 1993. The Upper Atmosphere Research Satellite Microwave Limb Sounder Instrument. *Journal of Geophysical Research-Atmospheres* **98**(D6), 10,751–10,762.

Becker, E. and Schmitz, G.: 1999. The Role of Orographically and Thermally Forced Stationary Waves in the Causation of the Residual Circulation. *Tellus Series A — Dynamic Meteorology and Oceanography* **51**(5), 902–913.

Black, R.: 1997. *Trajectory Mapping of Water Vapour Measured by the Microwave Limb Sounder.* Ph.D. thesis, The University of Edinburgh, United Kingdom.

Boering, K. A., Hintsa, E. J., Wofsy, S. C., Anderson, J. G., Daube, B. C., Dessler, A. E., Löewenstein, M., McCormick, M. P., Podolske, J. R., Weinstock, E. M.,

and Yue, G. K.: 1995. Measurements of Stratospheric Carbon Dioxide and Water Vapour at Northern Midlatitudes: Implications for Troposphere-to-Stratosphere Transport. *Geophysical Research Letters* **22**(20), 2737–2740.

Boering, K. A., Wofsy, S. C., Daube, B. C., Schneider, H. R., Löewenstein, M., and Podolske, J. R.: 1996. Stratospheric Mean Ages and Transport Rates from Observations of Carbon Dioxide and Nitrous Oxide. *Science* **274**(5291), 1340–1343.

Brewer, A. M.: 1949. Evidence for a World Circulation Provided by the Measurements of Helium and Water Vapour Distribution in the Stratosphere. *Quarterly Journal of the Royal Meteorological Society* **75**(326), 351–363.

Chen, P.: 1996. The Influences of Zonal Flow on Wave Breaking and Tropical-Extratropical Interaction in the Lower Stratosphere. *Journal of the Atmospheric Sciences* **53**(16), 2379–2392.

Chen, P., Holton, J. R., O'Neill, A., and Swinbank, R.: 1994. Isentropic Mass-Exchange Between the Tropics and the Extratropics in the Stratosphere. *Journal of the Atmospheric Sciences* **51**(20), 3006–3018.

Clark, H. L., Billingham, A., Harwood, R. S., and Pumphrey, H. C.: 2001. Water Vapour in the Tropical Lower Stratosphere During the Driest Phase of the Atmospheric "Tape Recorder". *Journal of Geophysical Research-Atmospheres* **106**(D19), 22,695–22,705.

Coy, L. and Swinbank, R.: 1997. Characteristics of Stratospheric Winds and Temperatures Produced by Data Assimilation. *Journal of Geophysical Research* **102**(122), 25,763–25,781.

Danielsen, E. F.: 1982. A Dehydration Mechanism for the Stratosphere. *Geophysical Research Letters* **9**(6), 605–608.

Danielsen, E. F.: 1993. In Situ Evidence of Rapid, Vertical Irreversible Transport of Lower Stratospheric Air into the Lower Tropical Stratosphere by Convective Cloud Turrets and by Larger-Scale Upwelling in Tropical Cyclones. *Journal of Geophysical Research-Atmospheres* **98**(D5), 8665–8681.

Dessler, A. E.: 1998. A Reexamination of the "Stratospheric Fountain" Hypothesis. *Geophysical Research Letters* **25**(22), 4165–4168.

Dessler, A. E.: 1999. Comment on "A Reexamination of the 'Stratospheric Fountain' Hypothesis" by A. E. Dessler. *Geophysical Research Letters* **26**(17), 2737–2738.

Dessler, A. E.: 2002. The Effect of Deep, Tropical Convection on the Tropical Tropopause Layer. *Journal of Geophysical Research-Atmospheres* **107**(D3). Art. no. 4033.

Dethof, A., O'Neill, A., Slingo, J. M., and Smit, H. G. J.: 1999. A Mechanism for Moistening the Lower Stratosphere Involving the Asian Summer Monsoon. *Quarterly Journal of the Royal Meteorological Society* **125**(556), 1079–1106.

Dickinson, R. E.: 1971. Analytic Model for Zonal Winds in the Tropics. I. Details of the Model and Simulation of Gross Features of the Zonal Mean Troposphere. *Monthly Weather Review* **99**(6), 501–510.

Dobson, G. M. B.: 1956. Origin and Distribution of Polyatomic Molecules in the Atmosphere. *Proceedings of the Royal Society of London* **A236**, 187–193.

Dunkerton, T.: 1978. On the Mean Meridional Mass Motions of the Stratosphere and Mesosphere. *Journal of the Atmospheric Sciences* **35**(12), 2325–2333.

Dunkerton, T. J.: 1995. Evidence of Meridional Motion in the Summer Lower Stratosphere Adjacent to Monsoon Circulations. *Journal of Geophysical Research-Atmospheres* **100**(D8), 16,675–16,688.

Dunkerton, T. J. and Baldwin, M. P.: 1991. Quasi-Biennial Modulation of Planetary-Wave Fluxes in the Northern-Hemisphere Winter. *Journal of the Atmospheric Sciences* **48**(8), 1043–1061.

for Environmental Prediction, N. C.: 2002. Cold and Warm Episodes by Season. http://www.cpc.ncep.noaa.gov/products/analysis_monitoring/lanina/.

Evans, M., Shallcross, D. E., Law, K. S., Wild, J. O. F., Simmonds, P. G., Spain, T. G., Berrisford, P., Methven, J., Lewis, A. C., McQuaid, J. B., Pilling, M. J., Bandy, B. J., Penkett, S. A., and Pyle, J. A.: 2000. Evaluation of a Lagrangian Box Model using Field Measurements from EASE 1996. *Atmospheric Environment* **34**(23), 3843–3863.

Folkins, I., Löewenstein, M., Podolske, J., Oltmans, S. J., and Proffitt, M.: 1999. A Barrier to Vertical Mixing at 14 km in the Tropics: Evidence from Ozonesondes and Aircraft Measurements. *Journal of Geophysical Research-Atmospheres* **104**(D18), 22,095–22,102.

Gettelman, A., Holton, J. R., and Douglass, A. R.: 2000. Simulations of Water Vapour in the Lower Stratosphere and Upper Troposphere. *Journal of Geophysical Research-Atmospheres* **105**(D7), 9003–9023.

Gettelman, A., Randel, W. J., Massie, S., Wu, F., Read, W. G., and Russell III, J. M.: 2001a. El-Niño as a Natural Experiment for Studying the Tropical Tropopause Region. *Journal of Climate* **14**(16), 3375–3392.

Gettelman, A., Salby, M. L., and Sassi, F.: 2002. The Distribution and Influence of Convection in the Tropical Tropopause Region. *Journal of Geophysical Research-Atmospheres* **107**(D10). Art. no. 4080.

Gettelman, A. and Sobel, A. H.: 2000. Direct Diagnoses of Stratospheric-Troposphere Exchange. *Journal of the Atmospheric Sciences* **57**(1), 3–16.

Gouget, H., Vaughan, G., Marenco, A., and Smit, H. G. J.: 2000. Decay of a Cut-Off Low and Contribution to Stratosphere-Troposphere Exchange. *Quarterly Journal of the Royal Meteorological Society* **126**(564), 1117–1141.

Grant, W. B., Browell, E. V., Long, C. S., Stowe, L. L., Grainger, R. G., and Lambert, A.: 1996. Use of Volcanic Aerosols to Study the Tropical Stratospheric Reservoir. *Journal of Geophysical Research* **101**(D2), 3973–3988.

Gray, L. J. and Russell III, J. M.: 1999. Interannual Variability of Trace Gases in the Subtropical Winter Stratosphere. *Journal of the Atmospheric Sciences* **56**(7), 977–993.

Hartmann, D. L., Holton, J. R., and Fu, Q.: 2001. The Heat Balance of the Tropical Tropopause, Cirrus, and Stratospheric Dehydration. *Geophysical Research Letters* **28**(10), 1969–1972.

Haynes, P. and Schuckburgh, E.: 2000a. Effective Diffusivity as a Diagnostic of Atmospheric Transport, 1. The Stratosphere. *Journal of Geophysical Research-Atmospheres* **105**(D18), 22,777–22,794.

Haynes, P. H., Marks, C. J., McIntyre, M. E., Shepherd, T. G., and Shine, K. P.: 1991. On the "Downward Control" of Extratropical Diabatic Circulations by Eddy-Induced Mean Zonal Forces. *Journal of the Atmospheric Sciences* **48**(4), 651–678.

Held, I. M. and Hou, A. Y.: 1980. Nonlinear Axially Symmetric Circulations in a Nearly Inviscid Atmosphere. *Journal of the Atmospheric Sciences* **37**(3), 515–533.

Highwood, E. J. and Hoskins, B. J.: 1998. The Tropical Tropopause. *Quarterly Journal of the Royal Meteorological Society* **124**(551), 1579–1604.

Hitchman, M. H., Leovy, C. B., Gille, J. C., and Bailey, P. L.: 1987. Quasi-Stationary Zonally Asymmetric Circulations in the Equatorial Lower Mesosphere. *Journal of the Atmospheric Sciences* **46**(16), 2219–2236.

Holton, J. R.: 1992. *An Introduction to dynamic Meteorology*, vol. 48 of *International Geophysics Series*. Academic Press.

Holton, J. R. and Austin, J.: 1991. The Influence of the Equatorial QBO on Sudden Stratospheric Warmings. *Journal of the Atmospheric Sciences* **48**(4), 607–618.

Holton, J. R. and Gettelman, A.: 2001. Horizontal Transport and Dehydration of the Stratosphere. *Geophysical Research Letters* **28**(14), 2799–2802.

Holton, J. R., Haynes, P. H., McIntyre, M. E., Douglass, A. R., Rood, R. B., and Pfister, L.: 1995. Stratosphere-Troposphere Exchange. *Reviews of Geophysics* **33**(4), 403–439.

Holton, J. R. and Lindzen, R. S.: 1972. An Updated Theory for the Quasi-Biennial Cycle of the Tropical Stratosphere. *Journal of the Atmospheric Sciences* **29**(6), 1076–1080.

Holton, J. R. and Tan, H.: 1980. The Influence of the Equatorial Quasi-Biennial Oscillation on the Global Circulation at 50 hPa. *Journal of the Atmospheric Sciences* **37**(10), 2200–2208.

Holton, J. R. and Tan, H.: 1982. The Quasi-Biennial Oscillation in the Northern Hemisphere Lower Stratosphere. *Journal of the Meteorological Society of Japan* **60**(1), 140–148.

Hoskins, B. J.: 1991. Towards a PV-Theta View of the General-Circulation. *Tellus Series A — Dynamic Meteorology and Oceanography* **43**(4), 27–35.

Jackson, D. R., Driscoll, S. J., Highwood, E. J., Harries, J. E., and Russell III, J. M.: 1998. Troposphere to Stratosphere Transport at Low Latitudes as Studied Using HALOE Observations of Water Vapour 1992–1997. *Quarterly Journal of the Royal Meteorological Society* **124**(545), 169–192.

Jackson, D. R., Methven, J., and Pope, V. D.: 2001. Transport in the Low-Latitude Tropopause Zone Diagnosed Using Particle Trajectories. *Journal of the Atmospheric Sciences* **58**, 173–192.

James, I. N.: 1994. *Introduction to Circulating Atmospheres.* Cambridge Atmospheric and Space Science series, Cambridge University Press.

Jensen, E. J., Read, W. G., Mergenthaler, J., Sandor, B. J., Pfister, L., and Tabazadeh, A.: 1999. High Humidities and Subvisible Cirrus Near the Tropical Tropopause. *Geophysical Research Letters* **26**(15), 2347–2350.

Kelly, K. K., Proffitt, M. H., Chan, K. R., Löewenstein, M., Podolske, J. R., Strahan, S. E., Wilson, J. C., and Kley, D.: 1993. Water Vapour and Cloud Water Measurements Over Darwin During the STEP 1987 Tropical Mission. *Journal of Geophysical Research-Atmospheres* **98**(D5), 8713–8723.

Kent, G. S., Williams, E. R., Wang, P. H., McCormick, M. P., and Skeens, K. M.: 1995. Surface-Temperature Related Variations in Tropical Cirrus Cloud as Measured by SAGE-II. *Journal of Climate* **8**(11), 2577–2594.

Kley, D., Stone, E. J., Henderson, W. R., Drummond, J. W., Harrop, W. J., Schmeltekopf, A. L., Thompson, T. L., and Winkler, R. H.: 1979. In Situ Measurements of the Mixing Ratio of Water Vapour in the Stratosphere. *Journal of the Atmospheric Sciences* **36**(12), 2513–2524.

Knudsen, B. M. and Carver, G. D.: 1994. Accuracy of the Trajectories Calculated for the EASOE Campaign. *Geophysical Research Letters* **21**(13), 1199–1202.

Knudsen, B. M., Rosen, J. M., Kjome, N. T., and Whitten, A. T.: 1996. Comparison of Analysed Stratospheric Temperatures and Calculated Trajectories with Long-Duration Balloon Data. *Journal of Geophysical Research-Atmospheres* **101**(D14), 19,137–19,145.

Kritz, M. A., Rosner, S. W., Kelly, K. K., Löwenstein, M., and Chan, K. R.: 1993. Radon Measurements in the Lower Tropical Stratosphere: Evidence for Rapid Vertical Transport and Dehydration of Tropospheric Air. *Journal of Geophysical Research-Atmospheres* **98**(D5), 8725–8736.

Lahoz, W. A., Suttie, M. R., Froidevaux, L., Harwood, R. S., Lau, C. L., Lungu, T. A., Peckham, G. E., Pumphrey, H. C., Read, W. G., Shippony, Z., Suttie, R. A., Waters, J. W., Nedoluha, G. E., Oltmans, S. J., M., R. I. J., and Traub, W. A.: 1996. Validation of UARS Microwave Limb Sounder 183 GHz H_2O Measurements. *Journal of Geophysical Research-Atmospheres* **101**(D6), 10,129–10,149.

Massie, S., Lowe, P., Tie, X. X., Hervig, M., Thomas, G., and Russell, J.: 2000. Effect of the 1997 El Niño on the Distribution of Upper Tropospheric Cirrus. *Journal of Geophysical Research-Atmospheres* **105**(D18), 22,725–22,741.

Mastenbrook, H. J.: 1974. Water Vapour Measurements in the Lower Stratosphere. *Canadian Journal of Chemistry* **52**(2), 1527–1531.

Mastenbrook, H. J. and Oltmans, S. J.: 1983. Stratospheric Water Vapour Variability for Washington, DC/Boulder, CO: 1964–82. *Journal of the Atmospheric Sciences* **40**(9), 2157–2165.

McIntyre, M. E. and Palmer, T. N.: 1983. Breaking Planetary Waves in the Stratosphere. *Nature* **305**(5935), 593–600.

McIntyre, M. E. and Palmer, T. N.: 1984. The Surf Zone in the Stratosphere. *Journal of Atmospheric and Terrestrial Physics* **46**(9), 825–849.

Methven, J.: 1997. Offline Trajectories: Calculation and Accuracy. *Technical Report 44*, UGAMP, CGAM, University of Reading, Earley Gate, Reading, RG6 6BB, United Kingdom. 18 pages.

Methven, J., Berrisford, P., and Hoskins, B. J.: 1999. A Lagrangian Climatology for the North Atlantic Storm Track. *Technical Note 9*, UKMO Hadley Centre, Hadley Centre for Climate Prediction and Research, The Met. Office, London Road, Bracknell, Berkshire, RG12 2SY, United Kingdom. 99 pages.

Michelsen, H. A., Irion, F. W., Manney, G. L., Toon, G. C., and Gunson, M. R.: 2000. Features and Trends in Atmospheric Trace Molecule Spectroscopy (ATMOS) Version 3 Stratospheric Water Vapor and Methane Measurements. *Journal of Geophysical Research-Atmospheres* **105**(D18), 22,713–22,724.

Morris, G. A., Schoeberl, M. R., L. C. Sparling, P. A. N., Lait, L. R., Elson, L., Waters, J., Suttie, R. A., Roche, A., Kumer, J., and Russell III, J. M.: 1995. Trajectory Mapping and Applications to Data from the Upper Atmosphere Research Satellite. *Journal of Geophysical Research-Atmospheres* **100**(D8), 16,491–16,505.

Mote, P. W., Dunkerton, T. J., McIntyre, M. E., Ray, E. A., Haynes, P. H., and Russell III, J. M.: 1998. Vertical Velocity, Vertical Diffusion and Dilution by Midlatitude Air in the Tropical Lower Stratosphere. *Journal of Geophysical Research-Atmospheres* **103**(D8), 8651–8666.

Mote, P. W., Rosenlof, K. H., Holton, J. R., Harwood, R. S., and Waters, J. W.: 1995. Seasonal Variations of Water Vapour in the Tropical Lower Stratosphere. *Geophysical Research Letters* **22**(9), 1093–1096.

Mote, P. W., Rosenlof, K. H., McIntyre, M. E., Carr, E. S., Gille, J. C., Holton, J. R., Kinnersley, J. S., Pumphrey, H. C., Russell III, J. M., and Waters, J. M.: 1996. An Atmospheric Tape Recorder: The Imprint of Tropical Tropopause Temperatures on Stratospheric Water Vapour. *Journal of Geophysical Research-Atmospheres* **101**(D2), 3989–4006.

Moyer, E. J., Irion, F. W., Yung, Y. L., and Gunson, M. R.: 1996. ATMOS Stratospheric Deuterated Water and Implications for Troposphere-Stratosphere Transport. *Geophysical Research Letters* **23**(17), 2385–2388.

Murgatroyd, R. J. and Singleton, F.: 1961. Possible Meridional Circulations in the Stratosphere and Mesosphere. *Quarterly Journal of the Royal Meteorological Society* **87**(372), 125–135.

Murphy, D. M., Fahey, D. W., Proffitt, M. H., Liu, C. S., Chan, K. R., Eubank, C. S., Kawa, S. R., and Kelly, K. K.: 1993. Reactive Nitrogen and its Correlation with Ozone in the Lower Stratosphere and Upper Troposphere. *Journal of Geophysical Research* **98**(D5), 8751–8773.

Nedoluha, G. E., Siskind, D. E., Bacmeister, J. T., Bevilacqua, R. M., and III, J. M. R.: 1998. Changes in Upper Stratospheric CH_4 and NO_2 as Measured by by HALOE and Implications for Changes in Transport. *Geophysical Research Letters* **25**(7), 987–990.

Neu, J. L. and Plumb, R. A.: 1999. Age of Air in a "Leaky Pipe" Model of Stratospheric Transport. *Journal of Geophysical Research-Atmospheres* **104**(D16), 19,243–19,255.

Newell, R. E. and Gould-Stewart, S.: 1981. A Stratospheric Fountain? *Journal of the Atmospheric Sciences* **38**(12), 2789–2796.

Niwano, M. and Shiotani, M.: 2001. Quasi-Biennial Oscillation in Vertical Velocity Inferred from Trace Gas Data in the Equatorial Lower Stratosphere. *Journal of Geophysical Research-Atmospheres* **106**(D7), 7281–7290.

Oltmans, S. J. and Hofmann, D. J.: 1995. Increase in Lower-Stratospheric Water-Vapour at a Mid-Latitude Northern-Hemisphere Site from 1981 to 1994. *Nature* **374**(6518), 146–149.

Pawson, S. and Fiorino, M.: 1998. A Comparison of Reanalyses in the Tropical Stratosphere, Part 1: Thermal Structure and the Annual Cycle. *Climate Dynamics* **14**(9), 631–644.

Pickering, K. E., Thompson, A. M., McNamara, D. P., Schoeberl, M. R., Fuelberg, H. E., Jr., R. O. L., Watson, M. V., Fakhruzzaman, K., and Bachmeier, A. S.: 1996. TRACE A Trajectory Intercomparison. 1. Effects of Different Input Analyses. *Journal of Geophysical Research-Atmospheres* **101**(D19), 23,903–23,925.

Pierce, R. B., Grose, W. L., III, J. M. R., and Tuck, A. F.: 1994. Evolution of Southern Hemisphere Spring Air Masses Observed by HALOE. *Geophysical Research Letters* **21**(3), 213–216.

Plumb, R. A.: 1977. The Interaction of Two Internal Waves with the Mean Flow: Implications for the Theory of the Quasi-Biennial Oscillation. *Journal of the Atmospheric Sciences* **34**(12), 1847–1858.

Plumb, R. A. and Eluszkiewicz, J.: 1999. The Brewer-Dobson Circulation: Dynamics of the Tropical Upwelling. *Journal of the Atmospheric Sciences* **56**(6), 868–890.

Plumb, R. A. and McEwan, A. D.: 1978. The Instability of a Forced Standing Wave in a Viscous Stratified Fluid: a Laboratory Analogue of the Quasi-Biennial Oscillation. *Journal of the Atmospheric Sciences* **35**(10), 1827–1839.

Polvani, M. W., Waugh, D. W., and Plumb, R. A.: 1995. On the Subtropical Edge of the Stratospheric Surf Zone. *Journal of the Atmospheric Sciences* **52**(9), 1288–1309.

Potter, B. E. and Holton, J. R.: 1995. The Role of Monsoon Convection in the Dehydration of the Lower Tropical Stratosphere. *Journal of the Atmospheric Sciences* **52**(8), 1034–1050.

Prabhakara, C., Kratz, D. P., Yoo, J. M., Dalu, G., and Vernekar, A.: 1993. Optically Thin Cirrus Clouds — Radiative Impact on the Warm Pool. *Journal of Quantitative Spectroscopy and Radiative Transfer* **49**(5), 467–483.

Pumphrey, H. C.: 1999. Validation of a New Prototype Water Vapour Retrieval for UARS MLS. *Journal of Geophysical Research-Atmospheres* **104**(D8), 9399–9412.

Pumphrey, H. C., Clark, H. L., and Harwood, R. S.: 2000. Lower Stratospheric Water Vapour Measured by UARS MLS. *Geophysical Research Letters* **27**(12), 1691–1694.

Randel, W. J., Gille, J. C., Roche, A. E., Kumer, J. B., Mergenthaler, J. L., Waters, J. W., Fishbein, E. F., and Lahoz, W. A.: 1993. Stratospheric Transport from the Tropics to Middle Latitudes by Planetary-Wave Mixing. *Nature* **365**(6446), 533–535.

Randel, W. J., Wu, F., and Gaffen, D. J.: 2000. Interannual Variability of the Tropical Tropopause Derived From Radiosonde Data and NCEP Reanalyses. *Journal of Geophysical Research-Atmospheres* **105**(D12), 15,509–15,523.

Randel, W. J., Wu, F., Russell III, J. M., Roche, A., and Waters, J. W.: 1998. Seasonal Cycle and QBO Variations in Stratospheric CH_4 and H_2O Observed in UARS HALOE Data. *Journal of the Atmospheric Sciences* **55**(2), 163–185.

Reber, C. A.: 1993. The Upper Atmosphere Research Satellite (UARS). *Geophysical Research Letters* **20**(12), 1215–1218.

Reid, G. C. and Gage, K. S.: 1996. The Tropical Tropopause Over the Western Pacific: Wave Driving, Convection and the Annual Cycle. *Journal of Geophysical Research-Atmospheres* **101**(D16), 21,233–21,241.

Robinson, G. D.: 1980. The Transport of Minor Atmospheric Constituents between Troposphere and Stratosphere. *Quarterly Journal of the Royal Meteorological Society* **106**(448), 227–253.

Rodgers, C. D.: 1976. Retrieval of Atmospheric Temperature and Composition from Remote Measurements of Thermal Radiation. *Reviews of Geophysics and Space Physics* **14**, 609–624.

Rolph, G. D. and Draxler, R. R.: 1990. Sensitivity of Three-Dimensional Trajectories to the Spatial and Temporal Densities of the Wind Field. *Journal of Applied Meteorology* **29**(10), 1043–1054.

Rosenfield, J. E., Considine, D. B., Schoeberl, M. R., and Browell, E. V.: 1998. The Impact of Subvisible Cirrus Clouds Near the Tropical Tropopause on Stratospheric Water Vapour. *Geophysical Research Letters* **25**(11), 1883–1886.

Rosenlof, K. H.: 1995. Seasonal Cycle of the Residual Mean Meridional Circulation in the Stratosphere. *Journal of Geophysical Research-Atmospheres* **100**(D3), 5173–5191.

Rosenlof, K. H. and Holton, J. R.: 1993. Estimates of the Stratospheric Residual Circulation using the Downward Control Principle. *Journal of Geophysical Research-Atmospheres* **98**(D6), 10,465–10,479.

Schoeberl, M. R. and Sparling, L. C.: 1995. Trajectory Modelling. *Diagnostic Tools in Atmospheric Physics*, edited by G. Fiocco and G. Visconti. Proceedings of the International School of Physics, Enrico Fermi, Course CXVI, North-Holland, pp. 289–305.

Seidel, D. J., Ross, R. J., Angell, J. K., and Reid, G. C.: 2001. Climatological Characteristics of the Tropical Tropopause as Revealed by Radiosondes. *Journal of Geophysical Research-Atmospheres* **106**(D8), 7857–7878.

Sherwood, S. C.: 2000. A "Stratospheric Drain" over the Maritime Continent. *Geophysical Research Letters* **27**(5), 677–680.

Sherwood, S. C. and Dessler, A. E.: 2000. On the Control of Stratospheric Humidity. *Geophysical Research Letters* **27**(16), 2513–2516.

Sherwood, S. C. and Dessler, A. E.: 2001. A Model for Transport Across the Tropical Tropopause. *Journal of the Atmospheric Sciences* **58**(7), 765–779.

Simmons, A. and Burridge, D.: 1981. An Energy and Angular-Momentum Conserving Vertical Finite-Difference Scheme in Hybrid Vertical Co-ordinates. *Monthly Weather Review* **109**(4), 758–766.

Simmons, A. J., Untch, A., Jakob, C., Kållberg, P., and Undén, P.: 1999. Stratospheric Water Vapour and Tropical Tropopause Temperatures in ECMWF Analyses and Multi-Year Simulations. *Quarterly Journal of the Royal Meteorological Society* **125**(553), 353–386.

Stohl, A.: 1998. Computation, Accuracy and Applications of Trajectories — A Review and Bibliography. *Atmospheric Environment* **32**(6), 947–966.

Stohl, A., Wotawa, G., Seibert, P., and Kromp-Kolb, H.: 1995. Interpolation Errors in the Wind Fields as a Function of Spatial and Temporal Resolution and their Impact on Different Types of Trajectories. *Journal of Applied Meteorology* **34**(10), 2149–2165.

Strahan, S. E., Douglass, A. R., Nielsen, J. E., and Boering, K. A.: 1998. The CO_2 Seasonal Cycle as a Tracer of Transport. *Journal of Geophysical Research-Atmospheres* **103**(D12), 13,729–13,741.

Sutton, R. T.: 1994. Langrangian Flow in the Middle Atmosphere. *Quarterly Journal of the Royal Meteorological Society* **120**(519), 1299–1321.

Sutton, R. T., Maclean, H., Swinbank, R., O'Neill, A., and Taylor, F. W.: 1994. High-Resolution Stratospheric Tracer Fields Estimated from Satellite Observations using Langrangian Trajectory Calculations. *Journal of the Atmospheric Sciences* **51**(20), 2995–3005.

Swinbank, R. and O'Neill, A.: 1994a. A Stratosphere-Troposphere Assimilation System. *Monthly Weather Review* **122**(4), 686–702.

Swinbank, R. and O'Neill, A.: 1994b. Quasi-Biennial and Semi-Annual Oscillation in Equatorial Wind Fields Constructed by Data Assimilation. *Geophysical Research Letters* **21**(19), 2099–2102.

Thuburn, J. and Craig, G. C.: 2000. Stratospheric Influence on Tropopause Height: The Radiative Constraint. *Journal of the Atmospheric Sciences* **57**(1), 17–28.

Trenberth, K. E. and Olson, J. G.: 1988a. An Evaluation and Intercomparison of Global Analyses from the National Meteorological Center and the European Centre for Medium Range Forecasts. *Bulletin of the American Meteorological Society* **69**(9), 1047–1057.

Trenberth, K. E. and Olson, J. G.: 1988b. Intercomparison of NMC and ECMWF Global Analyses: 1980–1986. *NCAR Tech. Note NCAR/TN-301+STR 81*, National Center for Atmospheric Research, Boulder, CO.

Trepte, C. R. and Hitchman, M. H.: 1992. Tropical Stratospheric Circulation Deduced from Satellite Aerosol Data. *Nature* **355**(6361), 626–628.

VanHaver, P., DeMuer, D., Beekmann, M., and Mancier, C.: 1996. Climatology of Tropopause Folds at Midlatitudes. *Geophysical Research Letters* **23**(9), 1033–1036.

van Velthoven, P. F. J. and Kelder, H.: 1996. Estimates of Stratosphere-Troposphere Exchange: Sensitivity to Model Formulation and Horizontal Resolution. *Journal of Geophysical Research-Atmospheres* **101**(D1), 1429–1434.

Volk, C. M., Elkins, J. W., Fahey, D. W., Salawitch, R. J., Dutton, G. S., Gilligan, J. M., Proffitt, M. H., Löewenstein, M., Podolske, J. R., Minschwaner, K., Margitan, J. J., and Chan, K. R.: 1996. Quantifying Transport Between the Tropical and Mid-Latitude Lower Stratosphere. *Science* **272**(5269), 1736–1768.

Vomel, H. and Oltmans, S. J.: 1999. Comment on "A Reexamination of the 'Stratospheric Fountain' Hypothesis" by A. E. Dessler. *Geophysical Research Letters* **26**(17), 2737–2738.

Vomel, H., Oltmans, S. J., Kley, D., and Crutzen, P. J.: 1995. New Evidence for the Stratospheric Dehydration Mechanism in the Equatorial Pacific. *Geophysical Research Letters* **22**(23), 3235–3238.

Walmsley, J. L. and Mailhot, J.: 1983. On the Numerical Accuracy of Trajectory Models for Long-Range Transport of Atmospheric Pollutants. *Atmos,-Ocean* **21**(1), 14–39.

Wang, P. H., Minnis, P., McCormick, M. P., Kent, G. S., and Skeens, K. M.: 1996. A 6-year Climatology of Cloud Occurrence Frequency from Stratospheric Aerosol and Gas Experiment II Observations (1985–1990). *Journal of Geophysical Research-Atmospheres* **101**(D23), 29,407–29,429.

Waters, J. W.: 1989. Microwave Limb Sounding of the Earth's Atmosphere. *Atmospheric Research*, vol. 23. Elsevier Science, pp. 391–410.

Waters, J. W.: 1993. Microwave Limb Sounding. *Atmospheric Remote Sensing by Microwave Radiometry*, edited by M. A. Janssen, chap. 8. No. 3 in Remote Sensing, Wiley, pp. 383–496.

Waugh, D. W. and Plumb, R. A.: 1994. Contour Advection with Surgery: A Technique for Investigating Finscale Structure in Tracer Transport. *Journal of the Atmospheric Sciences* **51**(4), 530–540.

Wei, M.-Y.: 1987. A New Formulation of the Exchange of Mass and Trace Constituents between the Stratosphere and Troposphere. *Journal of the Atmospheric Sciences* **44**(20), 3079–3086.

Winker, D. M. and Trepte, C. R.: 1998. Laminar Cirrus Observed Near the Tropical Tropopause by LITE. *Geophysical Research Letters* **25**(17), 3351–3354.

World Meteorological Organisation: 1986. Atmospheric Ozone 1985. *WMO* **16**. Geneva, Switzerland.

Yulaeva, E., Holton, J. R., and Wallace, J. M.: 1994. On the Cause of the Annual Cycle in Tropical Lower-Stratospheric Temperatures. *Journal of the Atmospheric Sciences* **51**(2), 169–174.

Zhang, C. D.: 1993. On the Annual Cycle in the Highest, Coldest Clouds in the Tropics. *Journal of Climate* **6**(10), 1987–1990.

Zhou, X., Geller, M. A., and Zhang, M.: 2001. Tropical Cold Point Tropopause Characteristics Derived From ECMWF Reanalysis and Soundings. *Journal of Climate* **14**(8), 1823–1838.

Index